

TRUCK/PAVEMENT/ECONOMIC MODELING AND IN-SITU FIELD TEST DATA ANALYSIS APPLICATIONS – VOLUME 2: VERIFICATION AND VALIDATION OF FINITE ELEMENT MODELS FOR RIGID PAVEMENT USING IN SITU DATA – SELECTION OF JOINT SPACING



Shad Sargand and Basel Abdalla

for the
Ohio Department of Transportation
Office of Research and Development

and the
United States Department of Transportation
Federal Highway Administration

State Job Number 147700 – SPR2(203)

June 2006



OHIO
UNIVERSITY

Ohio Research Institute for
Transportation and the Environment



1. Report No. FHWA/OH-2006/3B	2. Government Accession No.	3. Recipient's Catalog No.	
4. Title and Subtitle Truck/Pavement/Economic Modeling and In-Situ Field Test Data Analysis Applications – Volume 2: Verification and Validation of Finite Element Models for Rigid Pavement Using In-Situ Data – Selection of Joint Spacing		5. Report Date June 2006	6. Performing Organization Code
7. Author(s) Shad Sargand, Basel Abdalla		8. Performing Organization Report No.	
9. Performing Organization Name and Address Ohio Research Institute for Transportation and the Environment (ORITE) 141 Stocker Center Ohio University Athens OH 45701-2979		10. Work Unit No. (TRAIS)	
12. Sponsoring Agency Name and Address Ohio Department of Transportation Office of Research and Development 1980 West Broad St. Columbus OH 43223		11. Contract or Grant No. State Job No. 147700 – SPR2(203) Agreement No. 10212	
		13. Type of Report and Period Covered Technical Report	
		14. Sponsoring Agency Code	
15. Supplementary Notes Prepared in cooperation with the Ohio Department of Transportation (ODOT) and the U.S. Department of Transportation, Federal Highway Administration			
16. Abstract <p>This work is conducted to provide a complete verification and validation of four different finite element programs (ISLAB2000, JSLAB, EVREFE, and OU3D) for rigid pavement. The experimental data used in this process was collected from the Ohio SHRP Test Road (including four core sections with various geometry and pavement layers) and the Ohio University Accelerated Pavement Load Facility (three different loading conditions). The variety of the pavement sections and loading conditions makes this verification a complete and unique study. The verification outcomes are applied to optimize the joint spacing for least critical stresses within the pavement design life by using three concrete fatigue models (PCA, Huang, and Domenichini).</p> <p>The validation results show that the finite element models follow the general trend of the experimental data in strain, deflection, and vertical pressure. However, two issues are pointed out: stress reversals between the truck axle loads, and slab rocking.</p> <p>Experimental results show that moisture loss that occurred after placing concrete slabs produces a residual negative temperature gradient of -2.2°F/inch (-0.48°C/cm). This leads to a permanent loss of support (LOS) under the pavement corners. Thus, positive gradient-based curling will only reduce the amount of LOS without eliminating it. When tested under different loading conditions, ISLAB2000 shows some inaccuracy in modeling the joints under combined traffic and environmental loadings.</p> <p>With the presence of built-in negative temperature gradient due to the curing of concrete, the critical tensile stresses are located at the top of the slab, and are maximized when the two truck axle loads are positioned on the two edges of the slab. This fact is confirmed experimentally; the slab cracks are observed to initiate at the top and develop towards the bottom of the pavement.</p> <p>The review of the three fatigue models shows that the level of tensile stress overcomes the frequency of load application. This is due to the tensile stresses resulting from the built-in negative temperature gradient. For the four pavement sections in the study, 13 ft (4.0 m) slabs had the longest design life.</p>			
17. Key Words Rigid pavement system, joint spacing, finite element method, three-dimensional finite element method		18. Distribution Statement No Restrictions. This document is available to the public through the National Technical Information Service, Springfield, Virginia 22161	
19. Security Classif. (of this report) Unclassified	20. Security Classif. (of this page) Unclassified	21. No. of Pages 120	22. Price

SI* (MODERN METRIC) CONVERSION FACTORS

APPROXIMATE CONVERSIONS TO SI UNITS

Symbol When You Know Multiply By To Find Symbol

LENGTH

in	inches	25.4	millimetres	mm
ft	feet	0.305	metres	m
yd	yards	0.914	metres	m
mi	miles	1.61	kilometres	km

AREA

in ²	square inches	645.2	millimetres squared	mm ²
ft ²	square feet	0.093	metres squared	m ²
yd ²	square yards	0.836	metres squared	m ²
ac	acres	0.405	hectares	ha
mi ²	square miles	2.59	kilometres squared	km ²

VOLUME

fl oz	fluid ounces	29.57	millilitres	mL
gal	gallons	3.785	litres	L
ft ³	cubic feet	0.028	metres cubed	m ³
yd ³	cubic yards	0.765	metres cubed	m ³

MASS

oz	ounces	28.35	grams	g
lb	pounds	0.454	kilograms	kg
T	short tons (2000 lb)	0.907	megagrams	Mg

TEMPERATURE (exact)

°F	Fahrenheit temperature	$5(F-32)/9$	Celsius temperature	°C
----	------------------------	-------------	---------------------	----

NOTE: Volumes greater than 1000 L shall be shown in m³.

APPROXIMATE CONVERSIONS FROM SI UNITS

Symbol When You Know Multiply By To Find Symbol

LENGTH

mm	millimetres	0.039	inches	in
m	metres	3.28	feet	ft
m	metres	1.09	yards	yd
km	kilometres	0.621	miles	mi

AREA

mm ²	millimetres squared	0.0016	square inches	in ²
m ²	metres squared	10.764	square feet	ft ²
ha	hectares	2.47	acres	ac
km ²	kilometres squared	0.386	square miles	mi ²

VOLUME

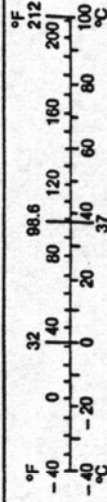
mL	millilitres	0.034	fluid ounces	fl oz
L	litres	0.264	gallons	gal
m ³	metres cubed	35.315	cubic feet	ft ³
m ³	metres cubed	1.308	cubic yards	yd ³

MASS

g	grams	0.035	ounces	oz
kg	kilograms	2.205	pounds	lb
Mg	megagrams	1.102	short tons (2000 lb)	T

TEMPERATURE (exact)

°C	Celsius temperature	$1.8C + 32$	Fahrenheit temperature	°F
----	---------------------	-------------	------------------------	----



* SI is the symbol for the International System of Measurement

(Revised April 1989)

Truck/Pavement/Economic Modeling and In-Situ Field Test Data Analysis Applications – Volume 2: Verification and Validation of Finite Element Models for Rigid Pavement Using In-Situ Data – Selection of Joint Spacing

Prepared in cooperation with the
Ohio Department of Transportation
and the
U.S. Department of Transportation, Federal Highway Administration

Prepared by

Shad M. Sargand
Basel Abdalla

Ohio Research Institute for Transportation and the Environment
Russ College of Engineering and Technology
Ohio University
Athens, Ohio 45701-2979

The contents of this report reflect the views of the authors who are responsible for the facts and the accuracy of the data presented herein. The contents do not necessarily reflect the official views or policies of the Ohio Department of Transportation or the Federal Highway Administration. This report does not constitute a standard, specification or regulation.

Final Report
June 2006

ACKNOWLEDGEMENTS

The authors would like to acknowledge the assistance and support of the pooled fund study members. The authors would like to acknowledge the contributions of the technical liaisons and project panel members to this project, including Roger Green.

The authors also acknowledge the contributions of ORITE Research Engineers Sam Khoury, Andrew Russ, and David Beegle to this project.

TABLE OF CONTENTS

1.	INTRODUCTION.....	1
1.1	BACKGROUND.....	1
1.2	RESEARCH OBJECTIVES	4
2	LITERATURE REVIEW	6
2.1	TWO-DIMENSIONAL FINITE ELEMENT MODELING.....	6
2.2	THREE-DIMENSIONAL FINITE ELEMENT MODELING.....	7
2.3	VERIFICATION OF FINITE ELEMENT MODELS.....	8
2.4	EFFECT OF SLAB SIZE ON RIGID PAVEMENT PERFORMANCE	9
3	VALIDATION OF MATHEMATICAL MODELS FOR RIGID PAVEMENT	12
3.1	INTRODUCTION	12
3.2	DESCRIPTION OF EXPERIMENTAL SECTIONS	12
3.2.1	PAVEMENT GEOMETRY	12
3.2.2	SENSOR LOCATIONS AND COORDINATE SYSTEM	13
3.2.3	MATERIAL PROPERTIES	15
3.2.4	DYNAMIC LOADS.....	17
3.3	BRIEF DESCRIPTION OF FINITE ELEMENT PROGRAMS.....	18
3.3.1	ISLAB2000	18
3.3.2	JSLAB	18
3.3.3	EVERFE.....	19
3.3.4	OU3D	19
3.4	PROGRAM PARAMETERS AND OPERATION	19
3.4.1	INPUT	19
3.4.2	MESH GENERATION	20
3.4.3	OUTPUT	20
3.5	DATA ANALYSIS AND RESULTS.....	20
3.6	SUMMARY	21
4	VALIDATION OF ISLAB2000.....	52
4.1	INTRODUCTION	52
4.2	EXPERIMENTAL DATA	52
4.3	EQUIVALENT TEMPERATURE GRADIENT DUE TO SLAB CURING	60

4.4	VERIFICATION FOR TEMPERATURE CYCLING – STAGE II	61
4.4.1	VALIDATION OF DEFLECTION PREDICTIONS	62
4.4.2	VALIDATION OF STRAIN PREDICTIONS	67
4.5	VERIFICATION FOR COMBINED LOAD AND TEMP. – STAGE III.....	72
4.5.1	VALIDATION OF STRAIN PREDICTIONS	82
4.6	SUMMARY	85
5	OPTIMIZATION OF SLAB JOINT SPACING	87
5.1	INTRODUCTION	87
5.2	TRAFFIC DATA: ODOT 23 WIM DATABASE	87
5.3	JOINT SPACING BASED ON FATIGUE MODEL	90
5.4	SUMMARY	98
6	SUMMARY AND CONCLUSIONS	99
6.1	GENERAL SUMMARY	99
6.2	CONCLUSIONS.....	100
6.2.1	Verification of Finite Element Models	100
6.2.2	Validation of ISLAB2000	100
6.2.3	Optimization of Joint Spacing	101
6.3	RECOMMENDATIONS FOR FUTURE STUDY	101
6.4	IMPLEMENTATION.....	102
7	REFERENCES.....	103

LIST OF FIGURES

Figure 1. Layout of Ohio SHRP Test Road (Sargand, 1994).	2
Figure 2. Sections of SPS1, SPS2, SPS8, and SPS9 in Ohio SHRP Test Road (Sargand, 1994).	3
Figure 3. Pavement Slab Geometry (1 inch = 2.54 cm).	13
Figure 4. Locations of Sensors within One Pavement Slab (1 in = 2.54 cm).	15
Figure 5. Dump Truck Footprints (1 inch = 2.54 cm, 100 psi = 689 kPa).	17
Figure 6. Comparison of Strains at D3 for Section 390201 (1 inch = 2.54 cm).	22
Figure 7. Comparison of Strains at D4 for Section 390201 (1 inch = 2.54 cm).	22
Figure 8. Comparison of Strains at D5 for Section 390201 (1 inch = 2.54 cm).	23
Figure 9. Comparison of Strains at D6 for Section 390201 (1 inch = 2.54 cm).	23
Figure 10. Comparison of Strains at D7 for Section 390201 (1 inch = 2.54 cm).	24
Figure 11. Comparison of Strains at D8 for Section 390201 (1 inch = 2.54 cm).	24
Figure 12. Comparison of Strains at K1 for Section 390201 (1 inch = 2.54 cm).	25
Figure 13. Comparison of Strains at K2 for Section 390201 (1 inch = 2.54 cm).	25
Figure 14. Comparison of Strains at K3 for Section 390201 (1 inch = 2.54 cm).	26
Figure 15. Comparison of Strains at K4 for Section 390201 (1 inch = 2.54 cm).	26
Figure 16. Comparison of Strains at K5 for Section 390201 (1 inch = 2.54 cm).	27
Figure 17. Comparison of Strains at K6 for Section 390201 (1 inch = 2.54 cm).	27
Figure 18. Comparison of Deflections at L4 for Section 390201 (1 inch = 2.54 cm).	28
Figure 19. Comparison of Deflections at L5 for Section 390201 (1 inch = 2.54 cm).	28
Figure 20. Comparison of Pressures at P1 for Section 390201 (1 inch = 2.54 cm).	29
Figure 21. Comparison of Strains at D3 for Section 390205 (1 inch = 2.54 cm).	29
Figure 22. Comparison of Strains at D4 for Section 390205 (1 inch = 2.54 cm).	30
Figure 23. Comparison of Strains at D5 for Section 390205 (1 inch = 2.54 cm).	30
Figure 24. Comparison of Strains at D6 for Section 390205 (1 inch = 2.54 cm).	31
Figure 25. Comparison of Strains at D7 for Section 390205 (1 inch = 2.54 cm).	31
Figure 26. Comparison of Strains at D8 for Section 390205 (1 inch = 2.54 cm).	32
Figure 27. Comparison of Strains at K1 for Section 390205 (1 inch = 2.54 cm).	32
Figure 28. Comparison of Strains at K2 for Section 390205 (1 inch = 2.54 cm).	33
Figure 29. Comparison of Strains at K3 for Section 390205 (1 inch = 2.54 cm).	33
Figure 30. Comparison of Strains at K4 for Section 390205 (1 inch = 2.54 cm).	34
Figure 31. Comparison of Strains at K5 for Section 390205 (1 inch = 2.54 cm).	34
Figure 32. Comparison of Strains at K6 for Section 390205 (1 inch = 2.54 cm).	35
Figure 33. Comparison of Deflections at L4 for Section 390205 (1 inch = 2.54 cm).	35
Figure 34. Comparison of Deflections at L5 for Section 390205 (1 inch = 2.54 cm).	36
Figure 35. Comparison of Pressures at P1 for Section 390205 (1 inch = 2.54 cm).	36
Figure 36. Comparison of Strains at D3 for Section 390208 (1 inch = 2.54 cm).	37
Figure 37. Comparison of Strains at D4 for Section 390208 (1 inch = 2.54 cm).	37
Figure 38. Comparison of Strains at D5 for Section 390208 (1 inch = 2.54 cm).	38
Figure 39. Comparison of Strains at D6 for Section 390208 (1 inch = 2.54 cm).	38
Figure 40. Comparison of Strains at D7 for Section 390208 (1 inch = 2.54 cm).	39
Figure 41. Comparison of Strains at D8 for Section 390208 (1 inch = 2.54 cm).	39
Figure 42. Comparison of Strains at K1 for Section 390208 (1 inch = 2.54 cm).	40
Figure 43. Comparison of Strains at K2 for Section 390208 (1 inch = 2.54 cm).	40
Figure 44. Comparison of Strains at K3 for Section 390208 (1 inch = 2.54 cm).	41

Figure 45. Comparison of Strains at K4 for Section 390208 (1 inch = 2.54 cm).....	41
Figure 46. Comparison of Strains at K5 for Section 390208 (1 inch = 2.54 cm).....	42
Figure 47. Comparison of Strains at K6 for Section 390208 (1 inch = 2.54 cm).....	42
Figure 48. Comparison of Deflections at L4 for Section 390208 (1 inch = 2.54 cm).....	43
Figure 49. Comparison of Deflections at L5 for Section 390208 (1 inch = 2.54 cm).....	43
Figure 50. Comparison of Pressures at P1 for Section 390208 (1 inch = 2.54 cm).....	44
Figure 51. Comparison of Strains at D3 for Section 390212 (1 inch = 2.54 cm).....	44
Figure 52. Comparison of Strains at D4 for Section 390212 (1 inch = 2.54 cm).....	45
Figure 53. Comparison of Strains at D5 for Section 390212 (1 inch = 2.54 cm).....	45
Figure 54. Comparison of Strains at D6 for Section 390212 (1 inch = 2.54 cm).....	46
Figure 55. Comparison of Strains at D7 for Section 390212 (1 inch = 2.54 cm).....	46
Figure 56. Comparison of Strains at D8 for Section 390212 (1 inch = 2.54 cm).....	47
Figure 57. Comparison of Strains at K1 for Section 390212 (1 inch = 2.54 cm).....	47
Figure 58. Comparison of Strains at K2 for Section 390212 (1 inch = 2.54 cm).....	48
Figure 59. Comparison of Strains at K3 for Section 390212 (1 inch = 2.54 cm).....	48
Figure 60. Comparison of Strains at K4 for Section 390212 (1 inch = 2.54 cm).....	49
Figure 61. Comparison of Strains at K5 for Section 390212 (1 inch = 2.54 cm).....	49
Figure 62. Comparison of Strains at K6 for Section 390212 (1 inch = 2.54 cm).....	50
Figure 63. Comparison of Deflections at L4 for Section 390212 (1 inch = 2.54 cm).....	50
Figure 64. Comparison of Deflections at L5 for Section 390212 (1 inch = 2.54 cm).....	51
Figure 65. Comparison of Pressures at P1 for Section 390212 (1 inch = 2.54 cm).....	51
Figure 66. PCC Doweled Slab Instrumentation. P1 through P5 indicate paths taken by the load; numbers indicate positions of measurement instrumentation. (1 m = 3.28 ft).....	54
Figure 67. Dipstick Path on Pavement. Numbers indicate positions of measurement instrumentation.....	54
Figure 68. Application of the Super Single Tire on Instrumented Pavement.....	55
Figure 69. Average Slab Temperature Gradient at Vibrating Wire Strain Gauges (1F° = 0.55C°).....	56
Figure 70. Top and Bottom Strain Development at Vibrating Wire Strain Gauge Location # 1.....	57
Figure 71. Top and Bottom Strain Development at Vibrating Wire Strain Gauge Location # 2.....	57
Figure 72. Top and Bottom Strain Development at Vibrating Wire Strain Gauge Location # 3.....	58
Figure 73. Top and Bottom Strain Development at Vibrating Wire Strain Gauge Location # 4.....	58
Figure 74. Average Slab Corner Deflection during Stages I and II (1 mm = 0.0394 inch).....	59
Figure 75. Average Slab Edge Deflection during Stages I and II (1mm = 0.039 in).....	59
Figure 76. Temperature Gradient at the Slab Center as Measured by Thermocouple (1F° = 0.55C°).....	60
Figure 77. Temperature Gradient at the Slab Center during Stage II (1F° = 0.55C°).....	62
Figure 78. Dipstick Profile along Diagonal Path on Slab (1 inch = 25.4 mm; 1 ft = 0.305 m).....	65
Figure 79. Upward Curling along the Diagonal. (left in English units, right in metric units).....	65
Figure 80. Loss of Support Model (Dimensions in feet, 1 foot = 0.305 m).....	65
Figure 81. Predicted and Measured Average Corner Deflection versus Test Time (1 mm = 0.0394 inch).....	67
Figure 82. Strain Predictions at the Slab Center, at the Top of Slab.....	70
Figure 83. Strain Predictions at the Slab Center, at the Bottom of Slab.....	70
Figure 84. Strain Predictions at the Slab Third Point, at the Top of Slab.....	71
Figure 85. Strain Predictions at the Slab Third Point, at the Bottom of Slab.....	71

Figure 86. Average Slab Temperature Gradient during Stage III ($1F^{\circ} = 0.55C^{\circ}$).....	72
Figure 87. Comparison between Measured and Combined Deflections along edge at study point A. Top: English units; bottom: metric units.....	74
Figure 88. Comparison between Measured and Combined Deflections along wheel path at study point A. Top: English units; bottom: metric units.	75
Figure 89. Comparison between Measured and Combined Deflections along edge at study point B. Top: English units; bottom: metric units.....	76
Figure 90. Comparison between Measured and Combined Deflections along wheel path at study point B Top: English units; bottom: metric units.....	77
Figure 91. Comparison between Measured and Combined Deflections along edge at study point C Top: English units; bottom: metric units.....	78
Figure 92. Comparison between Measured and Combined Deflections along wheel path at study point C Top: English units; bottom: metric units.....	79
Figure 93. Comparison between Measured and Combined Deflections along edge at study point D Top: English units; bottom: metric units.....	80
Figure 94. Comparison between Measured and Combined Deflections along wheel path at study point D Top: English units; bottom: metric units.	81
Figure 95. Longitudinal Predicted and Measured Strain at Study Point B along wheel path P4 at a load of 9000 lb (40.0 kN) (1 in = 2.54 cm).....	83
Figure 96. Transverse Predicted and Measured Strain at Study Point B along wheel path P4 at a load of 9000 lb (40.0 kN) (1 in = 2.54 cm).....	83
Figure 97. Longitudinal and Transverse Predicted and Measured Strain at Study Point A along wheel path P4 at a load of 12000 lb (53.4 kN) (1 in = 2.54 cm).	84
Figure 98. Longitudinal Predicted and Measured Strain at Study Point B along wheel path P4 at a load of 15000 lb (66.7 kN) (1 in = 2.54 cm).....	84
Figure 99. Transverse Predicted and Measured Strain at Study Point B along wheel path P4 at a load of 15000 lb (66.7 kN) (1 in = 2.54 cm).....	85
Figure 100. Traffic Frequencies and Axle Spacings on Ohio SHRP Test Road (1 foot = 0.305 m).	88
Figure 101. First and Second Truck Axle Weights (1 foot = 0.305 m, 1 kip = 4.448 kN).....	88
Figure 102. Number of Tracks per Month on Ohio SHRP Test Road as a function of axle spacing. (1 ft. = 0.305 m).....	89
Figure 103. Annual Number of Trucks on Ohio SHRP Test Road as a function of axle spacing. (1 ft. = 0.305 m).....	90
Figure 104. Maximum and Minimum Tensile Stresses at the Slab Top for Different Sections (1 psi = 6.89 kPa N, 1 foot = 0.305 m).....	93

LIST OF TABLES

Table 1. Portland Cement Concrete Sections in Ohio SHRP Test Road (adapted from Sargand, 1994).....	3
Table 2. Verification of Finite Element Models. Rows in italics designate ILLI-SLAB or ISLAB2000 verifications.....	9
Table 3. FAA recommended joint spacings on unstabilized subgrades (FAA, 1995, p. 87).....	10
Table 4. Dynamic Response Sensors.....	13
Table 5. Sensor Locations and Properties Measured (English units). For sensor abbreviations, see Table 4.....	14
Table 6. Sensor Locations and Properties Measured (metric units). For sensor abbreviations, see Table 4.....	14
Table 7. Material Properties of Core SPS-2 Sections (English units).....	16
Table 8. Material Properties of Core SPS-2 Sections (metric units).....	16
Table 9. Dump Truck Loads.....	17
Table 10. Required Locations of Truck.....	18
Table 11. Properties of Experimental Pavement Section (English units). Data for DGAB and subgrade (A-6) layers from Masada et al. (2004).....	53
Table 12. Properties of Experimental Pavement Section (metric units). Data for DGAB and subgrade (A-6) layers from Masada et al. (2004).....	53
Table 13. Nominal Temperature Conditions for Rolling Wheel Loads.....	55
Table 14. Trial Residual Temperature Gradients (English units).....	61
Table 15. Trial Residual Temperature Gradients (metric units).....	61
Table 16. Temperature Gradients for FE Analysis.....	63
Table 17. Dowel Bar Properties for FE Analysis.....	64
Table 18. Measured and Predicted Average Corner Deflection.....	66
Table 19. Comparison of Strain Test Reading with FE Analysis at Slab Center.....	68
Table 20. Comparison of Strain Test Reading with FE at Slab Third Point.....	68
Table 21. Correction of Predicted Strain at Slab Center.....	69
Table 22. Correction of Predicted Strain at Slab Third Point.....	69
Table 23. Cases used for Deflection Validation (English units). Tire Path P1 is along the edge and Tire Path P2 is in the wheel path 1 ft (30 cm) from the edge.....	73
Table 24. Cases used for Deflection Validation (metric units). Tire Path P1 is along the edge and Tire Path P2 is in the wheel path 1 ft (30 cm) from the edge.....	73
Table 25. Summary of Loading Conditions to Determine σ and σ_{min}	92
Table 26. Fatigue Model Calculations for Section 390201.....	94
Table 27. Fatigue Model Calculations for Section 390205.....	95
Table 28. Fatigue Model Calculations for Section 390208.....	96
Table 29. Fatigue Model Calculations for Section 390212.....	97

1. INTRODUCTION

1.1 BACKGROUND

The performance of rigid pavements depends on the stresses and deflections imposed by repeated traffic and environmental loading. Thus, understanding the response of rigid pavement structures under dynamic loads and thermal or moisture gradients is important for the design of new pavements, as well as the rehabilitation of existing ones. Two- and three- dimensional finite element (2DFE and 3DFE) modeling are powerful tools that can be used to investigate the combined effect of moving axle loads, thermal gradient through the slab thickness, concrete slab geometry, dowel bars at joints, and stiffness of foundation layers on the stresses induced in rigid pavements. A variety of finite element programs are available to the pavement engineer today. These programs can be divided into general-purpose finite element programs and finite element codes developed specifically for analysis of pavement systems (Khazanovich et al., 2003).

The National Cooperative Highway Research Program (NCHRP) developed the “Guide for Mechanistic-Empirical Design of New and Rehabilitated Pavement Structures” (Report NCHRP 1-37A) in 2002. The finite element program ISLAB2000 was selected as the structural response model for rigid pavements. ISLAB2000 is a plate theory-based pavement program and a revision of the finite element program ILLI-SLAB. ISLAB2000 is able to model all of the important features of the pavement systems, such as multiple slabs in each direction, multiple layers, mismatched joints, multiple loads, temperature curling, different subgrade models, and nonlinear temperature gradients (Khazanovich et al., 2003).

Validating the finite element model results is a key issue that highly affects the formulation of the model. Simply, validation is an investigation of the accuracy of the model to simulate the actual pavement behavior.

As the development of finite element models has progressed, many comparisons to theoretical solutions and experimental studies have been conducted for the purpose of verification. However, the majority of these experimental verifications have been limited to laboratory experiments and in situ tests that deal with idealized loads placed at critical locations on the slab.

The Ohio SHRP Test Road provides an excellent opportunity to compare realistic pavements and loadings to finite element models and to examine the effect of varying properties on the pavement response. As part of its support for the Strategic Highway Research Program (SHRP), the Ohio Department of Transportation, in conjunction with the Federal Highway Administration, developed a comprehensive test road encompassing four of nine experiments in the Specific Pavement Studies (SPS). This three-mile long project is located on U.S. 23 approximately 25 miles north of Columbus in Delaware County, and an overhead view is shown in Figure 1. To enhance the value of this test road, seasonal and dynamic response instrumentations were installed in 33 of the 38 test sections. The northbound lanes contain the SPS-2 experiment, while the southbound lanes contain the SPS-1 and SPS-9 experiments. The SPS-2 sections are presented in Figure 2. The variations of geometric and material properties between the slabs display the key roles that each property plays in the stress and deflection characteristics of the

slabs. The different base types and number of layers determine the influence of the base stiffness on the load response of rigid pavements. Dimensions, composition and strength values for the Portland Cement Concrete (PCC) sections are presented in Table 1.

In addition, some tests for this project were conducted at the Accelerated Pavement Load Facility (APLF). The APLF, located on the Lancaster Campus of Ohio University, is a state-of-the-art research facility designed for the testing of full-scale asphalt and concrete highway pavement sections under carefully controlled environmental and loading conditions. The pit where experimental sections of pavement are tested is 45 ft (13.7 m) long by 38 ft (11.6 m) wide by 8 ft (2.4 m) deep. Large 14 ft (4.3 m) high by 24 ft (7.3 m) wide doors are available at both ends of the building for access by equipment typically used to construct actual pavements. Air temperature in the facility can be maintained between 10°F (-12°C) and 130°F (54°C), and wheel loads of up to 30,000 lbs (133000 N) can be applied at a speed of up to 5 mph (8 km/h) with either dual or super single tires.

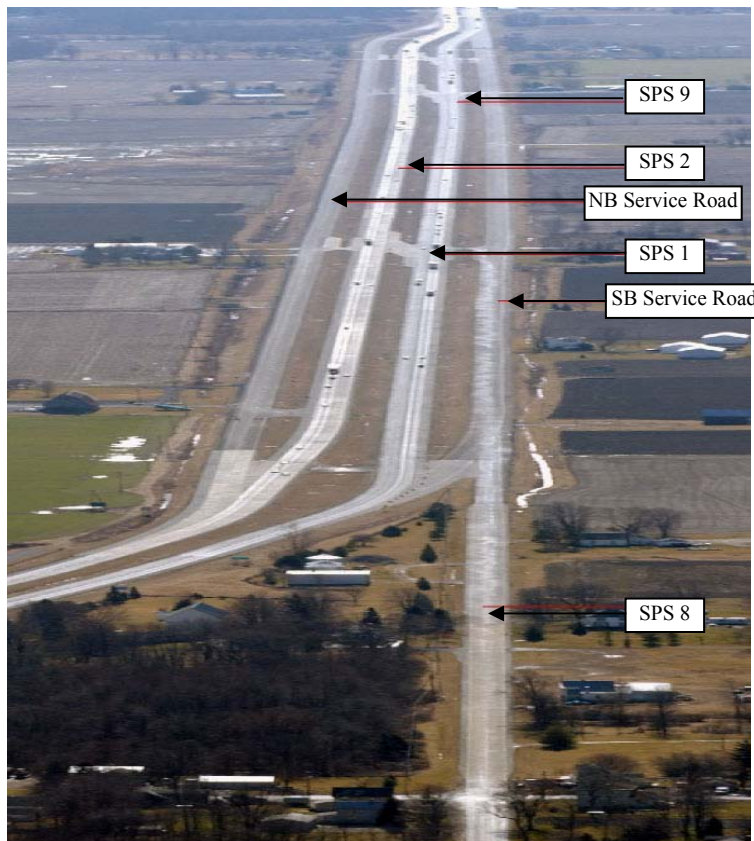


Figure 1. Layout of Ohio SHRP Test Road (Sargand, 1994).

In a previous project conducted by Sargand et al. (2003) to define the impact of curing, environmental cycling, and wheel loading on the performance of PCC pavements, the authors constructed 45 ft (13.7 m) long by 14 ft (4.3 m) wide by 10 in (0.25 m) thick slabs both doweled and undoweled in the APLF. Each pavement was sawn into three slabs, with joints spaced at 15 ft (4.6 m) intervals, and monitored from 12/17/1999 until 6/22/2000. The project provided massive amounts of data regarding the pavement strains and deflections under the effect of curing, temperature cycling, and combined dynamic loading and temperature cycling.

Table 1. Portland Cement Concrete Sections in Ohio SHRP Test Road (adapted from Sargand, 1994)

Portland Cement Concrete Studies on Ohio SHRP Test Road										
SPS-2										
Section	Lane Width		Strength		PCC Thickness		Base thickness		Base Type	Drainage
	(ft)	(m)	(psi)	(MPa)	(in)	(cm)	(in)	(cm)		
390201	12	3.66	ODOT	ODOT	8	20.3	6	15.2	DGAB	No
390202	14	4.27	900	6.21	8	20.3	6	15.2	DGAB	No
390203	14	4.27	ODOT	ODOT	11	27.9	6	15.2	DGAB	No
390204	12	3.66	900	6.21	11	27.9	6	15.2	DGAB	No
390205	12	3.66	ODOT	ODOT	8	20.3	6	15.2	LCB	No
390206	14	4.27	900	6.21	8	20.3	6	15.2	LCB	No
390207	14	4.27	ODOT	ODOT	11	27.9	6	15.2	LCB	No
390208	12	3.66	900	6.21	11	27.9	6	15.2	LCB	No
390209	12	3.66	ODOT	ODOT	8	20.3	8	20.3	half PATB/half DGAB	Yes
390210	14	4.27	900	6.21	8	20.3	8	20.3	half PATB/half DGAB	Yes
390211	14	4.27	ODOT	ODOT	11	27.9	8	20.3	half PATB/half DGAB	Yes
390212	12	3.66	900	6.21	11	27.9	8	20.3	half PATB/half DGAB	Yes
390259	12	3.66	900	6.21	11	27.9	6	15.2	DGAB	Yes
390260	12	3.66	ODOT	ODOT	11	27.9	8	20.3	half PATB/half DGAB	Yes
390261	14	4.27	ODOT	ODOT	11	27.9	8	20.3	half PCTB/half DGAB	Yes
390262	12	3.66	ODOT	ODOT	11	27.9	8	20.3	half PCTB/half DGAB	Yes
390263	14	4.27	ODOT	ODOT	11	27.9	6	15.2	DGAB	Yes
390264	12	3.66	ODOT	ODOT	11	27.9	6	15.2	DGAB	Yes
390265	12	3.66	ODOT	ODOT	11	27.9	8	20.3	half PATB/half DGAB	Yes
SPS-8										
390809	11	3.35	550	3.79	8	20.3	6	15.2	DGAB	No
390810	11	3.35	550	3.79	11	27.9	6	15.2	DGAB	No

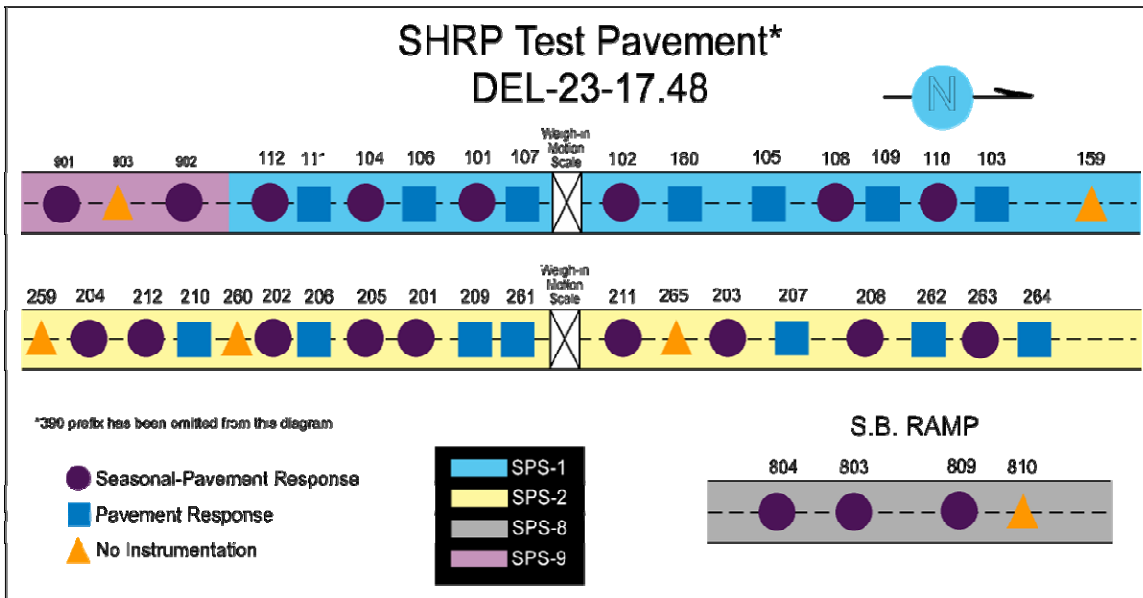


Figure 2. Sections of SPS1, SPS2, SPS8, and SPS9 in Ohio SHRP Test Road (Sargand, 1994)

As mentioned earlier, ISLAB2000 was selected for the NCHRP Guide as the final structural model. During the process of final model selection, ISLAB2000 predictions of maximum deflections and stresses were verified against PLITA by Khazanovich et al. (2003) and against ABAQUS by Hammons (1997). PLITA is a finite element program for analysis of slab-on-grade, and ABAQUS is a general-purpose, 3D, dynamic, nonlinear finite element code designed to address structural and heat transfer problems. The field verification of ISLAB2000 was conducted by using the main traffic loop measurements of the AASHO Road Test (Khazanovich et al., 2003). A flat slab condition was assumed, and the predicted bending stresses were compared with stresses calculated from measured strains. Although the ISLAB2000 predictions matched the measured stresses very closely, the main limitation of the field verification is that the experimental section was set up to measure the pavement edge response under moving truck loads only, without consideration of environmental loading. The PCC slab was assumed flat and in uniform contact with the underlying base material. Any loss of support from initial curing and from subsequent environmental curling and warping was ignored. However, the support that a base and embankment or roadbed subgrade provides to a PCC pavement was found to have a significant effect on the performance of the pavement (Darter et al., 1995). Research indicates that PCC slab edges begin to deform upward within a few hours after concrete placement and continue to deform throughout the traditional 28-day cure period and beyond, even when ambient conditions remain relatively constant. This displacement is caused primarily by a loss of moisture in the upper portion of the slab during the hydration process. As ambient temperature or moisture conditions change, further positive and negative displacements are superimposed on the slabs. Since the dynamic response of rigid pavements is affected by slab support, accurate response calculations require that the models properly account for non-uniform slab support.

Finite element models, if verified and validated, provide a powerful tool that can be used to accurately investigate the combined effect of various design features on the rigid pavement performance. Lee and Yen (2002) mentioned that the response behavior of rigid pavements is affected by various design features, including the PCC slab joint spacing. Field performance has shown that joint spacing has a considerable effect on the development of transverse cracks (Darter et al., 1995). Guo and Rice (1997) reported that joint spacing has a very significant effect on the pavement total stresses. Therefore, in order to enhance ride quality, it is necessary to optimize concrete slab joint spacing to reduce thermal- and moving traffic- induced stresses. Previous research on joint spacing (Parson et al., 2003, Lee et al., 2002, Guo et al., 1997) was mainly conducted on airport concrete pavements. However, no specific recommendation on rigid pavement joint spacing has been reported.

1.2 RESEARCH OBJECTIVES

The main objectives of this research are:

- Validation of four selected mathematical models for rigid pavement by the direct comparison to experimental data collected from the Ohio SHRP Test Road. The data include pavement strain, deflection, and vertical pressure. The models include two 3D-FE programs, EVERFE and OU3D, and two 2D-FE programs, ISLAB2000 and JSLAB. The results from this process also provide the opportunity to examine the influence of the base stiffness on the measured as well as predicted load response of rigid pavement.

- Verification and validation of ISLAB2000 rigid pavement response to curing, temperature cycling, and combined environmental and dynamic loading using the experimental data collected from the APLF. The 3D-FE program EVERFE is used to check the accuracy of the validation outcomes.
- Optimization of concrete slab joint spacing to reduce thermal and moving traffic induced stresses using the verified and validated ISLAB2000. The optimization is based on the analysis of rigid pavement fatigue model.

2 LITERATURE REVIEW

2.1 TWO-DIMENSIONAL FINITE ELEMENT MODELING

The enhanced computational capabilities of computers, along with the Finite Element (FE) method advanced the design and analysis of rigid pavements. Cheung and Zienkiewicz (1965) developed the first algorithm for the analysis of rigid pavements to solve the problem of isotropic and orthotropic slabs on both semi-infinite elastic continuum and Winkler foundation using the FE method. Huang and Wang (1973) followed the procedure of Cheung and Zienkiewicz to develop a FE method based on the classical theory of thin plates on Winkler foundations. However, the developed model was incapable of handling multilayer systems. Chou (1984) modified model developed by Huang and Wang (1973). The developed computer program, called WESLIQID, was able to handle multiple wheel loads on two-layered pavement system.

Tabatabaie (1978) developed a FE computer program ILLISLAB based on the classical theory of a medium-thick plate on a Winkler foundation. In the medium-thick plate theory, the plate is thick enough to carry a transverse load by flexure rather than by in-plane forces as in thin plate theory, and the plate is not so thick that transverse shear deformation becomes important. The model is capable of evaluating the effects of various load transfer mechanisms. Spring elements were used to model aggregate interlock and keyway joints that transfer forces between adjacent slabs by means of shear. Bar elements were used to model doweled joints that transfer moment as well as shear across the joints. Nasim et al. (1991) modified ILLI-SLAB to generate influence functions in order to predict the strain time histories at points of interest in the pavement. Additional capabilities were added to ILLISLAB including the incorporation of different subgrade models (Ioannides, 1984 and Khazanovich and Ioannides, 1993) and temperature loading (Korovesis, 1990).

ILSL2 (Khazanovich, 1994) is the most recent public domain revision of the finite element program ILLI-SLAB. The advantage of ILSL2 over ILLI-SLAB lies in its ability to analyze the separate action of two layers. ISLAB2000 is a proprietary revision of ILSL2 developed by ERES Consultants in cooperation with Michigan and Minnesota Departments of Transportation, Michigan Technical University, University of Michigan, Michigan State University, and University of Minnesota. ISLAB2000 is advantageous in having the ability to model several layers rather than just the two in ILSL2. ISLAB2000 can also model mismatched joints and has an increased maximum allowable number of nodes. Both these two programs have a technical superiority over programs specifically developed for rigid pavement analysis (Khazanovich and Yu, 1998). ISLAB2000 permits independent action of two pavement layers, linear and nonlinear temperature distribution, and partial-depth cracks.

Tayabji and Colley (1983) developed a computer program called JSLAB that allows only a linear temperature gradient. This program can analyze only a single layer slab when a temperature gradient is introduced. More details on JSLAB will be presented in Chapter 3.

Traditionally, dowel bars are modeled as bar elements. In order to examine the performance and failure of doweled joints closely, a two dimensional finite element model was developed by

Parson and Hjelmstad (1997). All of the components, including dowel bars, were modeled using four node quadrilateral finite elements.

Several other 2D-FE programs also exist, such as KENELS (Huang, 1974), KENSLABS (Huang, 1985), WESLAYER (Chou, 1981), KENSLAB (Huang, 1993), FEACONS-IV (Choubane and Tia, 1995), and ISLS97 (Roesler and Khazanovich, 1997).

The 2D-FE programs represent significant improvement over traditional pavement design methods. However, these programs have several limitations. They cannot accurately model realistic horizontal friction force at the interface between different pavement layers, or detailed local responses, such as stresses at dowel bar/concrete interfaces. These limitations can be overcome by using the three-dimensional finite element approach.

2.2 THREE-DIMENSIONAL FINITE ELEMENT MODELING

The approach of three-dimensional finite element modeling (3D-FEM) was adopted by many researchers to overcome the limitations of 2D-FEM and to better understand the reasons for some modes of pavement failure. Ioannides and Donnelly (1988) examined the effect of subgrade support conditions on rigid pavement slabs. In their study, the 3D-FE program GEOSYS was used to develop a model consisting of a single concrete slab and subgrade. The study examined the effect of mesh fineness, vertical and lateral subgrade extent, and boundary conditions on pavement response. GEOSYS can be used to analyze flexible or rigid pavements. Chatti (1992) developed the 3D-FEM called DYNA-SLAB, which is an extension of the static 2D-FE model ILLI-SLAB. Chatti showed that the maximum tensile stress occurs at the mid point of the slab bottom along the free edge, and observed stress reversal at the transverse joint.

Sargand and Beegle (1994) at Ohio University developed a 3D-FE program, OU3D, for the purpose of matching the data from the Ohio Test Road with mathematical models. In this program, all layers, including the soil foundation, are modeled using twenty-node hexahedral elements with linear elastic material properties. Special thin interface elements were used to model the behavior at the soil-concrete interface, and beam elements were used for joint dowels and ties. Thermal effects were also included. The program was capable of accurately predicting the displacements under thermal gradient loading.

In 1998, the University of Washington, in cooperation with the Washington state DOT, developed the 3D-FE analysis tool EVERFE. The program employed an intuitive graphical user interface that greatly simplified modal generation. EVERFE incorporated a novel technique for modeling aggregate interlock joint shear transfer. More details on both OU3D and EVERFE will be presented in Chapter 3.

Williams and Shoukry (2000) developed a 3D-FE program to investigate the applicability of Westergaard's thermal stress formulation to dowel-jointed concrete pavements. According to the model results, the authors proposed a corrected equation to calculate longitudinal curling stress.

General purpose 3D-FE packages such as NIKE3D, DYNA3D, TOPAZ3D, ANSYS, and ABAQUS are preferable for rigid pavement analysis because they incorporate advanced

modeling features such as interface algorithms and thermal modules. These packages have been in the process of development by private and public domain organizations since the 1970s, and have been used in different design problems.

Brill et al. (1997) presented a 3D-FE model of a rigid pavement structure with multiple elastic layers using NIKE3D. The model used two types of elements: 2D shell elements to represent the concrete slab and 3D hexahedrons for all other pavement system components, including joints.

Shoukry et al. (1996 and 1997) examined the dynamic response of rigid pavements to Falling Weight Deflectometer (FWD) impact using LS-DYNA. The results indicated the reliability of LS-DYNA in predicting the dynamic surface deflections measured during FWD tests. These results also demonstrated that pavement layer interface properties are very important considerations when modeling pavement structures.

Darter et al. (1995) developed a model called 3DPAVE using ABAQUS to investigate the effect of base support on slab stress and deformation response of rigid pavement. They proposed an improved methodology for better consideration of slab support in the AASHTO design procedure.

Hammons (1998) used ABAQUS to develop a FE model to predict the structural response of a jointed concrete airport pavement system. The concrete slabs were idealized as shell elements, while the base course was modeled by hexahedral continuum elements on Winkler foundation. Environmental factors were excluded in this research. The model predicted the stress-based load transfer efficiencies more accurately than the deflection-based efficiencies when compared to experimental data. Masad et al. (1996) developed a model using ABAQUS to study the effect of temperature variation on plain-jointed concrete pavements.

Harik et al. (1994) developed a 3D model using ANSYS for the study of rigid pavements subjected to temperature loading. The pavement was idealized as a thin isotropic plate resting on a Winkler foundation.

Kennedy et al. (1994) developed a 3D-FE interface for modeling pavement structures. This was basically a pavement-meshing algorithm, which relies on public domain FE equation solvers DYNA3D and NIKE3D. The model was verified using the results from a test section constructed in Ohio (Kennedy and Everhart, 1997). In this model, the bottom surface of the soil layer is supported by dynamic compliant boundaries (springs and dampers).

2.3 VERIFICATION OF FINITE ELEMENT MODELS

The key issue in the formulation of a theoretical model is to check the accuracy of the results obtained by the model, or to perform a model verification process. Verifying the results provides confidence in any analysis or conclusions reached from that model. Verification of finite element models has been conducted based on one or more of the following criteria: 1) comparison of the FE model results with field measurements for the same structure under identical loading conditions, 2) comparison of the FE model results with closed form solutions, and 3) comparison

of the FE model results with the results obtained from other FE programs (theoretical solutions) that are already verified.

The summary presented in Table 2 presents the verification method of the common FE models. The italic notation is given to ILLI-SLAB or ISLAB2000 verifications. While comparing theoretical results to experimentally measured results is the optimum verification criteria, this method is still limited to the quality of the measured data. On the other hand, matching model results with the results obtained from other previously verified FE programs depends on the quality of these programs and the obtained matching level.

Table 2. Verification of Finite Element Models. Rows in italics designate ILLI-SLAB or ISLAB2000 verifications.

Author	Year	Verification Method
Huang et al.	1973	Westergaard, Pickett and Ray, and AASHO Road Test
<i>Tabatabaie et al.</i>	<i>1978</i>	<i>Westergaard, Pickett and Ray, and AASHO Road Test</i>
Ioannides et al.	1988	Theoretical solutions (ILLI-SLAB)
Nasim et al.	1991	Instrumented rigid pavement sections of US-50 near Carlyle, Illinois
Chatti	1992	Theoretical solutions
Lee et al.	1994	AASHO Road Test and Arlington Road Test
Zaghloul et al.	1994	Westergaard solution and field results
Darter et al.	1995	AASHO, PCA, and Arlington Road Test
Tia et al.	1995	Florida Test Pavement
Masad et al.	1996	KENSLAB, ILLI-SLAB, JSLAB, and Bradbury analytical solution (Bradbury, 1938)
Kennedy et al.	1997	Measurements from Ohio Test Road
Hammons	1998	Data from the FAA's instrumented pavement at Denver International Airport (DIA)
Lee et al.	1998	Instrumented PCC runway in DIA
Davids et al.	1998	Laboratory-scale JPCCP models performed by Hammons (1997)
Sargand et al.	1998	Measurements from Ohio Test Road
<i>Lee et al.</i>	<i>1999</i>	<i>Test sections of Taiwan's second northern highway</i>
Shoukry	2000	Ohio Test Road results
Shoukry et al.	2003	Measurements from Robert Byrd Highway (Rt. 33), West Virginia
<i>Khazanovich et al.</i>	<i>2003</i>	<i>AASHO Road Test, PLITA, and ABAQUS</i>

2.4 EFFECT OF SLAB SIZE ON RIGID PAVEMENT PERFORMANCE

Joints should be provided in concrete pavements to relieve the stresses resulting from friction and environmental changes (i.e. temperature and moisture). Joints allow the transfer of load to the unloaded slab. In doweled joints, the load is transferred through shear action in the dowel and results in a more even distribution of loading to the foundation together with a reduction in the magnitude of local stresses in the loaded slab (Parson et al., 1997). The load transfer capabilities of joints are critical for pavement performance, since rigid pavement slabs have failed because of joint deterioration (Kuo, 1997).

The spacing of joints should be based on local experience, since a change in coarse aggregate types may have a significant effect on the concrete thermal coefficient, and consequently, the acceptable joint spacing (Huang, 1993). AASHTO (1986) limited the joint spacing in feet for plain concrete pavements to twice the slab thickness in inches, i.e. the maximum joint spacing was 24 times the slab thickness. The ratio of slab width to slab length was limited to 1.25. An FHWA technical Advisory (FHWA, 1990) recommends a maximum joint spacing of 15 ft. (4.6 m) for PCC slabs. The Federal Aviation Administration (FAA, 1995, p. 85ff) also recommends a maximum allowable joint spacing. For slabs on stabilized subgrades, a joint spacing of 4 to 6 times the radius of relative stiffness, as determined by Westergaard's formula is recommended. For joints on unstabilized subgrades, recommendations are as given in Table 3 below.

Table 3. FAA recommended joint spacings on unstabilized subgrades (FAA, 1995, p. 87).

Slab Thickness		Transverse		Longitudinal	
Inches	Millimeters	Feet	Meters	Feet	Meters
6	150	12.5	3.8	12.5	3.8
7-9	175-230	15	4.6	15	4.6
9-12	230-305	20	6.1	20	6.1
> 12	> 305	25	7.6	25	7.6

Note: The joint spacings shown in this table are recommended maximum values. Smaller joint spacings should be used if indicated by past experience. Pavements subject to extreme seasonal temperature differentials or extreme temperature differentials during placement may require smaller joint spacings. See also Chapter 5 for light load rigid pavement jointing.

Since longer and shorter slabs have both advantages and disadvantages, a compromise in joint spacing is required. The use of larger slabs reduces the number of joints, and consequently, the initial cost of pavements, reduces the joint maintenance fees, and provides smoother surface conditions. On the other hand, longer slabs have a higher possibility of earlier cracks and lower joint load transfer capabilities.

Shorter slab lengths require a larger number of joints and therefore higher construction costs. Shorter slabs have several advantages including less joint faulting, improved aggregate interlock, lower curling and warping stresses, fewer premature transverse cracks, reduced slab movement, and reduced shear stress.

A survey conducted in 1995 of current concrete pavement design practices in the US demonstrated that the mean joint spacing of JPCP is 15 ft (4.6 m) and ranges from 13 ft (4.0 m) to 20 ft (6.1 m) (Jiang et al., 1996).

Darter et al. (1995) reported that several design manuals provide rules for joint spacing as a function of slab thickness. These rules do not, however, adequately consider the effects of climate, frictional resistance, and base and subgrade stiffness.

Guo and Rice (1997) studied the effect of slab size on the critical responses in airport concrete pavements by calculating the critical response with varying slab sizes using the JSLAB program.

The study concluded that the slab size has a very significant effect on the total stresses if both load and temperature were considered.

In his study of the factors affecting the amount of slab curling due to shrinkage, Suprenant (2002) found that increasing slab thickness and reducing joint spacing decreases the amount of curling deflection. This is similar to conclusions by Leonards and Harr (1959) and by Childs and Kapernick (1958).

Ytterburg (1987) suggested that curling would not increase with an increase in joint spacing beyond 25 ft (7.6 m) to 30 ft (9.1 m). Also, reducing the joint spacing to 6 ft (1.8 m) to 8 ft (2.4 m) is unlikely to reduce the amount of curling deflection.

Lee and Yen (2002) investigated the effects of finite slab size on rigid airfield pavements. They used prediction models proposed by Lee et al. (1997) to estimate the critical edge stress for design. These models include adjustment factors for the effect of each design feature, such as different gear configuration, finite slab size, bounded or unbounded second layer, and the combined effect of loading plus daytime curling. The study concluded that the stress adjustment factors estimated in terms of R_w for finite slab width and R_L for finite slab length are indeed negligible (0.964 to 1.0) for the full-scale test pavements.

Shoukry and Fahmy (2002) studied the effect of slab geometry on thermal and moving traffic induced stresses in rigid pavement. They developed a 3D-FE model to simulate the response of rigid pavement to traffic and thermally induced loads. They concluded that short slab lengths can carry a larger number of vehicle passes to failure than longer slabs.

Parsons and Hall, Jr. (2003) studied the relationship between slab size (joint spacing) and pavement performance. Data was compiled from 48 inspections of military and civil airfields in the US, and was divided into small, medium, large, and extra large categories with respect to slab size. The study concluded that: 1) smaller slabs generally perform better, 2) pavements with joint spacing in excess of 25 ft (7.6 m) have the highest rate of deterioration, 3) slab thickness has the greatest effect on the relationship between pavement performance and slab size, and 4) pavements greater than 12 in (30.5 cm) thick deteriorate at approximately the same rate regardless of slab size.

Chen et al. (2004) presented an analytical model that used energy variation to predict the minimum and maximum crack spacings in continuous concrete pavements. They represented the pavement as a series of cohesive cracks and elastic bars. The model predictions correlated to what was found in practice.

Therefore, with the exclusion of Lee and Yen (2002) results, it can be concluded that joint spacing has a considerable effect on the performance of rigid pavement.

3 VALIDATION OF MATHEMATICAL MODELS FOR RIGID PAVEMENT

3.1 INTRODUCTION

The work completed in Finite Element (FE) modeling of rigid pavements from the beginning of the 1970's until the present is truly rich and led to a breakthrough in pavement analysis and design (Shoukry and Fahmy, 2002). However, validating the results of a theoretical model is one of the key issues in the formulation of the model. The massive instrumentation installed at the Ohio SHRP Test Road has provided a wealth of information concerning rigid pavements. This information is used as the basis for the validation of FE programs in this study. The output of four finite element programs, ISLAB2000, JSLAB, EVERFE, and OU3D, was compared to the experimental data obtained in the field. Computed results based on these four models, including strains, deflections, and vertical pressure, were compared to the experimental results from the four coinciding sections of the Ohio SHRP Test Road. JSLAB results were provided by a FHWA contractor, while the other three programs were run at Ohio University. The comparison focused on the trend rather than the absolute value of the computed pavement properties, which were dependent on input parameters. A direct comparison such as this has never before been conducted using these or any other models. The different programs were also compared for usability in terms of modeling, input and output data, and speed.

In this chapter, a description of the experimental sections is presented, followed by a brief summary of the finite element programs used. Although each program was developed for the same purpose, the programs utilize different methods of modeling the pavement structure. The following sections present the input data, mesh generation, and the output data of the models. Finally, the comparison results are presented in graphical form.

3.2 DESCRIPTION OF EXPERIMENTAL SECTIONS

3.2.1 PAVEMENT GEOMETRY

Four core LTPP instrumentation sections, 390201, 390205, 390208, and 390212, from the SPS-2 sections of the Ohio Test Road (U.S. 23) were used in this study. Each section had two 12-foot (3.66 m) lanes and a 10-foot (3.05 m) asphalt shoulder on the right side. Since the shoulder was not tied to the pavement, the shoulder could be ignored in this study. All instrumentation was located in the right lane. However, since the two lanes are tied together by 30-inch (76.2 cm)-long, 0.625-inch (15.88 mm)-diameter steel bars spaced every 30 inches (76.2 cm), both lanes were included in the solution. However the load transfer from the right to the left lane is small, so the left lane may be neglected. Thus the model may be considered symmetric about the longitudinal centerline of the right lane.

Figure 3 shows the geometry of one lane. The joint spacing is 15 feet (4.57 m), with 1.5-inch (38.1 mm)-diameter, 18-inch (45.7 cm)-long steel dowels spaced at 12 inches (30.5 cm) across each joint. Any appropriate finite element mesh may be used to model the geometry. The 8-inch (20.3 cm) thick sections (390201 and 390205 of those listed earlier), had 1.25-inch (31.8 mm) diameter steel dowels

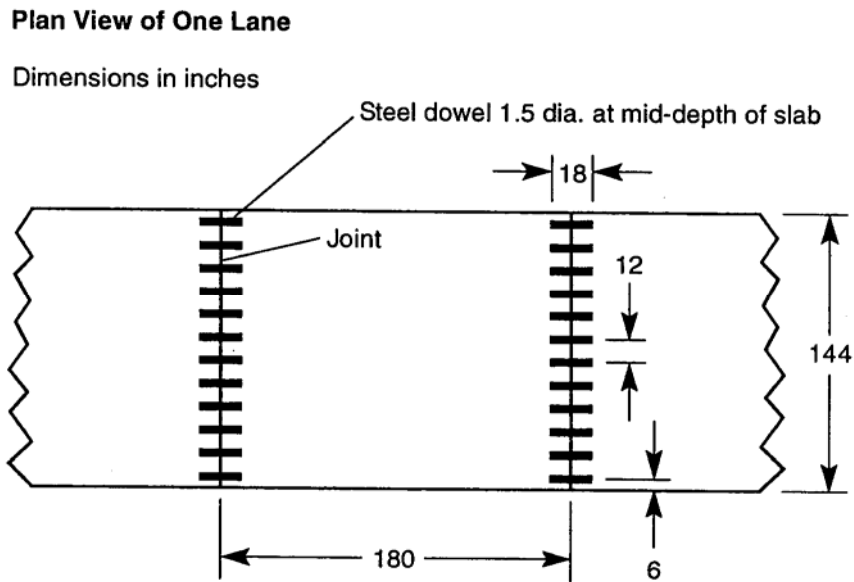


Figure 3. Pavement Slab Geometry (1 inch = 2.54 cm)

3.2.2 SENSOR LOCATIONS AND COORDINATE SYSTEM

Pressure cells, strain gauges, and deep reference LVDTs were installed at various locations along the centerline, right wheel path, and edge of the pavement section. Table 4 is a summary of dynamic sensors whose readings were used in this study. The sensor locations are shown in Figure 4. Experimental results obtained from these sensors were compared to the finite element models output at these locations. Table 5 and Table 6 list the sensor locations, which are the same in each section, in English and metric units, respectively. At the LVDT locations, the vertical deflection of the top pavement layer was measured. The pressure cells measured vertical pressure between the base and the subgrade. The strain gauges were embedded in the concrete in pairs, 1 inch (2.54 cm) from the slab bottom and approximately 1 inch (2.54 cm) from the top; all gauges measured strain in the longitudinal (x) direction.

The coordinates listed in Table 5 and Table 6 are measured as in Figure 4: The x- coordinate is measured from the first joint of the instrumented slab, and the y- coordinate is measured from the right edge of the lane. The z- coordinate is positive upward from the bottom of the slab.

Table 4. Dynamic Response Sensors.

Measured Parameter	Sensor	Abbreviation
Horizontal PCC Strain	Dynatest PAST-II PCC Strain Gauge	D
	TML KM-100B Strain Transducer	K
Vertical Deflection	Schaevitz GPD 121-500DC-LVDT	L
Vertical Pressure	Geokon Model 3500 Pressure Cell	P

Table 5. Sensor Locations and Properties Measured (English units). For sensor abbreviations, see Table 4.

Sensor	x (in)	y (in)	z (in above bottom of slab)	Property Measured
L4	132	30	Top of slab	Vertical deflection
L5	120	72	Top of slab	Vertical deflection
P1	60	30	Base-subgrade interface	Vertical pressure
D3	27	30	7.0 or 10.0*	Longitudinal strain
D4	27	30	1	Longitudinal strain
D5	60	30	7.0 or 10.0*	Longitudinal strain
D6	60	30	1	Longitudinal strain
D7	84	30	7.0 or 10.0*	Longitudinal strain
D8	84	30	1	Longitudinal strain
K1	27	72	7.0 or 10.0*	Longitudinal strain
K2	27	72	1	Longitudinal strain
K3	60	72	7.0 or 10.0*	Longitudinal strain
K4	60	72	1	Longitudinal strain
K5	90	72	7.0 or 10.0*	Longitudinal strain
K6	90	72	1	Longitudinal strain

* 7 in for Sections 390201 and 390205; 10 in for Sections 390208 and 390212

Table 6. Sensor Locations and Properties Measured (metric units). For sensor abbreviations, see Table 4.

Sensor	x (cm)	y (cm)	z (cm above bottom of slab)	Property Measured
L4	335	76	Top of slab	Vertical deflection
L5	305	183	Top of slab	Vertical deflection
P1	152	76	Base-subgrade interface	Vertical pressure
D3	69	76	17.8 or 25.4*	Longitudinal strain
D4	69	76	2.54	Longitudinal strain
D5	152	76	17.8 or 25.4*	Longitudinal strain
D6	152	76	2.54	Longitudinal strain
D7	213	76	17.8 or 25.4*	Longitudinal strain
D8	213	76	2.54	Longitudinal strain
K1	69	183	17.8 or 25.4*	Longitudinal strain
K2	69	183	2.54	Longitudinal strain
K3	152	183	17.8 or 25.4*	Longitudinal strain
K4	152	183	2.54	Longitudinal strain
K5	229	183	17.8 or 25.4*	Longitudinal strain
K6	229	183	2.54	Longitudinal strain

* 17.8 cm for Sections 390201 and 390205; 25.4 cm for Sections 390208 and 390212

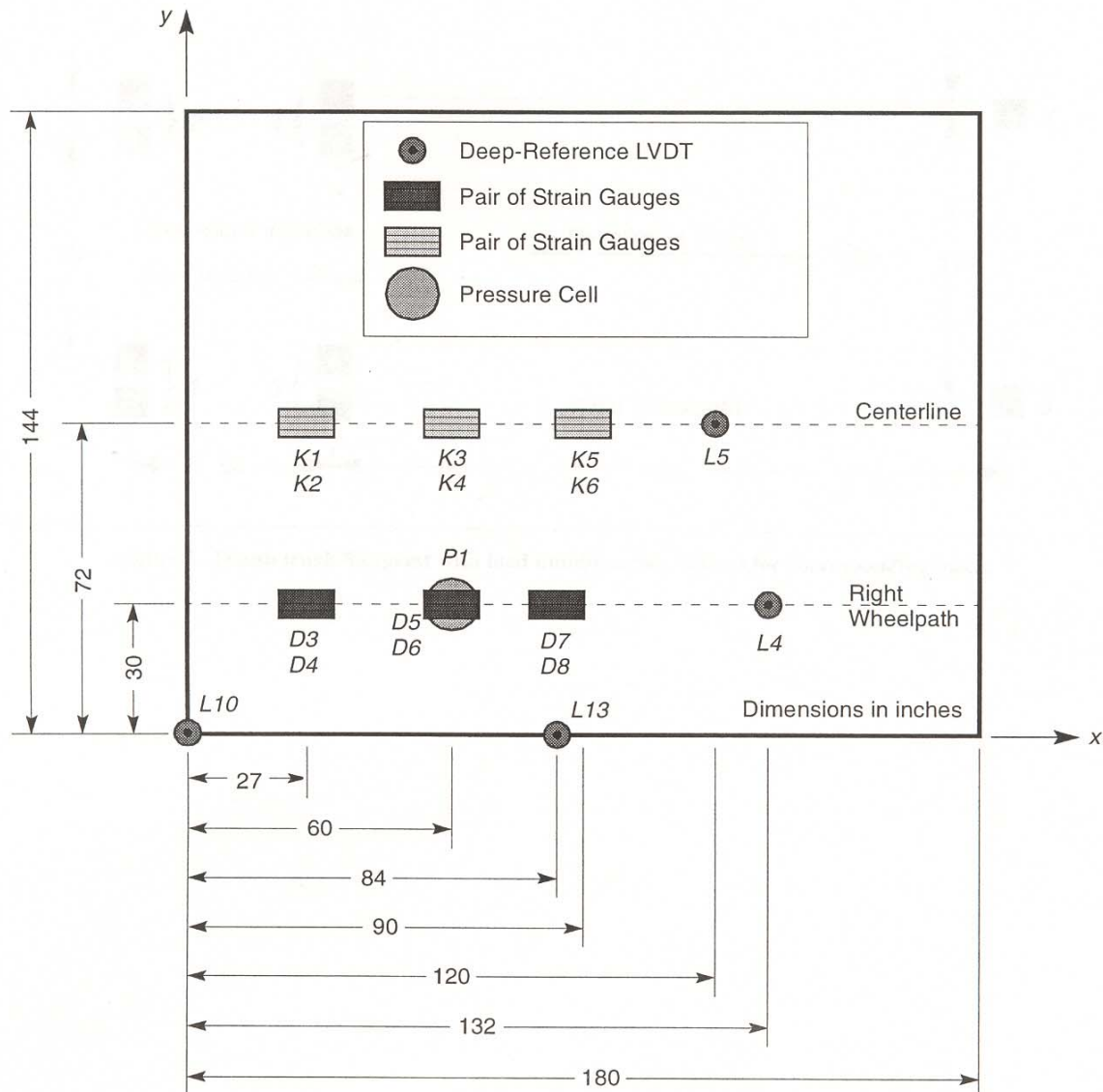


Figure 4. Locations of Sensors within One Pavement Slab (1 in = 2.54 cm)

3.2.3 MATERIAL PROPERTIES

The DEL23 database, compiled by ORITE at Ohio University, was the source consulted for the majority of the material properties. This database was included with the final report by Sargand and Masada (May 2001). The material properties of the four SPS sections are listed in Table 7 in English units and in Table 8 in metric units. These material properties were laboratory measured except for the modulus of subgrade reaction, which was determined after FWD data backcalculation, Boussinesq equation, and consultation with the Federal Aviation Administration's Dr. Edward Guo. The layers of each section are listed in order from top to bottom. All the materials may be assumed linear elastic.

Table 7. Material Properties of Core SPS-2 Sections (English units).

Section Number	layer	Thickness (in)	E (psi)	k (psi/in)	v	Density (lb/in ³)
390201	PCC	8.3	5.20E+06		0.29	8.22E-02
	DGAB	6	1.58E+04		0.35	7.37E-02
	Subgrade		9.04E+03	200	0.4	
390205	PCC	8.1	4.40E+06		0.2	8.22E-02
	LCB	6.3	2.50E+06		0.2	8.39E-02
	Subgrade		9.32E+03	95	0.4	
390208	PCC	11.2	5.40E+06		0.32	8.02E-02
	LCB	6.8	2.50E+06		0.2	8.39E-02
	Subgrade		1.63E+04	149	0.4	
390212	PCC	10.7	5.30E+06		0.21	8.30E-02
	PATB	4	5.90E+05		0.2	8.10E-02
	DGAB	4	1.58E+04		0.35	7.19E-02
	Subgrade		2.04E+04	300	0.4	
Properties of Steel Dowel Bars						
Length = 18 in		Dia. = 1.5 in		E = 2.90E+07 psi		v = 0.3

Table 8. Material Properties of Core SPS-2 Sections (metric units).

Section Number	layer	Thickness (cm)	E (MPa)	k (Pa/m)	v	Density (kg/m ³)
390201	PCC	21.1	3.59E+04		0.29	2.28E+03
	DGAB	15.2	1.09E+02		0.35	2.04E+03
	Subgrade		6.23E+01	5.43E+07	0.4	
390205	PCC	20.6	3.03E+04		0.2	2.28E+03
	LCB	16.0	1.72E+04		0.2	2.32E+03
	Subgrade		6.43E+01	2.58E+07	0.4	
390208	PCC	28.4	3.72E+04		0.32	2.22E+03
	LCB	17.3	1.72E+04		0.2	2.32E+03
	Subgrade		1.12E+02	4.04E+07	0.4	
390212	PCC	27.2	3.65E+04		0.21	2.30E+03
	PATB	10.2	4.07E+03		0.2	2.24E+03
	DGAB	10.2	1.09E+02		0.35	1.99E+03
	Subgrade		1.41E+02	8.14E+07	0.4	
Properties of Steel Dowel Bars						
Length = 45 cm		Dia. = 3.8 cm		E = 2.00E+05 MPa		v = 0.3

3.2.4 DYNAMIC LOADS

The load was applied using a three-axle dump truck. The footprints of the moving truck are shown in Figure 5. The labels 1 through 4 in the figure indicate dual tires which were weighed together, while labels 5 and 6 indicate individual tires. The dump truck loads are given in Table 9. The tire contact area may be assumed any convenient shape and size, but the tire pressure was approximately 100 psi (689 kPa).

The truck's location is defined as the x coordinate at the center of the front tire. Thus, when the truck is at $x = 0$, the front tire is centered on the first joint of the instrumented slab. When the truck is at $x = 84$ inches (2.13 m), the front tire is centered over strain gauges D7 and D8. The truck must be moved along the x direction from $x = -120$ inches (-3.05 m) to $x = 534$ inches (13.56 m). The specific locations listed in Table 10 are required to obtain the response at the location of sensors. The program response was obtained from enough other locations to produce a smooth response curve for each sensor. The finite element problem may be solved as either a true dynamic problem or as a quasi-static problem depending on the capabilities of the program.

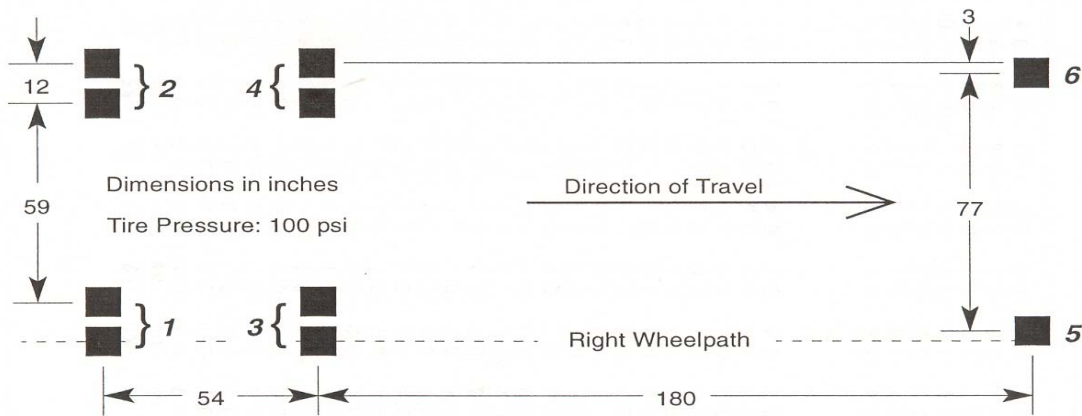


Figure 5. Dump Truck Footprints (1 inch = 2.54 cm, 100 psi = 689 kPa).

Table 9. Dump Truck Loads.

Testing time	Air Temp. (°F (°C))	Speed (mph (km/h))	Load (lb (N)) – Refer to Figure 5 for definition of load numbers					
			1	2	3	4	5	6
13:30 7/30/97	79 (26.1)	50 (80)	10,690 (47551)	10,690 (47551)	10,570 (47018)	10,570 (47018)	8,500 (37810)	8,500 (37810)

Table 10. Required Locations of Truck.

x coordinates (in (cm))			
0 (0)	132 (335)	264 (671)	324 (823)
27 (69)	180 (457)	270 (686)	339 (861)
60 (152)	207 (526)	294 (747)	354 (899)
84 (213)	234 (594)	300 (762)	366 (930)
90 (229)	240 (610)	312 (792)	
120 (305)	261 (663)	318 (808)	

3.3 BRIEF DESCRIPTION OF FINITE ELEMENT PROGRAMS

3.3.1 ISLAB2000

ISLAB2000 is a two-dimensional finite element program for the analysis of rigid pavements. The program was developed by the ERES Division of Applied Research Associates (ARA) in cooperation with Michigan and Minnesota Departments of Transportation, Michigan Technical University, University of Michigan, Michigan State University, and University of Minnesota. ISLAB2000 is a proprietary revision of ILSL2, the latest public domain version of the finite element program ILLI-SLAB, which is based on the medium-thick plate theory (Khazanovich et al., 2003). It employs four-node, 12-degree-of-freedom plate bending elements. The joints and aggregate interlock are modeled using shear springs, while the dowel bars are modeled by beam elements. The program also provides a variety of subgrade models (Spring, Winkler, Kerr, and Vlasov), analyzes the effect of linear and nonlinear temperature distribution throughout the pavement thickness, and includes an improved void analysis model. ISLAB2000 is able to analyze the effect of independent actions of two pavement layers using the Totsky model, where special 8-node, 24-degree-of-freedom elements are used. With this model, the multi-layered pavement system resting on a subgrade is modeled as a series of springs and plates. The plate elements model the bending, while the springs accommodate the direct compression that occurs in the system. ISLAB2000 has been recommended for the NCHRP “Guide for Mechanistic-Empirical Design of New and Rehabilitated Pavement Structures” based on computational practicality and prediction accuracy.

3.3.2 JSLAB

JSLAB is a two dimensional finite element program developed by Tayabji and Colley in 1986. The program can analyze a one- or two- layer pavement system resting on a Winkler foundation. The two layers may be unbonded or fully bonded. The slabs are modeled as rectangular plate elements, the dowels as thick beam elements, and the aggregate interlock as springs. Joints can be modeled as doweled, aggregate interlock, or keyed. The program can analyze curling behavior due to linear temperature variation in the slab, and can be used to determine curling restraint stresses. This program can analyze only a single layer pavement, with or without temperature gradient, when multiple slabs are modeled.

3.3.3 EVERFE

EVERFE is a finite element program for the linear and nonlinear three-dimensional analysis of jointed plain concrete pavements. The Universities of Maine and Washington jointly developed EVERFE with funding from the Washington and California State DOTs. EVERFE uses a Microsoft Windows based graphical user interface (GUI). The pavement layer is modeled with 20-node hexahedral elements, while base layer is modeled with 8-node brick elements. The dowels are modeled with embedded beam elements. The subgrade is modeled as a Winkler foundation. EVERFE provides a linear and a non-linear model for aggregate interlock that provides shear transfer across the vertical joint between two slabs.

3.3.4 OU3D

This finite element program was developed at Ohio University for the purpose of matching the data from the Ohio Test Road with mathematical models. OU3D uses 20-node, quadratic, isoparametric hexahedral elements for modeling concrete and soil. The program uses special thin interface elements to model the behavior of the top layer of soil under the slab. Concrete joints are also represented by interface elements. The interface element behaves as an ordinary element in compression, but in tension, it loses stiffness to allow joints to open or slabs to separate from soil. It uses three-node isoparametric beam elements which include both flexure and shear deformation in modeling of dowels and ties. Text input files are required for the mesh generator and a 64 bit system is required to run simulations.

3.4 PROGRAM PARAMETERS AND OPERATION

3.4.1 INPUT

The input data were similar for all four finite element programs. The input data were sufficient to model three continuous doweled slabs 15 feet (4.57 m) in length and 12 feet (3.66 m) in width. Material properties are shown in Table 7 in English units and Table 8 in metric units, while loads are shown in Table 9 in both English and metric units.

Additional input data were required by some of the programs: ISLAB2000 requires a dowel concrete interaction (DCI) factor, a property which was not available and was left at the default value (5.00E+05). Both EVERFE and ISLAB2000 require the foundation stiffness, or modulus of subgrade reaction, while OU3D requires the Young's modulus and Poisson's ratio of the soil foundation.

The pavement layer interface can be modeled as fully bounded or unbounded. In ISLAB2000, the additional interface option is the Totsky model. This approach models the multi-layered pavement system resting on subgrade as a series of springs and plates. The plate elements model the bending, whereas the springs accommodate the direct compression occurring in such a system.

OU3D uses a thin interface element for modeling the separation of pavement from base. The stiffness of the element is equal to the stiffness of the base material when it is in compression. In tension, the stiffness becomes relatively small to permit separation of layers. Furthermore, the interface formulation limits shearing stresses according to the Mohr-Coulomb criterion. The

friction angle between the pavement and the base is input as a material property. Interface elements are also employed in the pavement joints, where they permit the joints to open and close, thereby regulating the transfer of shear forces across the joints.

3.4.2 MESH GENERATION

Modeling of the finite element programs varies between fixing the finite element nominal size and selecting the number of elements in all the slab directions. As the element size decreases, the mesh becomes finer. This may increase the accuracy of the results, but also increases the running time. EVERFE and OU3D allow the selection of number of the elements in the longitudinal and transverse directions, and along the depth of the slab. ISLAB2000 allows the selection of the element size in both the longitudinal and transverse directions of the slab. The element size in the vertical direction is the slab thickness.

3.4.3 OUTPUT

The data output form varies among the finite element programs. ISLAB2000 saves the data in a tabular format, which can be easily displayed using spreadsheet software. The output data include displacement, rotation, and stresses at each node. In addition, the principal stresses and angles are displayed. Graphical outputs are also available, which display the analysis results and include stresses in the two plane directions, principal stresses and deflection. In EVERFE, the output format is user driven, where the desired location of the pavement response has to be specified. The output data include stresses and displacement in the three main directions. OU3D provides strains at each nodal location for all directions, along with the deflections and pressures.

3.5 DATA ANALYSIS AND RESULTS

The four SPS-2 sections were analyzed under one loading condition only. The testing time was 13:30 on July 30, 1997. The sensor readings were compared to the finite element programs output at the same location as the sensor. Comparison graphs present the distance of the front axle from the first joint in the x-direction, and the strains, deflections, and pressures obtained from the sensors, as well as the programs' outputs, in the y-direction.

The strain, deflection, and vertical pressure comparison plots are presented in Figure 6 through Figure 20 for section 390201, Figure 21 through Figure 35 for section 390205, Figure 36 through Figure 50 for section 390208, and Figure 51 through Figure 65 for section 390212. Where not presented, the experimental data were not collected. By analyzing the plots, the following details were noticed:

- 1) The computer simulations approximated the general experimental trend for all strains measured by Dynatest strain gauges (placed under the right wheel path) and KM-100B strain gauges (placed at the pavement centerline).
- 2) The pavement stress reversals between the first and second truck axles could be as high as the peak stresses under the truck axles. Stress reversal occurred when the first two axles were positioned on the slab joints. Thus, reversal stresses need to be considered in the pavement design, because they cause tension stress at the top of the slab.
- 3) The computer programs prediction followed the general experimental trend of pavement deflection. For ISLAB2000, JSLAB, and EVERFE, deflection values were highly dependent on the value of k. A small rocking of PCC slab was noticed in both ISLAB2000 and JSLAB.

Rocking in ISLAB2000 and JSLAB was more noticeable when a higher modulus of subgrade reaction was used.

- 4) The program EVERFE has no ability to predict the vertical pressure, but the other programs' predictions followed the general experimental trend.
- 5) Although ISLAB2000 and JSLAB are both 2-D FEM programs, the difference in trends can be justified by the differences in the base modeling and the dowel bar spacing.
- 6) Among the FE programs, OU3D produced the trend closest to the experimental data.
- 7) Based on the experimental results, it was found that the increase in the PCC thickness reduced both peak stresses and deflections. Also, the use of LCB instead of DGAB (i.e., stiffer base) reduced the reversal stresses, and the use of a thicker base slightly reduced the stresses.
- 8) The different programs were also compared for usability in terms of modeling, input and output data, and speed. As regards to input parameters, ISLAB2000, JSLAB, and EVERFE require the value of subgrade modulus of reaction, k . Precaution should be taken in choosing a value for k , or unrealistic values of deflection can result. The OU3D was designed to be fast and efficient, and it can solve multiple load cases. For static load cases, ISLAB2000 is the most computationally efficient.

3.6 SUMMARY

The current study was conducted to validate four finite element programs for rigid pavement using in-situ data. In the evaluation of the programs' output, the general output trend should be studied rather than the absolute value of predicted pavement properties, as these depend on the input parameters. Material properties for DEL23 data base were used for the input of finite element programs. These material properties were measured in the laboratory, except for the modulus of subgrade reaction (k). Generally, the FEM predictions follow the experimental trend of strains, deflections, and vertical pressure at the top of subgrade. However, it should be emphasized that loss of support caused by curling and pumping was not accounted for in this study; the pavement was treated as a flat slab.

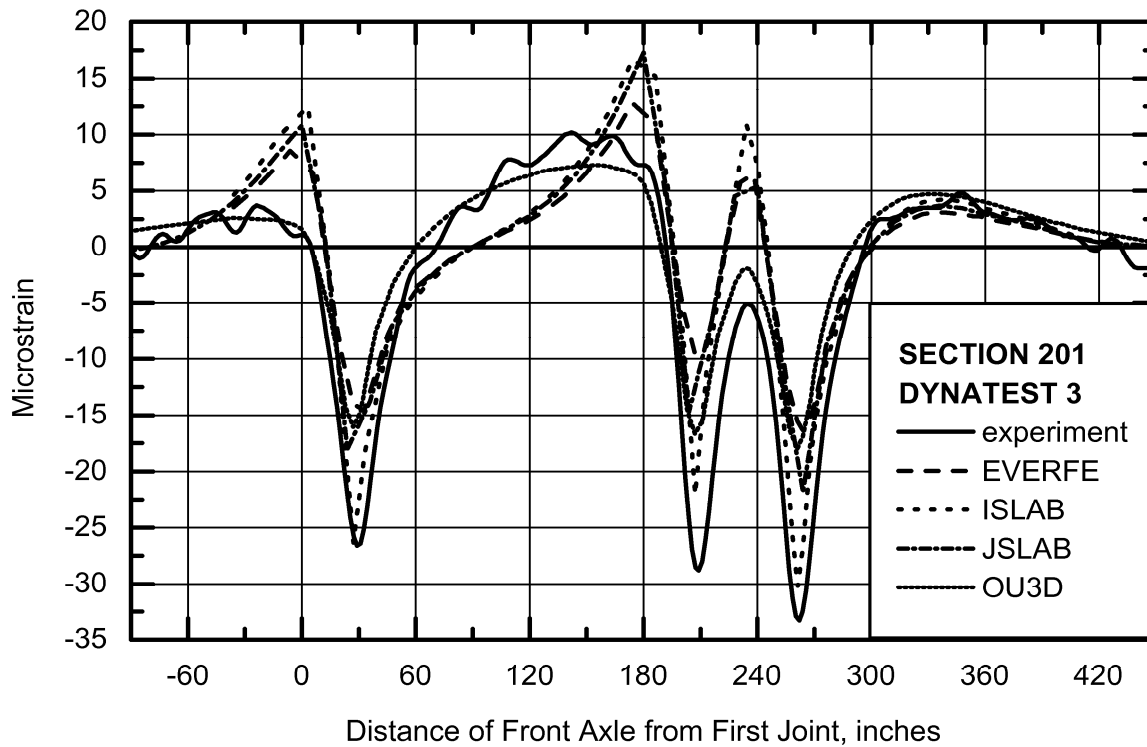


Figure 6. Comparison of Strains at D3 for Section 390201 (1 inch = 2.54 cm).

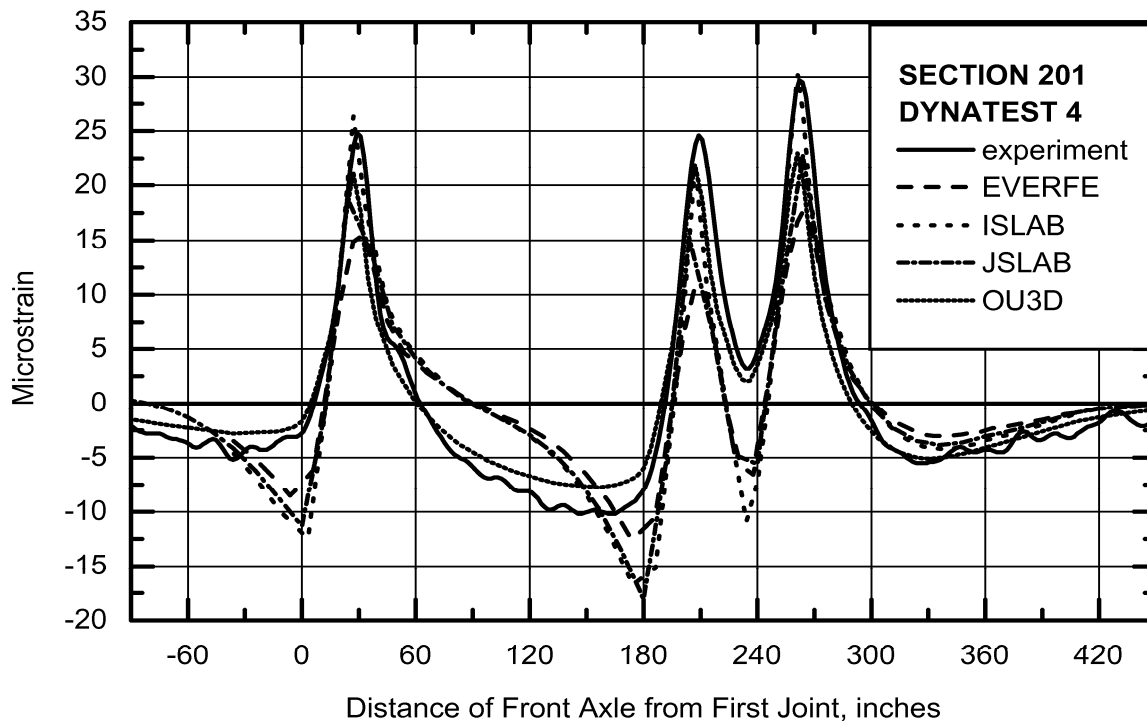


Figure 7. Comparison of Strains at D4 for Section 390201 (1 inch = 2.54 cm).

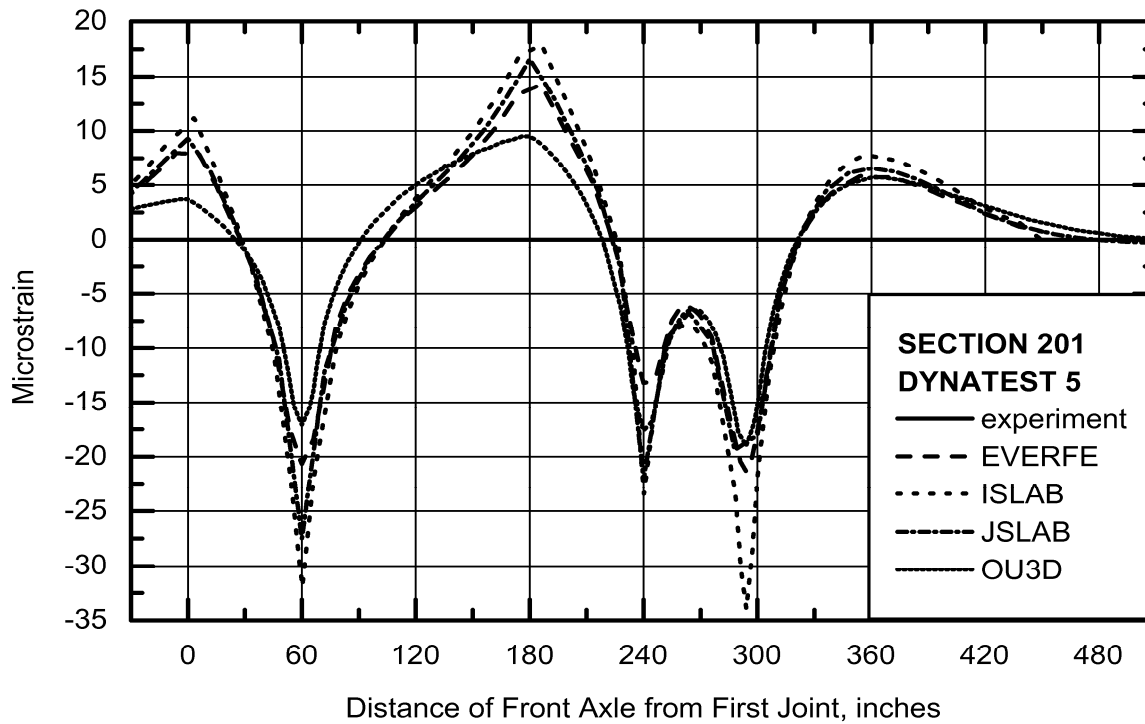


Figure 8. Comparison of Strains at D5 for Section 390201 (1 inch = 2.54 cm).

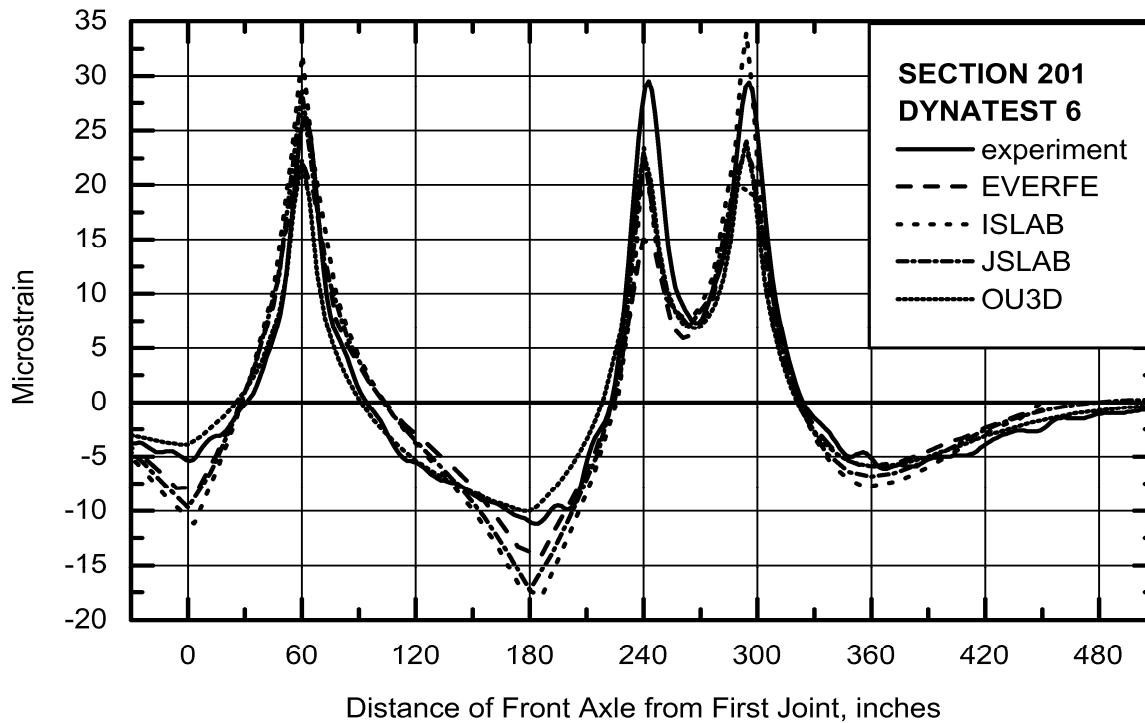


Figure 9. Comparison of Strains at D6 for Section 390201 (1 inch = 2.54 cm).

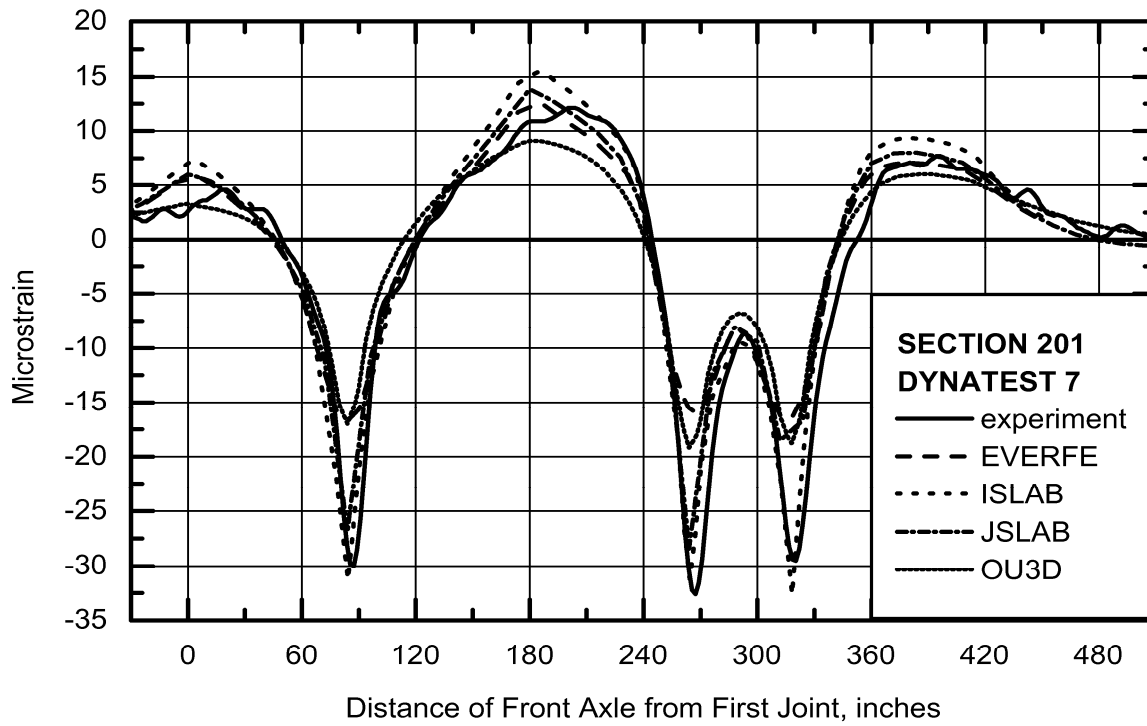


Figure 10. Comparison of Strains at D7 for Section 390201 (1 inch = 2.54 cm).

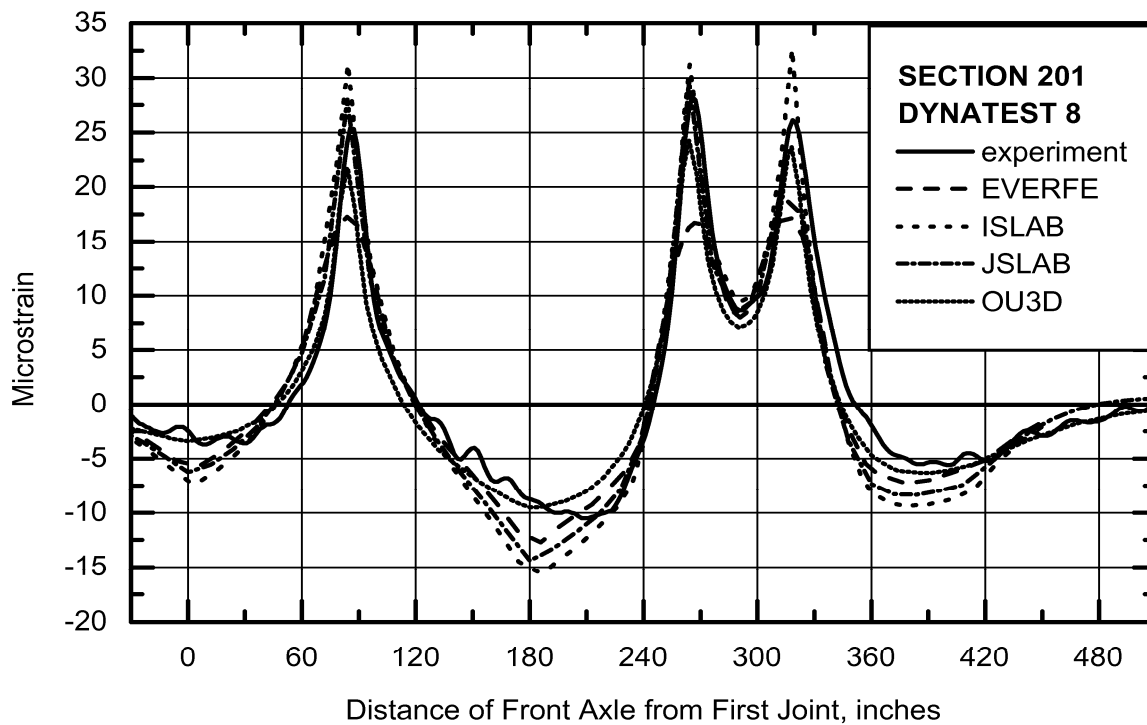


Figure 11. Comparison of Strains at D8 for Section 390201 (1 inch = 2.54 cm).

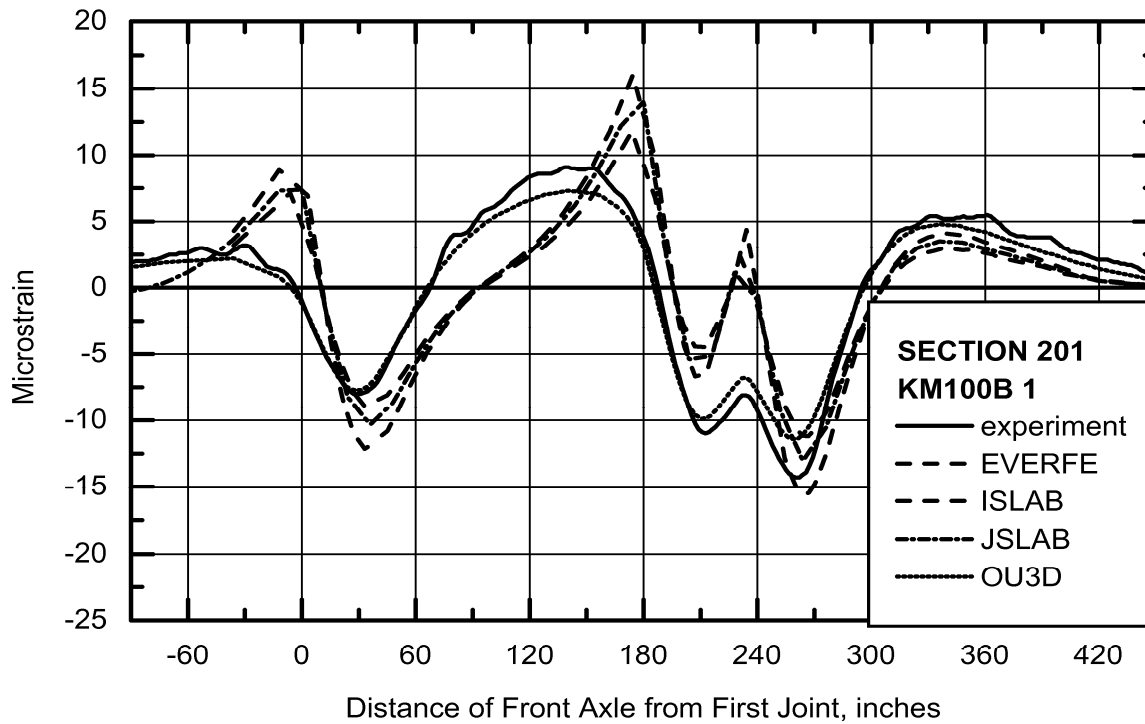


Figure 12. Comparison of Strains at K1 for Section 390201 (1 inch = 2.54 cm).

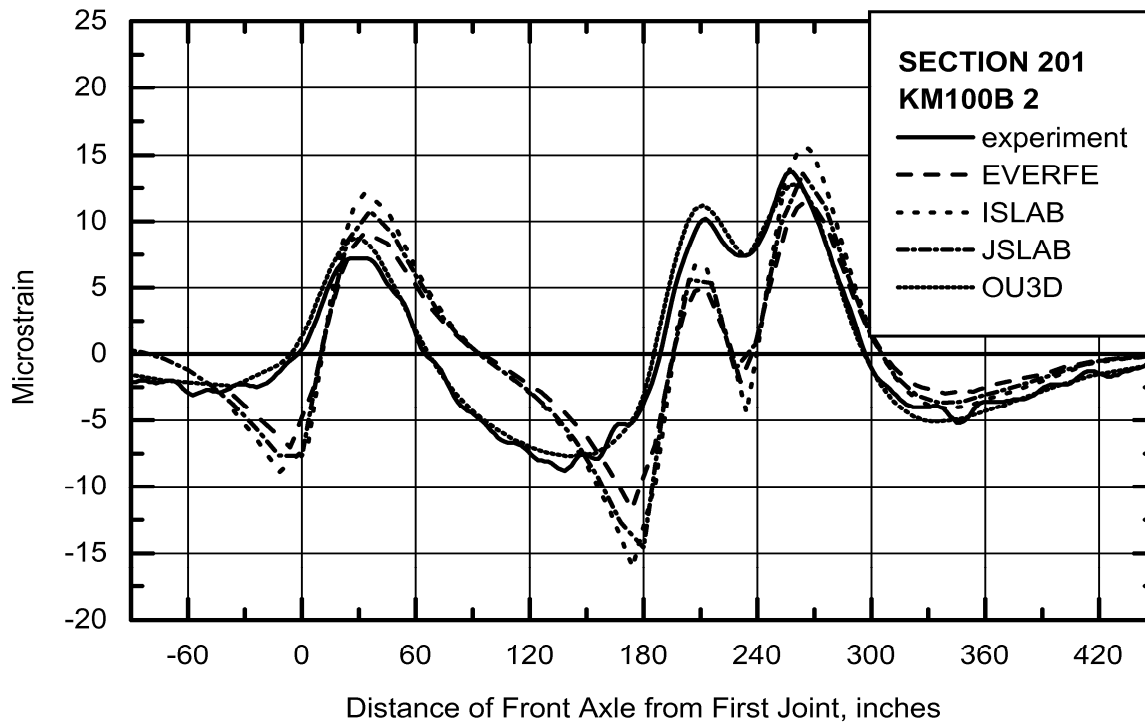


Figure 13. Comparison of Strains at K2 for Section 390201 (1 inch = 2.54 cm).

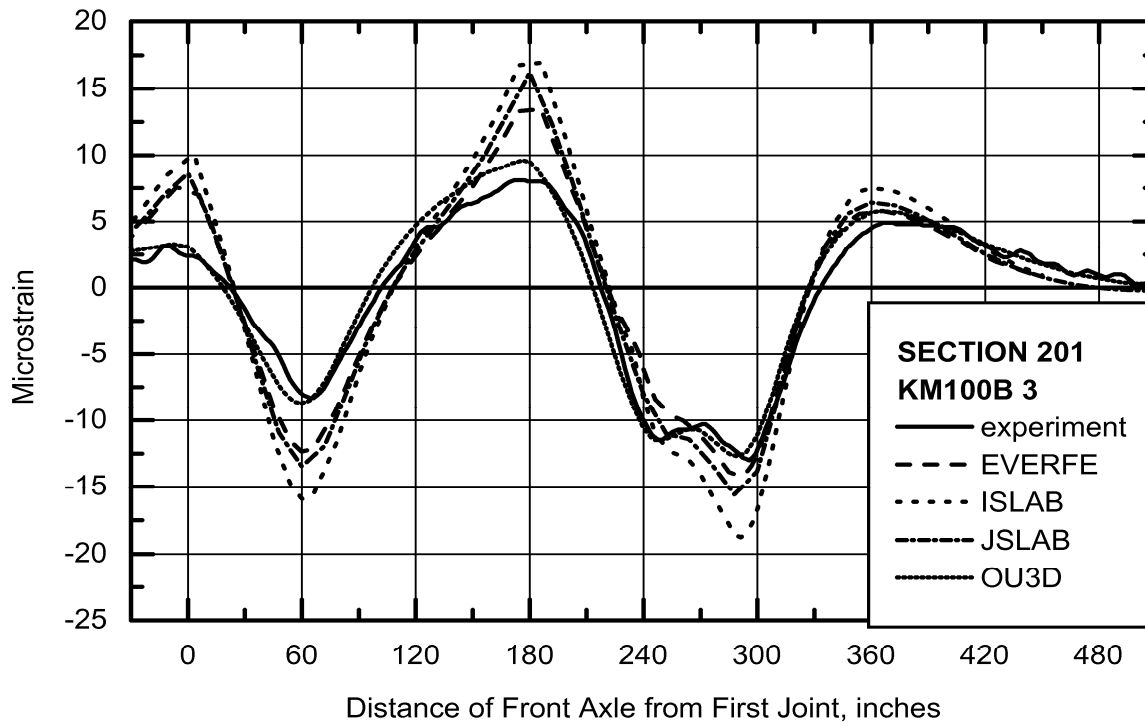


Figure 14. Comparison of Strains at K3 for Section 390201 (1 inch = 2.54 cm).

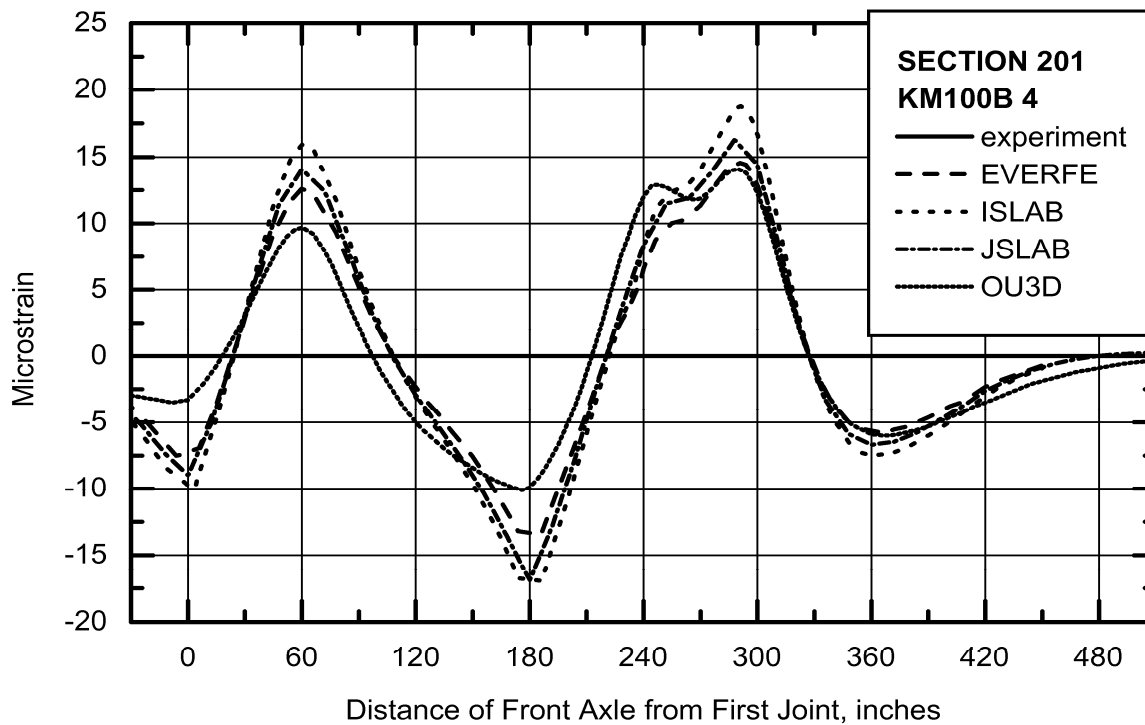


Figure 15. Comparison of Strains at K4 for Section 390201 (1 inch = 2.54 cm).

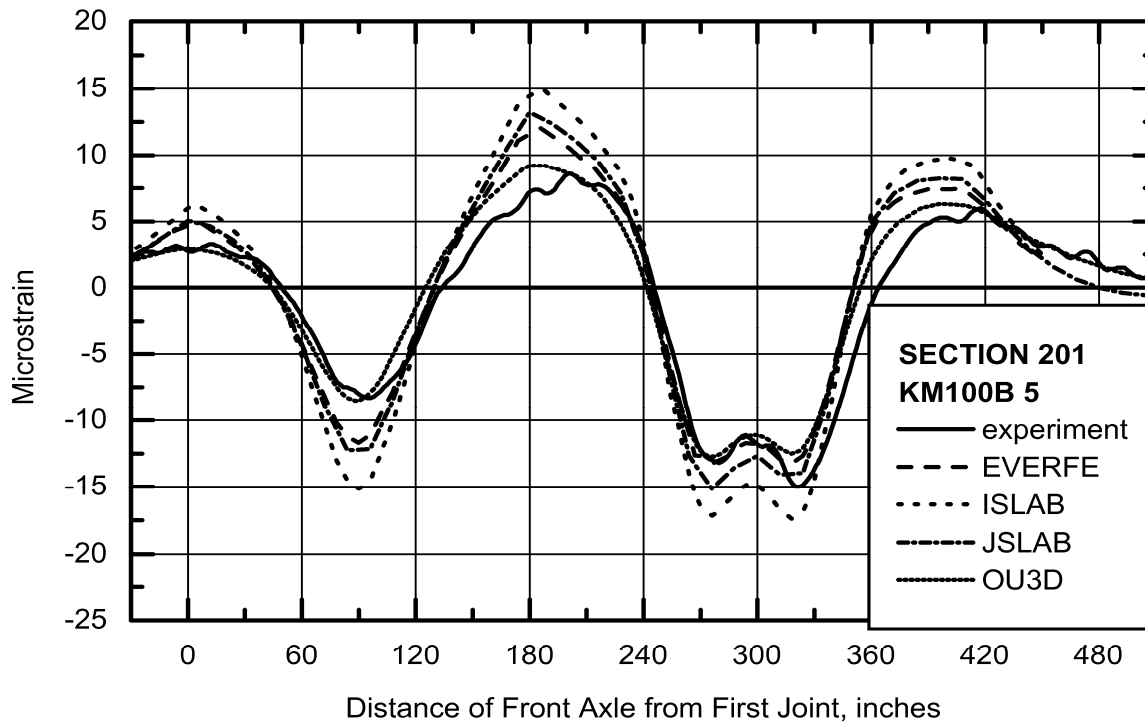


Figure 16. Comparison of Strains at K5 for Section 390201 (1 inch = 2.54 cm).

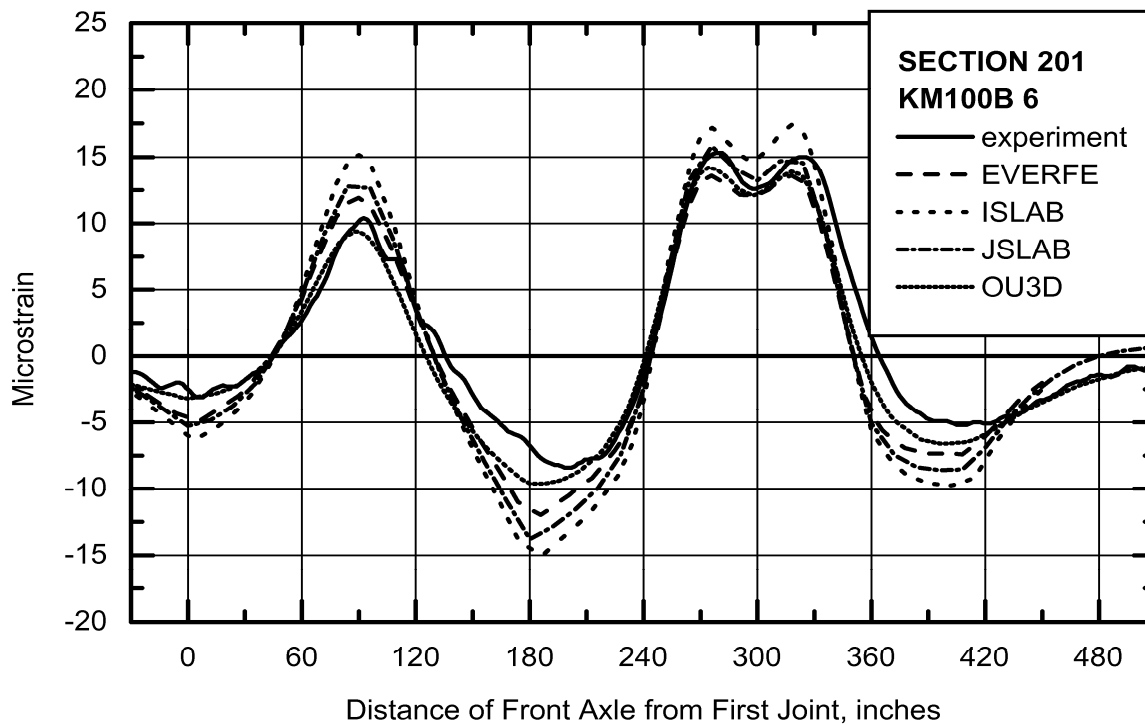


Figure 17. Comparison of Strains at K6 for Section 390201 (1 inch = 2.54 cm).

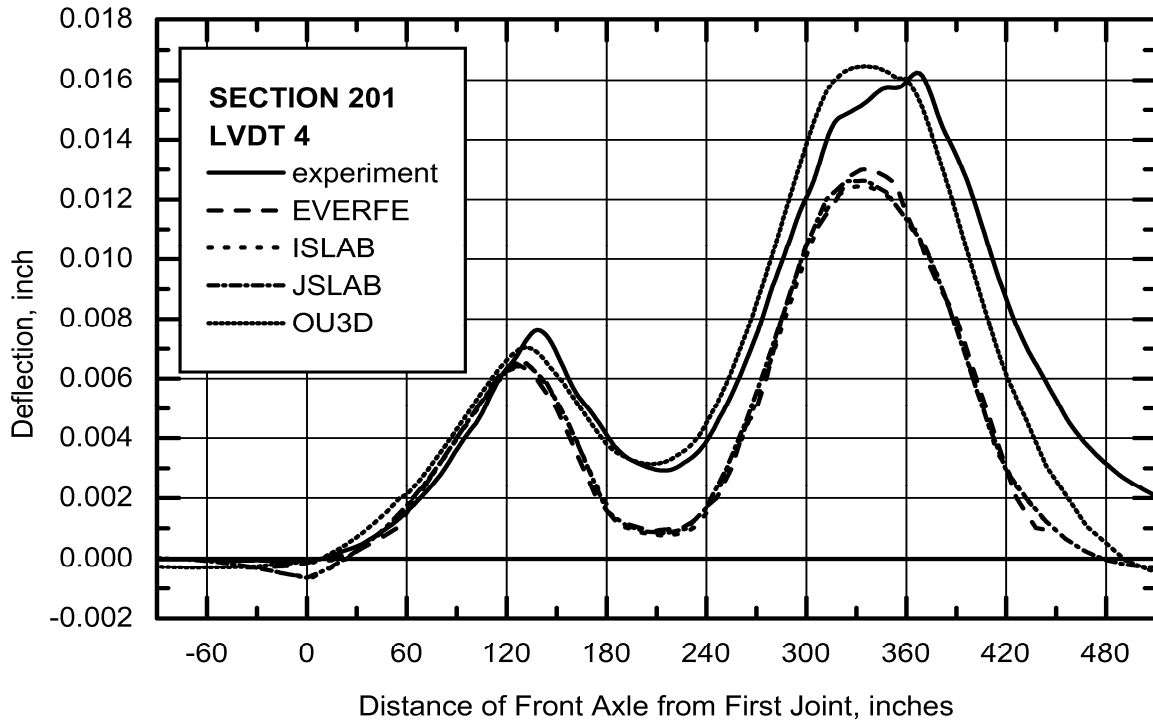


Figure 18. Comparison of Deflections at L4 for Section 390201 (1 inch = 2.54 cm).

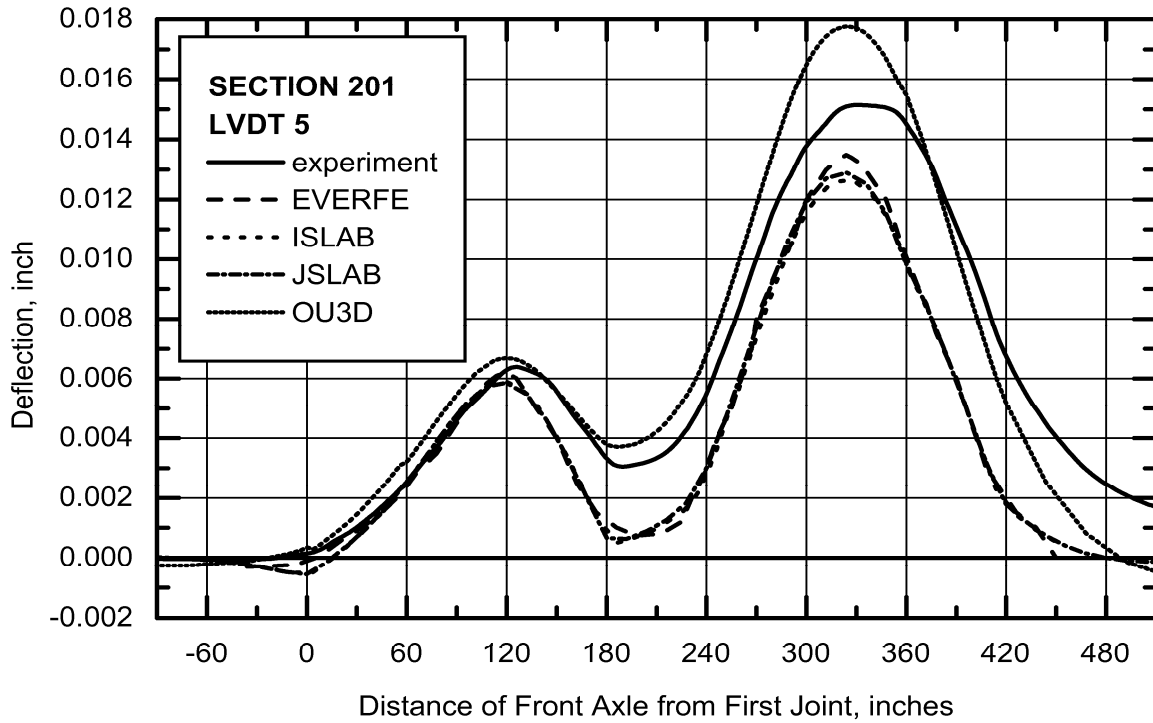


Figure 19. Comparison of Deflections at L5 for Section 390201 (1 inch = 2.54 cm).

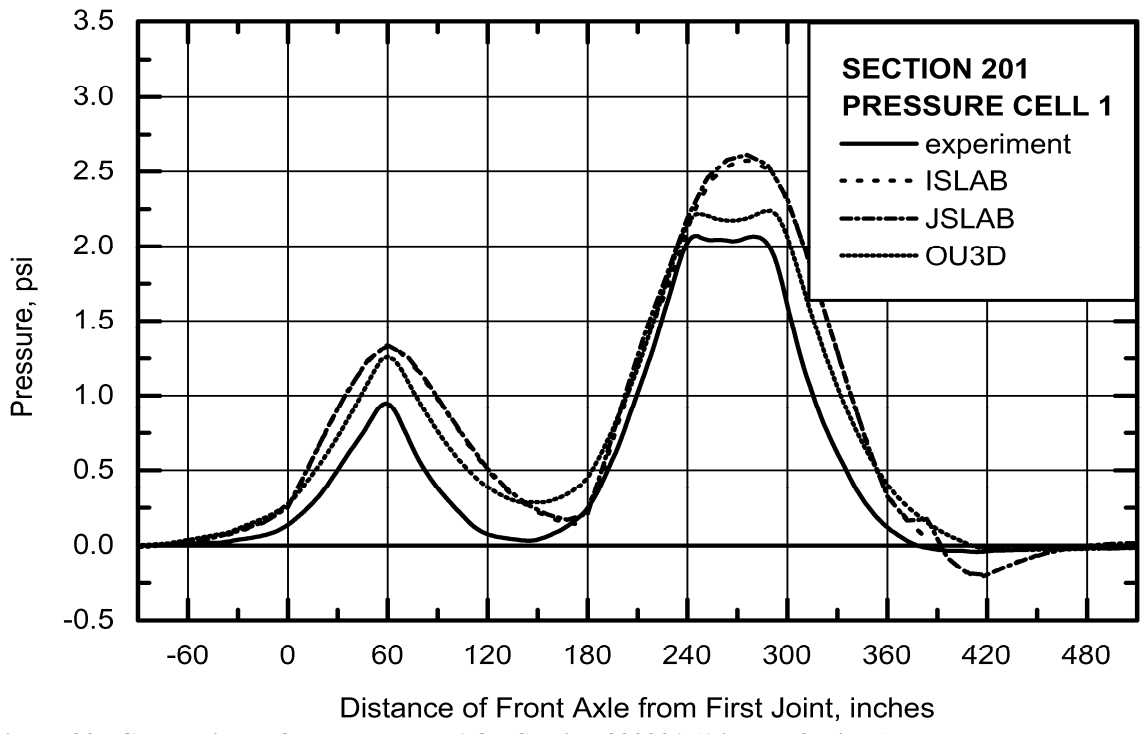


Figure 20. Comparison of Pressures at P1 for Section 390201 (1 inch = 2.54 cm).

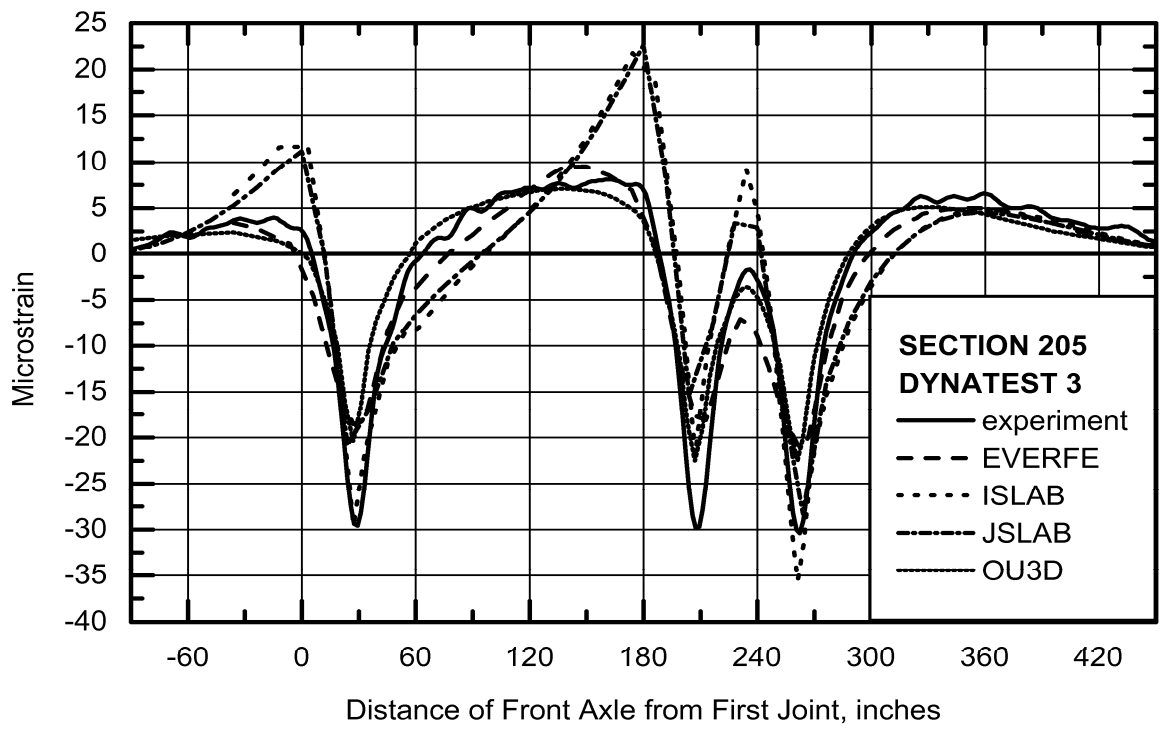


Figure 21. Comparison of Strains at D3 for Section 390205 (1 inch = 2.54 cm).

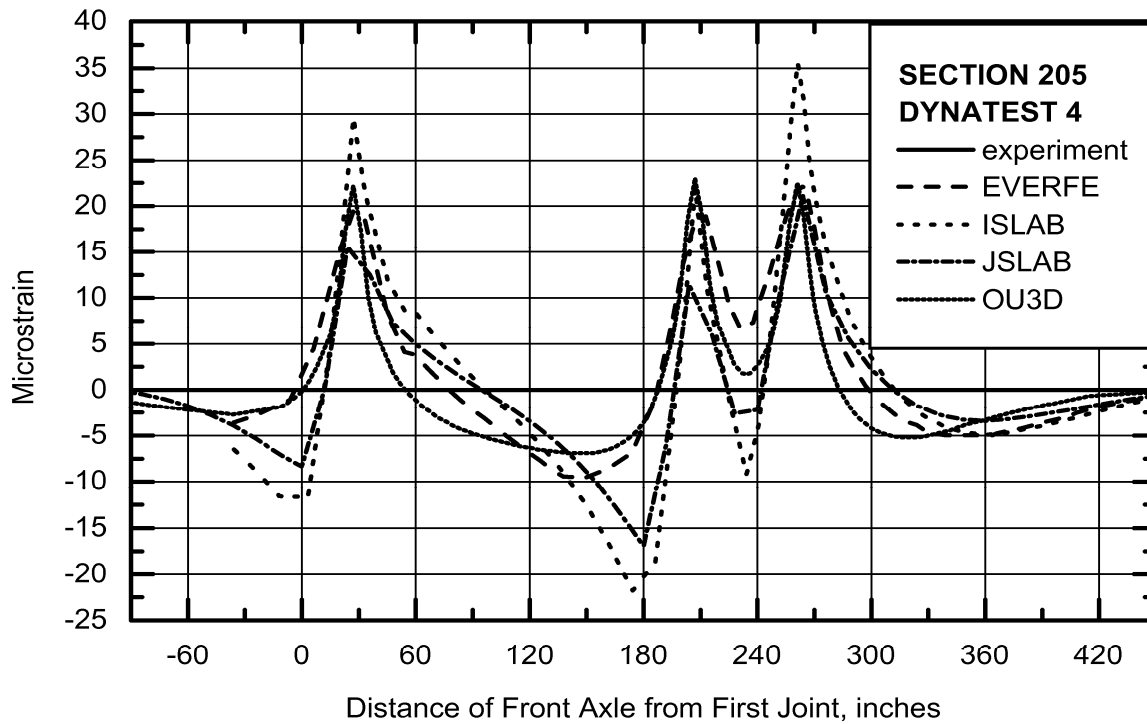


Figure 22. Comparison of Strains at D4 for Section 390205 (1 inch = 2.54 cm).

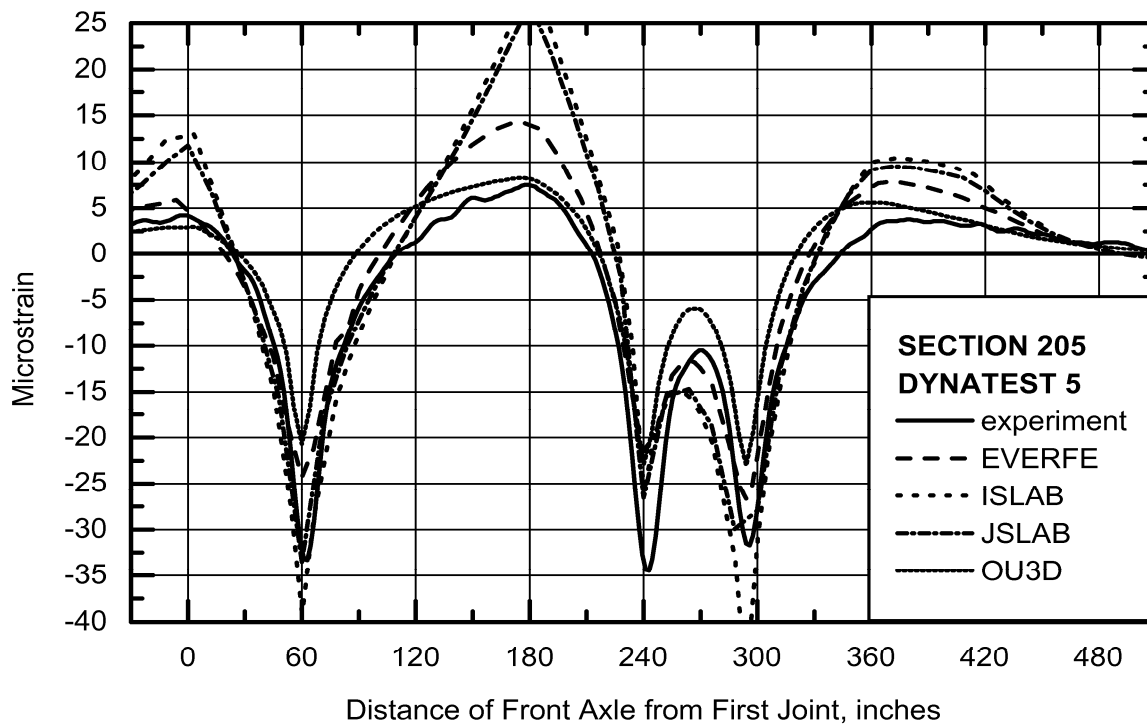


Figure 23. Comparison of Strains at D5 for Section 390205 (1 inch = 2.54 cm).

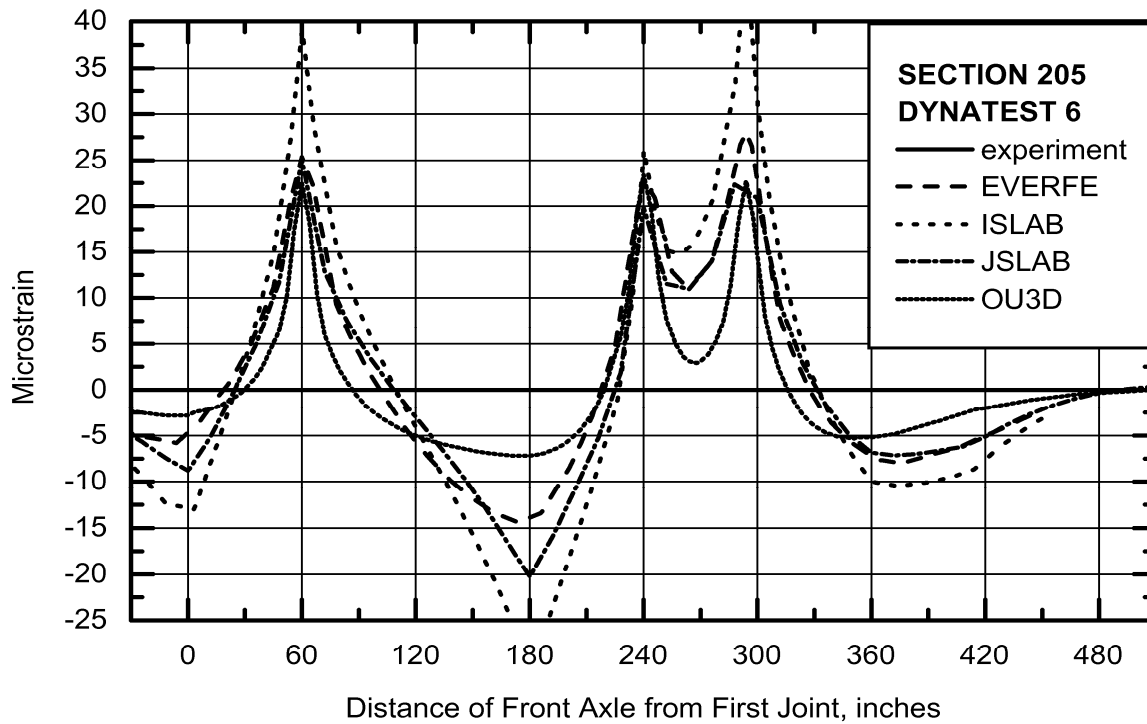


Figure 24. Comparison of Strains at D6 for Section 390205 (1 inch = 2.54 cm).

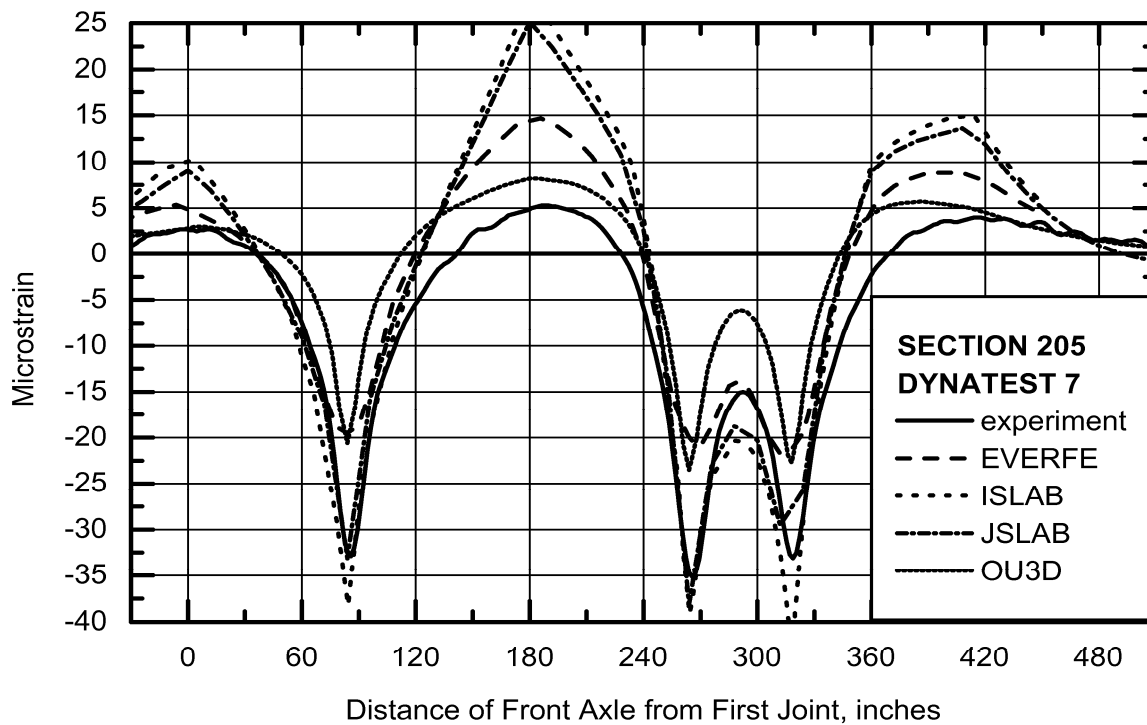


Figure 25. Comparison of Strains at D7 for Section 390205 (1 inch = 2.54 cm).

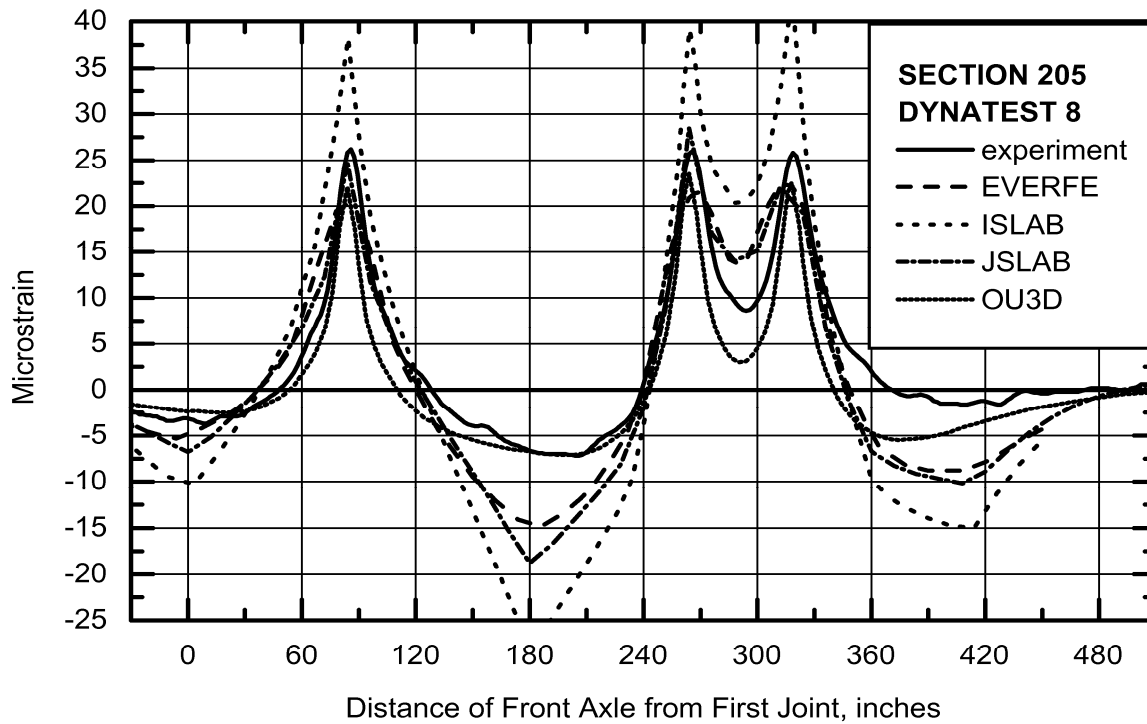


Figure 26. Comparison of Strains at D8 for Section 390205 (1 inch = 2.54 cm).

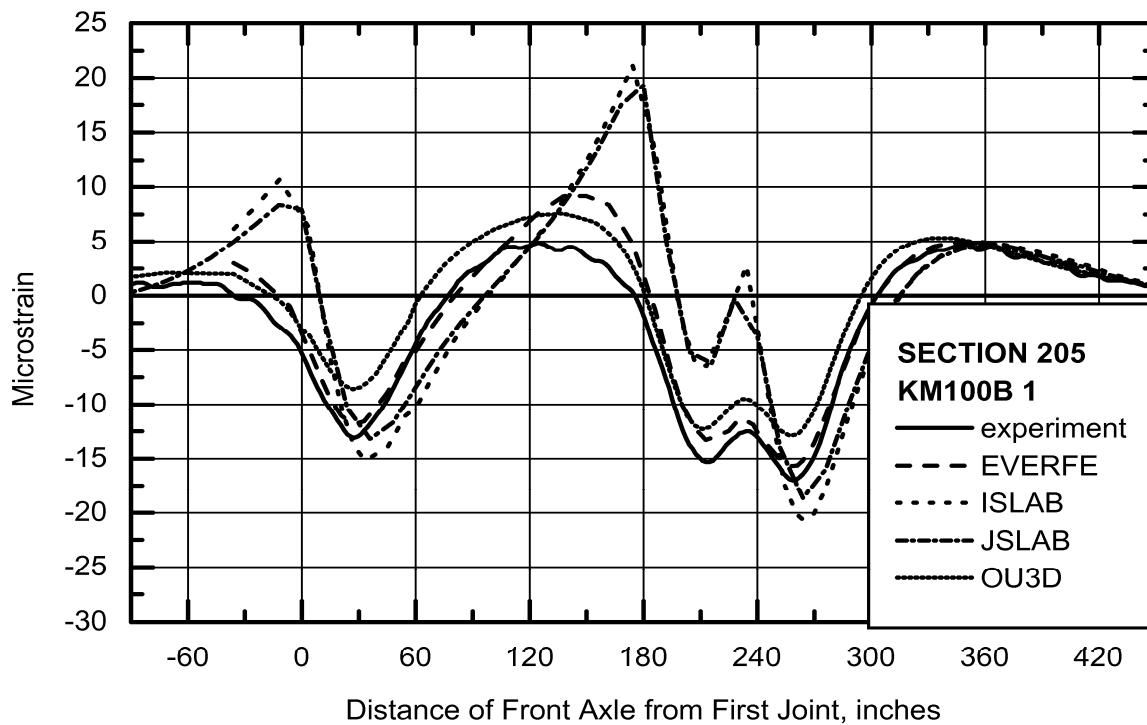


Figure 27. Comparison of Strains at K1 for Section 390205 (1 inch = 2.54 cm).

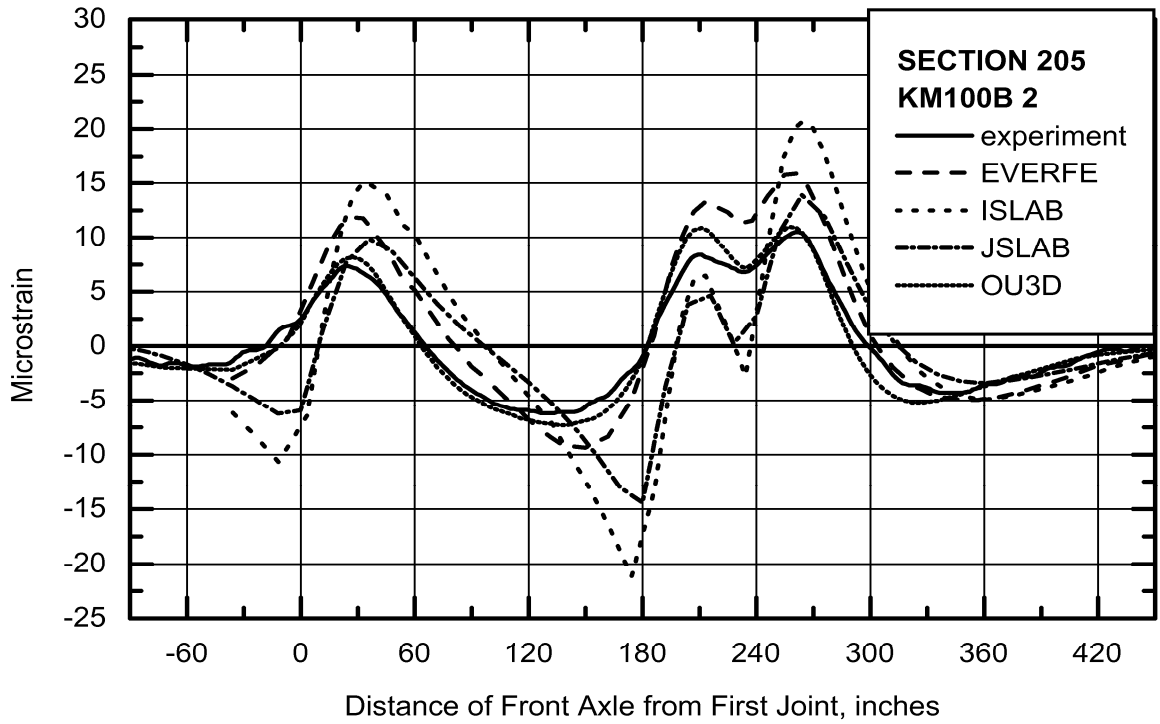


Figure 28. Comparison of Strains at K2 for Section 390205 (1 inch = 2.54 cm).

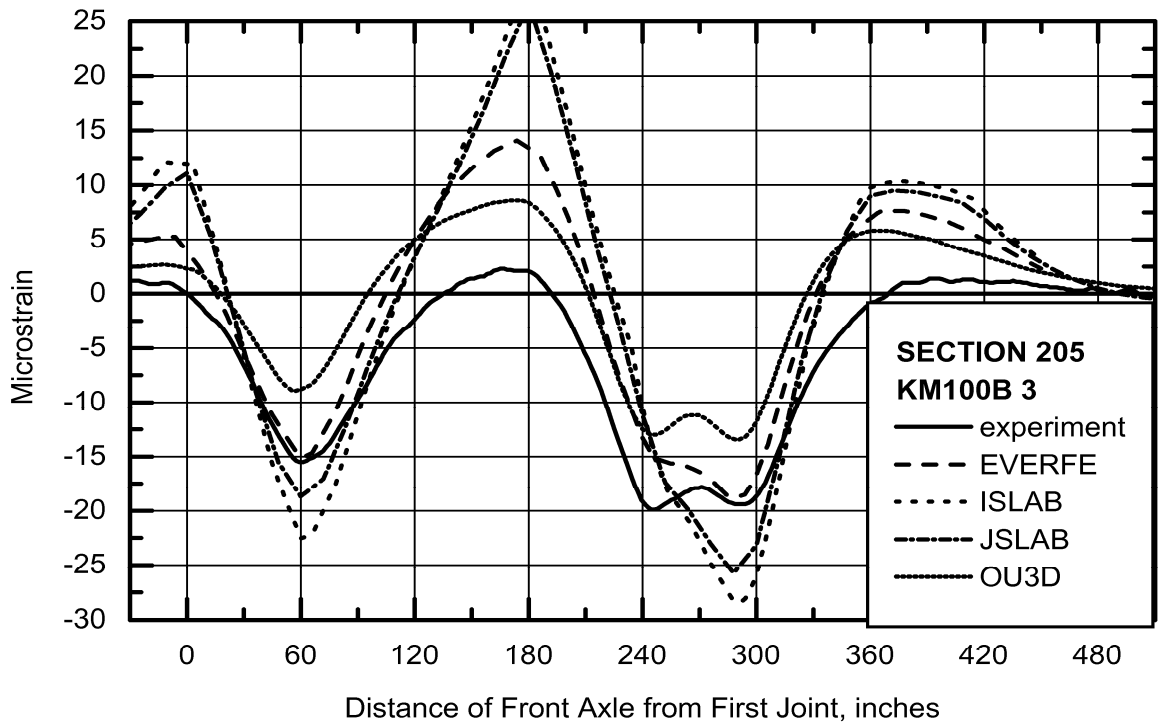


Figure 29. Comparison of Strains at K3 for Section 390205 (1 inch = 2.54 cm).

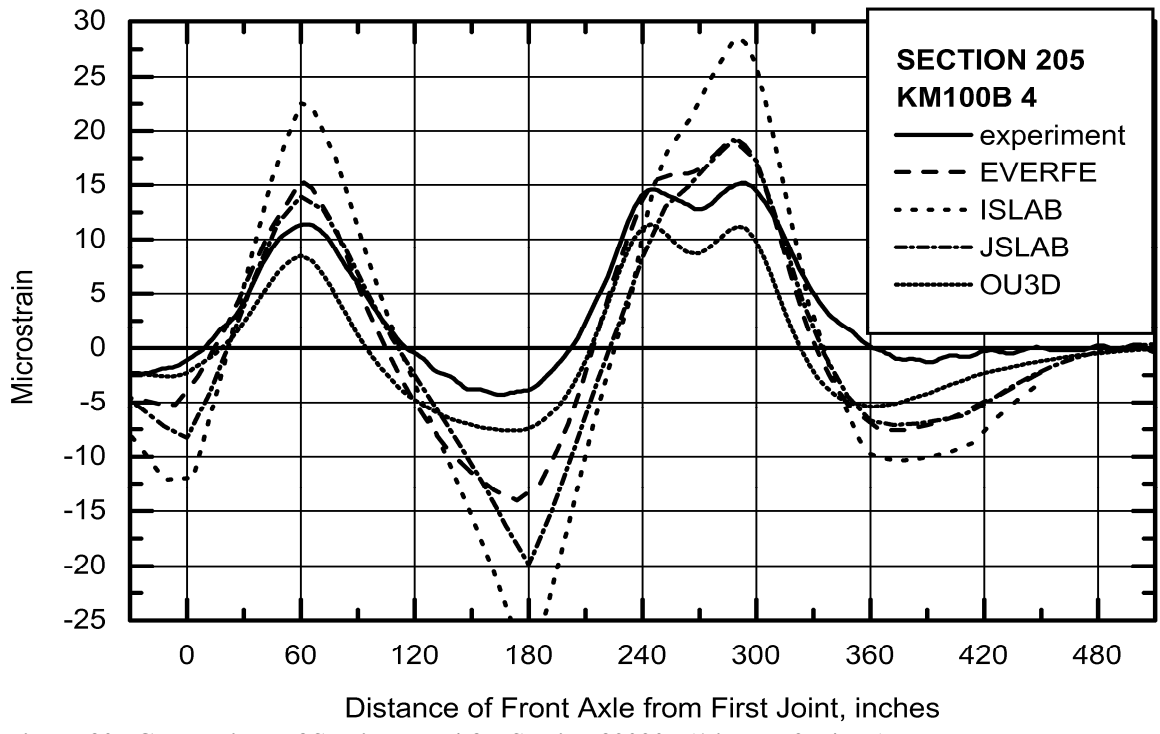


Figure 30. Comparison of Strains at K4 for Section 390205 (1 inch = 2.54 cm).

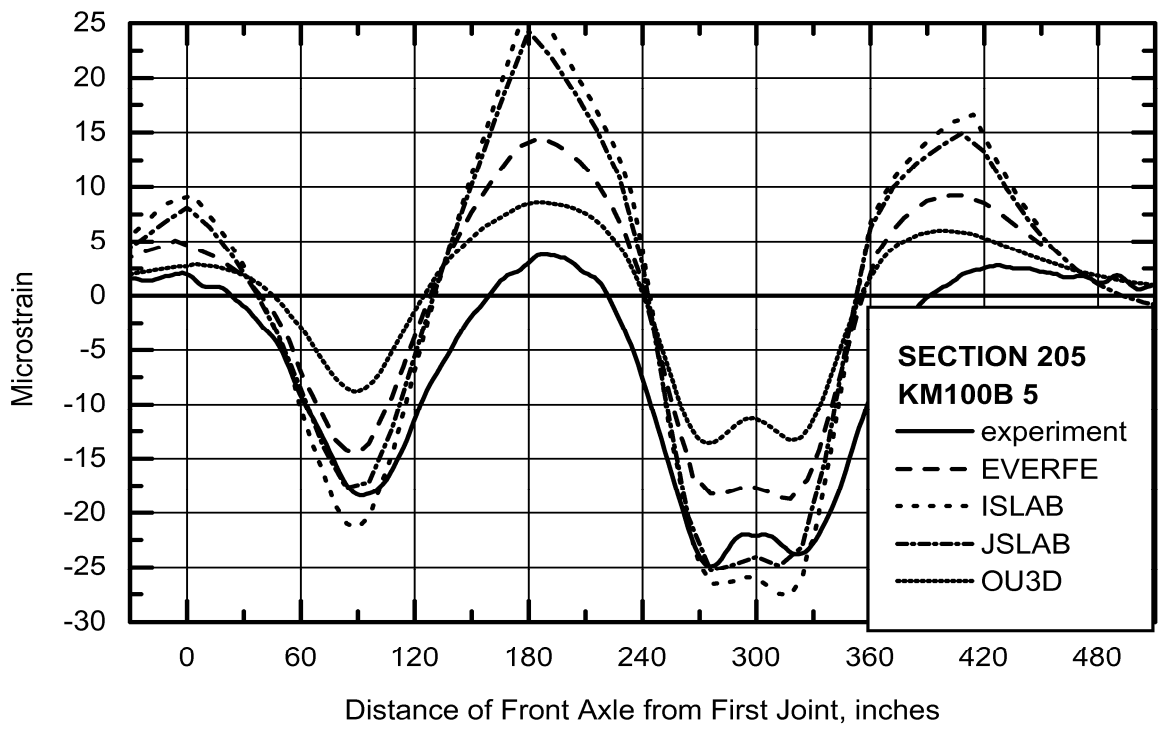


Figure 31. Comparison of Strains at K5 for Section 390205 (1 inch = 2.54 cm).

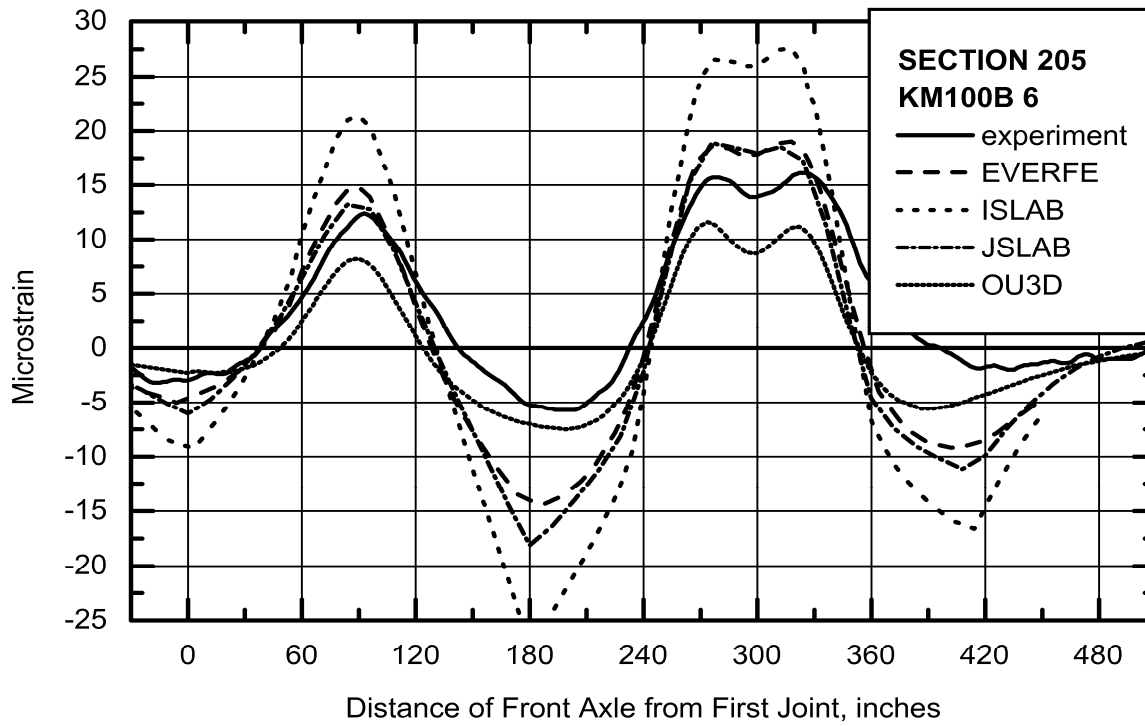


Figure 32. Comparison of Strains at K6 for Section 390205 (1 inch = 2.54 cm).

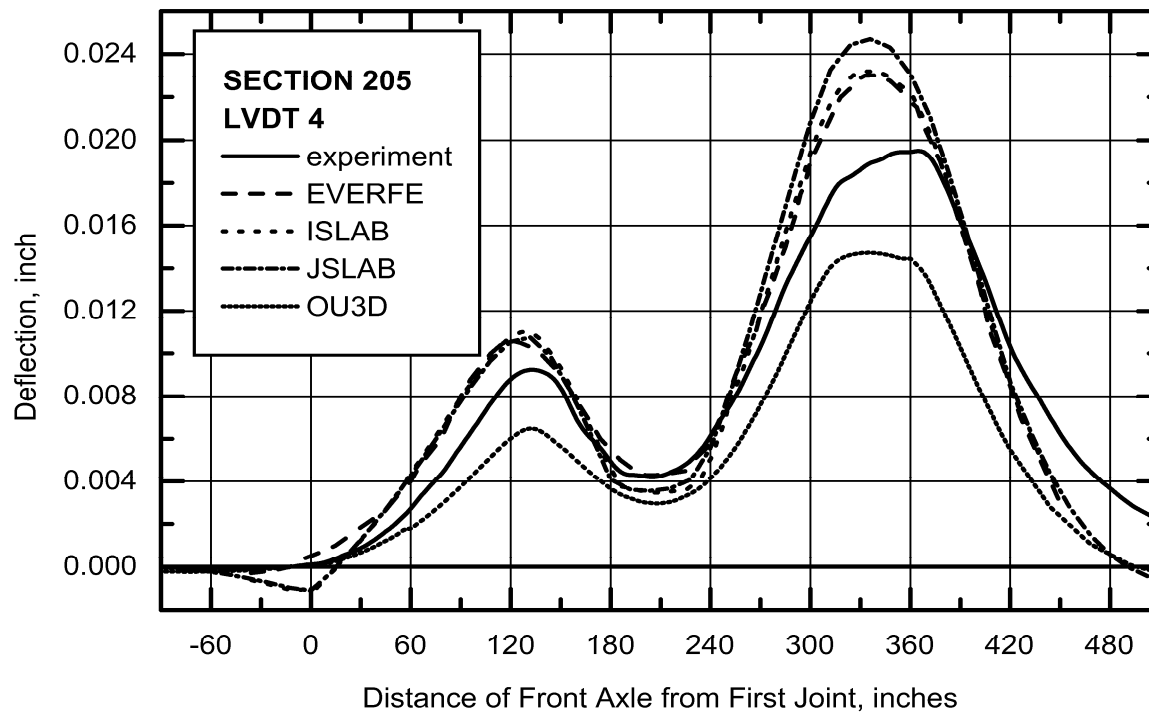


Figure 33. Comparison of Deflections at L4 for Section 390205 (1 inch = 2.54 cm).

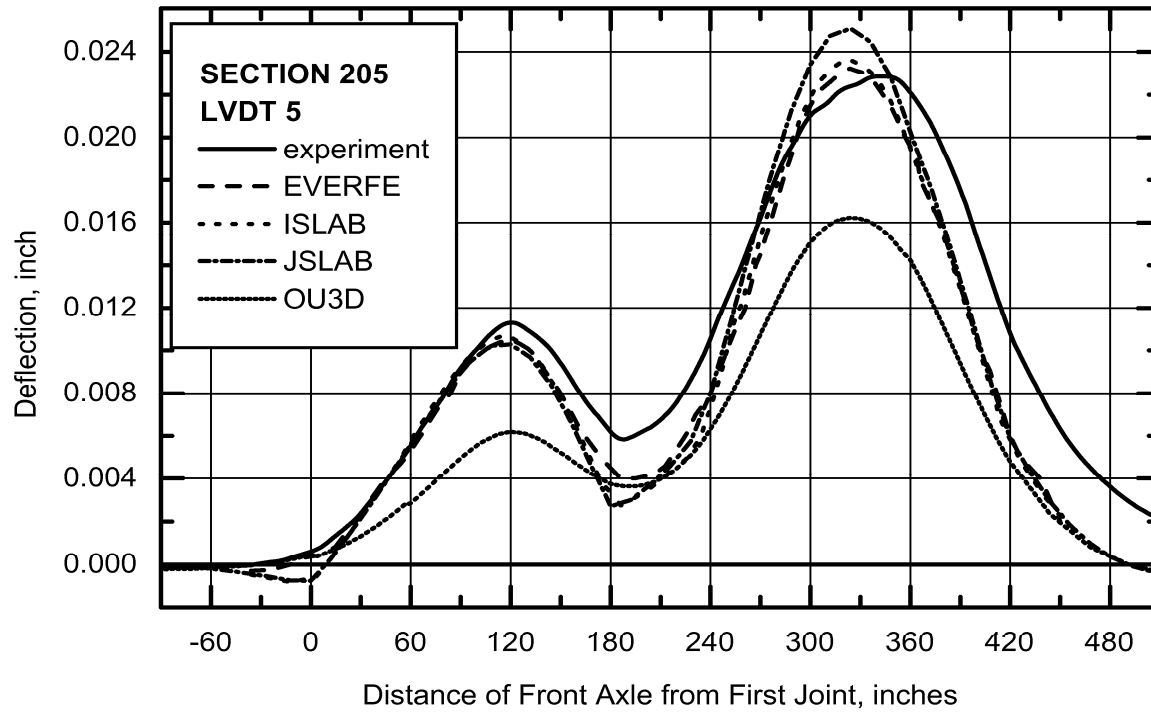


Figure 34. Comparison of Deflections at L5 for Section 390205 (1 inch = 2.54 cm).

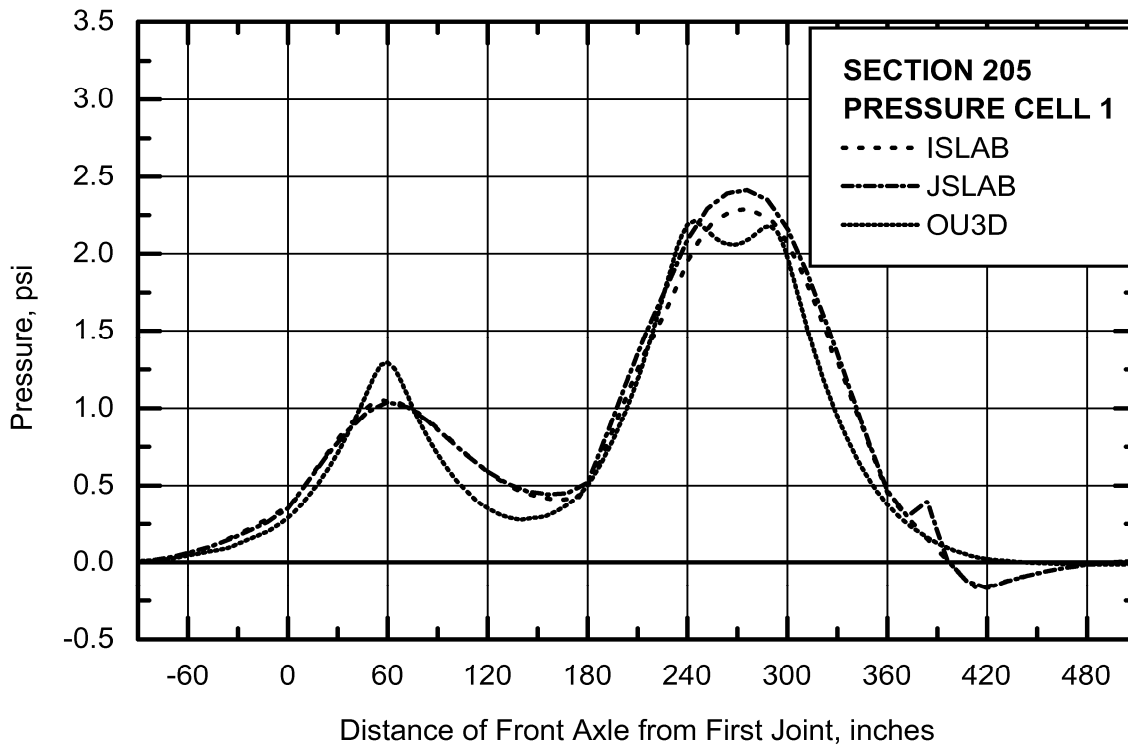


Figure 35. Comparison of Pressures at P1 for Section 390205 (1 inch = 2.54 cm).

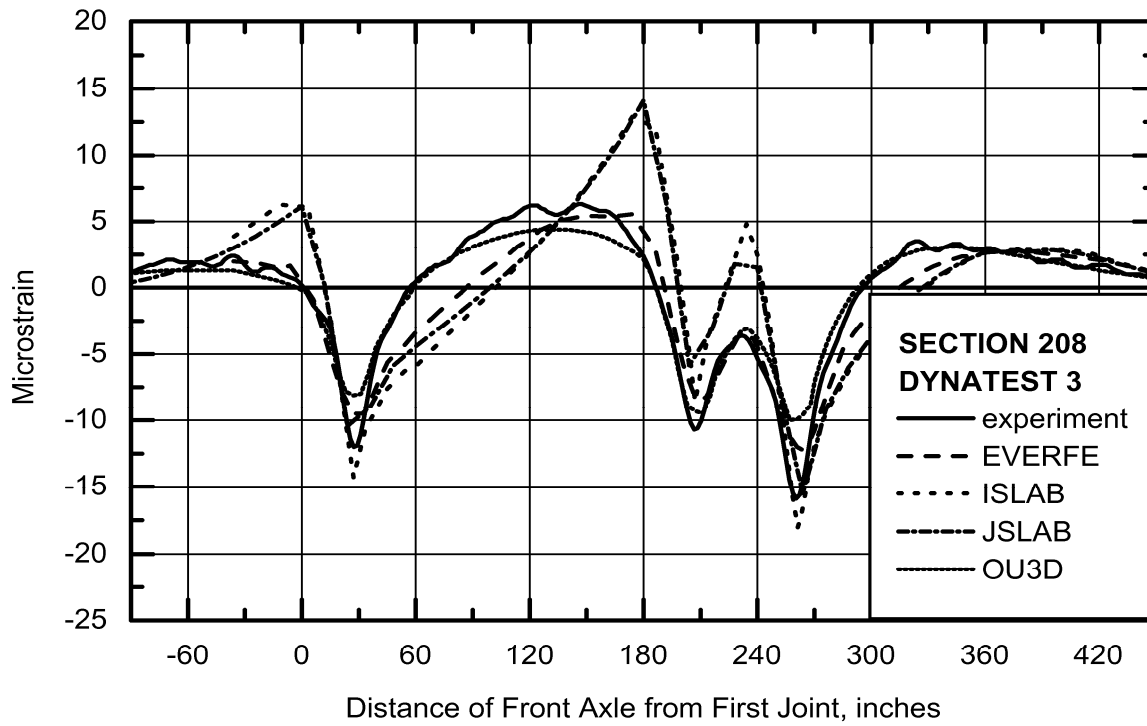


Figure 36. Comparison of Strains at D3 for Section 390208 (1 inch = 2.54 cm).

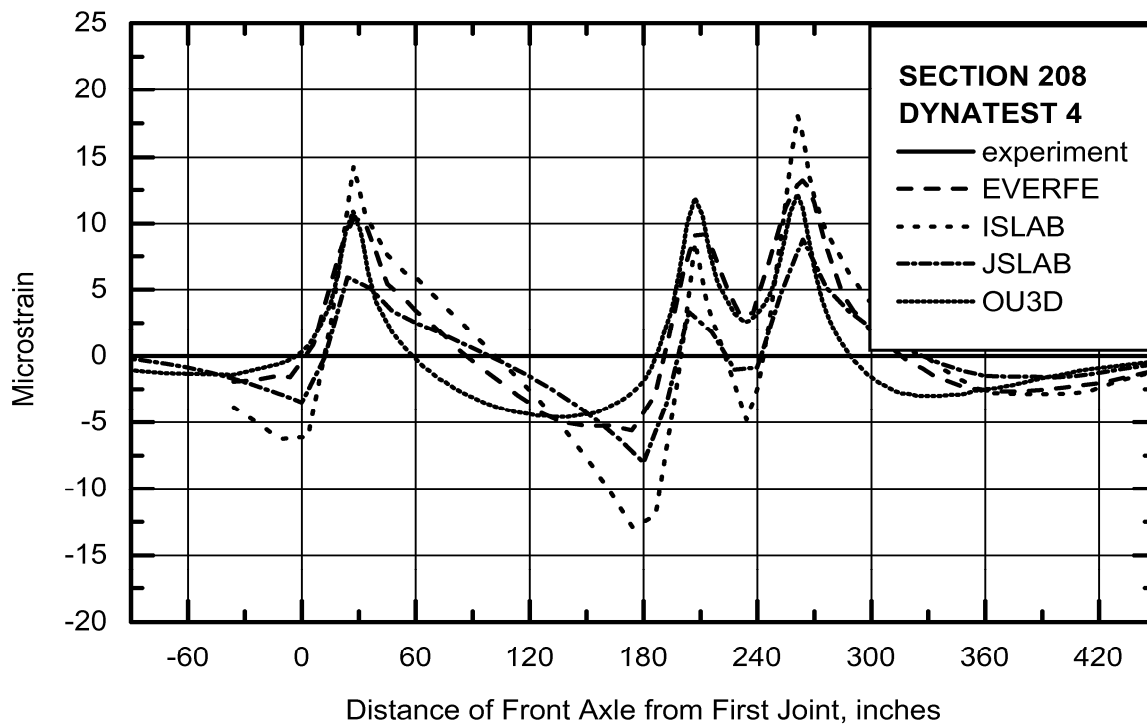


Figure 37. Comparison of Strains at D4 for Section 390208 (1 inch = 2.54 cm).

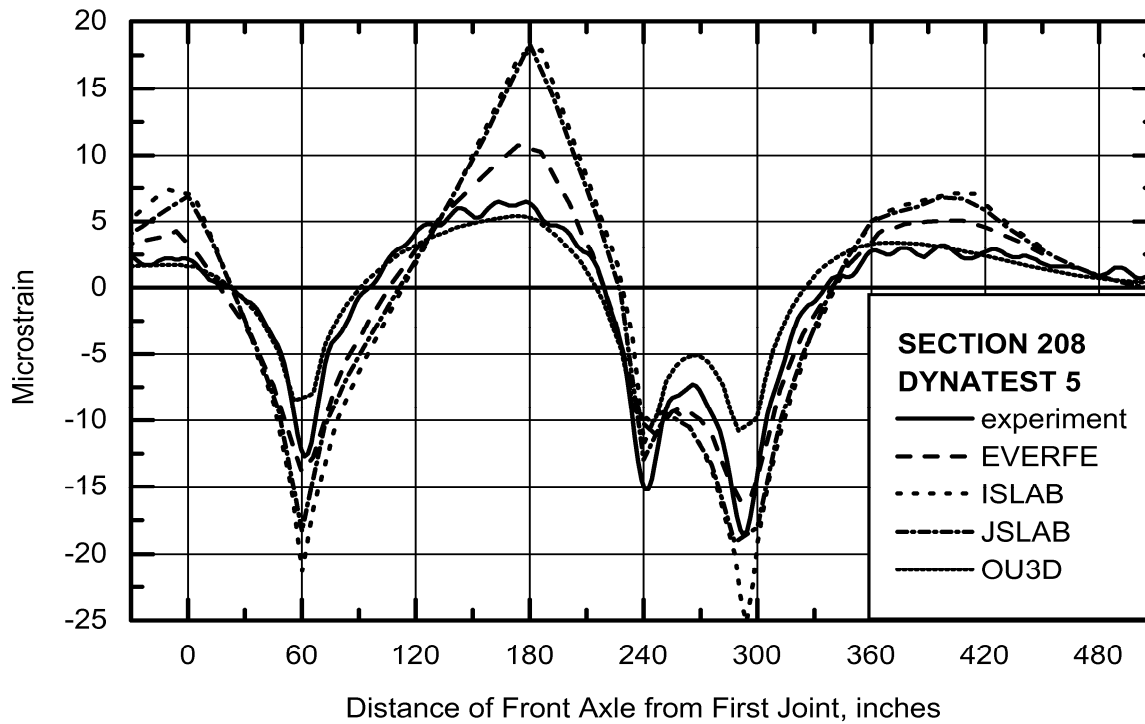


Figure 38. Comparison of Strains at D5 for Section 390208 (1 inch = 2.54 cm).

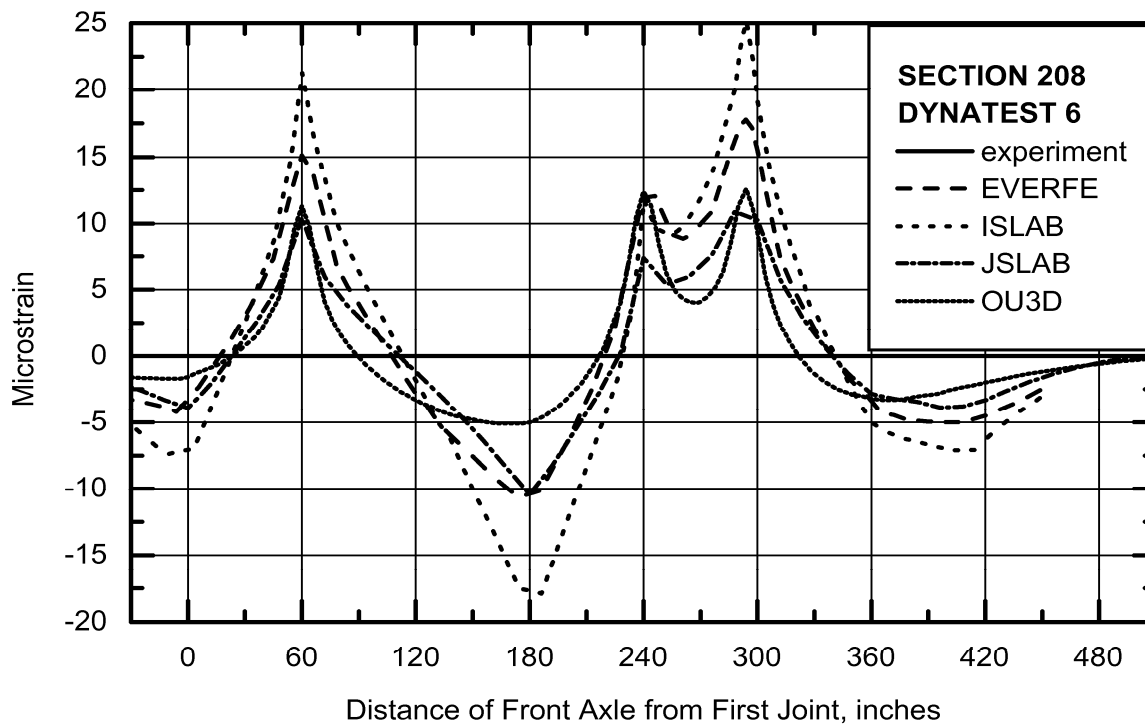


Figure 39. Comparison of Strains at D6 for Section 390208 (1 inch = 2.54 cm).

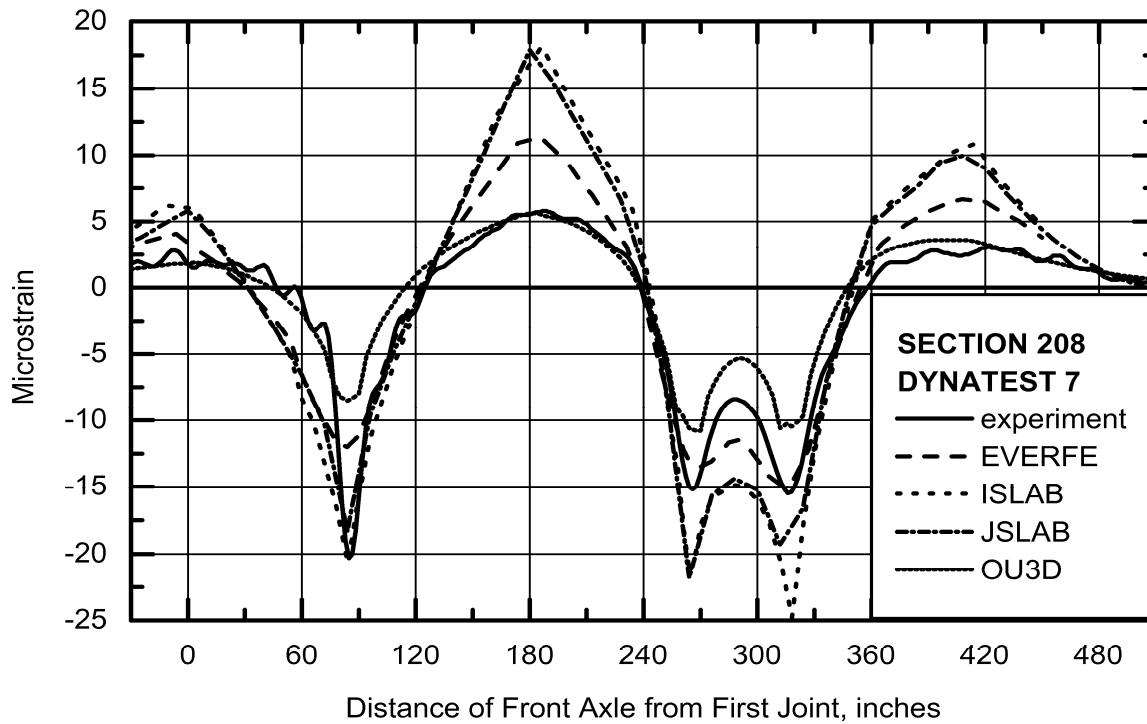


Figure 40. Comparison of Strains at D7 for Section 390208 (1 inch = 2.54 cm).

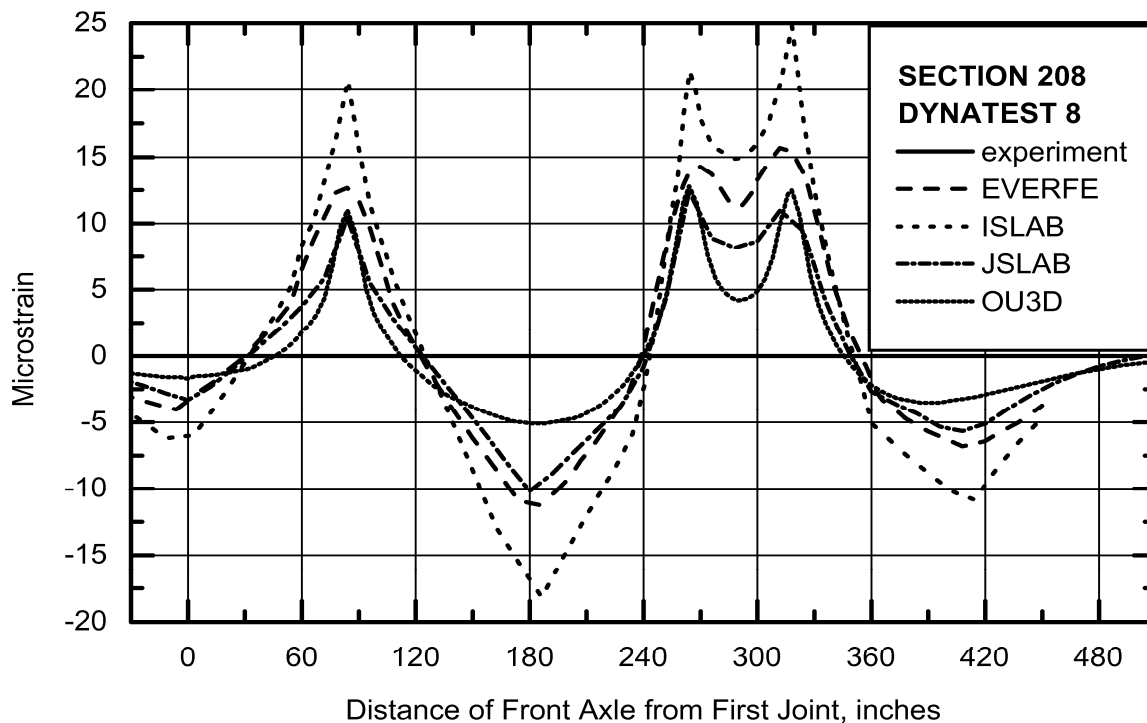


Figure 41. Comparison of Strains at D8 for Section 390208 (1 inch = 2.54 cm).

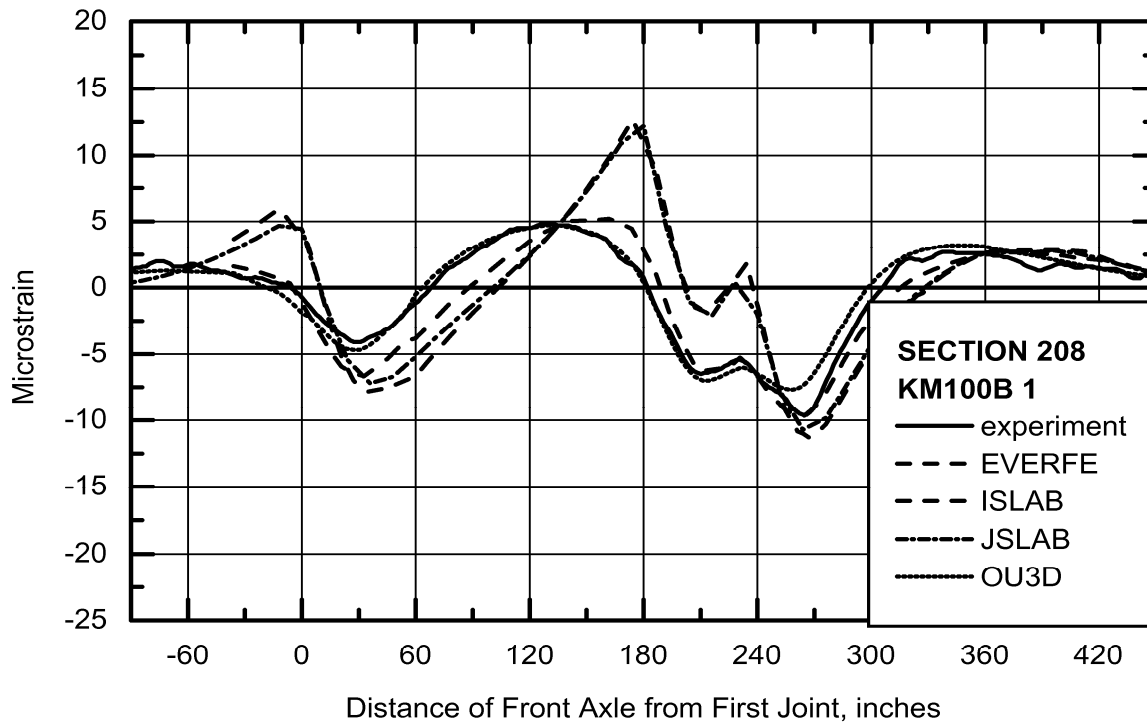


Figure 42. Comparison of Strains at K1 for Section 390208 (1 inch = 2.54 cm).

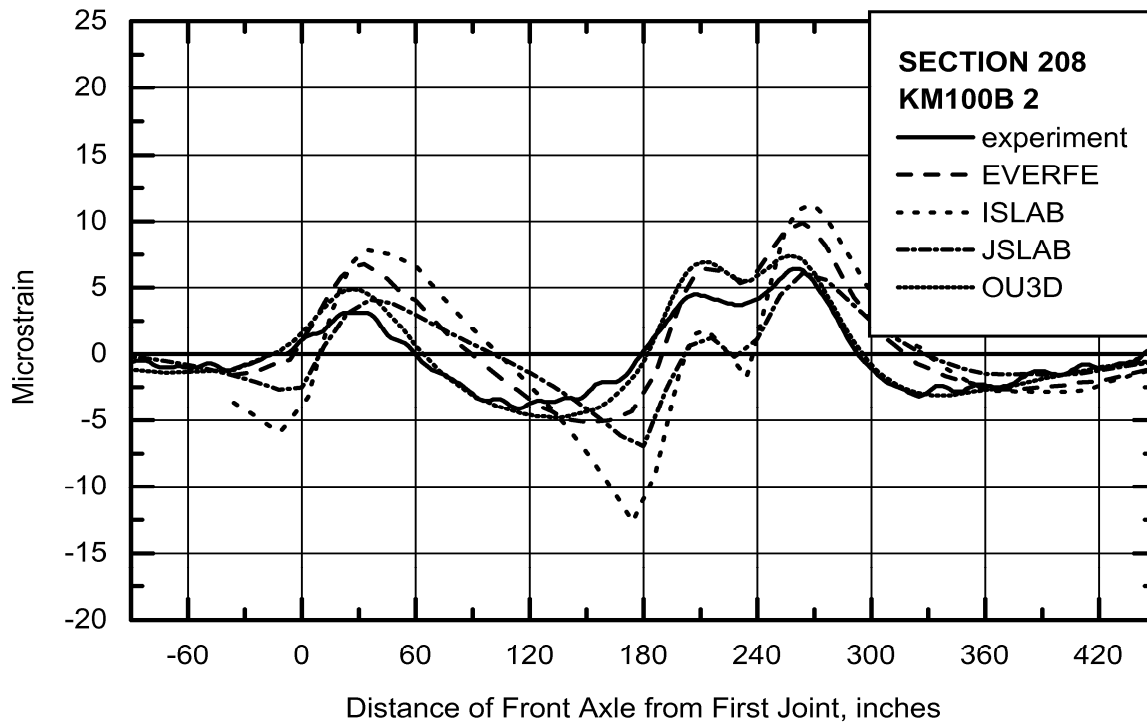


Figure 43. Comparison of Strains at K2 for Section 390208 (1 inch = 2.54 cm).

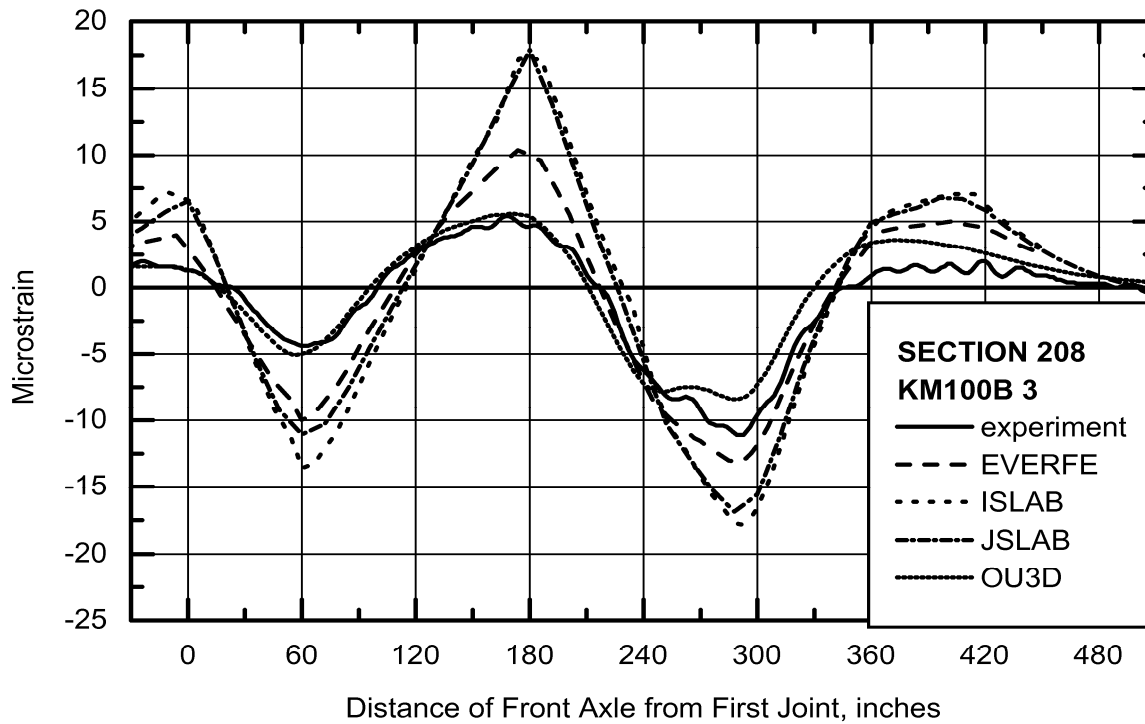


Figure 44. Comparison of Strains at K3 for Section 390208 (1 inch = 2.54 cm).

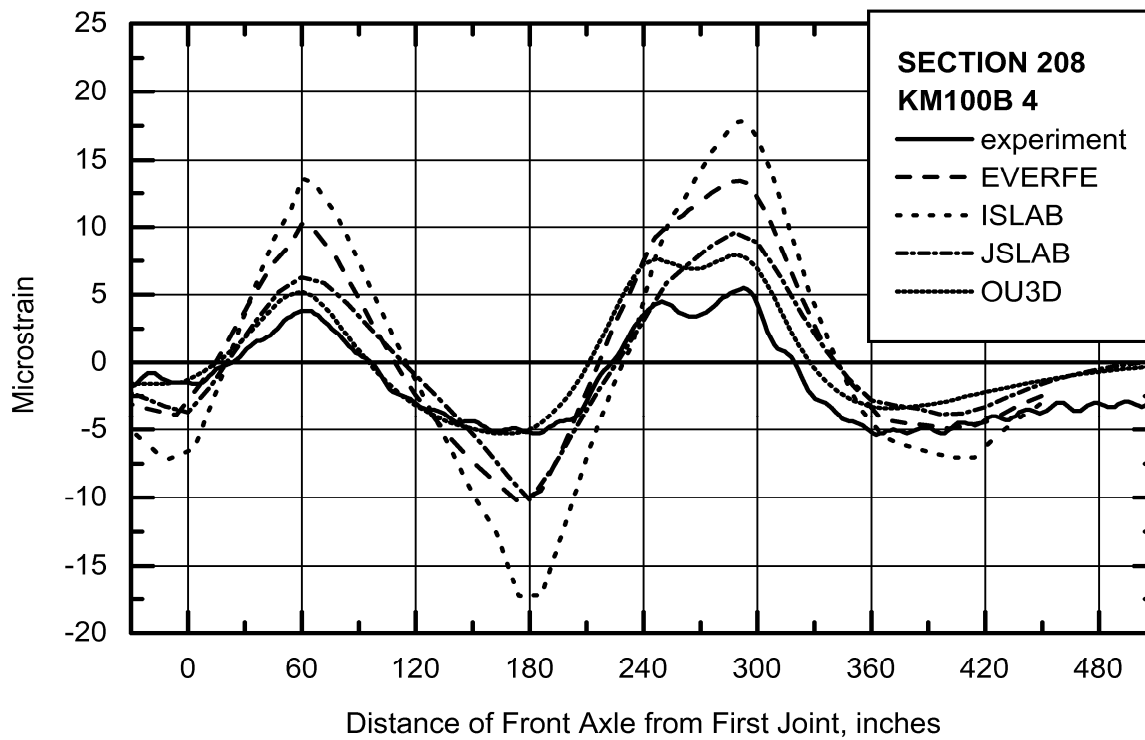


Figure 45. Comparison of Strains at K4 for Section 390208 (1 inch = 2.54 cm).

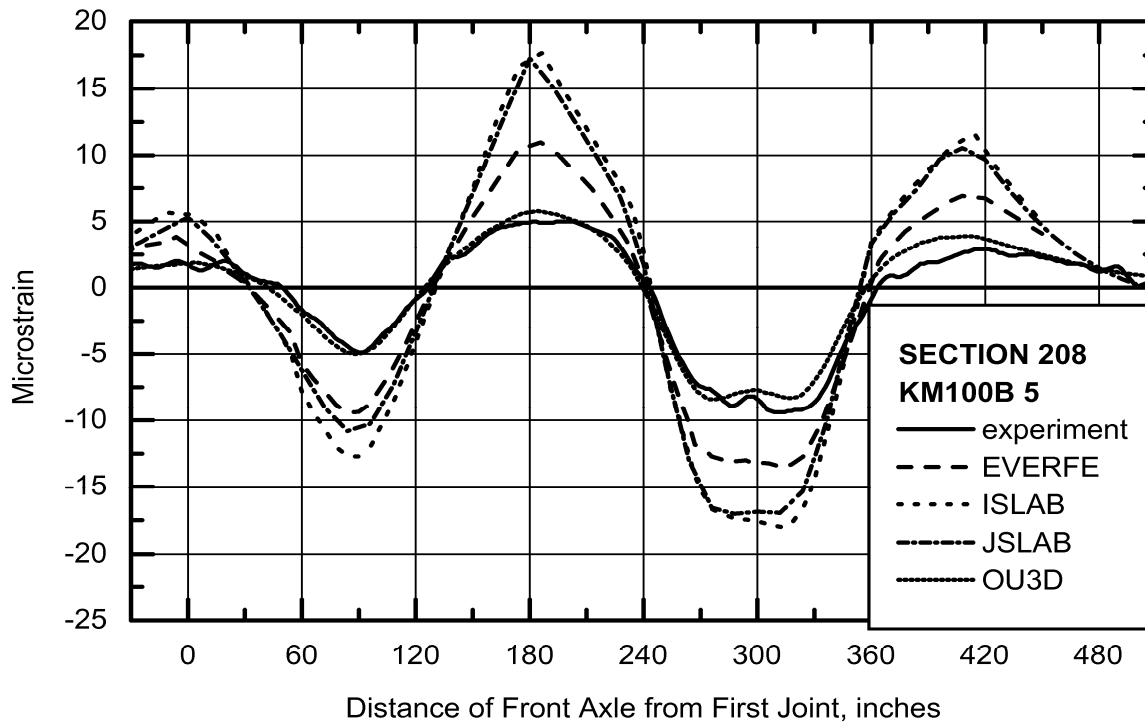


Figure 46. Comparison of Strains at K5 for Section 390208 (1 inch = 2.54 cm).

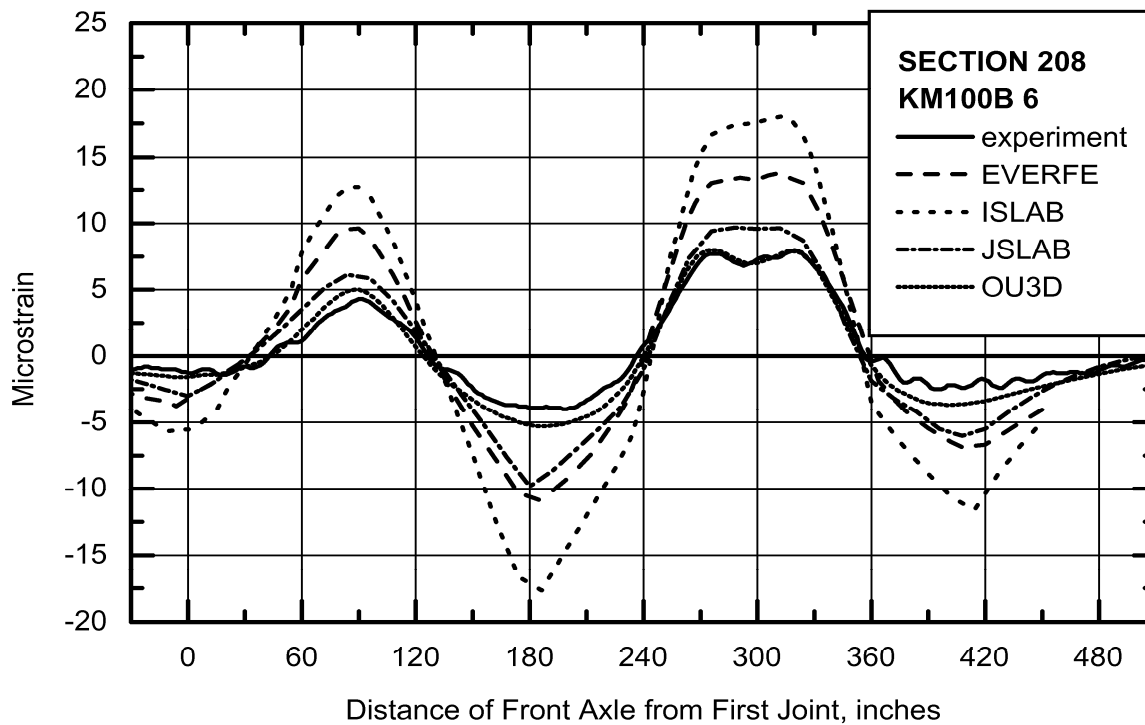


Figure 47. Comparison of Strains at K6 for Section 390208 (1 inch = 2.54 cm).

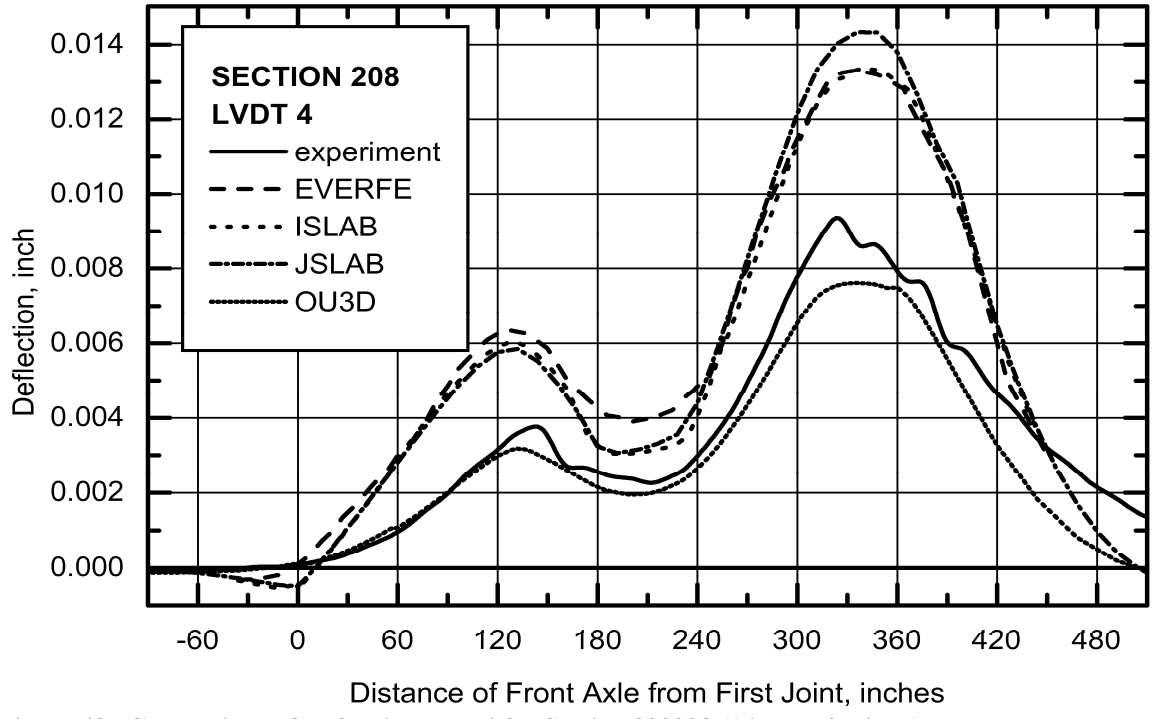


Figure 48. Comparison of Deflections at L4 for Section 390208 (1 inch = 2.54 cm).

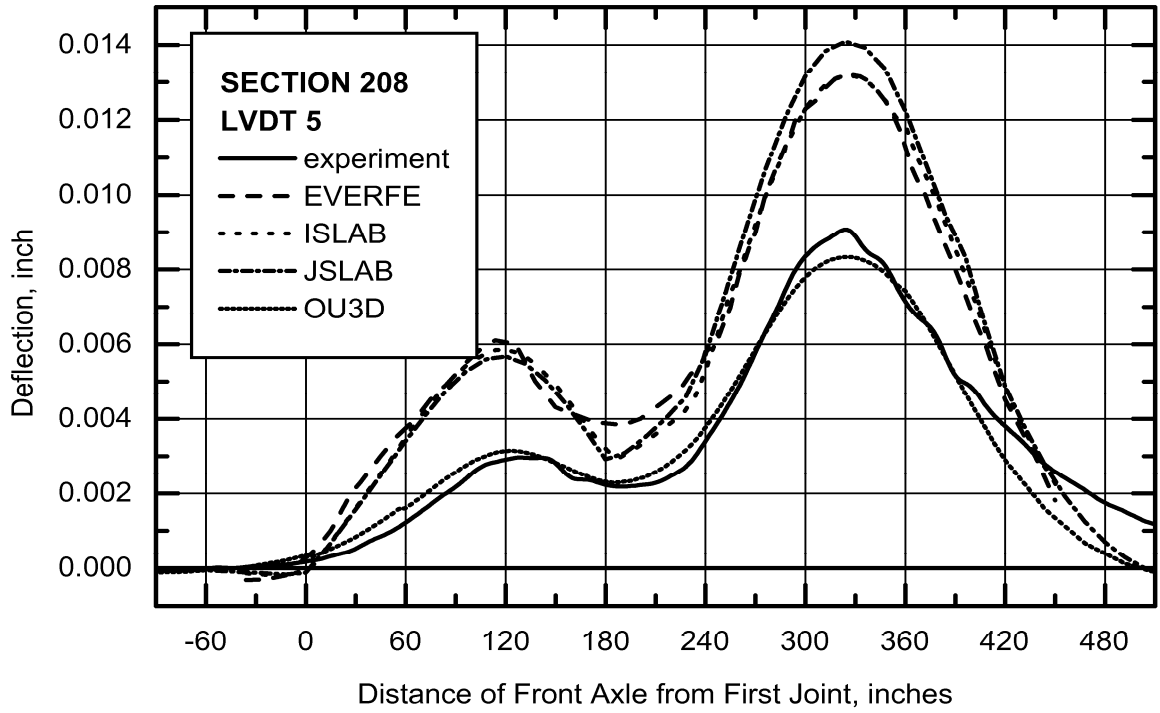


Figure 49. Comparison of Deflections at L5 for Section 390208 (1 inch = 2.54 cm).

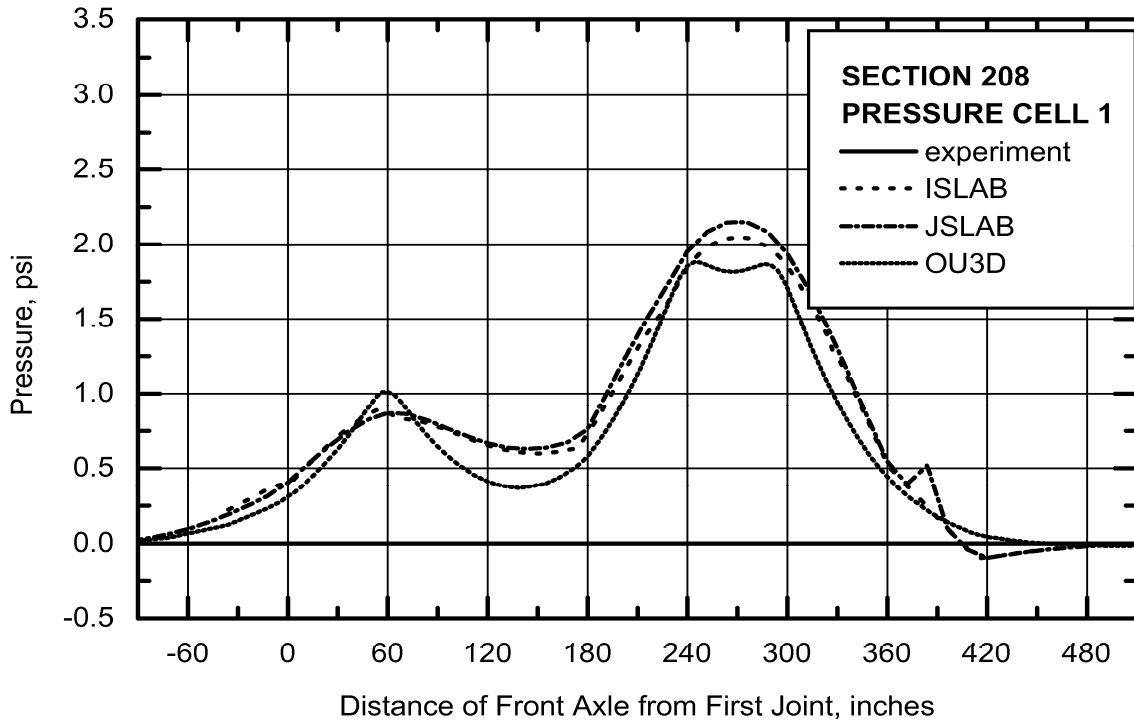


Figure 50. Comparison of Pressures at P1 for Section 390208 (1 inch = 2.54 cm).

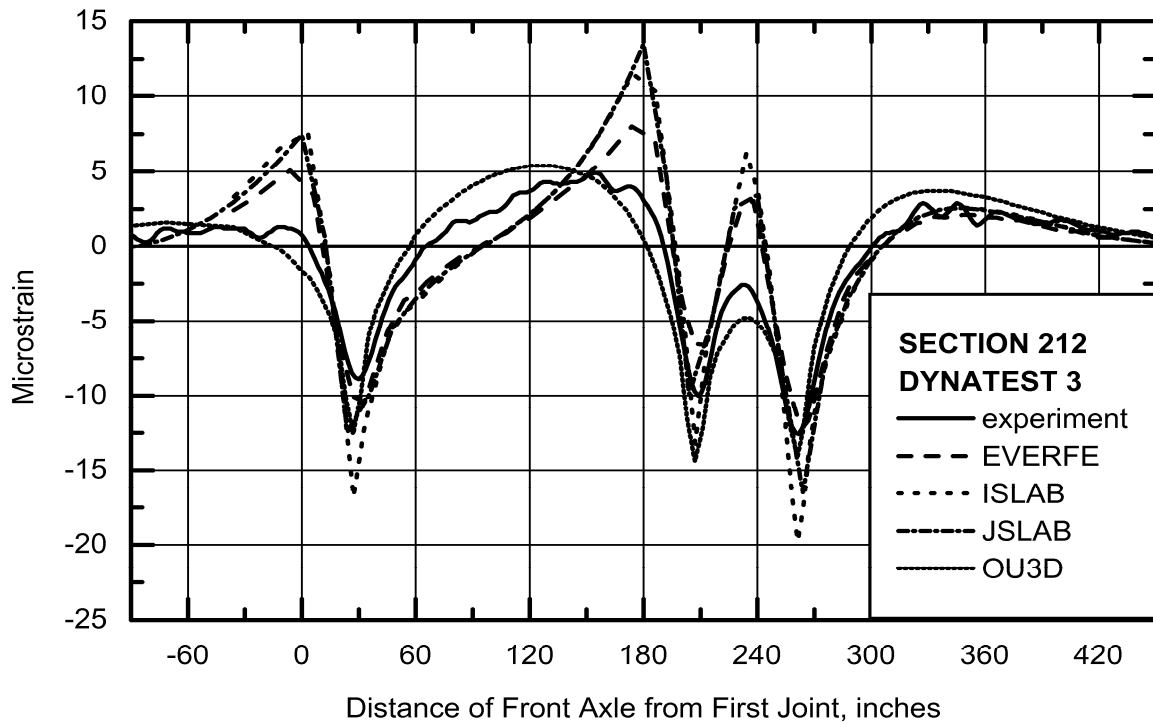


Figure 51. Comparison of Strains at D3 for Section 390212 (1 inch = 2.54 cm).

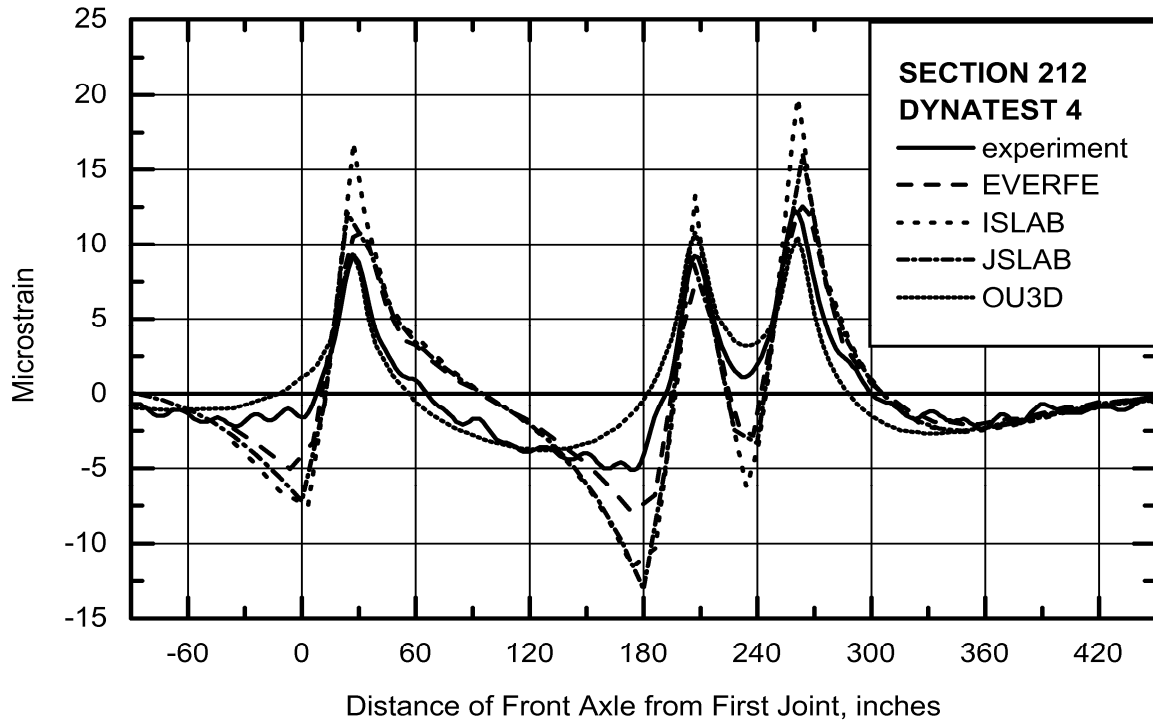


Figure 52. Comparison of Strains at D4 for Section 390212 (1 inch = 2.54 cm).

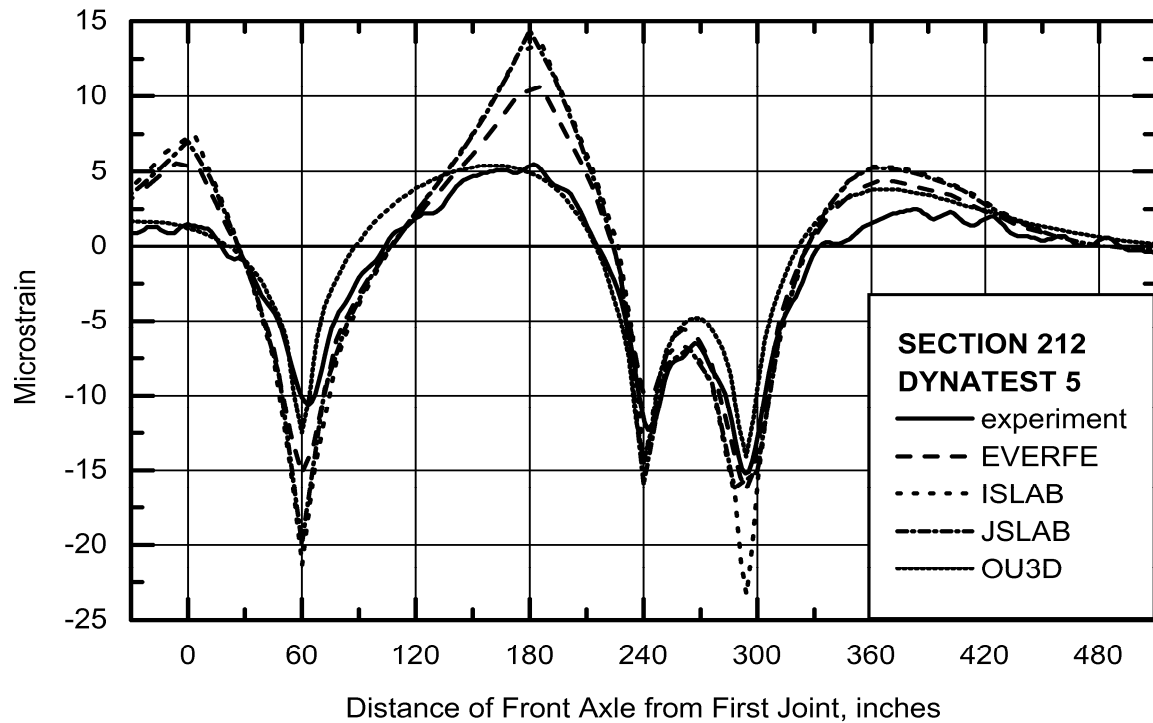


Figure 53. Comparison of Strains at D5 for Section 390212 (1 inch = 2.54 cm).

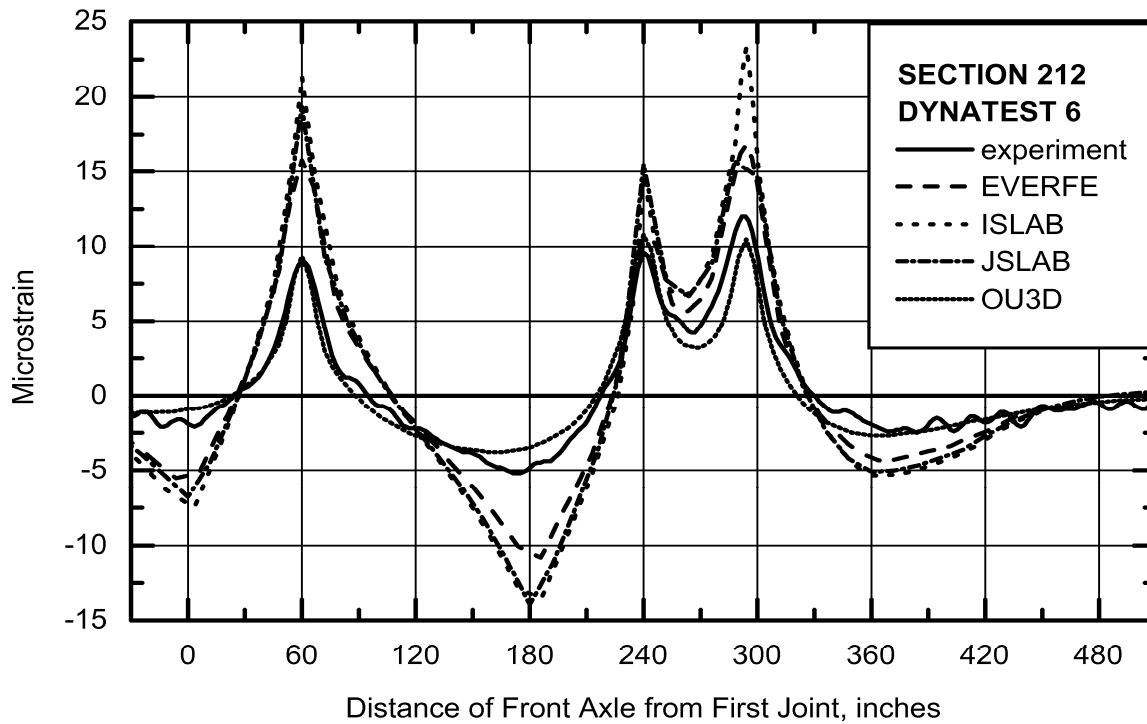


Figure 54. Comparison of Strains at D6 for Section 390212 (1 inch = 2.54 cm).

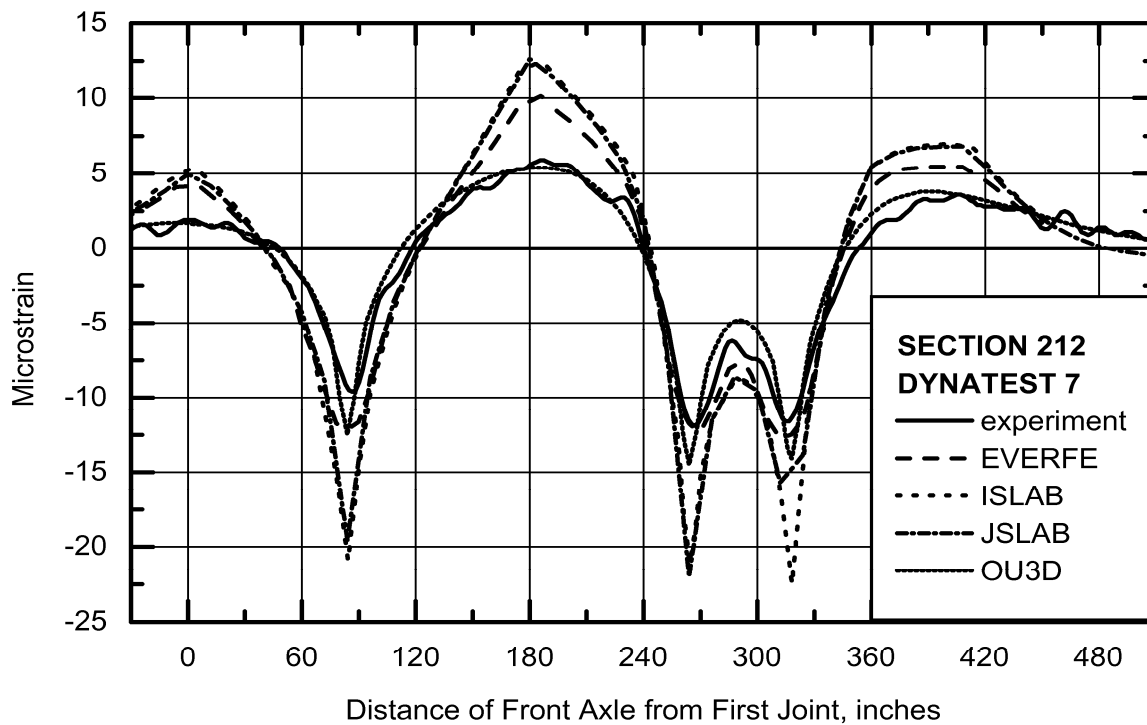


Figure 55. Comparison of Strains at D7 for Section 390212 (1 inch = 2.54 cm).

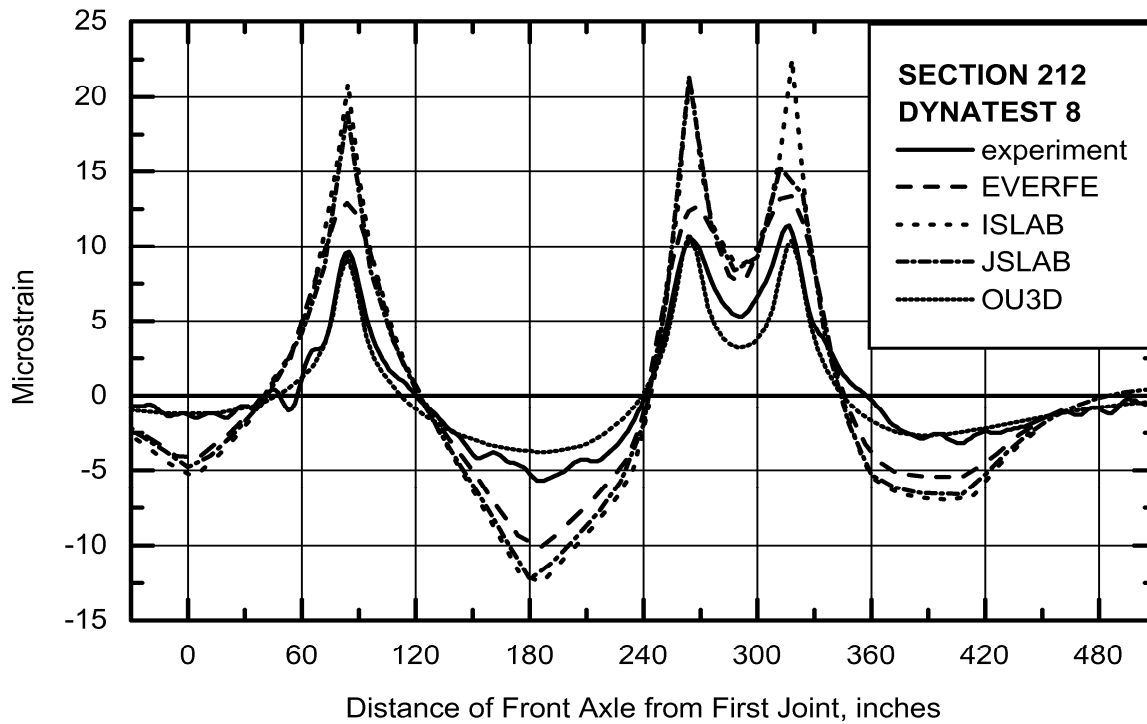


Figure 56. Comparison of Strains at D8 for Section 390212 (1 inch = 2.54 cm).

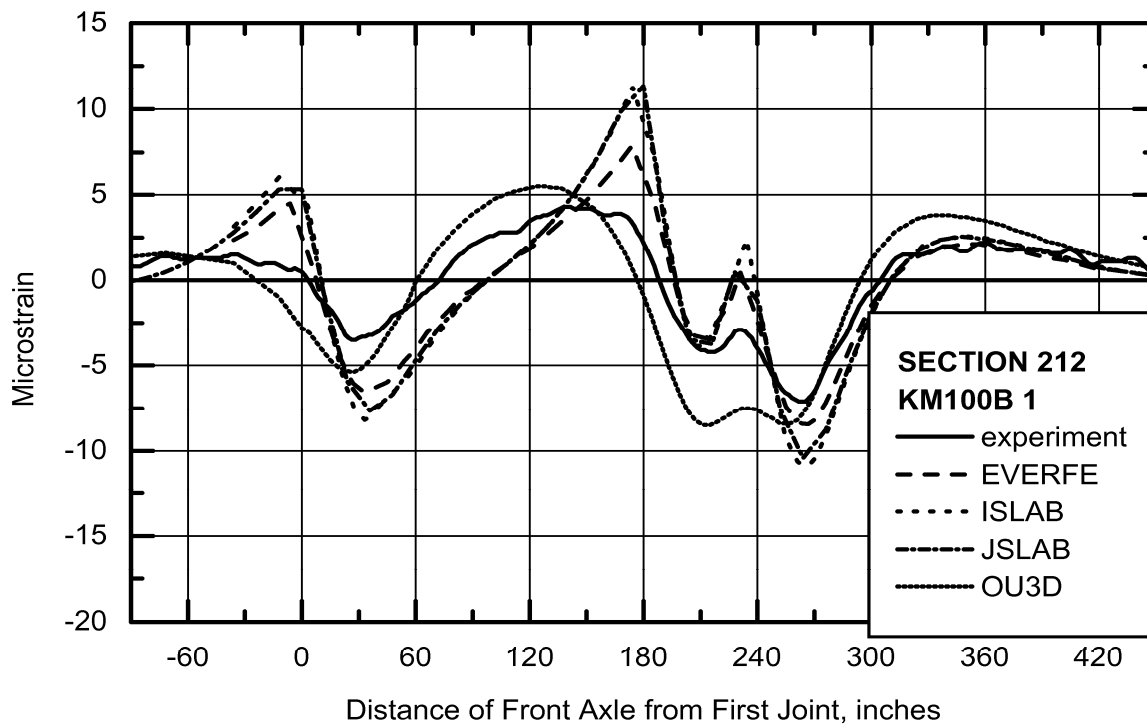


Figure 57. Comparison of Strains at K1 for Section 390212 (1 inch = 2.54 cm).

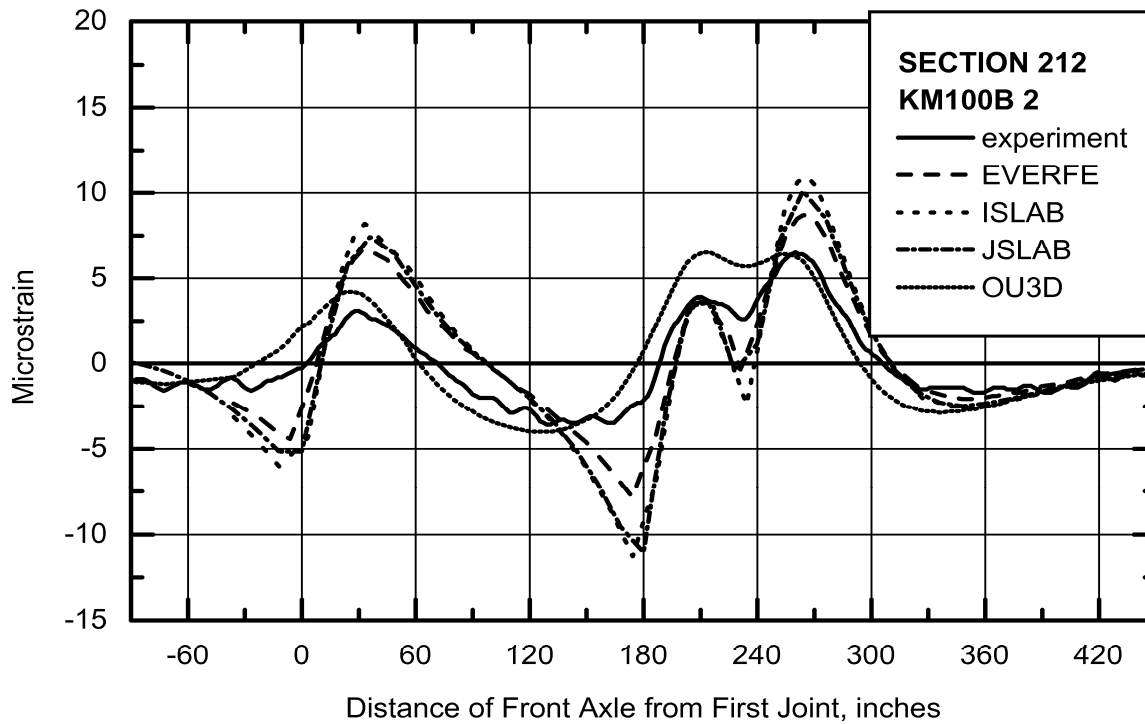


Figure 58. Comparison of Strains at K2 for Section 390212 (1 inch = 2.54 cm).

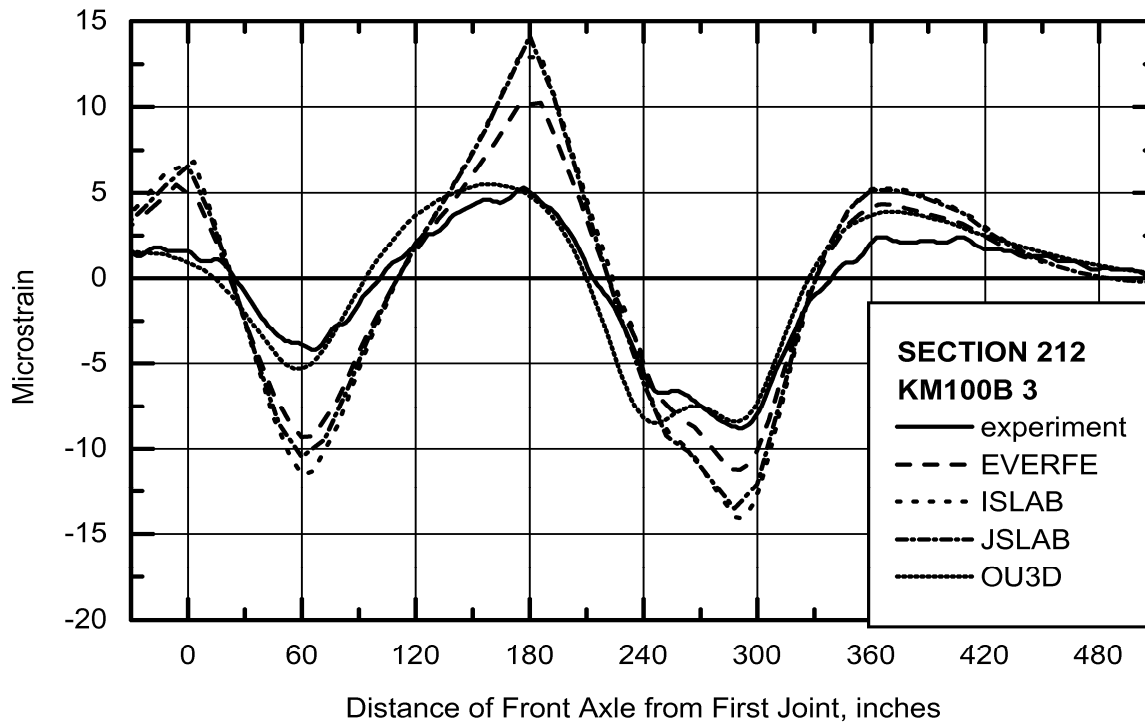


Figure 59. Comparison of Strains at K3 for Section 390212 (1 inch = 2.54 cm).

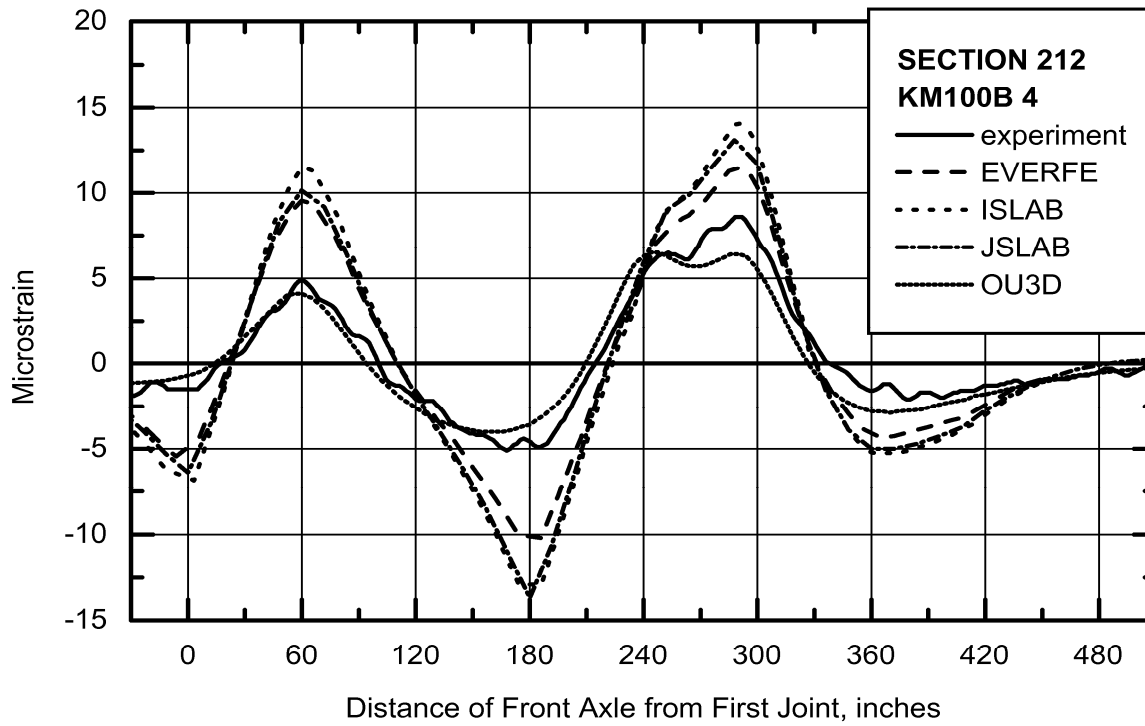


Figure 60. Comparison of Strains at K4 for Section 390212 (1 inch = 2.54 cm).

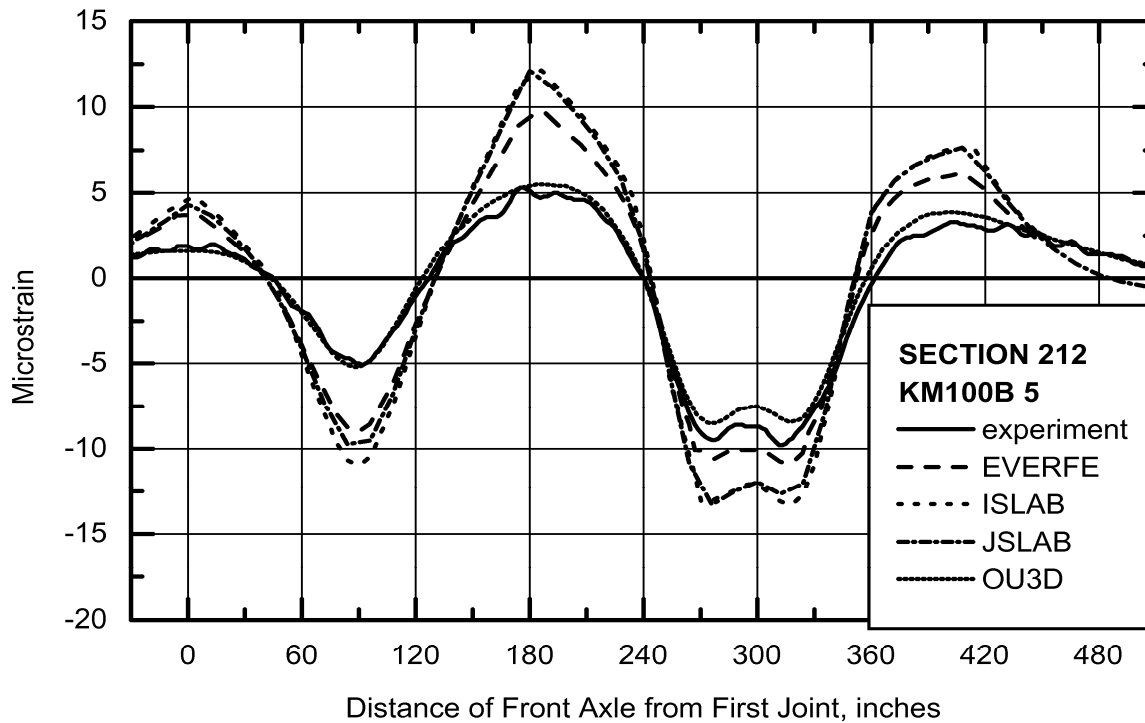


Figure 61. Comparison of Strains at K5 for Section 390212 (1 inch = 2.54 cm).

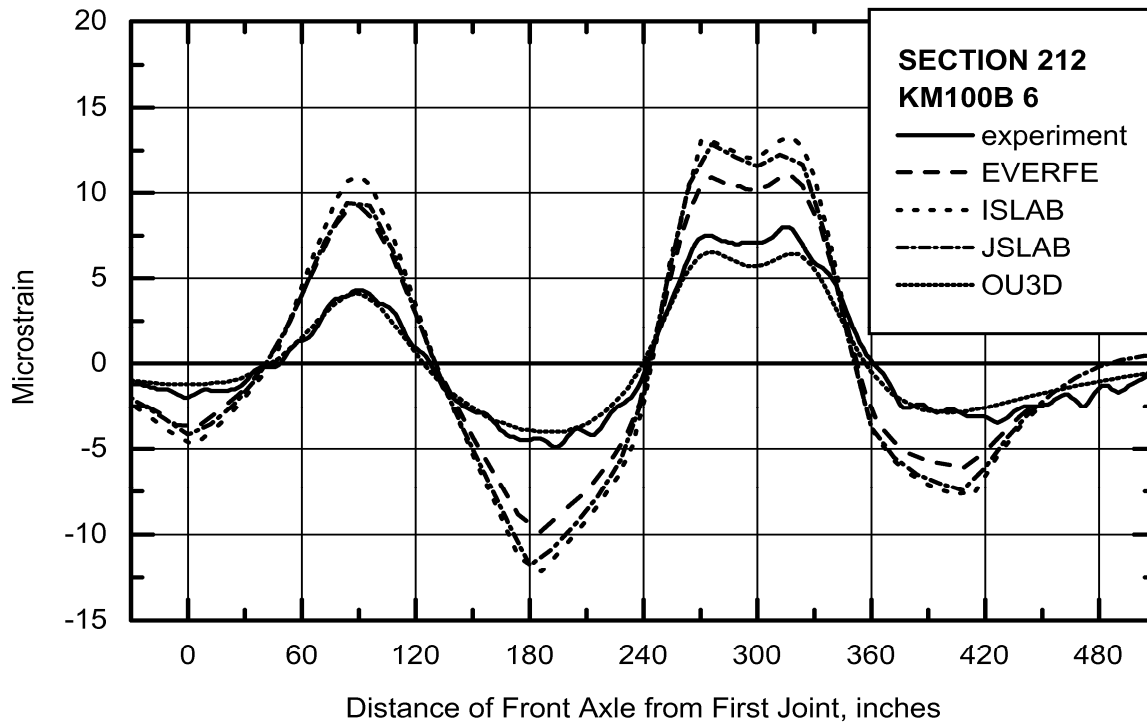


Figure 62. Comparison of Strains at K6 for Section 390212 (1 inch = 2.54 cm).

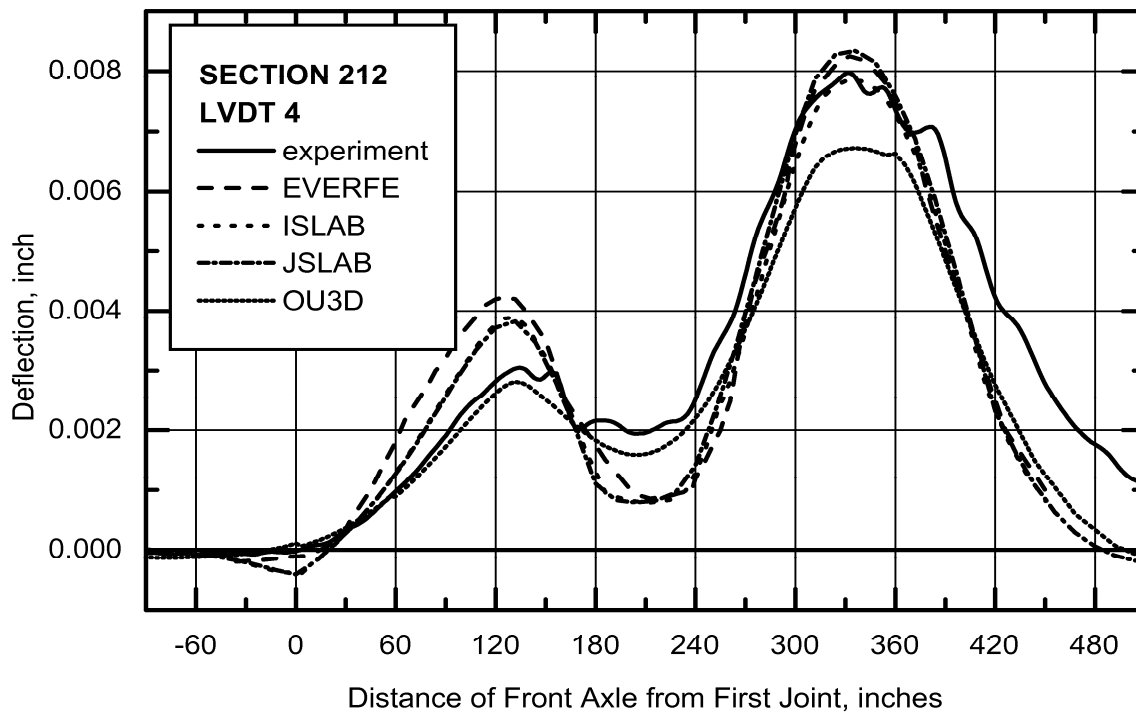


Figure 63. Comparison of Deflections at L4 for Section 390212 (1 inch = 2.54 cm).

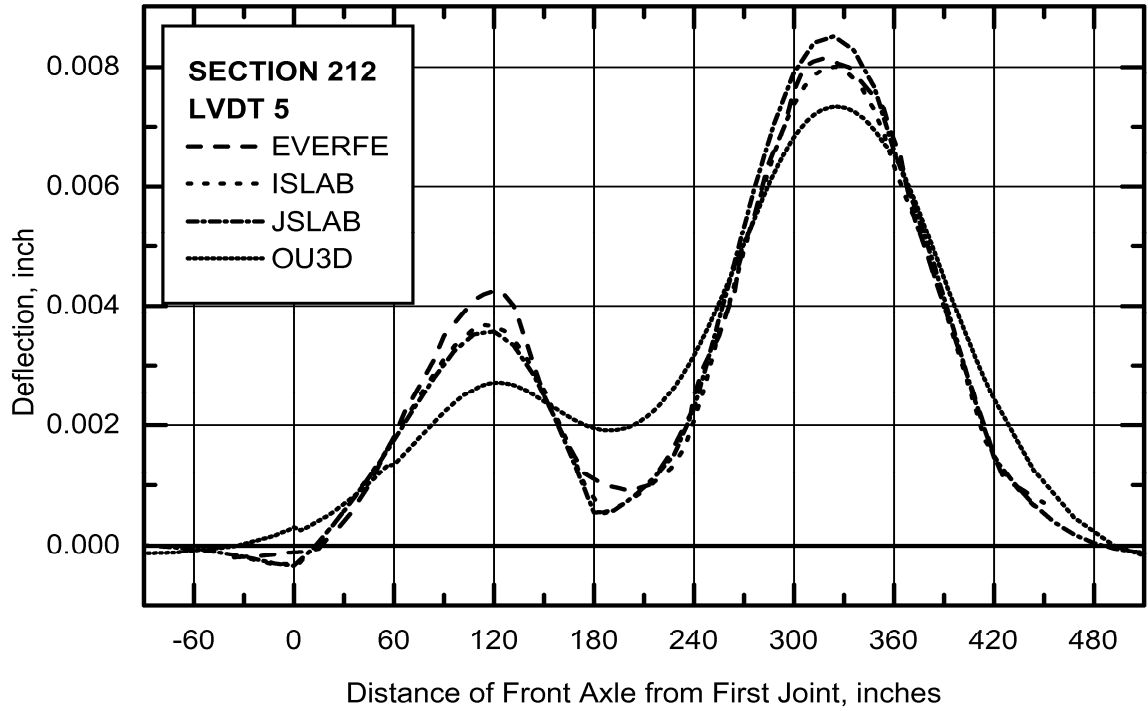


Figure 64. Comparison of Deflections at L5 for Section 390212 (1 inch = 2.54 cm).

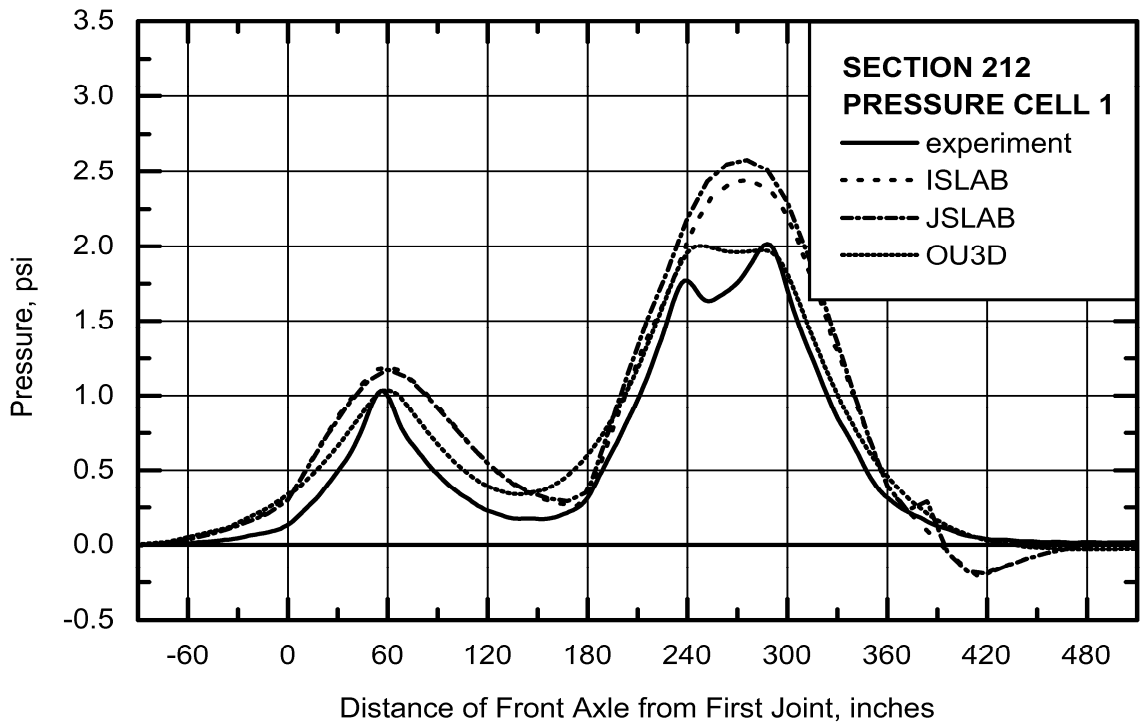


Figure 65. Comparison of Pressures at P1 for Section 390212 (1 inch = 2.54 cm).

4 VALIDATION OF ISLAB2000

4.1 INTRODUCTION

The research team for the National Cooperative Highway Research Program (NCHRP) Project 1-37 A: *Development of the 2002 Guide for the Design of New and Rehabilitated Pavement Structures* submitted the final document on structural response models for rigid pavements (Appendix QQ of that report) in July 2003. ISLAB2000 was selected as the finite element model for structure model development based on two criteria: 1) ability to model all of the important features of rigid pavements and 2) computational practicality. When compared to the 3D-FE ABAQUS, ISLAB2000 did not introduce significant errors in the predicted structural responses. Comparisons of the stresses predicted by ISLAB2000 with the measured stresses from the AASHO Road Test showed good correlation. It was mentioned earlier, however, that the field verification was limited to the structural response of slab edge under moving truck loads without the consideration of environmental effects.

For complete verification and validation, ISLAB2000 strain and deflection predictions were compared with the experimental data from the Accelerated Pavement Load Facility (APLF) where both dynamic and environmental loadings were considered. This chapter presents the experimental data obtained from APLF, followed by a detailed study of each particular condition the slab might be subjected to. These conditions are titled as follows: “stage I- curing period”, “stage II- temperature cycling period”, and “stage III- combined traffic and environmental loading period”. Concrete slab deflections and strains were compared with ISLAB2000 predictions. This validation will be used in finding the optimum slab joint spacing in chapter 5.

4.2 EXPERIMENTAL DATA

The database associated with the final copy of *Evaluation of Forces in Dowel Bars under Controlled Conditions* by Sargand et al. (2003) is the source of rigid pavement experimental responses. The main objective of that report was to quantitatively measure dowel bar and slab response under controlled conditions on doweled and undoweled pavements constructed in the APLF. These structural responses of a doweled slab were compiled through a period of 188 days. Within this period, the pavement was subjected to curing under constant temperature, a period of temperature cycling, and a combined effect of temperature cycling and moving loads. In this study, only the doweled slab will be considered for the verification and validation purposes. The pavement was constructed in accordance with Ohio Department of Transportation (ODOT) specifications with a dense-graded aggregate base (DGAB) and the A-6 subgrade under the pavement being typical of that found on high level rigid pavements in Ohio. Geometry and material properties of the pavement system are presented in Table 11 (English units) and Table 12 (metric units). The PCC material properties were laboratory measured, while the base properties and the modulus of subgrade reaction were recommended values from Masada et al. (2004).

Table 11. Properties of Experimental Pavement Section (English units). Data for DGAB and subgrade (A-6) layers from Masada et al. (2004).

Layer Name	Thickness (in)	Elastic Modulus (psi)	Coefficient of Thermal Expansion ((F°) ⁻¹)	Poisson's Ratio	Density (pci)	Modulus of Subgrade Reaction (psi/in)
PCC	10	3.42E+06	6.66E-06	0.22	0.0831	
DGAB	6	1.58E+04	6.33E-06	0.35	0.0737	
A-6						221
Note: Each slab was 180 inches in length by 144 inches in width						

Table 12. Properties of Experimental Pavement Section (metric units). Data for DGAB and subgrade (A-6) layers from Masada et al. (2004).

Layer Name	Thickness (cm)	Elastic Modulus (MPa)	Coefficient of Thermal Expansion ((C°) ⁻¹)	Poisson's Ratio	Density (kg/m ³)	Modulus of Subgrade Reaction (MPa/m)
PCC	25.4	2.35E+04	1.20E-05	0.22	2300	
DGAB	15.2	1.09E+02	1.14E-05	0.35	2040	
A-6						60.0
Note: Each slab was 4.57 m in length by 3.66 m in width						

Figure 66 presents the slab layout and instrumentation. Strain gauges and thermocouples were installed during concrete placement to measure strain and temperature in the concrete slab. Schaevitz 121-500 DC LVDTs, referenced to a depth of about seven feet, were installed along the pavement edges soon after placement to monitor vertical deflections at these locations. Two types of strain gauges were installed in the slabs. Geokon VCE 4200 Vibrating Wire (VW) strain gauges were embedded 1 inch (2.54 cm) from the top and bottom of the end slabs along the centerline to monitor environmental strain caused by changing temperature and moisture in the slabs. TML PMR-60 three-axis rosettes were mounted 1 inch (2.54 cm) from the top and bottom of the middle slabs to measure dynamic strain generated by the rolling test wheel. LVDTs measured vertical deflection from environmental and dynamic loadings. Also in the figure, the five paths traversed by the load are indicated: P1 and P5 are at the edge of the pavement; P2 and P4 are in the wheel paths 30 in (76 cm) from the edge; and P3 is along the centerline.

A Dipstick was used to obtain slab profiles by measuring vertical elevations to a thousandth of an inch (0.0254 mm) at 12 inch (30.5 cm) intervals. It included an LCD display, two footpads, and a main body housing an inclinometer positioned so that its axis and a line passing through the footpads were co-planar. Slab profiles were monitored periodically along a fixed traverse to determine the environmental response of the pavement during curing and temperature changes. The traverse, consisting of a rectangle 11 feet (3.35 m) by 14 feet (4.27 m) and one diagonal across the rectangle, was drawn on the middle slab as in Figure 67.

The environmental response testing included a curing period of five weeks under constant temperature, referred to as Stage I, followed by a period of controlled temperature changes for approximately three weeks, referred to as Stage II. The testing schedule was as follows: air temperature was increased from 20°C (68°F) to approximately 35°C (97°F) for one week, decreased to 22°C (72°F) for three days, decreased further to 5°C (41°F) for three days, and finally returned to 21°C (70°F).

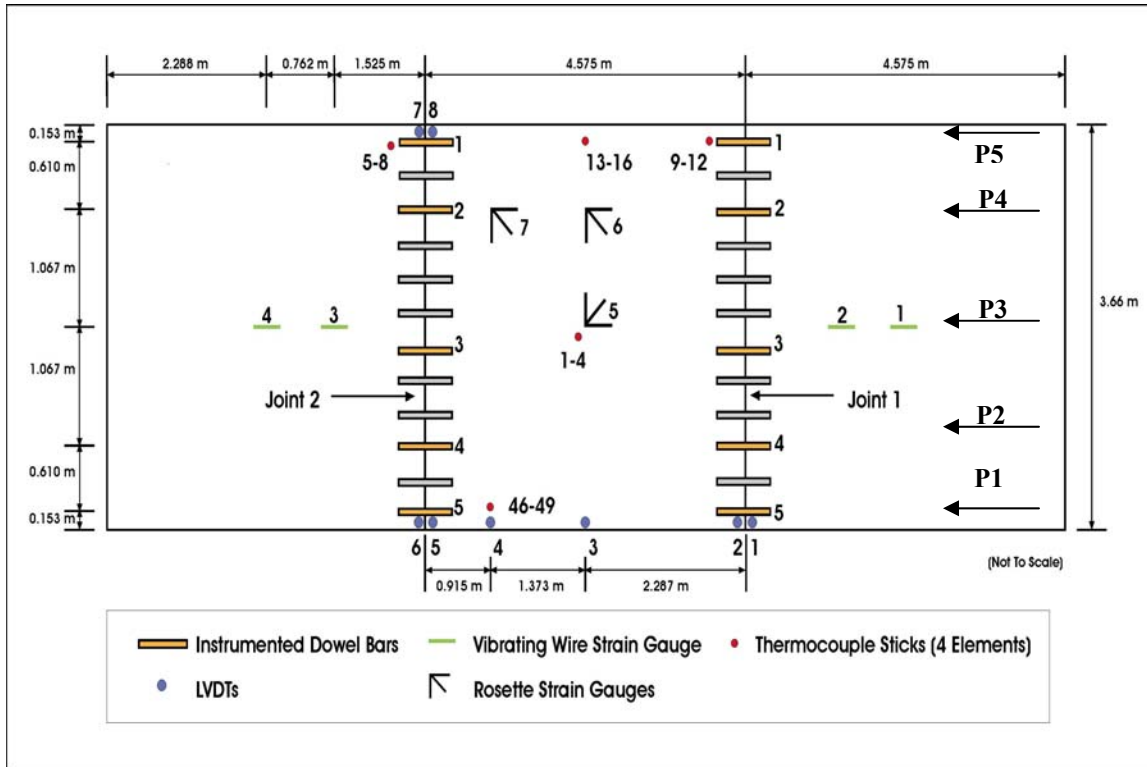


Figure 66. PCC Doweled Slab Instrumentation. P1 through P5 indicate paths taken by the load; numbers indicate positions of measurement instrumentation. (1 m = 3.28 ft).

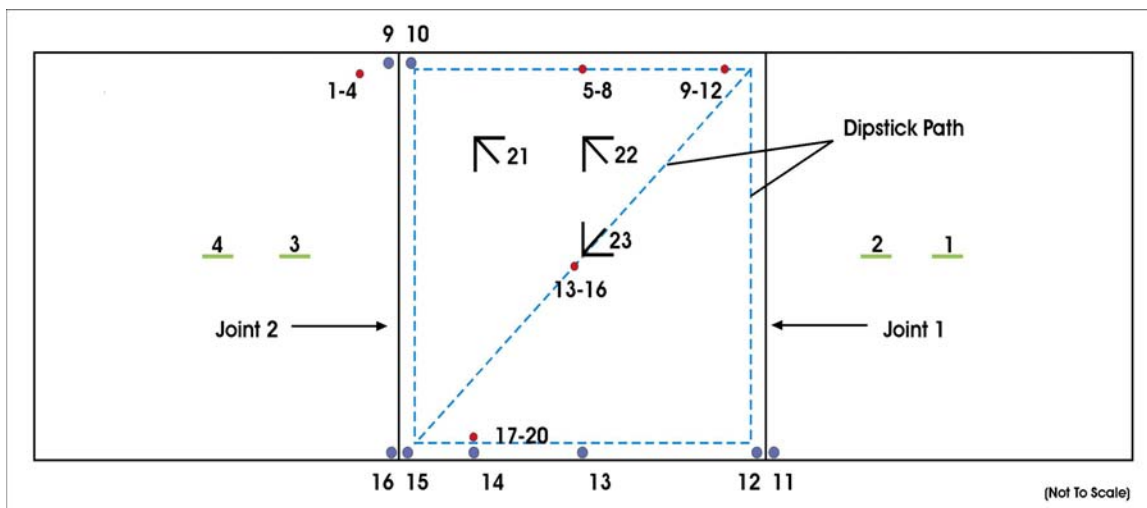


Figure 67. Dipstick Path on Pavement. Numbers indicate positions of measurement instrumentation.

After the initial curing period (Stage I) and temperature cycling (Stage II), rolling wheel loads of 9000 lb (40 kN), 12000 lb (53 kN), and 15000 lb (67 kN), traveling at 5 mph (8 km/h), were applied at five lateral positions or wheel paths with a super single tire. This period of the testing program was referred to as Stage III. The tire width equaled 13.5 inches (33.7 cm), and the tire pressure equaled 110 psi (758 kPa). These positions were at the nine nominal temperature conditions described in Table 13. The five test paths consisted of the pavement centerline, both wheel paths (30 inches (76 cm) from the pavement edges), and along the pavement edges. In terms of air temperature change, the maximum gradient was developed before running the super single tire. Because the tire speed was very low, the situation was treated as a static case. The application of the super single tire on the doweled pavement is shown in Figure 68.

Table 13. Nominal Temperature Conditions for Rolling Wheel Loads.

	Temperature Condition
1	Uniform temperature of 21°C (70°F)
2	Uniform temperature of 35°C (97°F)
3	Uniform temperature of 5°C (41°F)
4	Temperature rising from 20°C (68°F) to 35°C (97°F)
5	Temperature decreasing from 35°C (97°F) to 22°C (72°F)
6	Temperature decreasing from 22°C (72°F) to 5°C (41°F)
7	Temperature rising from 5°C (41°F) to 21°C (70°F)
8	Temperature rising from 4°C (40°F) to 35°C (97°F)
9	Temperature decreasing from 35°C (97°F) to 5°C (41°F)



Figure 68. Application of the Super Single Tire on Instrumented Pavement.

The time frame for each testing stage was as follows: Stage I extended from the testing hour 120 to the testing hour 838, Stage II fell directly after Stage I, and extended from hour 838 to hour 1319, and Stage III extended from hour 1765 to hour 2050.

The thermocouples were removed after the end of Stage II, and at the same time the rosette strain gauges were instrumented to measure the load induced strains in Stage III. LVDTs and vibrating wire strain gauges were installed over the entire testing period. Vibrating wire strain gauges provided temperature gradient and slab strain due to environmental loading through the entire time of testing. Figure 69 shows the slab temperature gradient during the full test time as measured by vibrating wire strain gauges. The slab top and bottom strains due to environmental changes are shown in Figure 70 through Figure 73 for strain gauges 1, 2, 3, and 4, respectively. The vibrating wire strain gauge temperature data as well as strain data were recorded every 30 minutes. The slab corner and edge deflections up to the end of Stage II, as measured by LVDTs, are also presented in Figure 74 and Figure 75, respectively. The positive reading implies an upward deflection, while the negative reading implies a downward deflection. An LVDT reading was obtained every 15 minutes. The corner deflection is the average of LVDTs 1, 2, 5, 6, 7, and 8, while the edge deflection is the average of LVDTs 2, 3, 4, and 5. For comparison purposes, Figure 76 shows the temperature gradient at the slab center through the end of Stage II as measured by thermocouples. Thermocouples data was recorded every 30 minutes. The slight difference between Figure 76 and Figure 69 for the same time period is because the thermocouples were installed at the top and the bottom of the slab, while the vibrating wire strain gauge were placed 1 inch (2.54 cm) above the bottom and 1 inch (2.54 cm) below the top of the slab. Detailed experimental data will be presented together with the finite element modeling data in the next sections.

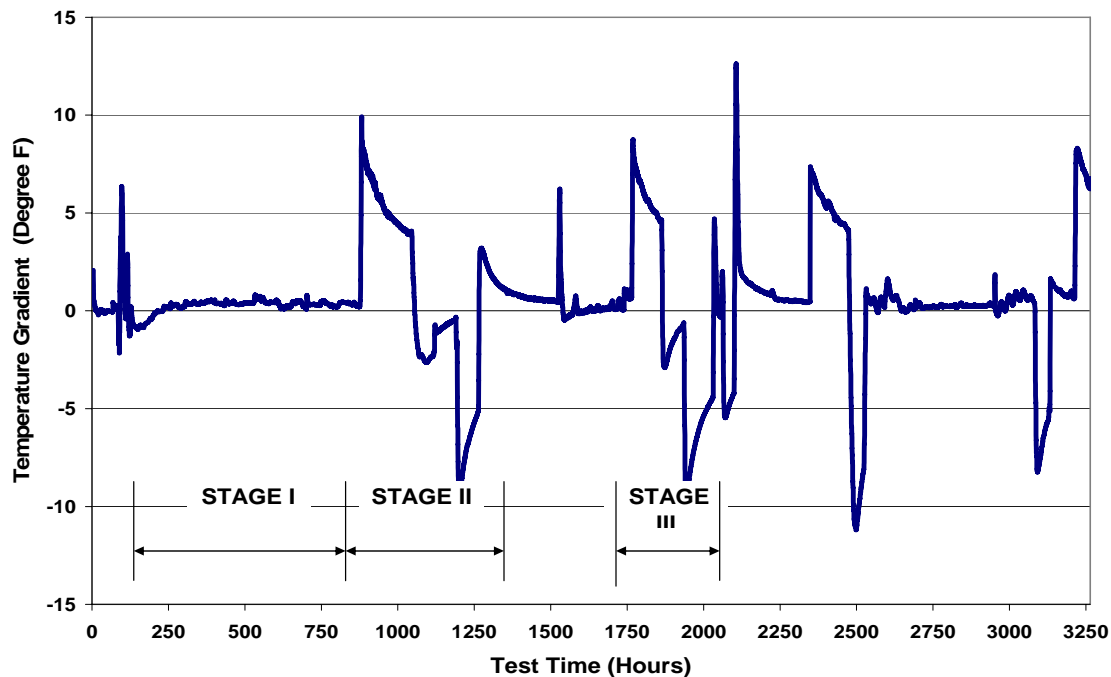


Figure 69. Average Slab Temperature Gradient at Vibrating Wire Strain Gauges (1F° = 0.55C°).

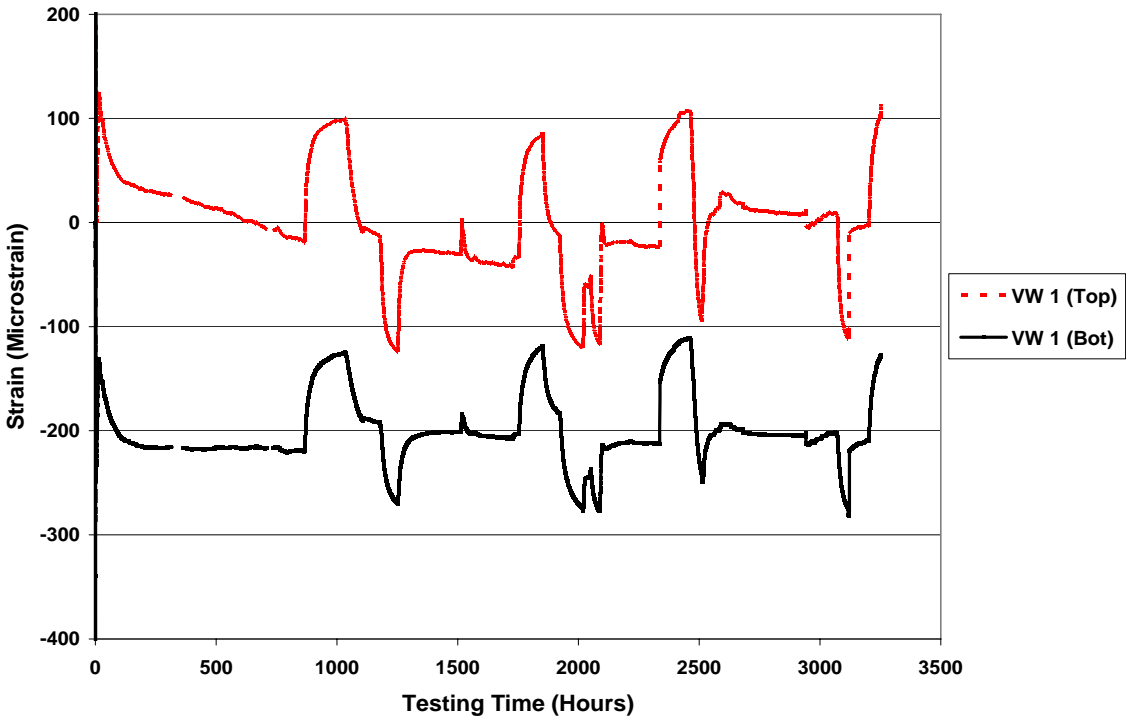


Figure 70. Top and Bottom Strain Development at Vibrating Wire Strain Gauge Location # 1.

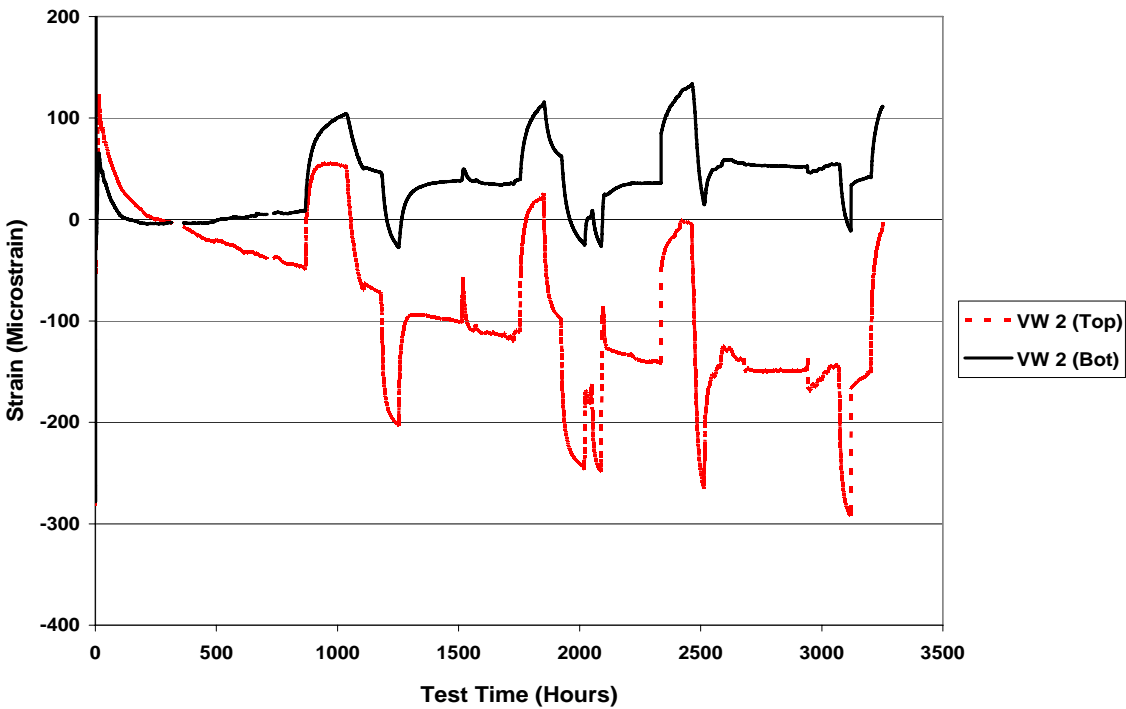


Figure 71. Top and Bottom Strain Development at Vibrating Wire Strain Gauge Location # 2.

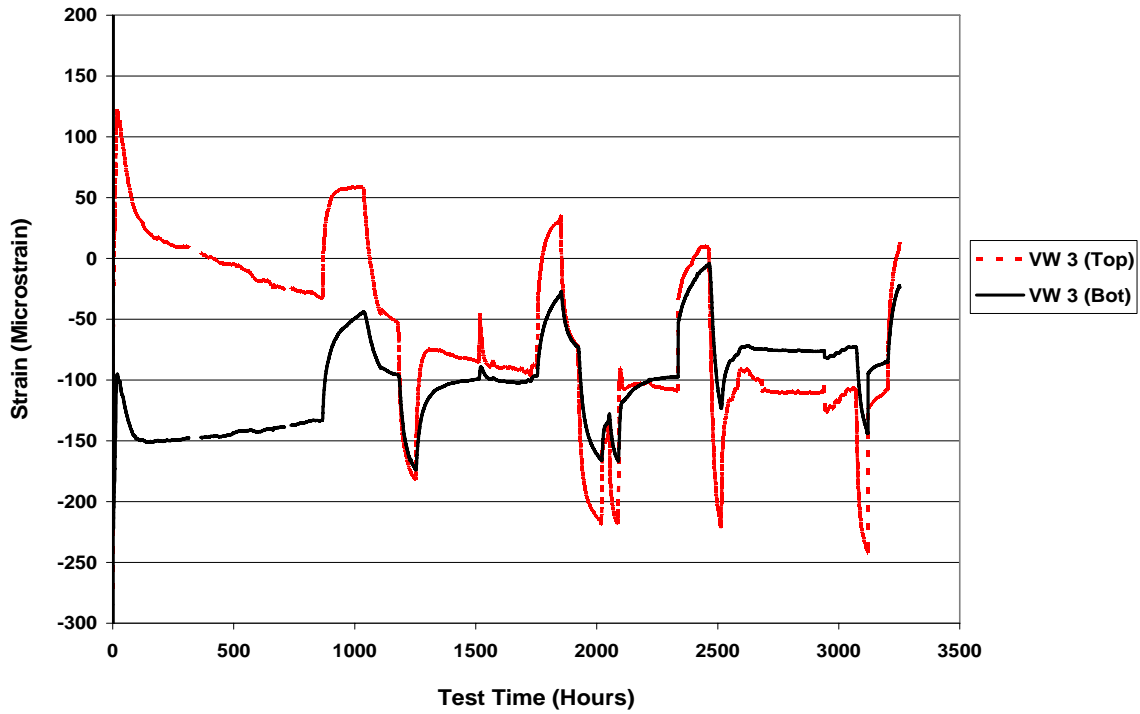


Figure 72. Top and Bottom Strain Development at Vibrating Wire Strain Gauge Location # 3.

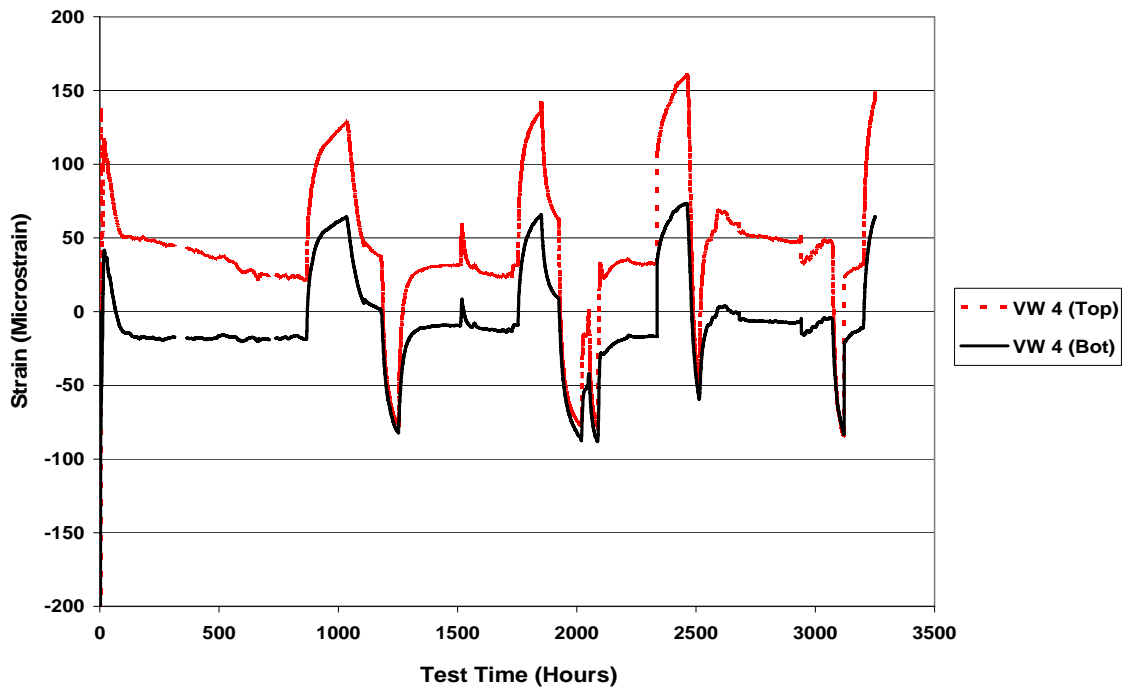


Figure 73. Top and Bottom Strain Development at Vibrating Wire Strain Gauge Location # 4.

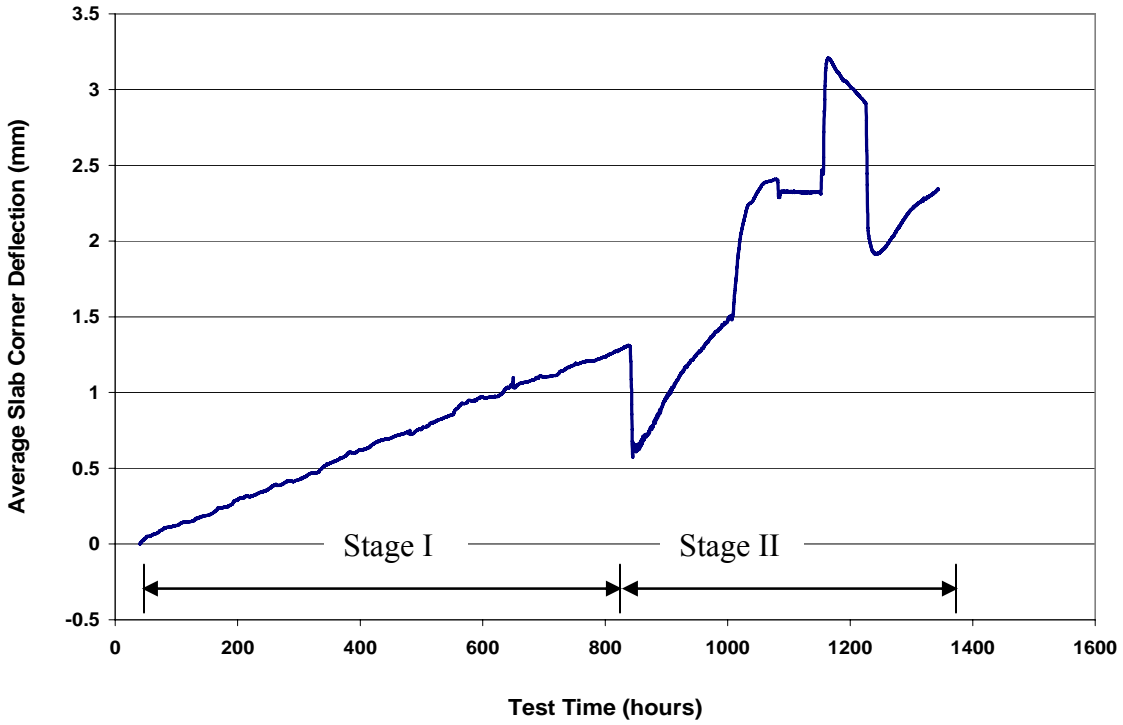


Figure 74. Average Slab Corner Deflection during Stages I and II (1 mm = 0.0394 inch).

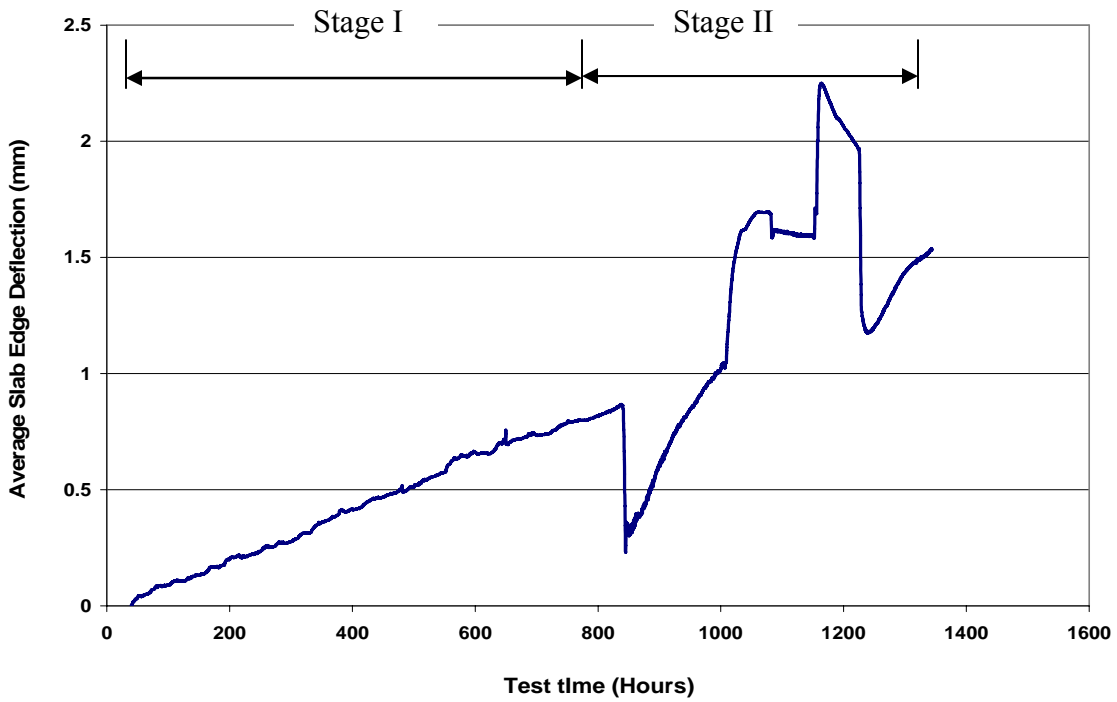


Figure 75. Average Slab Edge Deflection during Stages I and II (1mm = 0.039 in).

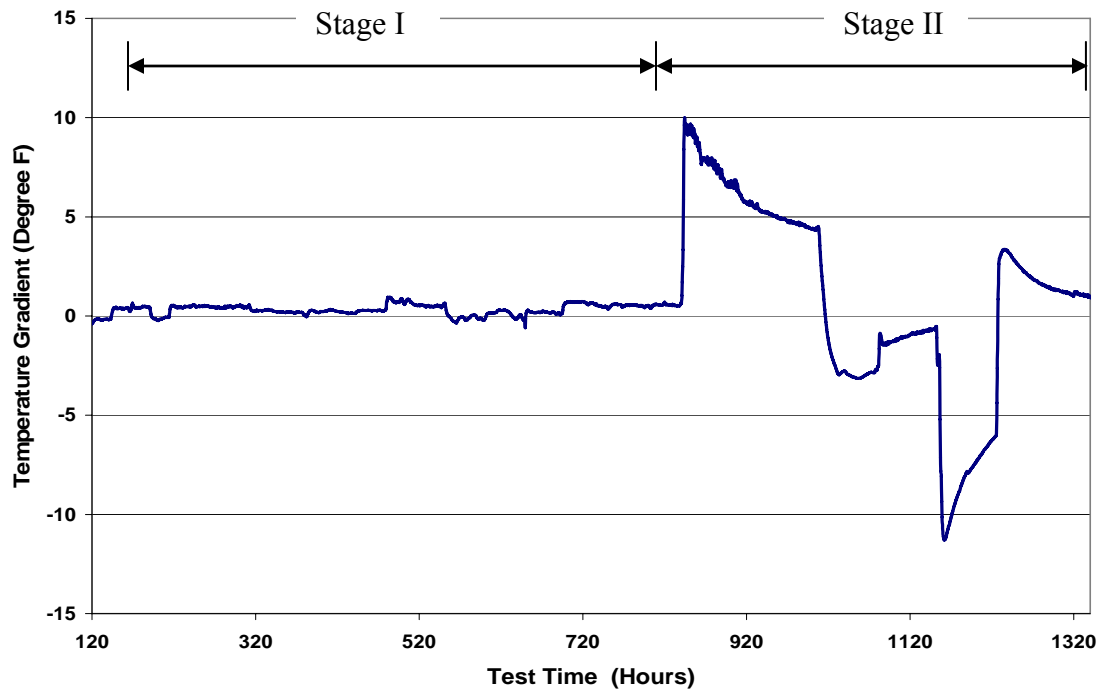


Figure 76. Temperature Gradient at the Slab Center as Measured by Thermocouple (1F° = 0.55C°).

4.3 EQUIVALENT TEMPERATURE GRADIENT DUE TO SLAB CURING

Portland cement concrete shrinks as it dries, essentially because water is removed as cement paste hardens. Moisture gradients in concrete pavements cause differential shrinkage between the top and the bottom of the pavement. Shrinkage causes upward warping, as moisture is lost primarily from the top of the slab. This leads to corner uplift and curling which results in the top of the pavement experiencing tension and the bottom of the pavement experiencing compression.

During the curing period, which lasted for five weeks, the air temperature in the APLF was kept constant. The temperature gradient within the slab thickness was approximately zero after 5 days (120 hours). Meanwhile, the average corner upward warping due to the moisture gradient was observed to be 1.3117 mm (0.0516 inch) at the end of the fifth week (Figure 74). This amount of warping can be simulated as a built-in negative temperature gradient. Using ISLAB2000, a number of temperatures were tried to match the calculated curling to the measured warping. A residual temperature gradient of -22F° (-12.2C°) gave a good match. This TG value is close to that obtained by Yu et al. (1995) (-20F° = -11.1C°, when adjusted to the sign convention used in this study). This warping would cause a permanent loss of support to the pavement. The trial built-in temperature gradients and the corresponding amount of curl are presented in Table 14 (English units) and Table 15 (metric units). The positive sign indicates an upward deflection.

Table 14. Trial Residual Temperature Gradients (English units).

Temperature Gradient (F°)	-18	-26	-20	-21	-23	-22
Upward Curl (mils)	36.2	63.4	42.5	45.7	53.9	50.0

Table 15. Trial Residual Temperature Gradients (metric units).

Temperature Gradient (C°)	-10.0	-14.4	-11.1	-11.7	-12.8	-12.2
Upward Curl (mm)	0.92	1.61	1.08	1.16	1.37	1.27

4.4 VERIFICATION FOR TEMPERATURE CYCLING – STAGE II

After the period of curing, a period of controlled temperature changes was applied from the fifth week to the eighth week. During this period, the air temperature was raised from 68°F (20°C) to 97°F (35°C) for one week after 838 hours of test time, decreased within 2 days back to 72°F (22°C) for 3 days, decreased further to 41°F (5°C) for 3 days, and eventually returned to 70°F (21°C). The temperature gradient within the slab thickness at the slab center is shown in Figure 77, which is a close-up of Figure 76. It should be mentioned that the maximum temperature gradient within the slab thickness occurred within a few hours of the time the air temperature was changed. Further, the gradient started to decrease as the temperature of the slab bottom surface started to follow the temperature of the slab top surface.

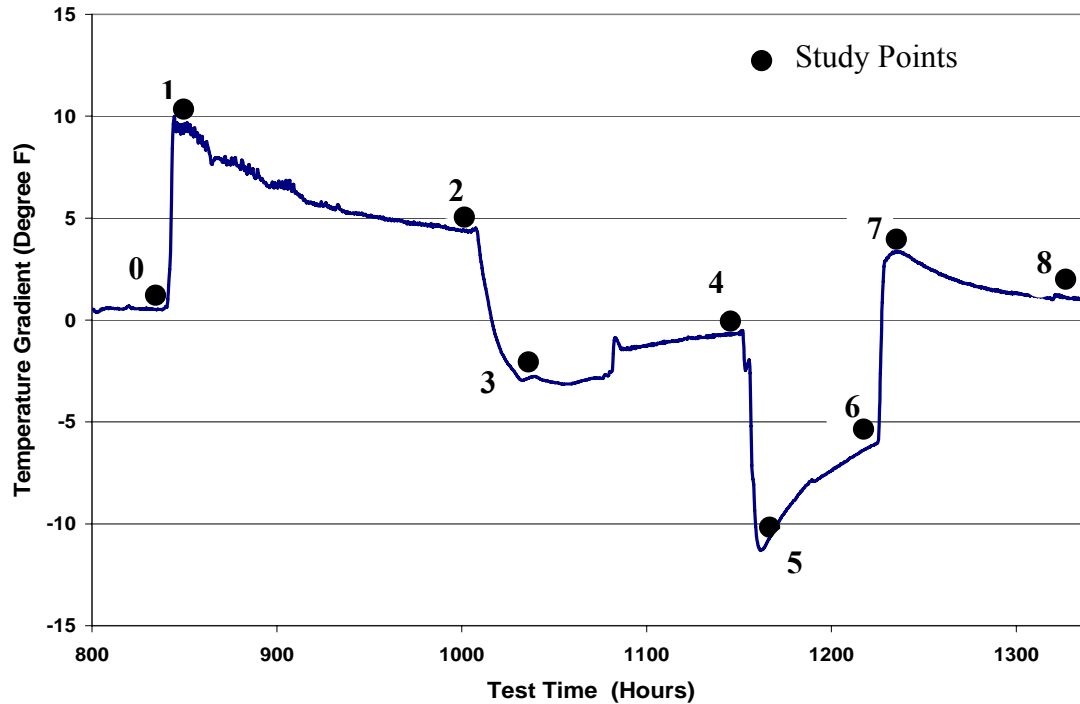


Figure 77. Temperature Gradient at the Slab Center during Stage II ($1F^{\circ} = 0.55C^{\circ}$).

Because the residual or equivalent temperature gradient from the curing period (ETG) is known, two approaches might be used to predict the pavement structural response under cycled temperature using ISLAB2000. The first approach is to assume a flat slab condition and to use the ETG as a reference gradient. For example, if the applied temperature gradient is $+10F^{\circ}$ ($5.55C^{\circ}$), then, the net temperature gradient value to be used in the model is $-22F^{\circ} + 10F^{\circ} = -12F^{\circ}$ ($-6.66C^{\circ}$). The second approach is to model the loss of support due to the curing period. In this case, the model uses the same temperature gradient as the experimental one, but in addition, uses the deformed slab shape as obtained after the curing period. Since the second approach models the field conditions closer, it was used in this study. The pavement response validation of ISLAB2000 was divided into two sections, validation of deflections and validation of strains.

4.4.1 VALIDATION OF DEFLECTION PREDICTIONS

To simplify the comparison process, slab deflections were predicted at nine key points in time. These key points, shown as black dots in Figure 77, present the maxima and minima as well as inflection points in the temperature gradient. Table 16 lists the selected key points and the corresponding temperature gradients. Positive temperature gradient occurs when the slab top surface is warmer than the bottom surface, which usually causes the slab to curl downward. In this case, the top surface is under compression stress while the bottom surface is under tension stress. The negative temperature gradient occurs when the slab top surface is cooler than the bottom surface, which usually causes the slab to lift upward. In this case, the top surface is under tension while the bottom surface is under compression. The measured corner deflection during Stage II, shown earlier in Figure 74, compared to Figure 76 implies that although the gradient at the beginning and end of Stage II is similar, the deflection of the corners is significantly different. This discrepancy is due to a combination of two influences. On one hand, there is an ongoing

moisture loss of the top pavement strata during Stage II that causes continuous rise of the corners. On the other hand, the deflection is based on the boundary conditions in terms of aggregate interlock in the transverse joints. The higher the absolute temperature of the pavement, the more aggregate interlock occurs, and the more the slab warping is restrained.

Table 16. Temperature Gradients for FE Analysis.

Point	0	1	2	3	4	5	6	7	8
Test Time (hours)	838	845	1007	1033	1152	1161	1225	1230	1319
Temperature Gradient (F°)	0.5	9.57	4.45	-2.97	-0.52	-11.21	-6.03	3.04	1
Relative Temperature Gradient (F°)	0	9.07	-5.12	-7.42	2.45	-10.69	5.18	9.07	-2.04
Temperature Gradient (C°)	0.28	5.32	2.47	-1.65	-0.29	-6.23	-3.35	1.69	0.56
Relative Temperature Gradient (C°)	0.00	5.04	-2.84	-4.12	1.36	-5.94	2.88	5.04	-1.13

For each of the nine key points, the model input parameters included: Geometry, Areas, Layers, Subgrade, Joints, Temperature, Load, Voids.

Geometry: Three slabs in the longitudinal direction, and one slab in the transverse direction, fine mesh with nominal element size of 3 in (7.5 cm).

Areas: This is to define the areas that have special input values. The areas will be used to define the Loss of Support (LOS) due to the moisture gradient, (ETG = -22F° (-12C°)).

Layers: 10 inches (25.4 cm) PCC over 6 inches (15.2 cm) DGAB over A-6 subgrade. Table 11 (English units) and Table 12 (metric units) include the material properties of these layers. Unbonded slab/base interface was selected to allow the slab curling, and thus, separation.

Subgrade: Winkler model with modulus of subgrade reaction 221 psi/inch (60 MPa/m).

Joints: Doweled joints. Aggregate interlock was ignored. The dowel bars were spaced 12 inches (30.5 cm) apart, 6 inches (15.2 cm) at the edges, and their properties are listed in Table 17. There are two dowel models available in ISLAB2000; The Guo model and the Tabatabaie model that was originally implemented in ILLISLAB. Both models treat the dowel as a beam element and adjust stiffness to account for dowel-concrete interaction. However, the models differ in the way this interaction is accounted for. The Tabatabaie model assumes an infinite length of the dowel bar to achieve that stiffness; in this case, the length of the dowel bar should be entered as zero. The Guo model, on the other hand, accounts for the length of the dowel bar, and exact length should be entered.

Temperature: The temperature gradient within the slab thickness is presented in Table 16. No temperature gradient was considered through the base.

Loads: No traffic loads.

voids: This is to specify the depth of voids under the PCC slab. The voids apply to the rectangular areas previously defined.

Table 17. Dowel Bar Properties for FE Analysis.

Diameter (in (cm))	Joints Width (in (cm))	Elastic Modulus (psi (MPa))	Length (in (cm))	Poisson's Ratio	Dowel Model
1.5 (3.81)	0.1 (0.25)	2.90 E+07 (2.00 E+05)	18 (40.7)	0.3	Guo Model

The crucial parameter is the voids parameter, which represents the LOS under the PCC slab. The actual LOS can be estimated using the Dipstick data recorded at the end of the curing period, i.e. the end of the fifth week, or at 838 hours. Figure 78 shows the Dipstick data across the slab diagonal measured after 838 and 1167 hours of test time. Notice that the end of the curing period occurred after 838 hours of test time, while the maximum positive gradient occurred after 845 hours, about 7 hours after the increase of the air temperature. This period of 7 hours was needed to achieve the maximum difference between the top and bottom surfaces of the slab. The slab deflections along the slab diagonal shown in Figure 78 were referenced to the deflection of the corner as a base line; however deflections should be referenced to zero deflection line. The horizontal distance of 38 feet represents the slab diagonal being measured twice, forward and backward. The horizontal dotted line at 0.0516 inch (1.3117 mm) represents the zero deflection line to separate between the upward and downward curling. It is shown that the upward lift across the diagonal is 3.5 feet (107 cm). As a sign convention, upward curling has a positive sign, and downward curling has a negative sign. Using simple geometry, and assuming symmetrical uplift, the upward curling can be found as 2.2 feet (67 cm) in the longitudinal direction, and 2.7 feet (82 cm) in the transverse direction, as shown in Figure 79. ISLAB2000 considers rectangular LOS only. The LOS model is shown in Figure 80; the hatched area represents unsupported areas.

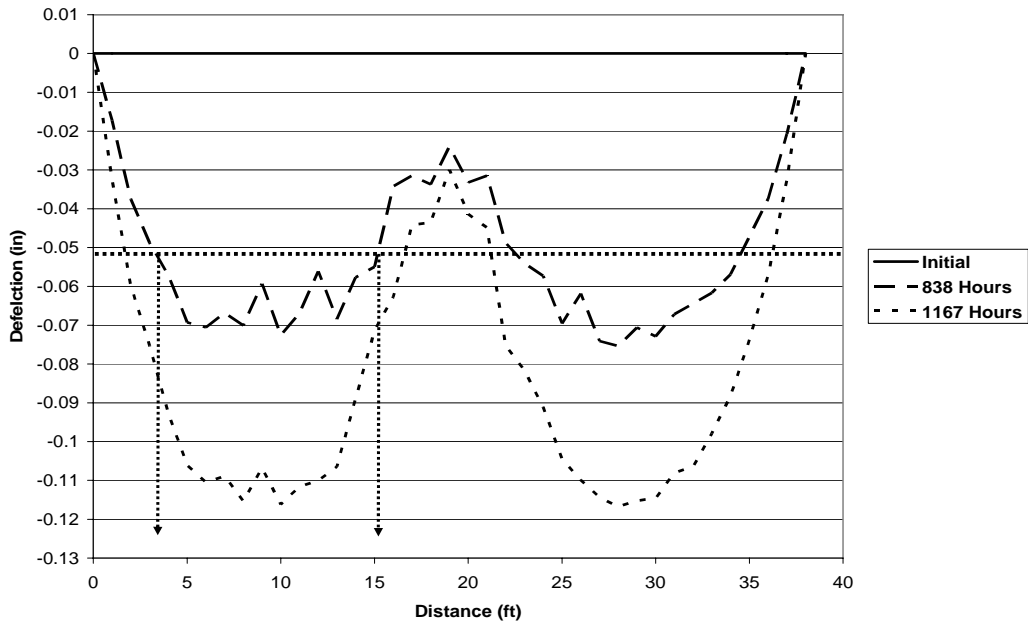


Figure 78. Dipstick Profile along Diagonal Path on Slab (1 inch = 25.4 mm; 1 ft = 0.305 m).



Figure 79. Upward Curling along the Diagonal. (left in English units, right in metric units).

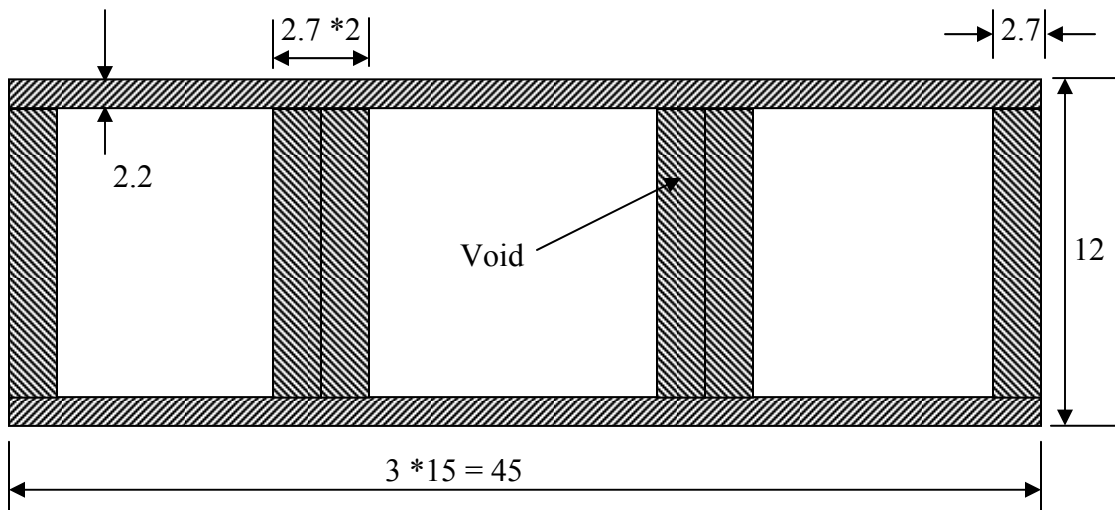


Figure 80. Loss of Support Model (Dimensions in feet, 1 foot = 0.305 m).

When comparing the predicted corner deflection to the measured ones, relative values of TG and relative change in the corner deflection should be considered instead of absolute values. For example, if the TG changed from 9.5°F (5.3°C) to 4.4°F (2.4°C), then, a TG of -5.1°F (-2.8°C)

should be used. This approach simulates the actual change in TG that the pavement experienced. The actual and relative temperature gradients are shown in Table 16 above.

The average measured corner deflection from the LVDTs 1, 2, 5, 6, 7, 8 and the average predicted corner deflections from ISLAB2000 are listed in Table 18. The comparison plot is shown in Figure 81. Positive deflection values indicate an upward deflection.

Table 18. Measured and Predicted Average Corner Deflection.

Test Points	Measured corner deflection		Measured Corner Deflection Relative to Point 0		Predicted Relative Corner Deflection	
	(mils)	(mm)	(mils)	(mm)	(mils)	(mm)
Point 0 (838 hrs)	51.64	1.311753				
Point 1 (845 hrs)	22.59	0.573835	-29.05	-0.7379	-31.75	-0.8064
Point 2 (1007 hrs)	58.31	1.481094	35.72	0.9072	17.96	0.4561
Point 3 (1033 hrs)	88.02	2.23572	29.71	0.7546	25.99	0.6601
Point 4 (1152 hrs)	91.04	2.31236	3.02	0.0766	-8.54	-0.2168
Point 5 (1161 hrs)	124.81	3.17022	33.77	0.8578	37.53	0.9532
Point 6 (1225 hrs)	114.77	2.915051	-10.04	-0.2551	-18.13	-0.4605
Point 7 (1230 hrs)	80.34	2.040529	-34.43	-0.8745	-31.73	-0.806
Point 8 (1319 hrs)	89.09	2.262906	8.75	0.2223	7.20	0.183

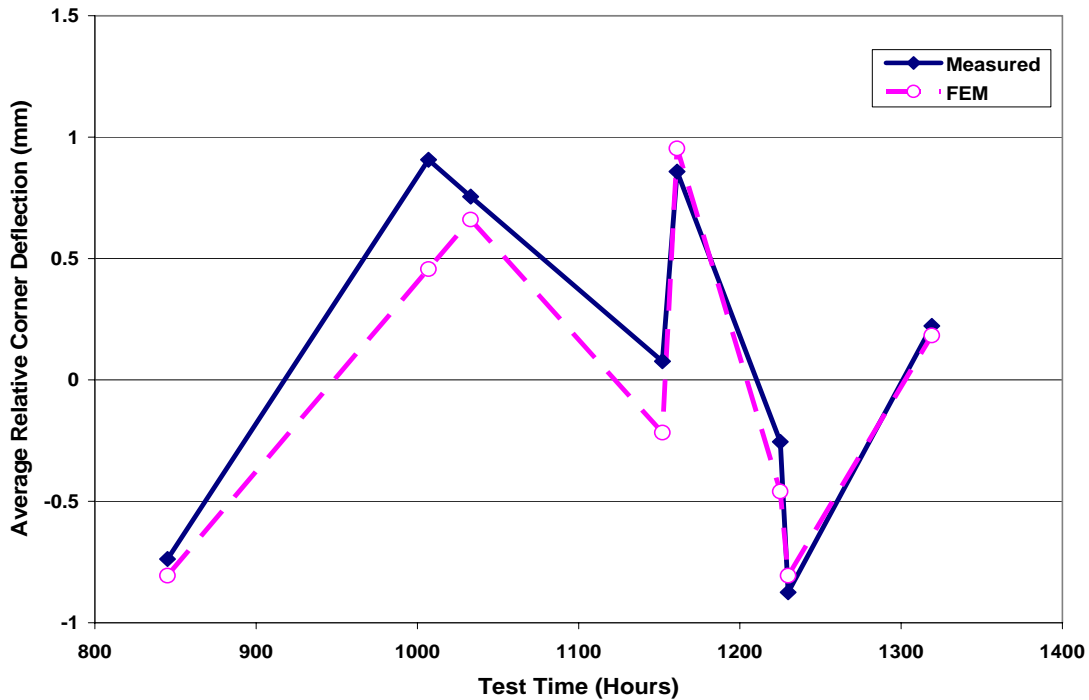


Figure 81. Predicted and Measured Average Corner Deflection versus Test Time (1 mm = 0.0394 inch).

In general, the finite element modeling using the LOS described earlier showed good agreement with the measured deflections in Figure 81. The differences between measured and predicted values can be justified by the combination of two factors. First, as mentioned earlier, there is an ongoing warping process during Stage II, which is clear from Figure 74. Warping during Stage II caused an additional rise in corner deflection of more than .039 in (1.0 mm), as clearly shown in the values measured at Point 4. Second, the LOS defined in Figure 80 was used in all the nine test points. However, when the slab was subjected to a positive TG, the pavement experienced a smaller LOS. This is clearly shown in the disagreement of deflection at Point 2.

4.4.2 VALIDATION OF STRAIN PREDICTIONS

The same procedure as in the previous section was used here to validate ISLAB2000 predictions of the pavement strains during Stage II. Although the LOS was derived from the corner deflection, it is still appropriate for strain determination as it showed good deflection agreement. The relative measured and predicted top and bottom strain values at the slab center (average of location # 1 & 4) and the slab third point (average of location # 2 & 3) are shown in Table 19 and Table 20, respectively. The positive strain means tension, and the negative means compression. The presence of tension stresses on the top of the slab and compression stresses on the bottom of the slab in the finite element predictions is due to the presence of negative TG all the time, or LOS.

Table 19. Comparison of Strain Test Reading with FE Analysis at Slab Center.

Test Point	Measured Strain (Microstrain)		Relative Measured Strain (Microstrain)		Predicted Strain (Microstrain)	
	Top	Bottom	Top	Bottom	Top	Bottom
0	-1.6	23.3	0	0	0	0
1	30.6	45.7	32.2	22.4	13.6	-13.6
2	111.4	112.5	80.8	66.8	26.2	-26.2
3	67.4	84.1	-44	-28.4	28.3	-28.3
4	10.0	47.8	-57.4	-36.3	19.5	-19.5
5	-27.4	28.3	-37.4	-19.5	31.1	-31.1
6	-102.4	-33.1	-75	-61.4	16.9	-16.9
7	-70.7	-19.7	31.7	13.4	13.6	-13.6
8	-1.8	35.3	68.9	55.0	23.4	-23.4

Table 20. Comparison of Strain Test Reading with FE at Slab Third Point.

Test Point	Measured Strain (Microstrain)		Relative Measured Strain (Microstrain)		Predicted Strain (Microstrain)	
	Top	Bottom	Top	Bottom	Top	Bottom
0	-51.0	39.7	0	0	0	0
1	-15.7	56.5	35.3	16.8	15.2	-15.2
2	45.2	132.0	60.9	75.5	23.4	-23.4
3	-13.2	113.9	-58.4	-18.1	24.9	-24.9
4	-72.5	77.7	-59.3	-36.2	19.3	-19.3
5	-131.4	67.8	-58.9	-9.9	26.7	-26.7
6	-202.4	1.9	-71	-65.9	17.6	-17.6
7	-159.6	7.4	42.8	5.5	15.2	-15.2
8	-95.2	65.0	64.4	57.6	21.9	-21.9

In order to compare the vibrating wire readings with the analysis, a certain amount of strain should be added to or subtracted from the model strain output due to the change in joint opening. This amount for all specific key points was calculated by multiplying the temperature difference of two consecutive (top and bottom) points by the coefficient of thermal expansion ($6.66 \text{ E-}06 \text{ F}^{-1}$ ($12 \text{ E-}06 \text{ C}^{-1}$)), which was determined experimentally. The relative measured, predicted, and corrected predicted strains at the slab top and bottom are presented in Table 21 and Table 22 for locations at slab center and slab third point respectively.

Table 21. Correction of Predicted Strain at Slab Center.

Test Point	Relative Measured Strain (Microstrain)		Predicted Strain (Microstrain)		Corrected Predicted Strain (Microstrain)	
	Top	Bottom	Top	Bottom	Top	Bottom
0	0	0	0	0	0	0
1	32.2	22.4	13.6	-13.6	66.9	16.37
2	80.8	66.8	26.2	-26.2	101.3	87.3
3	-44	-28.4	28.3	-28.3	-47.2	-53.4
4	-57.4	-36.3	19.5	-19.5	-47.6	-55.1
5	-37.4	-19.5	31.1	-31.1	-59.6	-51.8
6	-75	-61.4	16.9	-16.9	-47.3	-90.8
7	31.7	13.4	13.6	-13.6	67.1	5.6
8	68.9	55	23.4	-23.4	86.9	54.5

Table 22. Correction of Predicted Strain at Slab Third Point.

Test Point	Relative Measured Strain (Microstrain)		Predicted Strain (Microstrain)		Corrected Predicted Strain (Microstrain)	
	Top	Bottom	Top	Bottom	Top	Bottom
0	0	0	0	0	0	0
1	35.3	16.8	15.2	-15.2	71.9	7.57
2	60.9	75.5	23.4	-23.4	83.3	87.6
3	-58.4	-18.1	24.9	-24.9	-43.4	-40.0
4	-59.3	-36.2	19.3	-19.3	-46.6	-54.4
5	-58.9	-9.9	26.7	-26.7	-76.4	-25.1
6	-71	-65.9	17.6	-17.6	-36.4	-92.9
7	42.8	5.5	15.2	-15.2	68.4	3.02
8	64.4	57.6	21.9	-21.9	85.4	54.8

The above strain values are plotted in Figure 82 through Figure 85. The plots show fairly good trend agreement. The divergence at some points can be explained by the approximate values used for material properties of base and subgrade, and the ongoing moisture loss, which was not accounted for in the analysis. This is clearly seen in the values of measured strain at point 4 where the temperature gradient is almost zero. On the other hand, the disagreement implies that the joint response to the temperature variations, a key issue in strain analysis, cannot be modeled correctly in ISLAB2000.

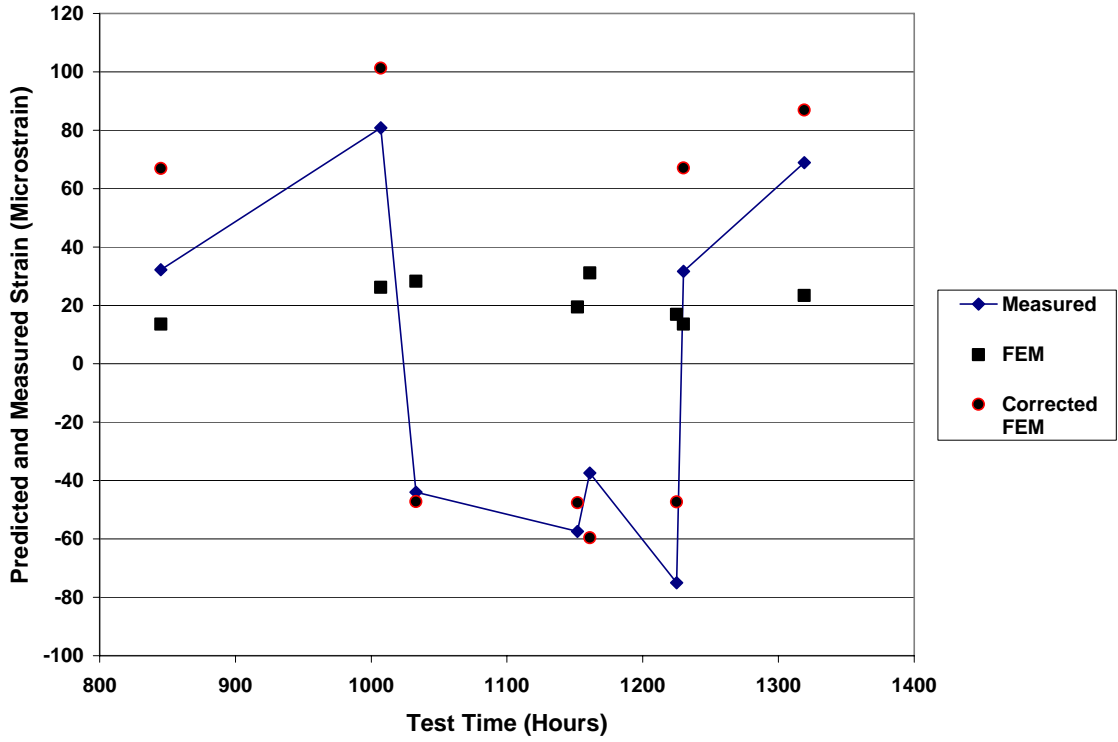


Figure 82. Strain Predictions at the Slab Center, at the Top of Slab.

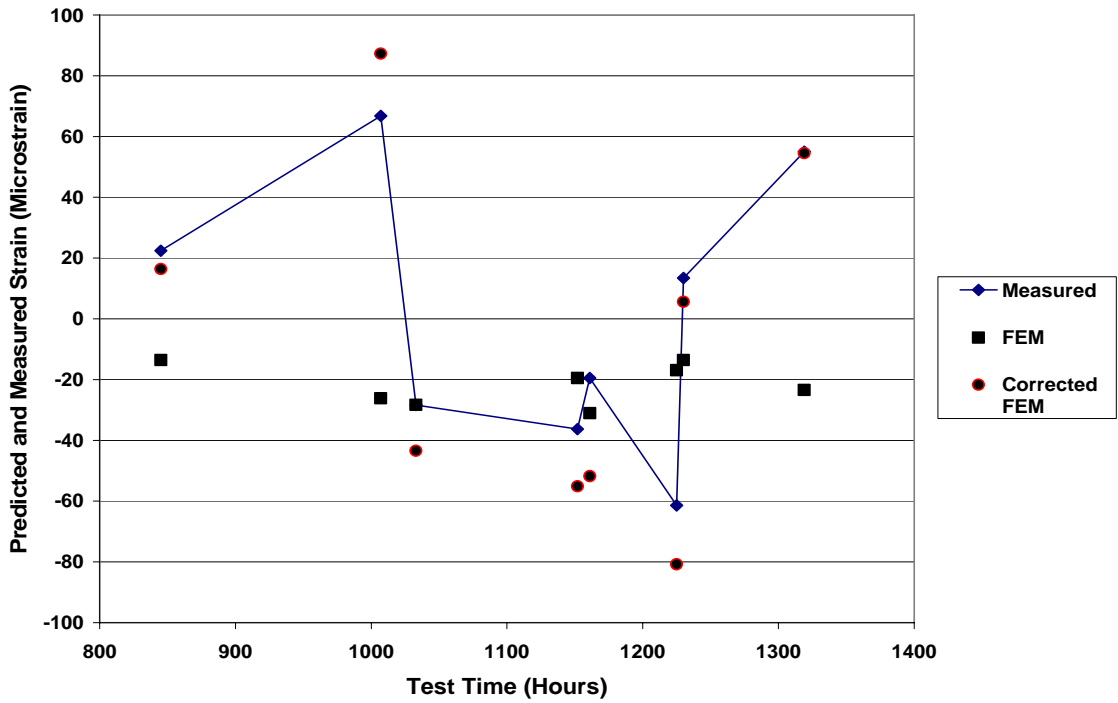


Figure 83. Strain Predictions at the Slab Center, at the Bottom of Slab.

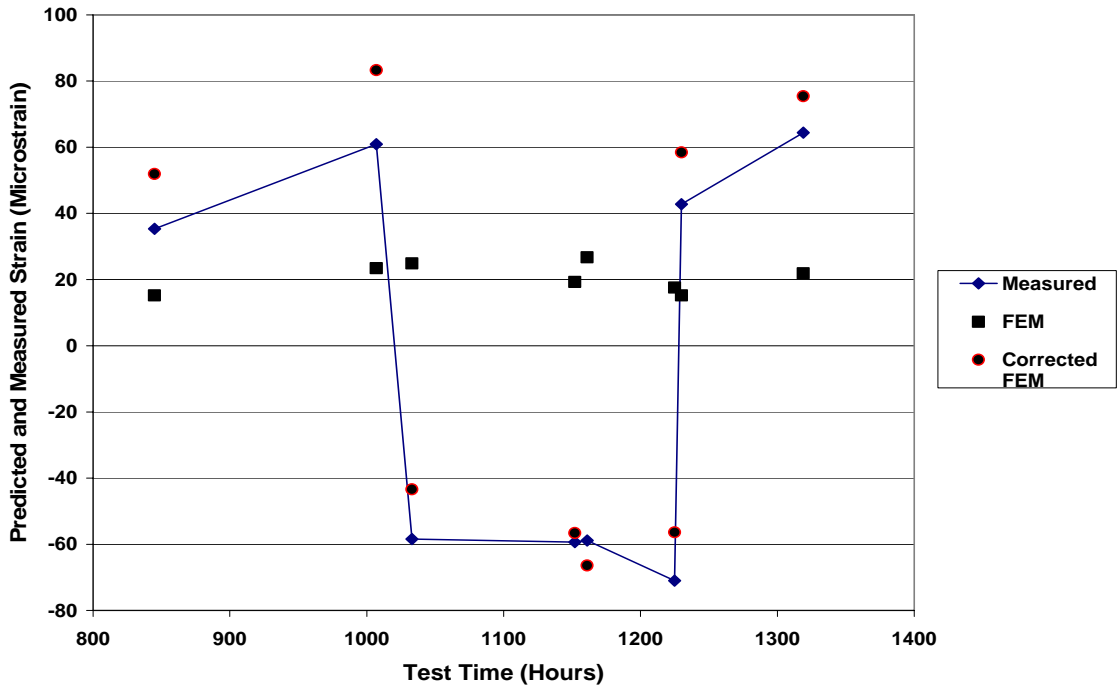


Figure 84. Strain Predictions at the Slab Third Point, at the Top of Slab.

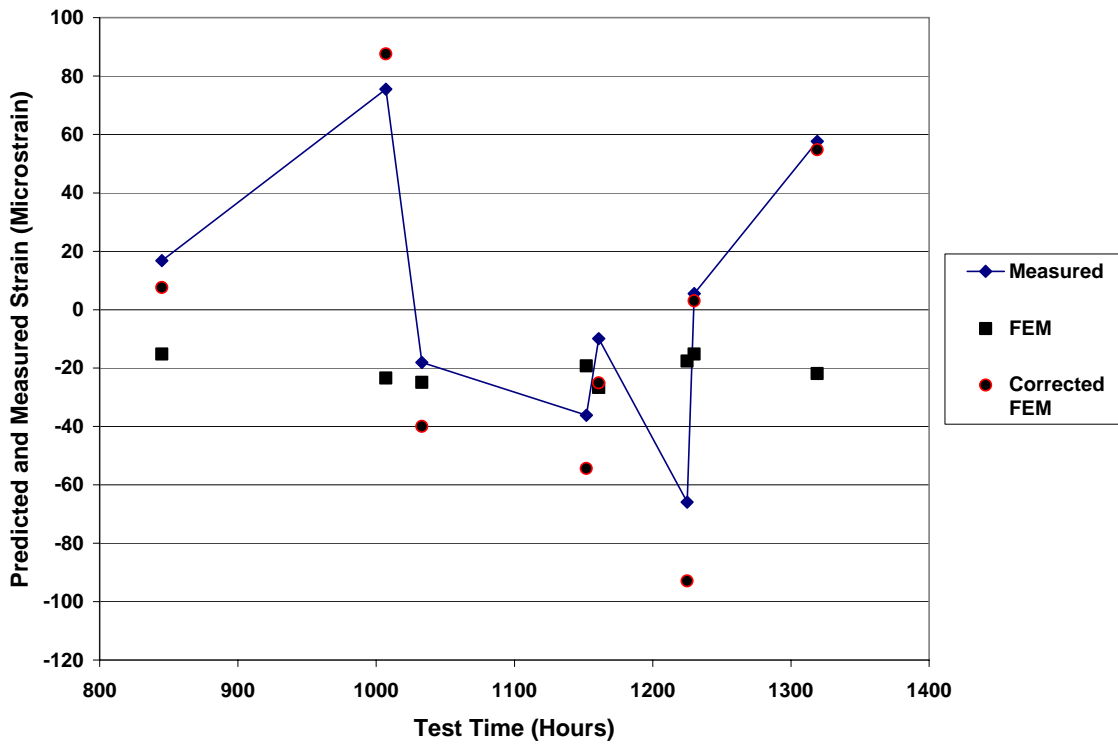


Figure 85. Strain Predictions at the Slab Third Point, at the Bottom of Slab.

4.5 VERIFICATION FOR COMBINED LOAD AND TEMP. – STAGE III

The verification and validation of ISLAB2000 for combined effect of environmental and traffic loads was done in this section. The first step was to obtain the TG during Stage III, shown in Figure 86. The TG in Figure 86 was monitored by VW gauges, and represents the average TG at VW locations 1, 2, 3, and 4. There are more than 135 combinations of traffic and environmental test results, including 9 temperature conditions (shown in Table 13), 5 wheel paths, and 3 tire load values. Because of a lack of sufficient resources to check all these cases, a set of representative cases was studied. The experimental data included the corner deflection due to combined effect, the strain due to the load passes obtained by the rosette strain gauges, and the environmental strain monitored by VW gauges. It should be mentioned that the experimental tire footprints showed a non-uniform pressure distribution since the tire edges have a higher stiffness.

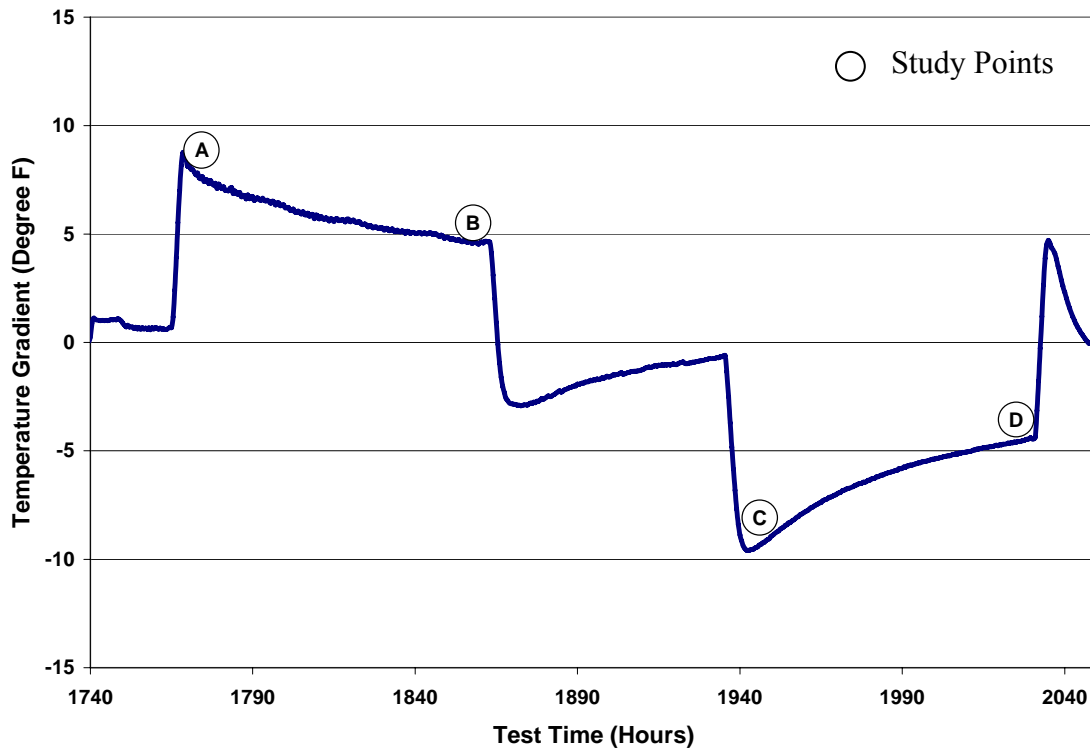


Figure 86. Average Slab Temperature Gradient during Stage III ($1F^{\circ} = 0.55C^{\circ}$).

4.5.1 VALIDATION OF DEFLECTION PREDICTIONS

The experimental data chosen to validate the combined deflection predictions included four temperature cases, presented by letters A through D in Figure 86, two tire paths, one at the edge (P1), and the other in a wheel path 30 in (76.2 cm) from the edge (P2) as in Figure 66, and randomly chosen tire load values. The experimental data showed the deflection of the slab corners and edge due to tire load in reference to the curled shape due to the environmental effect. Since the expected deflection is downward, a positive value means downward deflection, while a negative value means upward deflection. No Dipstick data were available to determine the actual loss of support, thus, a reasonable estimated loss of support (LOS) had to be assumed. For points

A & B, and as concluded from the previous section, it is relevant to use a smaller LOS than the one used in Stage II because of the positive gradient. Hence, 2.0 feet by 1.5 feet (61 cm by 46 cm) can be used, where 2.0 feet (61 cm) is the curled distance from each side of the slab in the longitudinal direction, and 1.5 feet (46 cm) is the curled distance from each side in the transverse direction. For points C & D, 2.7 feet by 2.2 feet (82 cm by 67 cm) can be used because this LOS showed good agreement at negative gradients in Stage II.

To clarify the cases, Table 23 (English units) and Table 24 (metric units) list each case with corresponding properties. Figure 87 through Figure 94 show the experimental and predicted deflections. The numbers 1, 4, and 5 in the plot legends refer to the sensor locations in Figure 66. The horizontal distance represents the path traveled by the tire relative to the right joint of the middle slab.

Table 23. Cases used for Deflection Validation (English units). Tire Path P1 is along the edge and Tire Path P2 is in the wheel path 1 ft (30 cm) from the edge.

Point	Case No.	Tire Load (lb)	Tire Path	T.G. (F°)	Actual T.G. (F°)	LOS (Long.-ft, Transv.-ft)	Air Temp. (°F)
A	1	12000	P1	8.5	-13.5	(2.0, 1.5)	70-100
	2	9000	P2	8.5	-13.5	(2.0, 1.5)	70-100
B	3	15000	P1	4.7	-17.3	(2.0, 1.5)	100
	4	12000	P2	4.7	-17.3	(2.0, 1.5)	100
C	5	12000	P1	-9.5	-31.5	(2.7, 2.2)	70-40
	6	12000	P2	-9.5	-31.5	(2.7, 2.2)	70-40
D	7	12000	P1	-4.4	-26.4	(2.7, 2.2)	40
	8	12000	P2	-4.4	-26.4	(2.7, 2.2)	40

Table 24. Cases used for Deflection Validation (metric units). Tire Path P1 is along the edge and Tire Path P2 is in the wheel path 1 ft (30 cm) from the edge.

Point	Case No.	Tire Load (N)	Tire Path	T.G. (C°)	Actual T.G. (C°)	LOS (Long.-m, Transv.-m)	Air Temp. (°C)
A	1	53.38	P1	4.72	-7.50	(0.61, 0.46)	21.1-37.8
	2	40.03	P2	4.72	-7.50	(0.61, 0.46)	21.1-37.8
B	3	66.72	P1	2.61	-9.61	(0.61, 0.46)	37.8
	4	53.38	P2	2.61	-9.61	(0.61, 0.46)	37.8
C	5	53.38	P1	-5.28	-17.50	(0.82, 0.67)	21.1-4.4
	6	53.38	P2	-5.28	-17.50	(0.82, 0.67)	21.1-4.4
D	7	53.38	P1	-2.44	-14.67	(0.82, 0.67)	4.4
	8	53.38	P2	-2.44	-14.67	(0.82, 0.67)	4.4

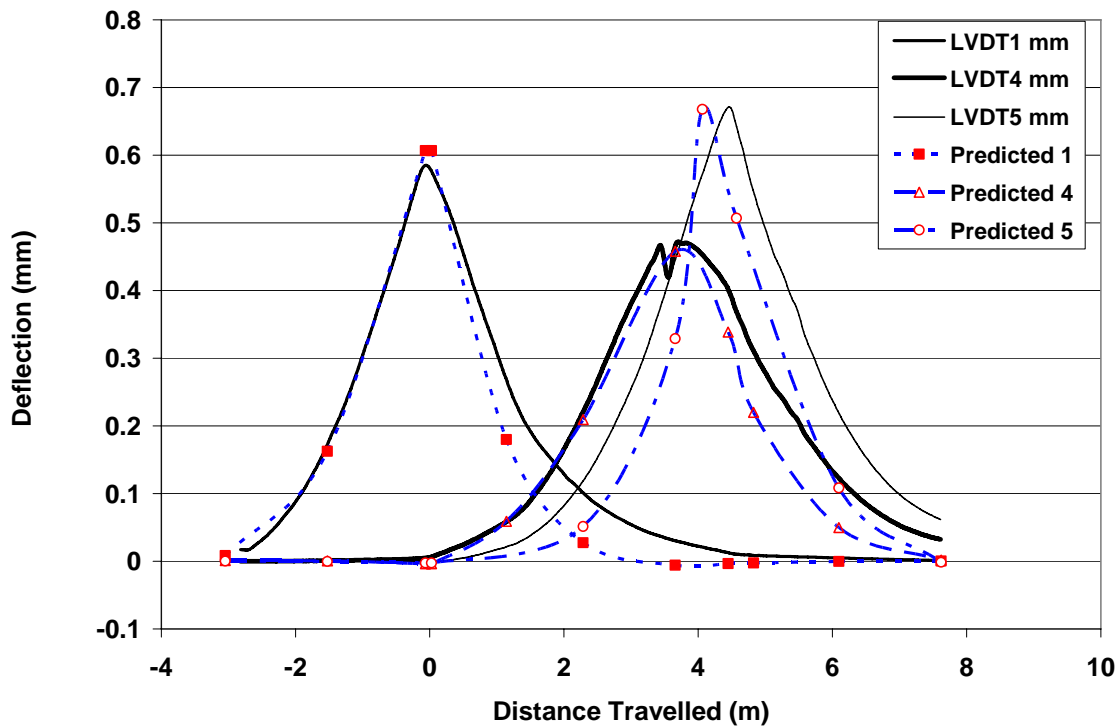
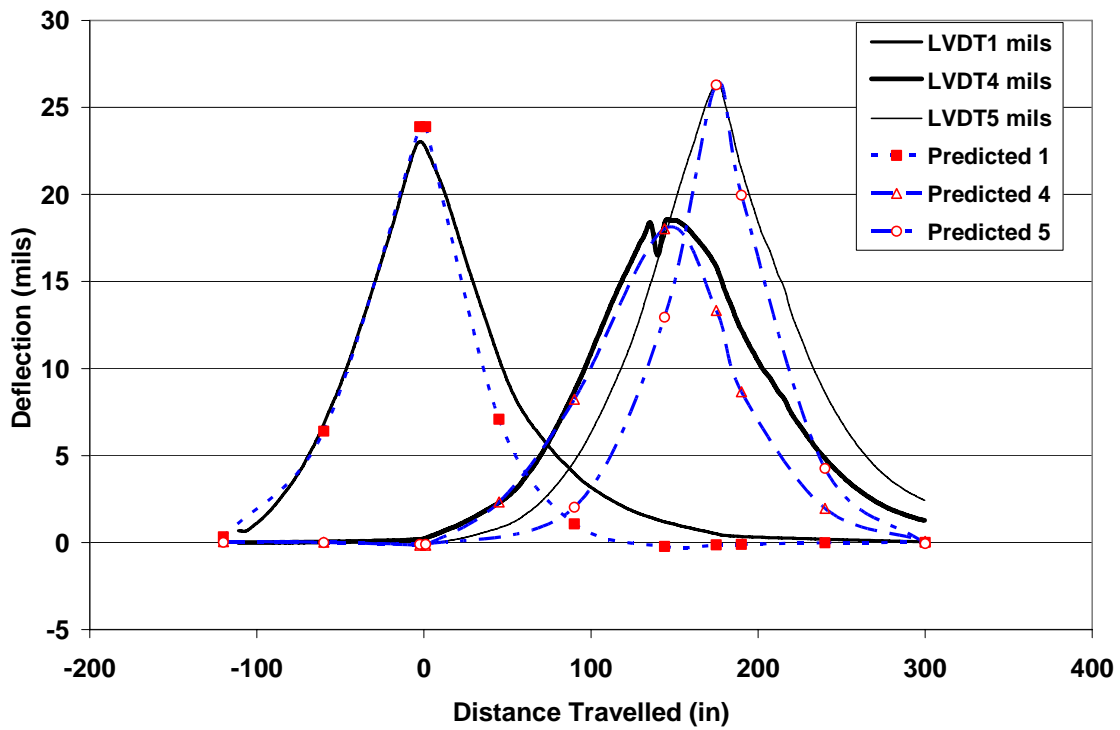


Figure 87. Comparison between Measured and Combined Deflections along edge at study point A. Top: English units; bottom: metric units.

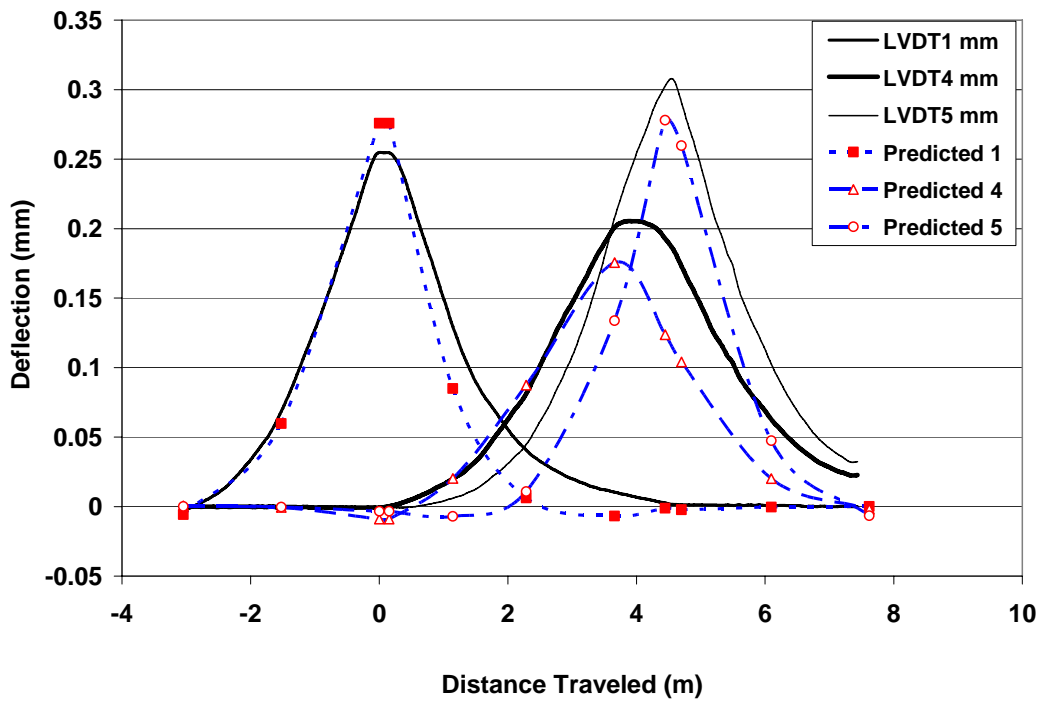
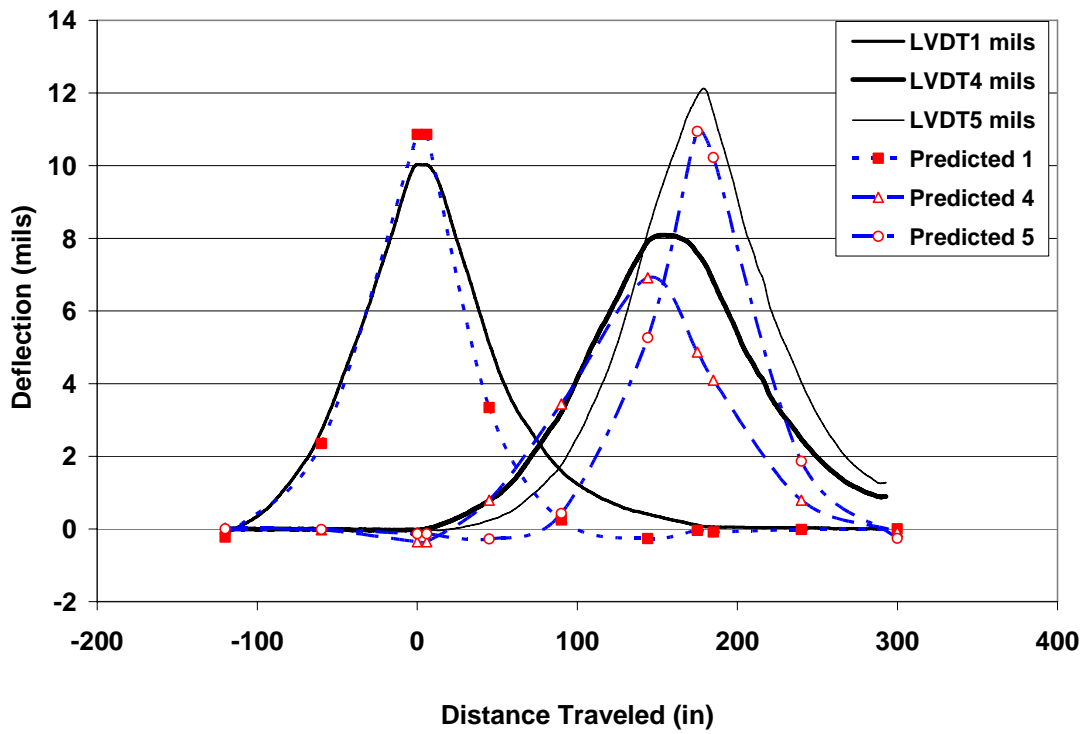


Figure 88. Comparison between Measured and Combined Deflections along wheel path at study point A. Top: English units; bottom: metric units.

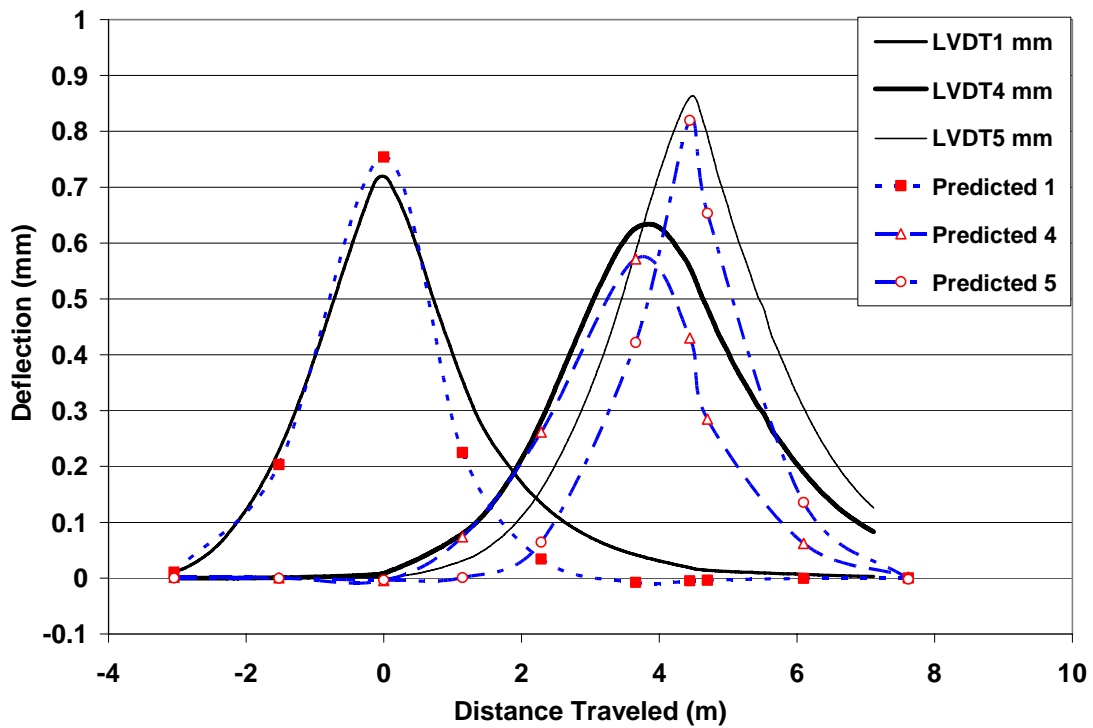
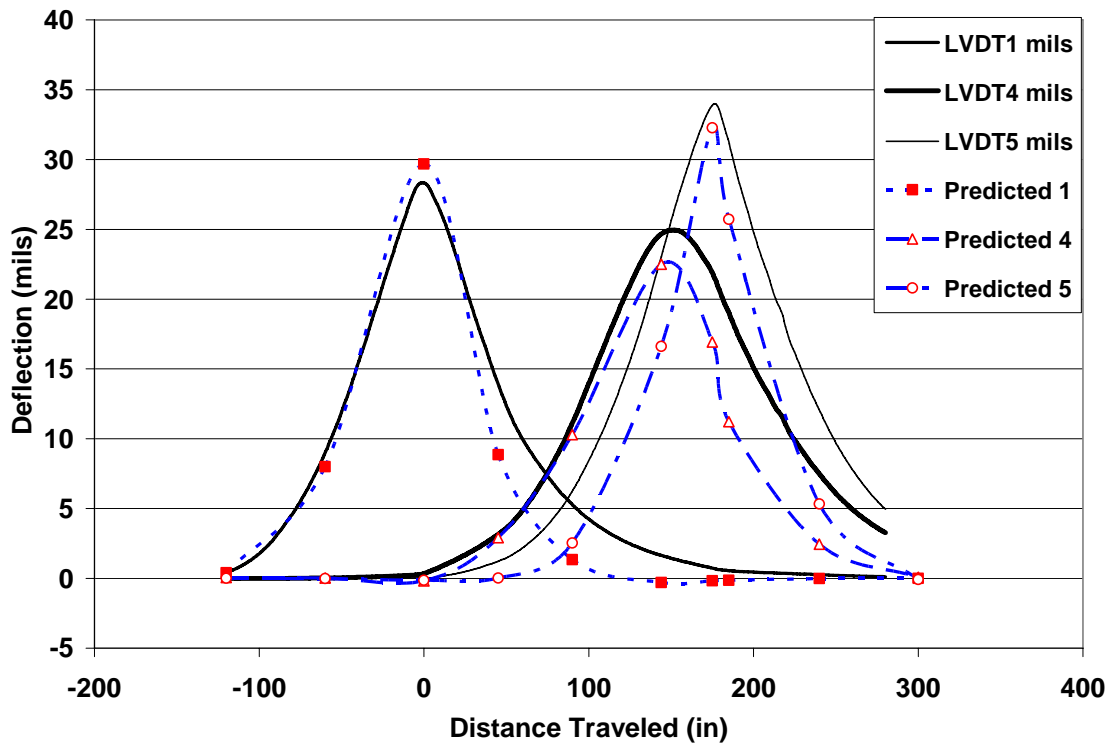


Figure 89. Comparison between Measured and Combined Deflections along edge at study point B. Top: English units; bottom: metric units.

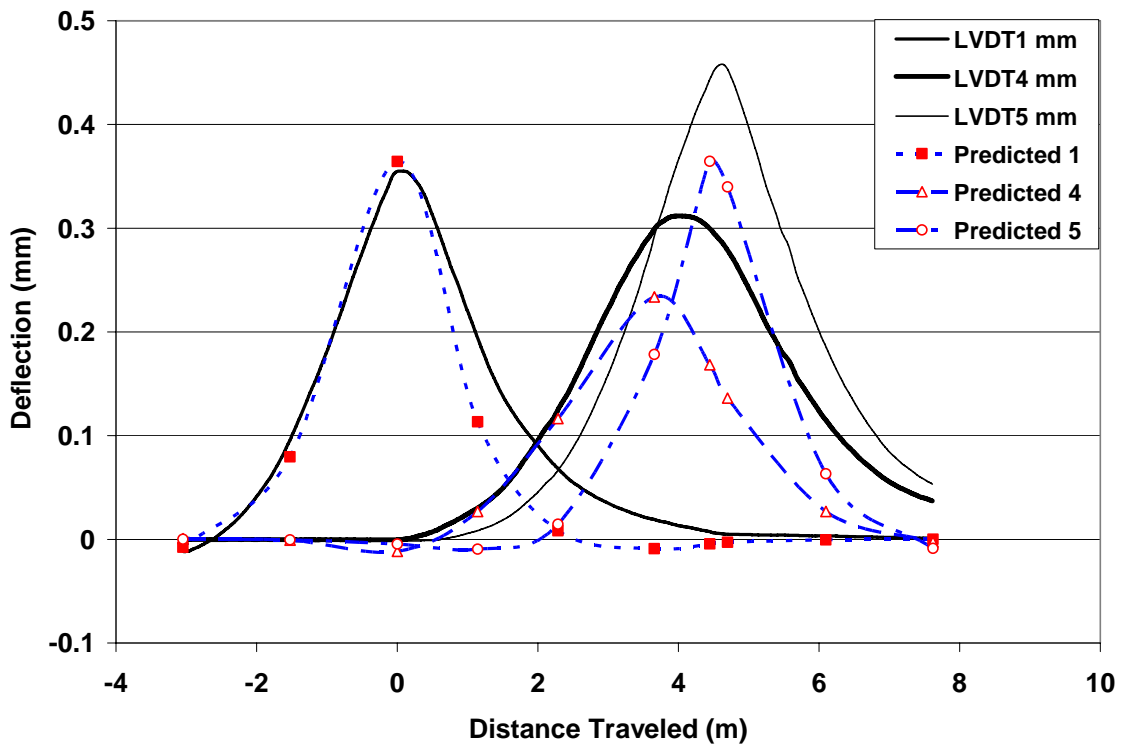
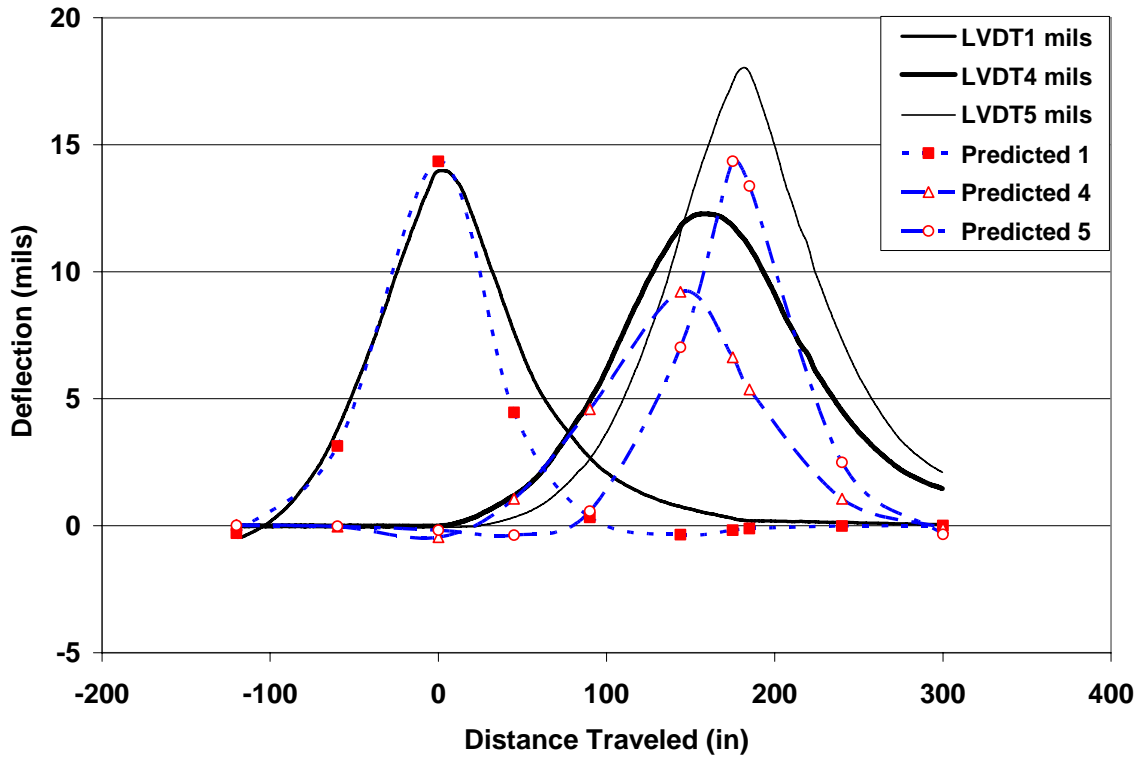


Figure 90. Comparison between Measured and Combined Deflections along wheel path at study point B Top: English units; bottom: metric units.

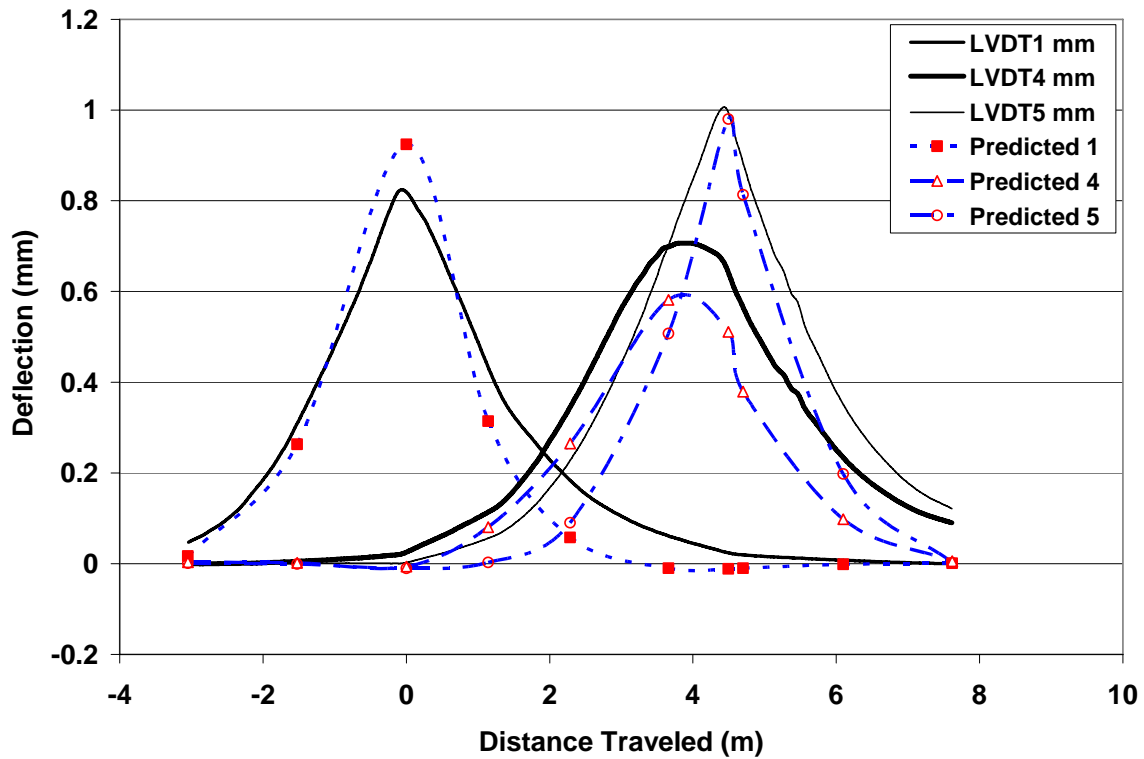
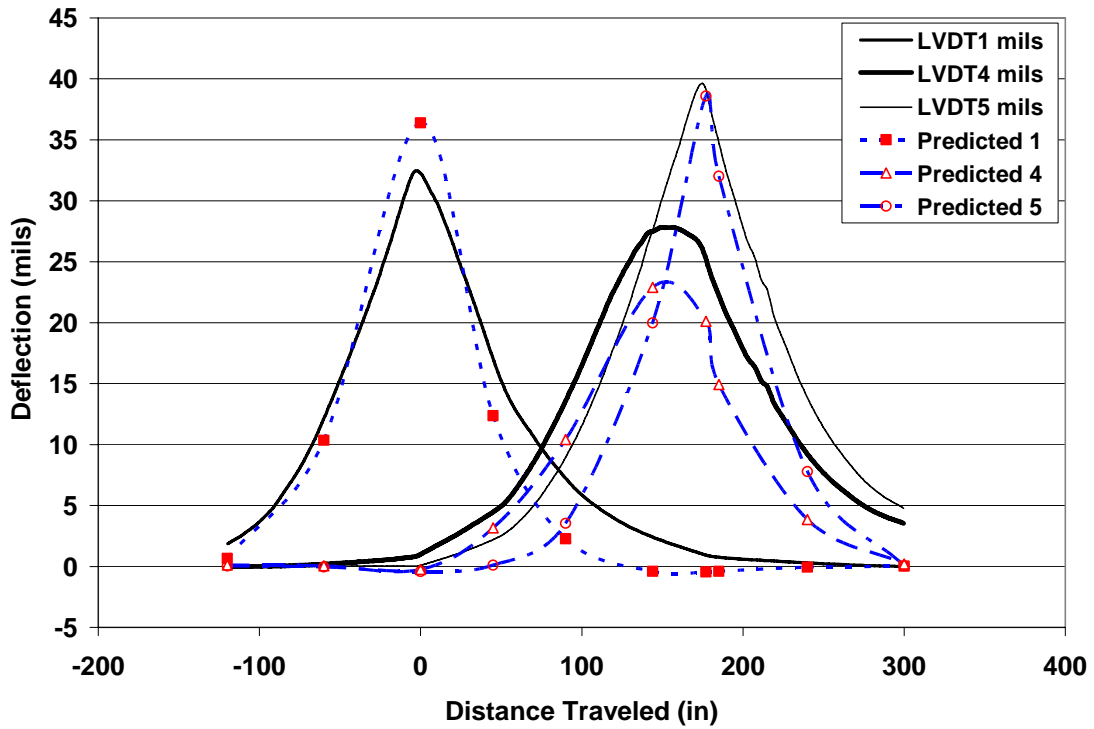


Figure 91. Comparison between Measured and Combined Deflections along edge at study point C Top: English units; bottom: metric units.

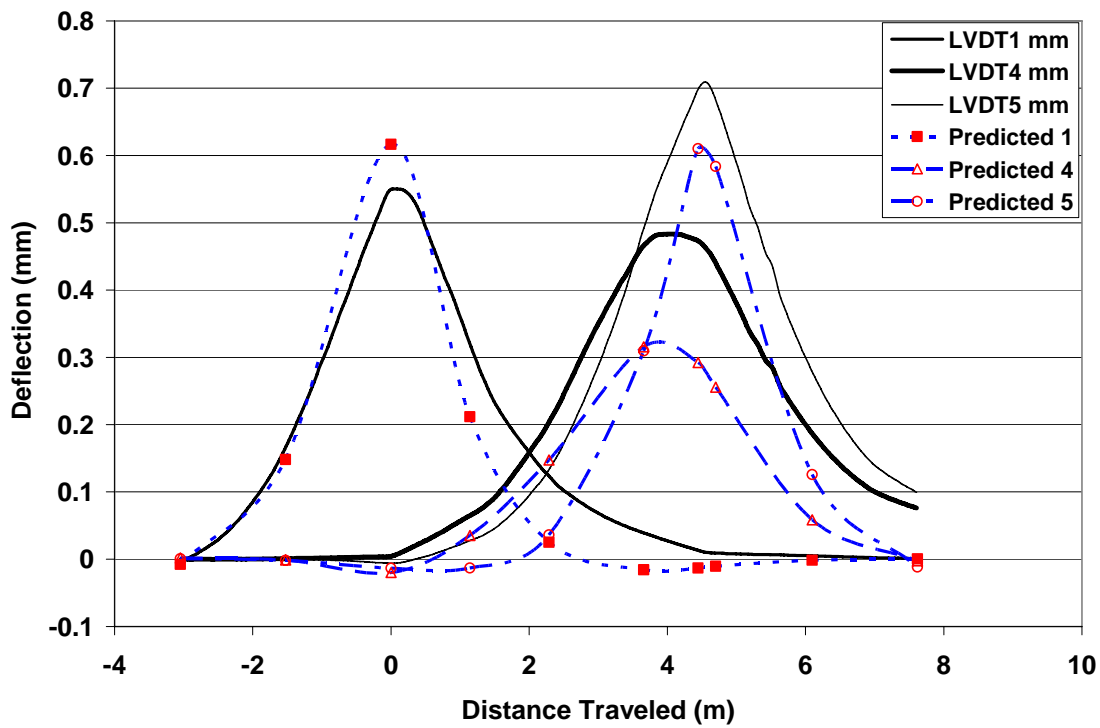
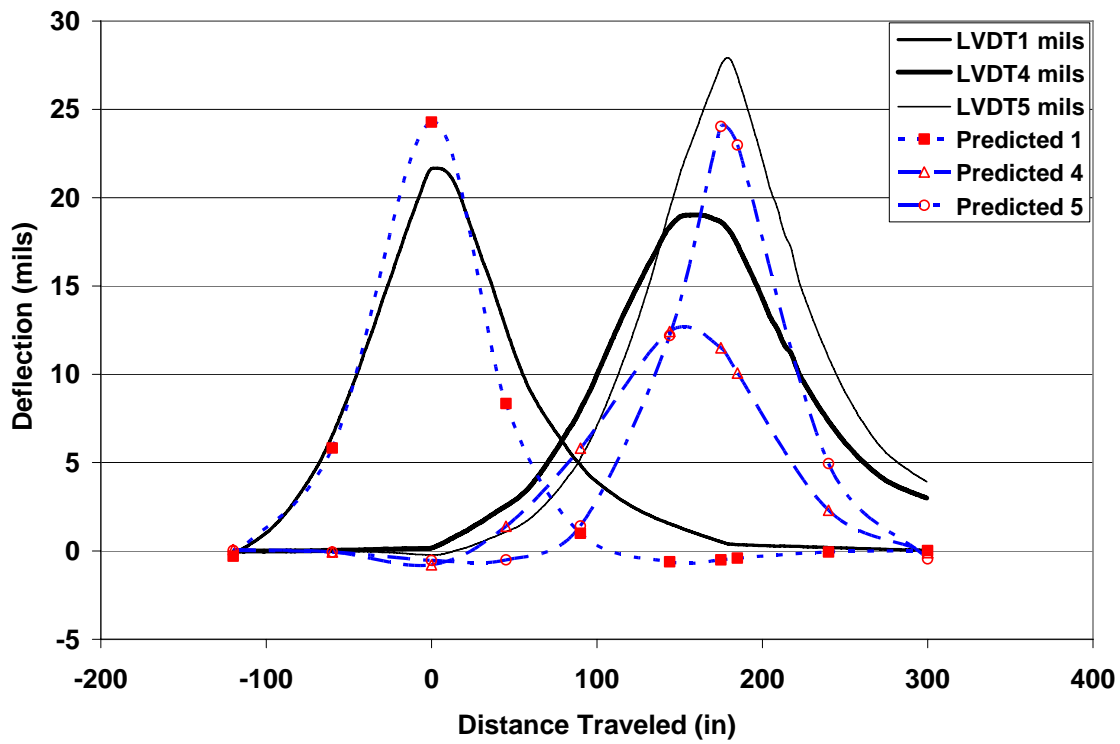
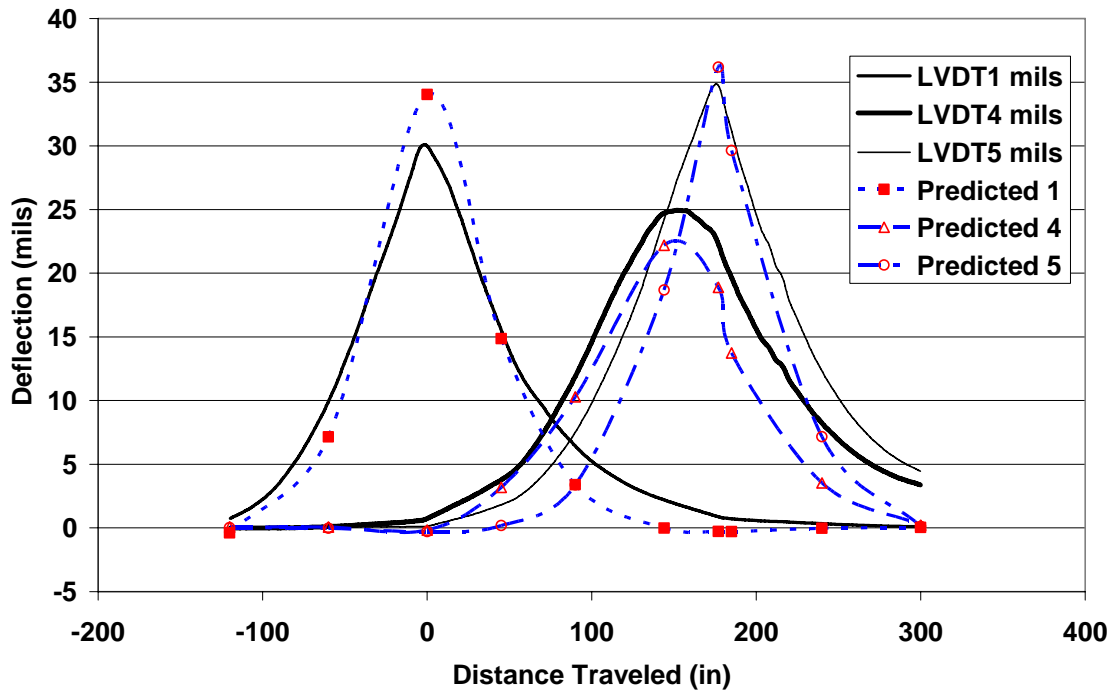


Figure 92. Comparison between Measured and Combined Deflections along wheel path at study point C Top: English units; bottom: metric units.

Load applied along edge, temperature 40°F (4.4°C)



Load applied along edge, temperature 40°F (4.4°C)

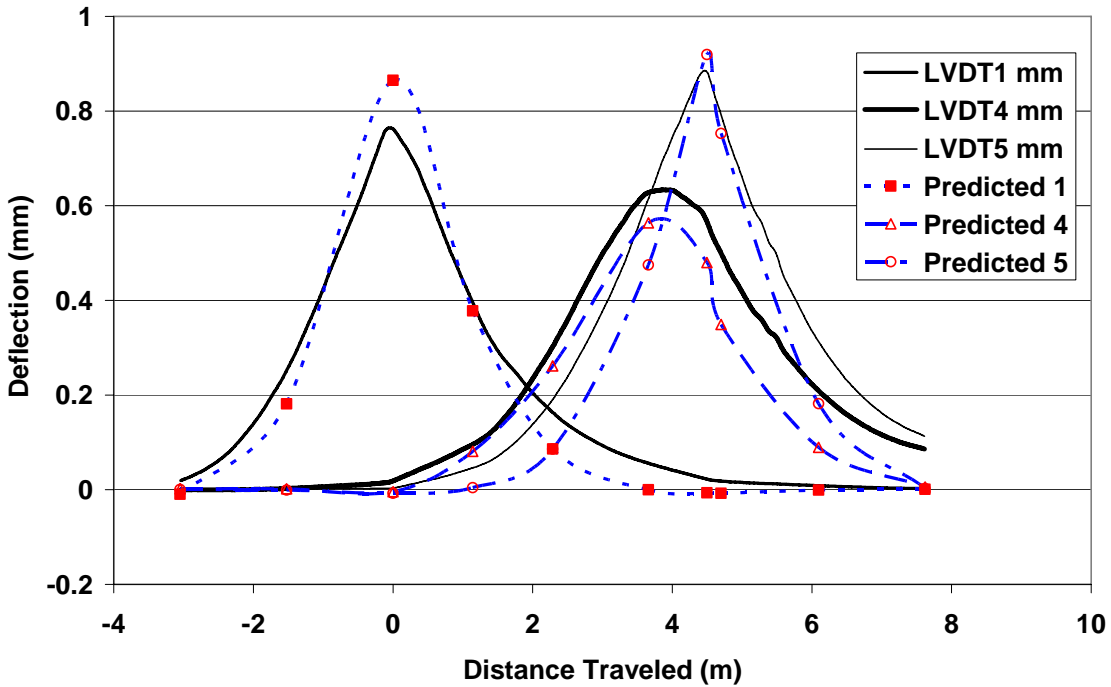


Figure 93. Comparison between Measured and Combined Deflections along edge at study point D Top: English units; bottom: metric units.

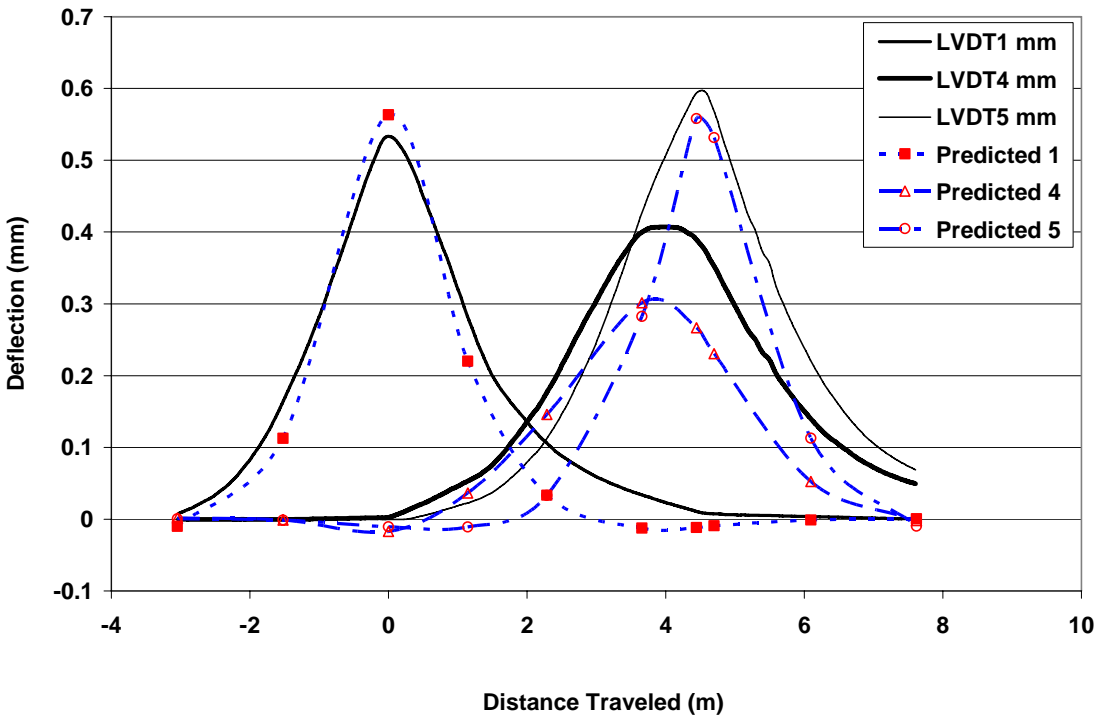
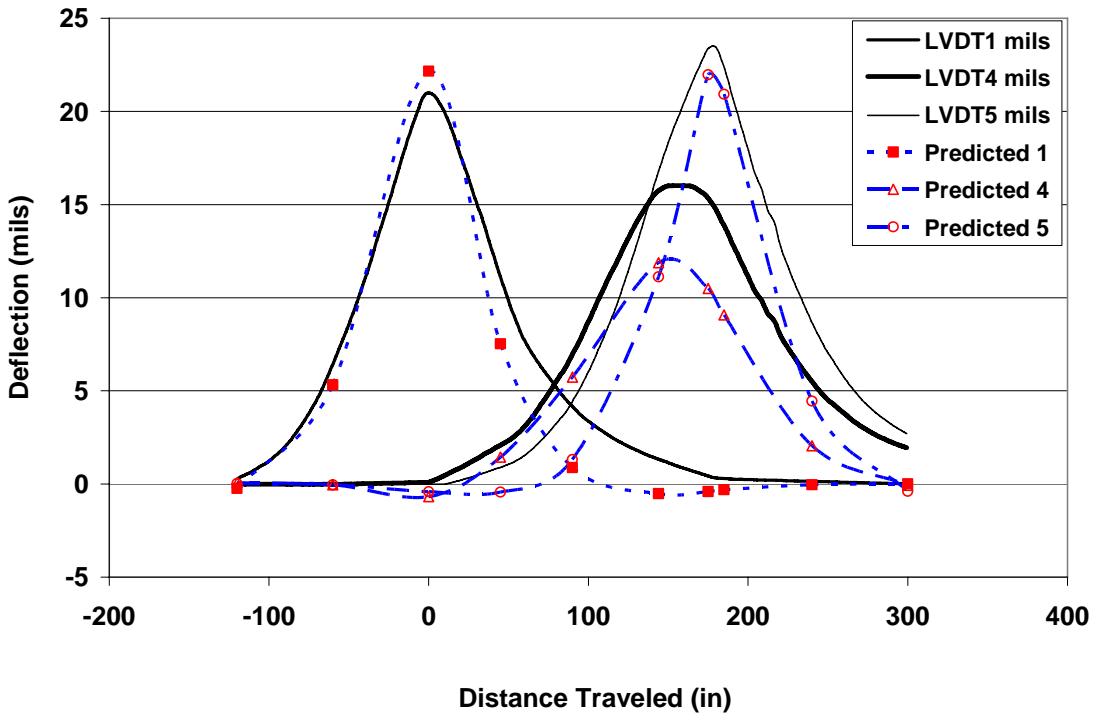


Figure 94. Comparison between Measured and Combined Deflections along wheel path at study point D Top: English units; bottom: metric units.

The experimental results show that the deflection of the corner and the edge increased due to the tire load with the decrease in temperature. The explanation of this is that when the temperature drops, the corner and edge curl up, thus creating a higher unsupported area that will deflect more upon the application of tire load. The predictions follow the general trend of deflections of both corner and edge points. The difference in the measured peak deflection between LVDT 1 and LVDT 5 can be explained as due to the non-uniformity in the materials, construction, corner lift, etc. The FE predictions of corner and edge deflections show good agreement with the measurement trend. The measured edge deflections were always higher than the predicted ones. This implies that a slightly modified LOS needed to be considered in the model.

4.5.1 VALIDATION OF STRAIN PREDICTIONS

The experimental instrumentation to measure the strain due to a moving load on a curled slab included 3 rosette locations. The rosettes in location 6 of Figure 66, tire path P4 (the wheel path 30 in (76 cm) from the edge), three tire load values, and randomly selected temperature points A and B (in Figure 86) were chosen to validate the combined strain predictions. The measured strain shows that the strain reversals increased as the temperature dropped, while the peak strain value was not affected by the temperature variations. This implies that at the point when the tire is directly on the rosette gauge, there is a full slab contact with the base. Figure 95 through Figure 99 present the strain validation result, with the positive sign implying tension. The longitudinal and transverse strains were compared. ROS 9 *ue* is in the longitudinal direction of the top rosette, ROS 12 *ue* is in the longitudinal direction of the bottom rosette, ROS 7 *ue* is in the transverse direction of the top rosette, and ROS 10 *ue* is in the transverse direction of the bottom rosette. The strains measured in the diagonal directions in the rosettes are not used because the simulations programs could not compute diagonal strains. The predicted peak strains in the longitudinal direction were always higher than the measured strain, due to the input material properties, and the joint modeling inaccuracy. Moreover, the rosette measured the strain one inch (2.54 cm) below the top and one inch (2.54 cm) above the bottom of the slab, while the FE produced the strain at the top and bottom of the slab. Nevertheless, the model with the LOS described above showed an agreement with the general trend.

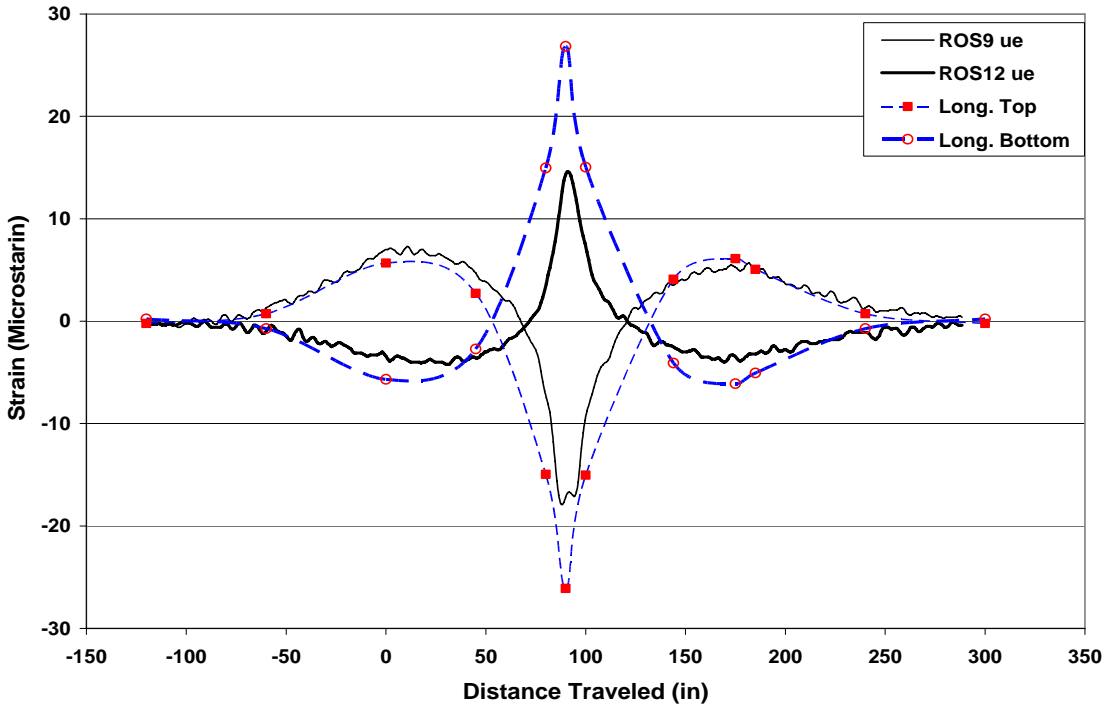


Figure 95. Longitudinal Predicted and Measured Strain at Study Point B along wheel path P4 at a load of 9000 lb (40.0 kN) (1 in = 2.54 cm).

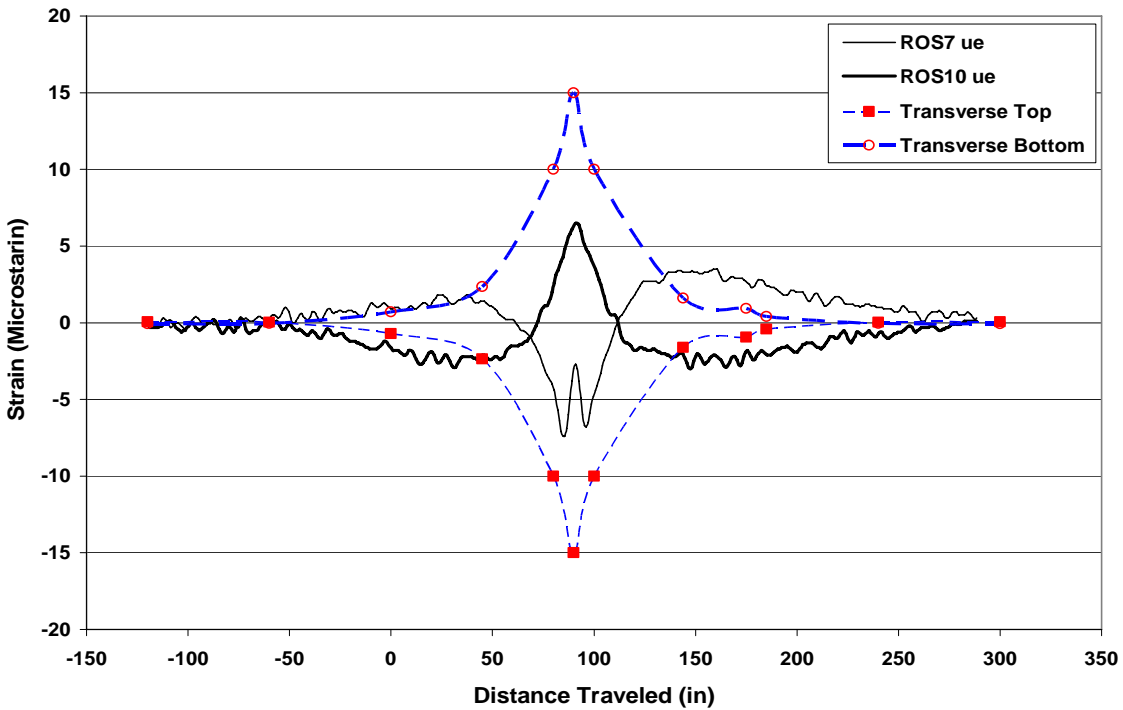


Figure 96. Transverse Predicted and Measured Strain at Study Point B along wheel path P4 at a load of 9000 lb (40.0 kN) (1 in = 2.54 cm).

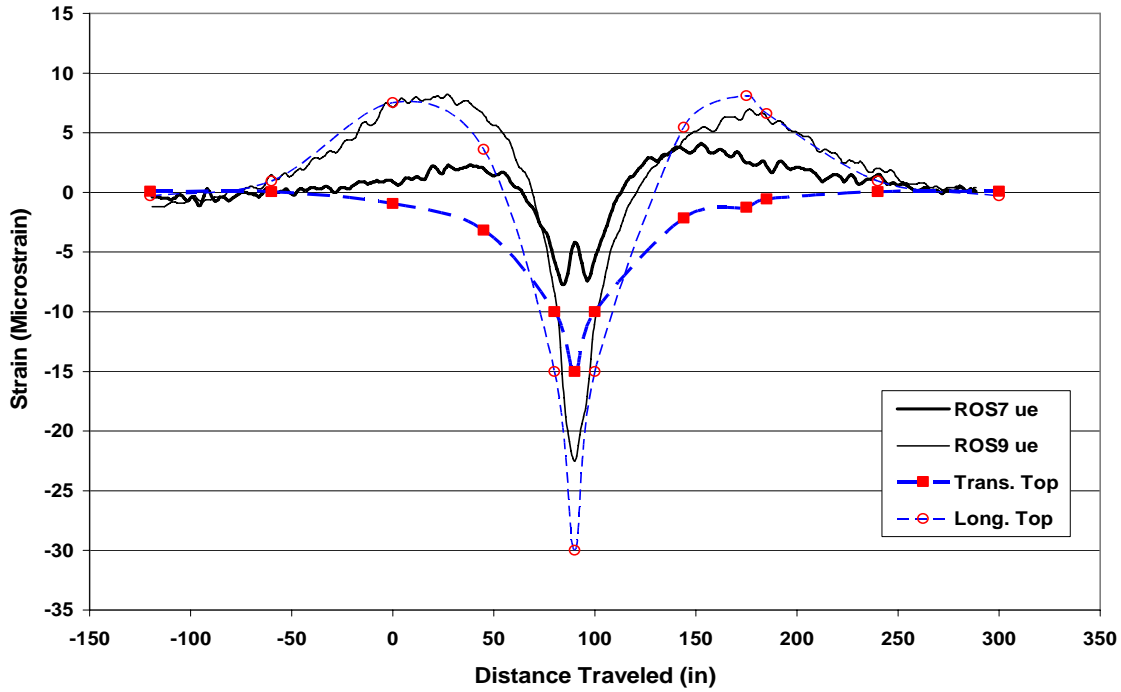


Figure 97. Longitudinal and Transverse Predicted and Measured Strain at Study Point A along wheel path P4 at a load of 12000 lb (53.4 kN) (1 in = 2.54 cm).

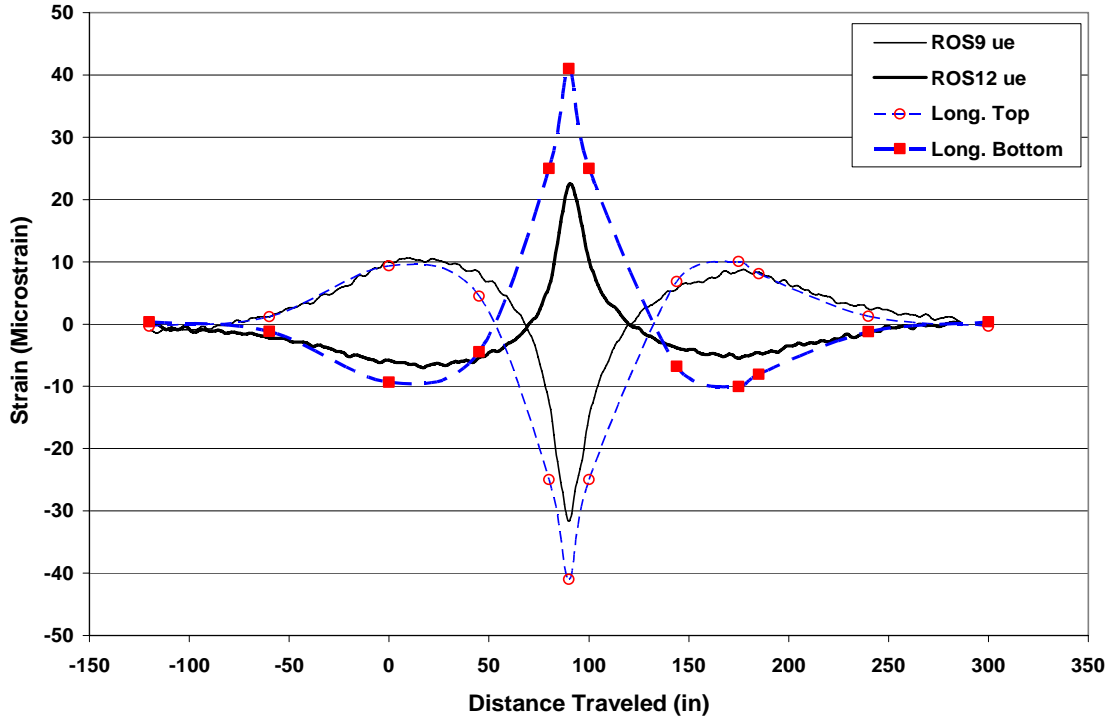


Figure 98. Longitudinal Predicted and Measured Strain at Study Point B along wheel path P4 at a load of 15000 lb (66.7 kN) (1 in = 2.54 cm).

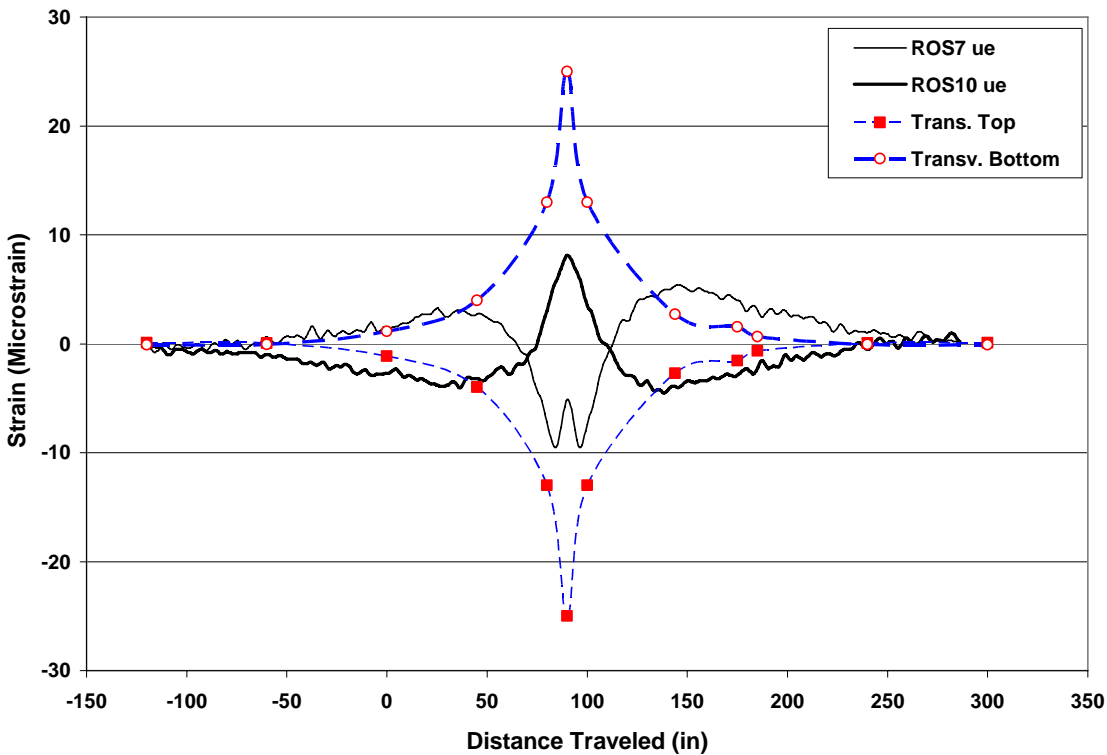


Figure 99. Transverse Predicted and Measured Strain at Study Point B along wheel path P4 at a load of 15000 lb (66.7 kN) (1 in = 2.54 cm).

4.6 SUMMARY

The chapter dealt mainly with the verification and validation of ISLAB2000 response to the different loading conditions. The testing conducted at the APLF provided numerous experimental data for the verification process. The experimental data were divided into three stages: stage I which presented the slab curing, stage II which presented the period of temperature variations, and stage III which presented the application of load while the temperature was varied. It was found that a residual temperature gradient of -22F° (-12.2C°) developed within the slab thickness due to the moisture loss only. Moreover, the corner upward deflection due to this residual TG increased approximately 1 mm (0.0394 in) after 8 weeks of the slab placing even when 10F° (5.55C°) positive TG was applied. Thus, warping could cause a permanent loss of support (LOS) for the pavement. Positive gradient based curling would only reduce the amount of LOS without eliminating it. However, it is questionable if warping in this magnitude could be observed under field conditions. In the test, the pavement was subjected to pure environmental loads. Within the 8 week test period, no dynamic loads were applied to the pavement. In the field the conditions are different, and early traffic loading would cause a greater compressive stresses on the slab and therefore, a smaller slab curvature due to warping.

A proper selection of LOS is crucial to predict the deflections and strains due to temperature- and load- induced stresses. Although their general trend follows the experimental data, disagreement in the absolute predicted values was justified by several reasons: First, there was a continuous moisture loss in the top pavement strata during the change in temperature that was not

considered in the model. Second, the boundary conditions in terms of aggregate interlock were not modified according to the change in temperature. Third, the material properties of the base and the subgrade were estimated from the literature. Fourth, the location of the strain measurements was slightly different than the location of the predicted strain values. This also applied to the TG obtained from the VW gauges. Finally, the FE showed some inaccuracy in modeling the joints under combined traffic and environmental loadings.

5 OPTIMIZATION OF SLAB JOINT SPACING

5.1 INTRODUCTION

Previous studies (Darter et al., 1995, Guo et al., 1997, Parson et al., 2003 and others) have shown that joint spacing in rigid pavement has a major effect on slab cracking and faulting. Traditionally, slab size is determined from minimum pavement thickness, which in turn, is determined from structural requirements. It has been shown that longer slabs deteriorate faster, thicker slabs perform better, and the width does not have a significant effect on the performance of rigid pavement. However, an optimization of slab length to produce minimum critical stresses has not been developed.

Two parameters are considered to have a significant effect on the slab performance: The truck axle spacing and the frequency of the load application. These parameters are related by the fatigue model. The Ohio Department of Transportation Weigh-in-Motion (WIM) data base was utilized to obtain traffic data. Truck axle spacing, axle weight, and frequency were collected over a period of four years on the Ohio SHRP Test Road on US Route 23 in Delaware County. On the other hand, finite element programs were used to obtain the slab stresses of Ohio SHRP Test Road sections. Based on the traffic data and the finite element results, the joint spacing corresponding to the least fatigue was recommended.

5.2 TRAFFIC DATA: ODOT 23 WIM DATABASE

The Ohio Department of Transportation (ODOT) WIM database was utilized to determine the truck axle spacing, axle weights, and repetition on the Ohio SHRP Test Road. The spacing between the first and second truck axles was of a concern, because if these two axles were placed at both ends of the slab, tensile stress reversals would occur at the top of the slab. These tensile stresses at the slab top were found to be the critical stresses when the slab is subjected to a high negative temperature gradient. Thus, there is a relation between the spacing of the first and second truck axles and the slab joint spacing. The axle spacings were divided into 1 foot (0.305 m) ranges. For example, all the axle spacings between 11 feet (3.35 m) and 12 feet (3.66 m) were grouped in a single 11-11.99 feet (3.35-3.65 m) axle spacing category. This axle spacing category was associated with a slab length of 12 feet (3.66 m), or a joint spacing of 12 feet (3.66 m), in order to have the critical load positions just described. Experimental results from 15 days of monitoring during the period 1998-2001 were chosen to classify the traffic. Figure 100 shows the daily number of trucks with a certain axle spacing category versus the joint spacing upon which the two axles were placed at the slab ends. The number of trucks represents one day of monitoring on the 4 lanes. It is clearly noticed that a joint spacing of 15 feet (4.57 m) has the least repetition of trucks in a slab length range between 11 feet (3.35 m) and 22 feet (6.71 m). Thus, although a slab length of 13 feet (3.96 m) produces a lower tensile stress than 15 feet (4.57 m), the load frequency for 15 feet (4.57 m) is lower. To clarify this discrepancy, a fatigue model was used. The average weights of the first and second axles were monitored; Figure 101 shows that there is not a well defined relation between the axle spacing and the weight.

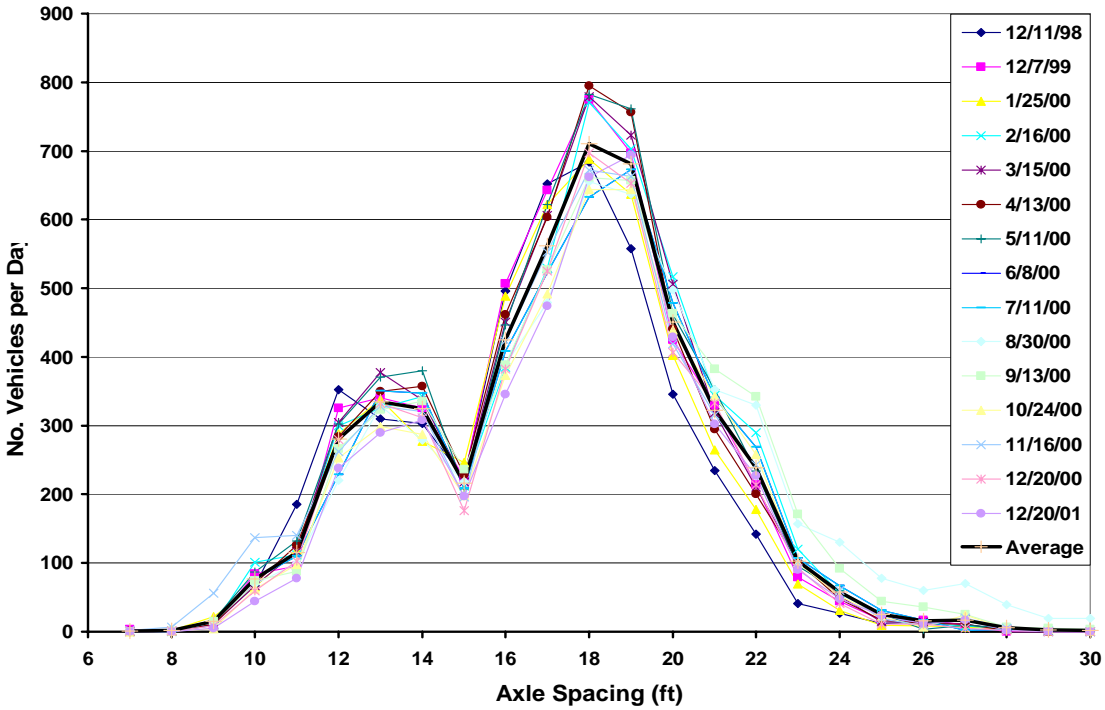


Figure 100. Traffic Frequencies and Axle Spacings on Ohio SHRP Test Road (1 foot = 0.305 m).

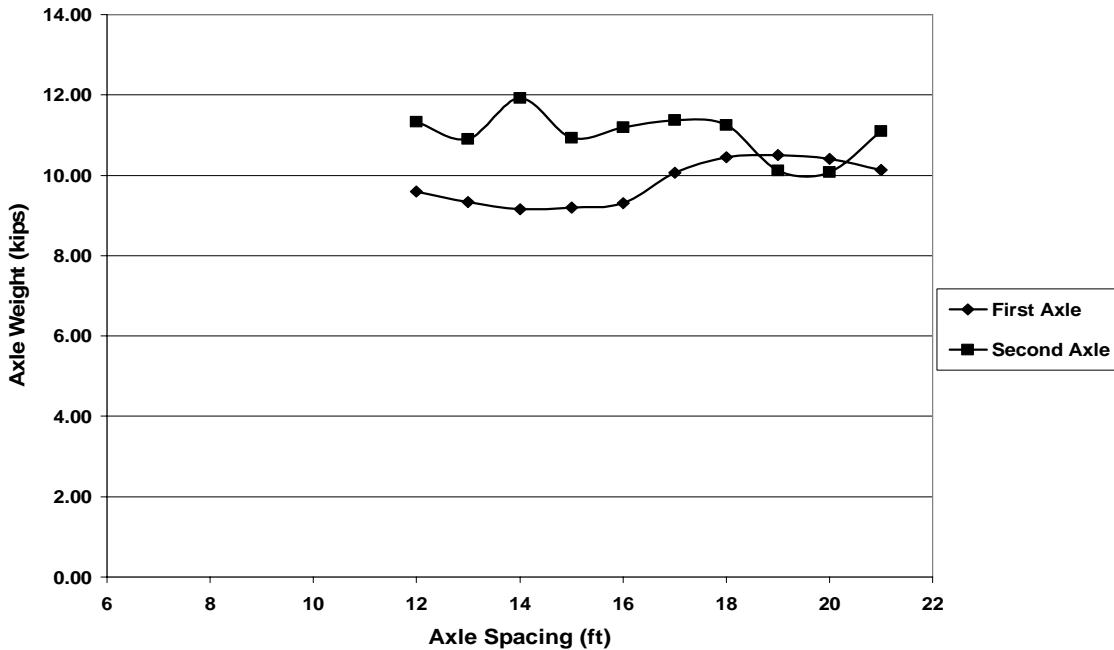


Figure 101. First and Second Truck Axle Weights (1 foot = 0.305 m, 1 kip = 4.448 kN).

It might be more relevant to study the traffic count for a complete year. The traffic count and corresponding axle spacing for one weekday per month of the year 2000 are shown in Figure 102. To extrapolate this data to annual traffic data, the traffic size was assumed to be cut in half on

weekends. Because the joint spacing optimization is a relative comparison between the different slab spacing, this assumption is acceptable. Since there are 52 weeks and one day per year, there are 261 (52*5 +1) weekdays and 104 (52*2) weekend days per year, or 21.75 weekdays and 8.67 weekend days per month on average.

For each axle spacing range, the annual traffic then can be obtained by the following relation:

$$\text{Annual Number of Trucks} = \sum_{n=1}^{12} [(21.75 * x_n) + (8.67 * \frac{x_n}{2})] \quad (5.1)$$

where x_n = daily number of trucks of certain axle spacing.

The number of trucks of axle spacing range between 6 feet (1.83 m) and 30 feet (9.15 m) on the 4 lanes of US 23 per month is represented in Figure 102. Figure 103 shows the annual number of trucks versus the axle spacing.

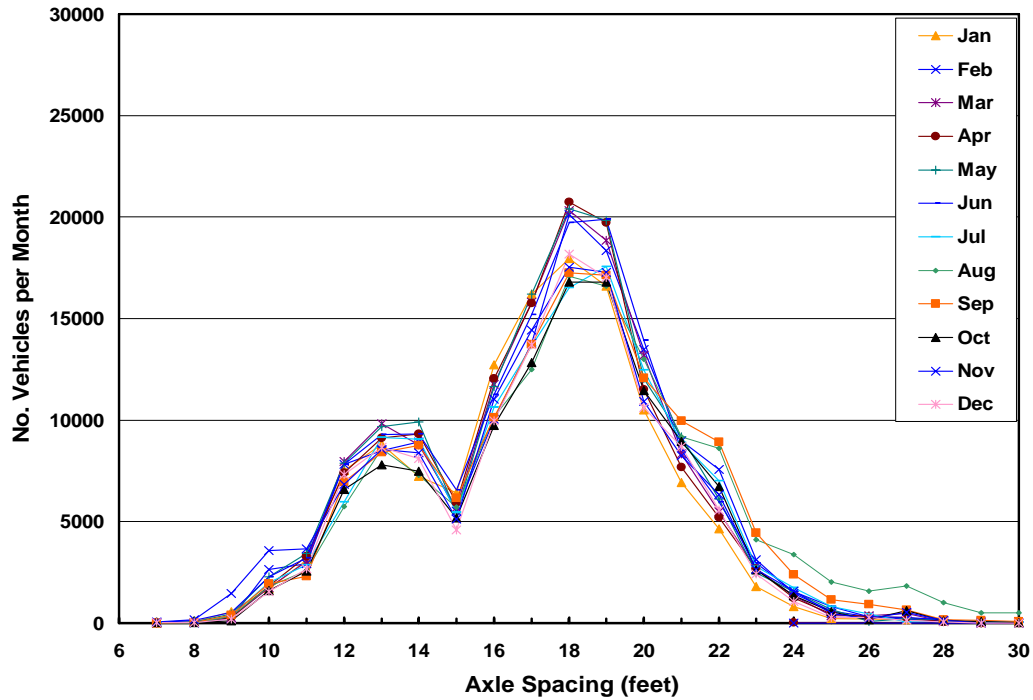


Figure 102. Number of Trucks per Month on Ohio SHRP Test Road as a function of axle spacing. (1 ft. = 0.305 m).

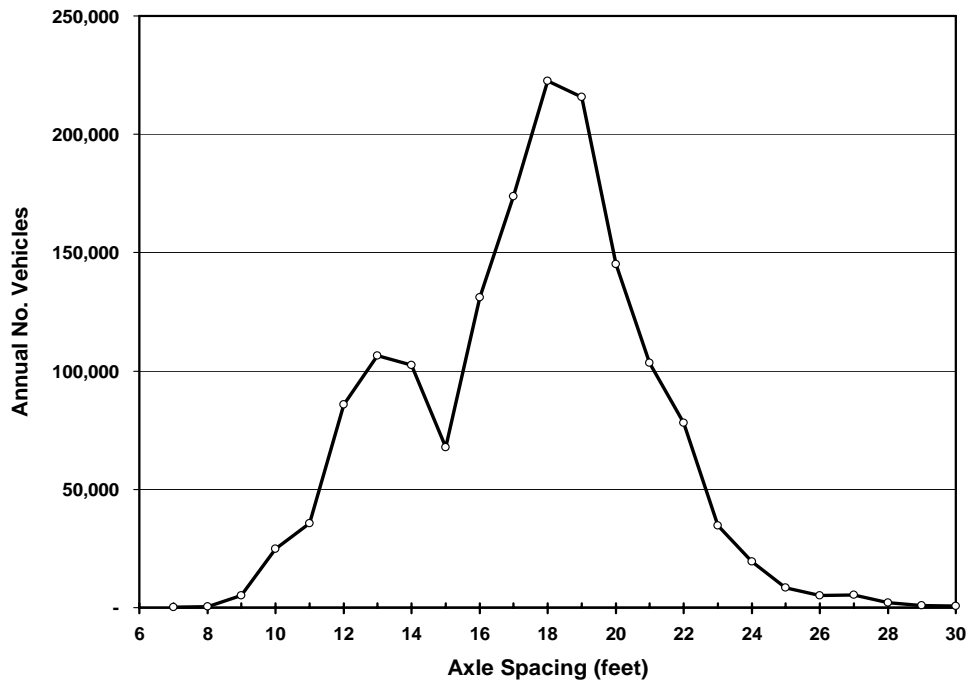


Figure 103. Annual Number of Trucks on Ohio SHRP Test Road as a function of axle spacing. (1 ft. = 0.305 m).

5.3 JOINT SPACING BASED ON FATIGUE MODEL

After the intensive parametric study and the presentation of traffic data, a fatigue model was needed to define the contribution of various design factors to the slab stresses. A plain concrete fatigue model is simply a combination of the concrete strength and non-uniform cyclic loading to predict the number of loads to failure, where failure is indicated by the development of cracking. Three concrete fatigue models were used in this study. The Portland Cement Association (PCA) (Packard and Tayabji, 1985) proposed the fatigue model shown in Equation 5.2. Note that for the PCA model, if the ratio of flexural tensile stress to modulus of rupture is less than 0.45, the slab will never fail. Huang (1993) concluded that the PCA model is very conservative and proposed another fatigue model represented by Equation 5.3. Both models may be used if the bending stresses dominate the shear stresses. The third model was proposed by Domenichini and Marchionna (1981), and presented by equation 5.4.

$$\left. \begin{aligned}
 \log N_f &= 11.737 - 12.077 \left(\frac{\sigma}{S_c} \right) && \text{for } \left(\frac{\sigma}{S_c} \right) \geq 0.55 \\
 N_f &= \left(\frac{4.2577}{\sigma/S_c - 0.4325} \right)^{3.268} && \text{for } 0.45 < \left(\frac{\sigma}{S_c} \right) < 0.55 \\
 N_f &= \text{Unlimited} && \text{for } \left(\frac{\sigma}{S_c} \right) \leq 0.45
 \end{aligned} \right\} \quad (5.2)$$

$$\log N_f = 17.61 - 17.61 \left(\frac{\sigma}{S_c} \right) \quad (5.3)$$

$$\log N_f = \frac{1 - \frac{\sigma}{S_c}}{0.0954(1 - R)} \quad (5.4)$$

where N_f = number of repetitions to failure, σ = maximum slab tensile stress due to combined load and curl stresses, $R = (\sigma/\sigma_{\min})$, σ_{\min} = curling stresses, and S_c = modulus of rupture of the concrete, which can be obtained from the following equation by the American Concrete Institute (ACI):

$$S_c = K * \sqrt{f_c'} \quad (5.5)$$

where $K = 8.4$ for S_c in psi, and $f_c' = 28$ -day concrete compressive strength in psi. Equation 5.6 relates the concrete elastic modulus, E_c to the 28-day compressive strength.

$$E_c = 57000 * \sqrt{f_c'} \quad (5.6)$$

where E_c and f_c' are in psi.

As was discussed earlier in Chapter 4, the warping stresses in a concrete slab may be represented by an equivalent temperature gradient of -22F° (-12.2C°) for a 10 inch (25.4 cm) slab thickness, or $-2.2\text{F}^\circ/\text{in}$ ($-0.48\text{C}^\circ/\text{cm}$). This implies that the upward lifting of slab edges stays even in the warm seasons, a fact that was proven experimentally in the APLF. On the other hand, it was reported by Sargand (1994) that the maximum negative TG observed through the thickness of a 9 in (22.9 cm) slab at Ohio SHRP Test Road was -15.6F° (-8.67C°), i.e., $-1.73\text{F}^\circ/\text{in}$ ($-0.378\text{C}^\circ/\text{cm}$). When a negative gradient is applied together with axle loads, the critical load position would be such as the two truck axles are positioned on both slab joints. The case of the axle positioned at the middle of the slab would be critical if the slab underwent an opposite behavior, i.e. curled downwards; such a behavior was not observed experimentally. Moreover, it was noticed by the author that slab cracks initiate at the slab top and develop towards the bottom. Therefore, it was reasonable to study the combination of maximum negative temperature gradient and the first two truck axles at the slab joints. To determine σ , a total TG of $-3.93\text{F}^\circ/\text{in}$ ($-0.85\text{C}^\circ/\text{cm}$) representing the warping and curling stresses combined was used together with the axle loads presented in Figure 101. When unavailable, an average value of axle loading was used. To determine σ_{\min} , only warping stresses were considered, i.e., only a TG of $-2.2\text{F}^\circ/\text{in}$ ($-0.48\text{C}^\circ/\text{cm}$) across the slab thickness was used. Table 25 summarizes the loading conditions used in the determination of σ and σ_{\min} .

Table 25. Summary of Loading Conditions to Determine σ and σ_{min} .

		To Determine σ			
Joint Spacing		First Axle Load		Second Axle Load	
(ft)	(m)	(kips)	(kN)	(kips)	(kN)
13	3.96	9.33	41.50	10.9	48.48
14	4.27	9.16	40.74	11.92	53.02
15	4.57	9.2	40.92	10.93	48.62
16	4.88	9.3	41.37	11.2	49.82
17	5.18	10.06	44.75	11.38	50.62
18	5.49	10.45	46.48	11.24	50.00
19	5.79	10.5	46.70	10.12	45.01
20	6.10	10.41	46.30	10.07	44.79
21	6.40	10.13	45.06	11.09	49.33
22	6.71	9.81	43.63	11.02	49.02
23	7.01	9.81	43.63	11.02	49.02
24	7.32	9.81	43.63	11.02	49.02

Note: To Determine σ a temperature gradient of $-3.93 \text{ F}^\circ/\text{in}$ ($-0.86 \text{ C}^\circ/\text{cm}$) was used.
 To Determine σ_{min} , a temperature gradient of $-2.2 \text{ F}^\circ/\text{in}$ ($-0.48 \text{ C}^\circ/\text{cm}$) was used.

The main input in the fatigue model was the tensile stress at the top of the slab when the truck axles were placed at the two ends of the slab. This stress was roughly located at the center of the slab. Since the stress value depended on the pavement section used, all of the four sections discussed earlier in Chapter 3 were analyzed (390201, 390205, 390208, and 390212). At this point, optimum axle spacing was expected for each pavement section, i.e. for each slab thickness and base type. The dimensions of the four sections, as well as the material properties were the same as in Chapter 3. However, the length was set as the joint spacing, equal to the axle spacing in this analysis. The load configuration and the tire pressure were the same as in Chapter 3. However, the right wheel path was modified so that the truck will be centered within the width of the slab (144 inch (3.66 m)), as this would produce the maximum stresses. ISLAB2000 was used to obtain the maximum tensile stresses, i.e., the longitudinal stresses at the top of the slab. These stresses were also compared to those obtained by EVERFE. While having the same trend, an average of 5% difference was observed between the outputs of the two finite element programs. Although EVERFE is a 3-D program, ISLAB2000 values were used in the subsequent sections due to the fact that EVERFE may result in some errors when the loads are placed very close to the joints (as mentioned in the “help” section of EVERFE). The tensile stresses, corresponding to both maximum and minimum loading conditions described earlier in Table 25, for all the section are shown in Figure 104. The fatigue model calculations for the Ohio SHRP Test Road sections are presented in Table 26, Table 27, Table 28, and Table 29 for sections 390201, 390205, 390208, and 390212 respectively.

The maximum tensile stress was roughly located at the geometric center of the top surface of the slab. Minimum tensile stress referred to the warping stresses only. The allowable number of repetitions for each slab length was calculated by the three models, and compared to the actual number of truck repetitions from the traffic data presented in the previous section. The ratio of the two numbers determined the time needed for the pavement to fail by fatigue.

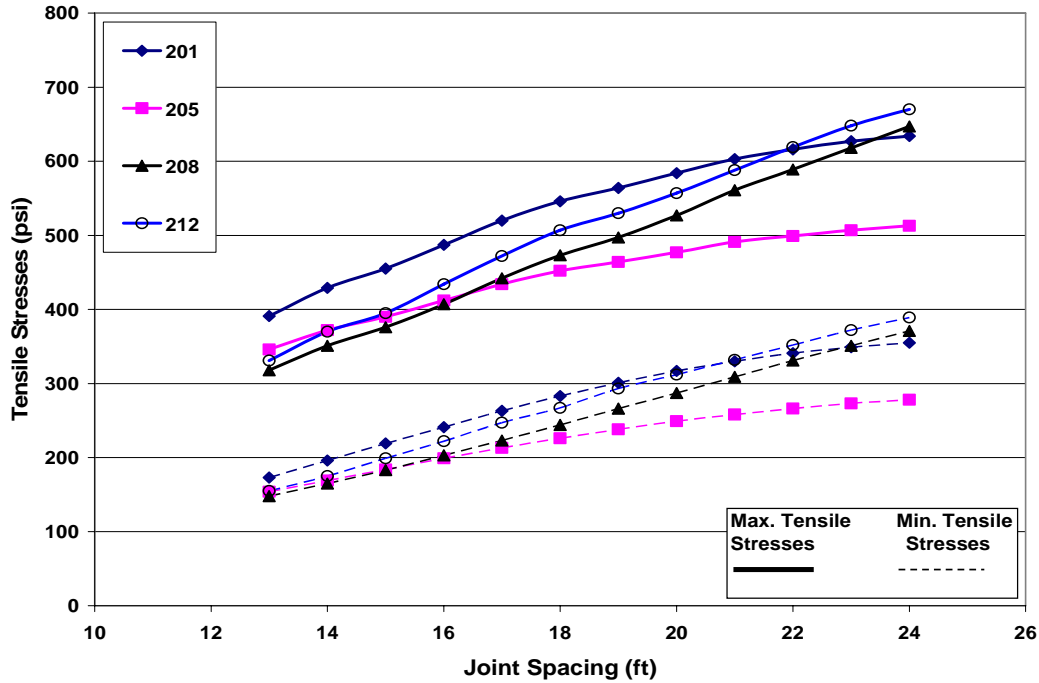


Figure 104. Maximum and Minimum Tensile Stresses at the Slab Top for Different Sections (1 psi = 6.89 kPa N, 1 foot = 0.305 m).

Table 26. Fatigue Model Calculations for Section 390201.

Joint Spacing (ft) (m)		σ		Shear stress		Annual Trucks Number	PCA Fatigue Model		Huang Fatigue Model	
		(psi)	(MPa)	(psi)	(kPa)		N_f	Design Life (yr)	N_f	Design Life (yr)
13	3.96	391	2.70	0.28	1.93	106421	480436.6343	4.51449	421490484.7	3960.59
14	4.27	429	2.96	0.32	2.21	102535	94631.69241	0.92292	56434494.96	550.392
15	4.57	455	3.14	0.3	2.07	67739	36836.74519	0.5438	14258127.7	210.486
16	4.88	487	3.36	0.22	1.52	131148	11533.65521	0.08794	2622405.594	19.9957
17	5.18	520	3.59	0.26	1.79	173847	3482.513889	0.02003	457464.2315	2.63141
18	5.49	546	3.76	0.41	2.83	222571	1355.618541	0.00609	115577.9534	0.51928
19	5.79	564	3.89	0.56	3.86	215711	705.4410279	0.00327	44589.59384	0.2067
20	6.10	584	4.03	0.51	3.52	145181	341.4006045	0.00235	15475.04313	0.10659
21	6.40	603	4.16	0.39	2.69	103500	171.327737	0.00165	5662.527213	0.05471
22	6.71	616	4.25	0.74	5.10	78173	106.8931807	0.00136	2846.225012	0.0364
23	7.01	627	4.32	0.54	3.72	34692	71.71202137	0.00206	1590.333928	0.04584
24	7.32	634	4.37	0.61	4.21	19485	55.62540862	0.00285	1098.064237	0.05635

Joint Spacing (ft) (m)		σ		σ_{min}		R	Annual Trucks Number	Domenichini Fatigue Model	
		(psi)	(MPa)	(psi)	(MPa)			N_f	Design Life (yr)
13	3.96	391	2.70	173	1.19	0.442	106421	1614014966	15166.32
14	4.27	429	2.96	196	1.35	0.456	102535	312868665	3051.335
15	4.57	455	3.14	219	1.51	0.481	67739	162189734.5	2394.333
16	4.88	487	3.36	241	1.66	0.494	131148	36616833.94	279.2023
17	5.18	520	3.59	263	1.81	0.505	173847	6564543.441	37.76046
18	5.49	546	3.76	283	1.95	0.518	222571	1804790.566	8.10883
19	5.79	564	3.89	301	2.08	0.533	215711	860350.8706	3.988442
20	6.10	584	4.03	317	2.19	0.542	145181	284895.4728	1.962346
21	6.40	603	4.16	330	2.28	0.547	103500	85963.27586	0.830563
22	6.71	616	4.25	341	2.35	0.553	78173	40337.4794	0.516002
23	7.01	627	4.32	349	2.41	0.556	34692	19861.18695	0.5725
24	7.32	634	4.37	355	2.45	0.559	19485	12966.66501	0.665469

Note: $S_c = 766$ psi (5.28 MPa)

Table 27. Fatigue Model Calculations for Section 390205.

Joint Spacing (ft) (m)		σ		Shear stress		Annual Trucks Number	PCA Fatigue Model		Huang Fatigue Model	
		(psi)	(MPa)	(psi)	(kPa)		N_f	Design Life (yr)	N_f	Design Life (yr)
13	3.96	346	2.39	0.13	0.90	106421	203499.1586	1.9122	163393730.9	1535.35
14	4.27	372	2.56	0.25	1.72	102535	64329.38738	0.62738	32145495.9	313.507
15	4.57	390	2.69	0.68	4.69	67739	29727.27033	0.43885	10429682.89	153.968
16	4.88	412	2.84	0.62	4.27	131148	11571.76686	0.08823	2635050.611	20.0921
17	5.18	434	2.99	0.16	1.10	173847	4504.476424	0.02591	665743.3211	3.82947
18	5.49	452	3.12	0.79	5.45	222571	2081.564799	0.00935	216002.0099	0.97048
19	5.79	464	3.20	0.46	3.17	215711	1244.190878	0.00576	101990.1996	0.4728
20	6.10	477	3.29	0.91	6.27	145181	712.457311	0.0049	45237.73078	0.31159
21	6.40	491	3.39	0.16	1.10	103500	390.84579	0.00377	18848.85192	0.18211
22	6.71	499	3.44	0.1	0.69	78173	277.3342393	0.00354	11429.27464	0.1462
23	7.01	507	3.50	0.23	1.59	34692	196.7893278	0.00567	6930.306387	0.19976
24	7.32	513	3.54	0.47	3.24	19485	152.1423364	0.0078	4762.146589	0.2444

Joint Spacing (ft) (m)		σ		σ_{min}		R	Annual Trucks Number	Domenichini Fatigue Model	
		(psi)	(MPa)	(psi)	(MPa)			N_f	Design Life (yr)
13	3.96	346	2.39	154	1.06	0.445	106421	645820146.4	6068.54
14	4.27	372	2.56	169	1.17	0.454	102535	154402489.7	1505.852
15	4.57	390	2.69	184	1.27	0.471	67739	81090055.39	1197.096
16	4.88	412	2.84	199	1.37	0.483	131148	24695521.89	188.3027
17	5.18	434	2.99	213	1.47	0.49	173847	6412939.869	36.88841
18	5.49	452	3.12	226	1.56	0.5	222571	2241649.31	10.07161
19	5.79	464	3.20	238	1.64	0.512	215711	1320960.225	6.12375
20	6.10	477	3.29	249	1.72	0.522	145181	627363.6715	4.321252
21	6.40	491	3.39	258	1.78	0.525	103500	230511.492	2.227164
22	6.71	499	3.44	266	1.83	0.533	78173	148970.6542	1.905654
23	7.01	507	3.50	273	1.88	0.538	34692	89819.17162	2.589046
24	7.32	513	3.54	278	1.92	0.541	19485	60106.98013	3.084782

Note: $S_c = 648$ psi (4.47 MPa)

Table 28. Fatigue Model Calculations for Section 390208.

Joint Spacing (ft) (m)		σ		Shear stress		Annual Trucks Number	PCA Fatigue Model		Huang Fatigue Model	
		(psi)	(MPa)	(psi)	(kPa)		N_f	Design Life (yr)	N_f	Design Life (yr)
13	3.96	318	2.19	0.13	0.90	106421	Unlimited	Unlimited	3.74E+10	351528.6
14	4.27	351	2.42	0.25	1.72	102535	Unlimited	Unlimited	6961969925	67898.47
15	4.57	376	2.59	0.34	2.34	67739	4217755.989	62.26481	1947636642	28752.07
16	4.88	407	2.81	0.12	0.83	131148	456819.622	3.483237	401337666	3060.188
17	5.18	442	3.05	0.68	4.69	173847	106943.1673	0.615156	67452186.4	387.9974
18	5.49	473	3.26	0.91	6.27	222571	36198.71782	0.162639	13899462.8	62.44956
19	5.79	497	3.43	0.92	6.34	215711	15648.26541	0.072542	4091690.52	18.96839
20	6.10	527	3.63	0.46	3.17	145181	5485.073778	0.03778	887224.917	6.111164
21	6.40	561	3.87	0.81	5.58	103500	1671.838207	0.016153	156909.345	1.516032
22	6.71	589	4.06	0.43	2.96	78173	628.4384728	0.008039	37673.65	0.481926
23	7.01	618	4.26	0.35	2.41	34692	228.1156907	0.006575	8596.02399	0.247781
24	7.32	647	4.46	0.26	1.79	19485	82.80328239	0.004249	1961.36102	0.10066

Joint Spacing (ft) (m)		σ		σ_{min}		R	Annual Trucks Number	Domenichini Fatigue Model	
		(psi)	(MPa)	(psi)	(MPa)			N_f	Design Life (yr)
13	3.96	318	2.19	154	1.06	0.465	106421	5.92E+11	5564926.5
14	4.27	351	2.42	169	1.17	0.47	102535	1.14E+11	1109766.6
15	4.57	376	2.59	184	1.27	0.486	67739	59220968807	874252.18
16	4.88	407	2.81	199	1.37	0.498	131148	16489466056	125731.73
17	5.18	442	3.05	213	1.47	0.504	173847	2543216006	14629.047
18	5.49	473	3.26	226	1.56	0.515	222571	605482508.4	2720.4016
19	5.79	497	3.43	238	1.64	0.535	215711	293531457.1	1360.7625
20	6.10	527	3.63	249	1.72	0.544	145181	59479524.41	409.6922
21	6.40	561	3.87	258	1.78	0.55	103500	7670935.608	74.115319
22	6.71	589	4.06	266	1.83	0.561	78173	1653418.437	21.150761
23	7.01	618	4.26	273	1.88	0.567	34692	263309.6976	7.5899255
24	7.32	647	4.46	278	1.92	0.573	19485	39293.05266	2.0165795

Note: $S_c = 796$ psi (5.49 MPa)

Table 29. Fatigue Model Calculations for Section 390212.

Joint Spacing (ft) (m)		σ		Shear stress		Annual Trucks Number	PCA Fatigue Model		Huang Fatigue Model	
		(psi)	(MPa)	(psi)	(kPa)		N_f	Design Life (yr)	N_f	Design Life (yr)
13	3.96	331	2.28	0.42	2.90	106421	Unlimited	Unlimited	14031685378	131850.7
14	4.27	370	2.55	0.86	5.93	102535	3819287.241	37.24862	1852663289	18068.5
15	4.57	395	2.72	0.61	4.21	67739	583960.7859	8.6207471	505980869.5	7469.56
16	4.88	434	2.99	0.39	2.69	131148	106240.3818	0.8100801	66806813.06	509.4
17	5.18	472	3.25	0.47	3.24	173847	27460.97185	0.1579606	9290817.052	53.4424
18	5.49	507	3.50	0.52	3.59	222571	7898.226468	0.0354863	1509824.783	6.78356
19	5.79	530	3.65	0.16	1.10	215711	3482.513889	0.0161444	457464.2315	2.12072
20	6.10	557	3.84	0.42	2.90	145181	1331.699592	0.0091727	112616.429	0.77569
21	6.40	588	4.05	0.63	4.34	103500	441.641434	0.0042671	22524.77064	0.21763
22	6.71	619	4.27	0.43	2.96	78173	146.4648313	0.0018736	4505.251114	0.05763
23	7.01	648	4.47	0.26	1.79	34692	52.15810843	0.0015035	999.7021358	0.02881
24	7.32	670	4.62	0.19	1.31	19485	23.83129124	0.0012231	319.0418896	0.01637

Joint Spacing (ft) (m)		σ		σ_{min}		R	Annual Trucks Number	Domenichini Fatigue Model	
		(psi)	(MPa)	(psi)	(MPa)			N_f	Design Life (yr)
13	3.96	331	2.28	155	1.07	0.468	106421	2.29E+11	2148970.6
14	4.27	370	2.55	175	1.21	0.472	102535	29331137651	286059.76
15	4.57	395	2.72	199	1.37	0.503	67739	27631420065	407910.06
16	4.88	434	2.99	222	1.53	0.511	131148	3427649857	26135.738
17	5.18	472	3.25	247	1.70	0.523	173847	502205491.7	2888.7785
18	5.49	507	3.50	267	1.84	0.526	222571	58838296.71	264.35742
19	5.79	530	3.65	293	2.02	0.552	215711	34249909.9	158.77683
20	6.10	557	3.84	312	2.15	0.56	145181	6856977.332	47.230542
21	6.40	588	4.05	332	2.29	0.564	103500	893149.4044	8.6294628
22	6.71	619	4.27	352	2.43	0.568	78173	110165.5912	1.4092537
23	7.01	648	4.47	372	2.56	0.574	34692	15573.30345	0.4489018
24	7.32	670	4.62	389	2.68	0.58	19485	3577.675872	0.1836118

Note: $S_c = 781$ psi (5.38 MPa)

5.4 SUMMARY

It was experimentally shown that a positive temperature gradient (slab curl downwards) did not develop in the concrete slab during the usual variations in air temperature, due to the build up of a high negative temperature gradient during the slab curing. Another experimental fact is that the cracks in the concrete slab initiated at the top and developed downwards due to the same reason. Therefore, the critical tensile stresses are located on the top of the PCC slab. This happened when the two truck axle loads were positioned on the two ends of the slab, i.e. when the axle spacing was the same as the joint spacing. In addition to the truck axle loads, loading conditions consisted of the maximum negative temperature gradient observed on Ohio SHRP Test Road ($-1.73\text{F}^\circ/\text{in}$ ($-0.38\text{C}^\circ/\text{cm}$)), and the built in negative gradient observed from the APLF ($-2.2\text{F}^\circ/\text{in}$ ($-0.48\text{C}^\circ/\text{cm}$)). With traffic data from ODOT WIM data base, finite element and fatigue models were used to evaluate the failure time of four different pavement sections. ISLAB2000 was used for the finite element modeling, and the slab stresses were checked against EVERFE. The pavement sections and the traffic data represented Ohio SHRP Test Road.

The review of the three fatigue models (PCA, Huang, and Domenichini) showed that, under the given loading conditions, the tensile stress level overcame the frequency of load application. For example, the axle load repetition on the 15 feet (4.5 m) slabs was less than two thirds (0.62) of that on the 13 feet (4.0 m) slabs, however, the design life of 13 feet (4.0 m) slabs was higher. Again, this is due to the tensile stresses resulting from the built-in negative TG. For each of the four pavement sections in the study, 13 feet (4.0 m) slabs showed the highest expected design life.

6 SUMMARY AND CONCLUSIONS

6.1 GENERAL SUMMARY

The current study was conducted mainly to provide a complete verification and validation of finite element models for rigid pavements. The experimental data used in this process were obtained at the Ohio SHRP Test Road and the Ohio University Accelerated Pavement Load Facility. The variety of the pavement sections and loading conditions makes this verification a complete and unique study. At the Ohio SHRP Test Road, four core sections with various geometry and pavement layers were included in the study, while at the APLF, three different loading conditions were investigated. Additionally, four different finite element programs were studied. The validation outcomes were applied to optimize the pavement joint spacing for minimizing critical stresses during the design life.

Background information on finite element modeling for rigid pavement was presented, followed by a detailed literature search on two and three dimensional finite element models. The literature search revealed a shortcoming in the verification process, as previous evaluations were conducted by applying the surface load at critical locations without the consideration of the effects of environmentally induced stresses. This was typical for the verifications of ISLAB2000, a 2D-FE program recommended for use in the *Development of the 2002 Guide for the Design for the design of new and Rehabilitated Pavement Structures*.

In this study, verification of four selected finite element programs was performed using the experimental data from the Ohio SHRP Test Road. All the pavement responses due to a dynamic load were covered in the verification, i.e., strains, deflections, and vertical pressures at the top of subgrade. The four finite element programs ISLAB2000, JSLAB, EVERFE, and OU3D were selected as being most widely used. The performance of the FEM programs with different base stiffness values was also included in this study.

The third part of this study focused on the verification and validation of ISLAB2000. This process is a complementary step of the experimental verification conducted by the NCHRP project 1-37A research team on *Structural Response Models for Rigid Pavements*. In this section, all the possible loading conditions were considered. The experimental data for verification were obtained from the APLF, a research facility designed for the testing of full-scale asphalt and concrete highway pavement sections under carefully controlled environmental and loading conditions. The FE pavement response was studied under curing conditions, temperature variations, and simultaneous tire load and temperature variations.

The last part of the study focused on the optimization of joint spacing to minimize critical tensile stresses. The critical loading condition was found to be when the two truck axles are placed at the slab joints with the application of a negative temperature gradient (TG). For such loading conditions, the critical stresses were located at the top of the pavement at the center of the slab. A pavement fatigue model was applied to four different pavement sections as constructed on the Ohio SHRP Test Road, with different base stiffness values to determine the highest joint spacing producing a reasonable design life.

6.2 CONCLUSIONS

Due to the multi-phase nature of the current study, conclusions reached by the author are presented here in segments:

6.2.1 Verification of Finite Element Models

- The computer simulations approximated the general experimental trend for strains measured under the right wheel path and at the pavement centerline, deflections, and vertical pressures at the top of subgrade.
- The pavement stress reversals between the first and second truck axles could be as high as the peak stresses under the truck axles. Maximum stress reversal occurred when the first two axles were positioned on the slab joints. Reversal stresses are critical in the pavement design, because they cause tension stress at the top of the slab.
- Slab rocking was noticed in the predictions of ISLAB2000 and JSLAB. The amount of slab rocking increases with higher modulus of subgrade reaction.
- Based on the experimental results, it was found that the increase in the PCC thickness reduces both peak stresses and deflections. Also the use of a thicker base slightly reduces peak stresses. The use of the stiffer LCB instead of DGAB reduces the reversal stresses.
- The different programs were also compared for usability in terms of modeling, input and output data, and speed. As regards to input parameters, ISLAB2000, JSLAB, and EVERFE require the value of subgrade modulus of reaction, k . The OU3D was designed to be fast and efficient, as it solves multiple load cases. For static load cases, ISLAB2000 is the most computationally efficient.
- It should be emphasized that loss of support caused by curling and pumping was not accounted for in this study. The pavement was treated as a flat slab.

6.2.2 Validation of ISLAB2000

- Moisture loss that occurred after placing concrete slabs produced a residual negative temperature gradient. This TG was found to be -22 F° (-12.2 C°) based on the amount of curl measured after 5 weeks. However, it was also found that the amount of curl continues to increase after the fifth week of curing. A curl of 1 mm (0.039 in) was measured between the fifth and eighth week even after a positive temperature gradient of 10 F° (5.5 C°) was applied. Thus, positive gradient based curling would only reduce the amount of loss of support (LOS).
- With a good assumption of LOS, ISLAB2000 proved to predict the trend of deflections and strains fairly well under the variation of temperature. However, strain values need to be corrected to account for the joint opening. Precaution should be taken while assuming LOS, as the unsupported area will change due to the combination of many factors: the change in TG, the change in the boundary conditions, and the ongoing moisture loss.

- When the slab is curled due to environmental loads, the traffic induced deflections increase with a decrease in temperature. This is because reducing the temperature will produce a higher negative gradient, which in turn will produce a larger unsupported area. A similar conclusion was also reached concerning the strain reversals due to traffic load. These stresses increase with a decrease in temperature. On the other hand, if the slab is in full contact with the base, load induced strains will not change significantly with the temperature variations.
- ISLAB2000 predictions of combined load and temperature induced strains were higher than the actual measured strains. The divergence can be modified with a proper estimation of material properties and LOS. On the other hand, ISLAB2000 showed some inaccuracy in modeling the joints under combined traffic and environmental loadings.
- EVERFE was unable to model the LOS; thus an equivalent negative gradient was applied instead, after which the program showed good agreement with ISLAB2000 predictions.

6.2.3 Optimization of Joint Spacing

- With the presence of built-in negative TG due to the curing of concrete, the critical tensile stresses were located at the top of the slab and were maximized when the two truck axle loads were positioned on the two edges of the slab. This fact was confirmed experimentally; the slab cracks were observed to initiate at the top center of the slab and propagate towards the bottom of the pavement.
- The review of the three fatigue models (PCA, Huang, and Domenichini) showed that, under the given loading conditions, the tensile stress level overcame the frequency of load application. For example, the axle load repetition on the 15 ft (4.5 m) slabs was less than two thirds (0.62) that on the 13 ft (4.0 m) slabs, however, the design life of 13 ft (4.0 m) slabs was higher. This is due to the tensile stresses from the built-in negative TG. For the four pavement sections in the study, the shortest (13 ft (4.0 m)) slabs had the longest design life, or the best performance.

6.3 RECOMMENDATIONS FOR FUTURE STUDY

The idea that cracks initiate at the top of concrete slabs and spread towards the bottom, i.e., top-to-bottom cracks, contradicts the traditional rigid pavement design method, where critical tensile stresses were expected at the slab bottom. Based on the accomplishments made in the current study, the following plans are recommended by the author for future studies:

- A sensitivity study of the slab rocking and its effect on the rigid pavement design.
- The influence of early traffic on reducing the upward deflection due to warping effects.

- A detailed study of the change in loss of support under the slab due to variations in temperature, with and without traffic loading.
- The validation process needs to be carried out further to predict possible distresses in the pavement system and compare them to the actual distresses exhibited by the pavement system in the field.

6.4 IMPLEMENTATION

The joint spacing results will be verified by constructing test sections on the SHRP test road on US 23 in Delaware County. Once the results are verified, ODOT construction specifications can be modified to incorporate the new information. The load response analysis in this report can be used as input in implementing the mechanistic-empirical design process recommended in the guidelines developed under NCHRP Project 1-37A.

It is important to bear in mind that the long-term serviceability depends upon proper M-E design. For rigid pavements the critical design parameters are mainly slab deflection and tensile stresses. A key pillar of M-E Design is the software used to compute the load response. In this report, we have indicated how four different programs, EVERFE, ISLAB2000, JSLAB, and OU3D, predict load response. This report also discusses the limitations on these programs. For routine applications, ISLAB2000 is easy to use, practical, and fast. When more in-depth computation is needed then EVERFE may be used.

7 REFERENCES

Al-Nasra, M., and Wang, R. L. (1994). "Parametric Study of Slab-on-Grade Problems due to Initial Warping and Point Loads". *ACI Structural Journal*, American Concrete Institute, Vol. 91, No. 1, pp.198-210.

Applied Research Associates, Inc., ERES Division. (2003). "Guide for Mechanistic-Empirical Design of New and Rehabilitated Pavement Structures, Appendix QQ: Structural Response Models for Rigid Pavements". NCHRP Report.

Bathe, K. J. (1982). Finite Element Procedures in Engineering Analysis. Prentice-Hall, Inc., Englewood Cliffs, New Jersey 07632.

Beegle, D. J. (1998). "Three-Dimensional Modeling of Rigid Pavement". Master's Thesis, Ohio University, Athens, Ohio.

Beegle, D., and Sargand, S. M. (2003). "Comparisons of Measured and Predicted Primary Response of Rigid Pavement for Different Truck Axle Spacings". A Paper Presented at the International Conference on Highway Pavement Data, Analysis and Mechanistic Design Applications, Columbus, Ohio.

Beegle, D.J., and Sargand, S. M. (1995). "Three-Dimensional Modeling of Rigid Pavement". Report ST/ SS/95-002. Ohio Department of Transportation and FHWA, U.S. Department of Transportation.

Beegle, D.J., and Sargand, S.M. (2003). "Comparison of Measured and Predicted Primary Response of Rigid Pavement for Different Truck Axle Spacing." A paper presented at the International Conference on Highway Pavement Data, Analysis and Mechanistic Design Applications. Columbus, Ohio, Volume II, pp. 213–224.

Bendaña, J. and Jason, W. (2003). "Environmental Effects of Early Age and Long Term Response of PCC Pavement". A Paper Presented at the International Conference on Highway Pavement Data, Analysis and Mechanistic Design Applications, Columbus, Ohio.

Brill, D. R., Hayhoe, G. F., and Lee, X. (1997). "Three-Dimensional Finite Element Modeling of Rigid Pavement Structures". A Paper Presented at the Aircraft/Pavement Technology in the Midst of Change Conference, Seattle, Washington.

Chen, G., and Baker, G. (2004). "Analytical Model for Prediction of Crack Spacing due to Shrinkage in Concrete Pavements". *Journal of Structural Engineering*, Vol. 130, No. 10, pp. 1529-1533.

Childs, L.D., and Kapernick, J.W., "Tests of Concrete Pavements on Gravel Subbases", *Proceedings of the American Society of Civil Engineers*, V. 84, HW3, Oct. 1958.

- Chou, Y. T. (1984). "Stress Analysis of Small Concrete Slabs on Grade". *Journal of Transportation Engineering*, ASCE, Vol. 110, No. 5, pp. 481-492.
- Choubane, B., and Tia, M. (1992). "Nonlinear Temperature Gradient Effect on Maximum Warping Stresses in Rigid Pavements". *Transportation Research Record* 1370, pp. 11-19.
- Choubane, B., and Tia, M. (1995). "Analysis and Verification of Thermal-Gradient Effects on Concrete Pavement". *Journal of Transportation Engineering*, Vol. 121, No. 1, pp. 75-81.
- Crovetti, J. A. (2002). "Deflection-Based Analysis Techniques for Jointed Concrete Pavement Systems". *Transportation Research record* 1809, pp. 3-11.
- Darter, M. I., Hall, K. T., and Kuo, C-M. (1995). "Support under Portland Cement Concrete Pavements". NCHRP Report, Issue 372, 56 p.
- Domenichini, L., and Marchionna A. (1981). "Influence of Stress Range on Plain Concrete Pavement Fatigue Design". Proceedings of 2nd International Conference on Concrete Pavement Design, Purdue University, Indiana.
- Dong, M., Hayhoe, G. F., and Fang, Y. W. (1997). "Runway Instrumentation at Denver International Airport: Dynamic Sensor Data Processing". A Paper Presented at the Aircraft/Pavement Technology in the Midst of Change Conference, Seattle, Washington.
- Faraggi, V., Jofre, C., and Kraemer, C. (1887). "Combined Effect of Traffic Loads and Thermal Gradients on Concrete Pavement Design". *Transportation Research Record* 1136, pp. 108-118.
- Federal Aviation Administration (FAA) (1995), *Airport Pavement Design and Evaluation*, Advisory Circular AC150/5320-6D, p. 85ff, available online at http://www.faa.gov/airports_airtraffic/airports/resources/advisory_circulars/media/150-5320-6D/150_5320_6d_part4.pdf, accessed June 7, 2006.
- Federal Highway Administration (FHWA) (1990), "Concrete Pavement Joints", Technical advisory T5040.30, Washington DC, November 30, 1990, available online at <http://www.fhwa.dot.gov/legregs/directives/techadvts/t504030.htm>, accessed June 7, 2006.
- Frabizzio, M. A., and Buch, N. J. (1999). "Performance of Transverse Cracking in Jointed Concrete Pavements". *Journal of Performance of Constructed Facilities*, ASCE, Vol. 13, No. 4.
- Guo, E. H., and Rice, J. L. (1997). "Effects of Slab Size on Critical Responses in Airport Concrete Pavements". A Paper Presented at the Aircraft/Pavement Technology in the Midst of Change Conference, Seattle, Washington.
- Hammons, M. I. (1998). "Validation of Three-Dimensional Finite Element Modeling Technique for Joints in Concrete Airport Pavements". *Transportation Research Record* 1629, pp. 67-75.

- Hammons, M. I., and Metcalf, J. B. (1999). "Effect of Transverse Shear on Edge Stresses in Rigid Pavements". *Journal of Transportation Engineering*, ASCE, Vol. 125, No. 2, pp. 93-100.
- Hansen, W., Smiley, D. L., Peng, Y., and Jensen, E. A. (2002). "Validating Top-Down Premature Transverse Slab Cracking in Jointed Plain Concrete Pavement". *Transportation Research Record* 1809, pp. 52-59.
- Harik, I. E., Jianping, P., Southgate, H., and Allen, D. (1994). "Temperature Effects on Rigid Pavements". *Journal of Transportation Engineering*, Vol. 120, No. 1, pp. 127-143.
- Harrison, J. A. (1997). "Analysis of Rigid Pavement Response Data Induced by Military Aircraft at Denver International Airport". Master Thesis, Mississippi State University, Mississippi.
- Hjelmstad, K. D., Kim, J., and Zuo, Q. H. (1997). "Finite Element Procedures for Three-Dimensional Pavement Analysis". A Paper Presented at the Aircraft/Pavement Technology in the Midst of Change Conference, Seattle, Washington.
- Huang, Y. H., and Wang, S. T. (1973). "Finite-Element Analysis of Concrete Slabs and its Implications for Rigid Pavement Design". *Transportation Research Record* 466, pp. 55-69.
- Hudson, W. R., and Flanagan, P. R. (1987). "An Examination of Environmental Versus Load Effects on Pavements". *Transportation Research Record* 1121, pp. 34-39.
- Hui, C. (1999). "Investigation into the Analysis and Prediction of Transverse Cracking in Rigid Pavement". Proposal for Dissertation Research, Civil Engineering Dept., Ohio University, Ohio.
- Ioannides, A. M., and Donnelly, J. P. (1988). "Three-Dimensional Analysis of Slab on Stress-Dependent Foundation". *Transportation Research Record* 1196, pp. 72-84.
- Ioannides, A. M., and Khazanovich, L. (1998). "Nonlinear Temperature Effects on Multilayered Concrete Pavements". *Journal of Transportation Engineering*, Vol. 124, No. 2, pp. 127-136.
- Ioannides, A. M., and Salsilli-Murua, R. A. (1989). "Temperature Curling in Rigid Pavements: An Application of Dimensional Analysis". *Transportation Research Record* 1227, pp 1-11.
- Jaghoory, S. (1981). "Effects of Various Design Parameters on the Movement of Jointed concrete Pavements". Ph.D. Thesis, University of Cincinnati, Ohio.
- Janssen, D. J. (1987). "Moisture in Portland Cement Concrete". *Transportation Research Record* 1121, pp. 40-44.
- Jensen, E. A., and Hansen, W. (2002). "Crack Resistance of Jointed Plain Concrete Pavements". *Transportation Research Record* 1809, pp. 60-65.
- Jiang, Y., Darter, M. I., and Owusu-Antwi, E. (1996). "Analysis of Current State Rigid Pavement Design Practices in the United States". *Transportation Research Record* 1525, pp. 72-82.

Kennedy, J. C., Everhart, R. D., Forte, T. P., Hadden, J. A., and Majidzadeh, K. (1994). "Development of a Governing Primary Response Model (GPRM) for Airport Pavement Design and Analysis, Volume I". Final Report submitted to Volpe National Transportation Systems center, Kendall Square, Cambridge, MA.

Kerr A. D. (1993). "Mathematical Models of Airport Pavements". Airport Pavement Innovations: Theory to Practice, ASCE, New York, New York, 10017, pp. 31-45.

Khazanovich, L., and Ioannides, A. M. (1993). "Finite Element Analysis of Slabs-On-Grade Using Higher Order Subgrade Soil Models". Airport Pavement Innovations: Theory to Practice, ASCE, New York, New York, 10017, pp. 16-30.

Khazanovich, L., Selezneva, O. I., Yu H. T., and Darter M. I. (2001). "Development of Rapid Solutions for Prediction of Critical Continuously Reinforced Concrete Pavement Stresses". *Transportation Research Record 1778*, pp. 64-72.

Kim, J., Hjelmstad, K. D., and Zuo, Q. H. (1997). "Three-Dimensional Finite Element Study of Wheel Load Interaction". A Paper Presented at the Aircraft/Pavement Technology in the Midst of Change Conference, Seattle, Washington.

Kim, S-M., Won, M. C., and McCullough, B. F. (2002). "Airport Pavement Response under Moving Dynamic Aircraft Loads". A Paper Presented at the Twenty-Seventh International Air Transport Conference, ASCE, Orlando, Florida.

Lee, Y-H. (1999). "TKUPAV: Stress Analysis and Thickness Design Program for Rigid Pavements". *Journal of Transportation Engineering*, ASCE, Vol. 125, No. 4, pp. 338-346.

Lee, Y-H., and Darter, M. I. (1994). "Loading and Curling Stress Models for Concrete Pavement Design". *Transportation Research Record 1449*, pp. 101-113.

Lee, Y-H., and Yen, S-T. (2002). "Effects of Various Design Features on Rigid Airfield Pavement Design". A Paper Presented at the Twenty-Seventh International Air Transport Conference, ASCE, Orlando, Florida.

Mallela, J., and George, K. P. (1994). "Three-Dimensional Dynamic Response Model for Rigid Pavements". *Transportation Research Record 1448*, pp. 92-99.

Masad, E., Taha, R., and Muhunthan, B. (1996). "Finite-Element Analysis of Temperature Effects on plain-Jointed Concrete Pavements". *Journal of Transportation Engineering*, ASCE, Vol. 122, No. 5, pp. 388-398.

Masada, T., Sargand, S. M., Abdalla, B., and Figueroa, J. L. (2004). "Material Properties for Implementation of Mechanistic-Empirical (M-E) Pavement Design Procedures". Final Report to Ohio Department of Transportation & Federal Highway Administration, ORITE, Department of Civil Engineering, Ohio University, Athens, Ohio, 267 p.

- Mohamed, A. R., and Hansen, W. (1997). "Effect of Nonlinear Temperature Gradient on Curling Stress in Concrete Pavements". *Transportation Research Record* 1568, pp.65-71.
- Nasim, M. A., Karamihas, S. M., Gillespie, W. H., and David S. (1991). "Behavior of a Rigid Pavement under Moving Dynamic Loads". *Transportation Research Record* 1307, pp. 129-135.
- Pane, I., Hansen, W., and Mohamed, A. R. (1998). "Three-Dimensional Finite Element Study on Effects of Nonlinear Temperature Gradients in Concrete Pavements". *Transportation Research Record* 1629, pp. 58-66.
- Parson, I. D., Eom, I. S., and Hjelmstad, K. D. (1997). "Numerical Solutions of Load Transfer Between Doweled Pavement Slabs". A Paper Presented at the Aircraft/Pavement Technology in the Midst of Change Conference, Seattle, Washington.
- Parsons, T. A., and Hall Jr., J. W. (2003). "The Effects of Slab Size on PCC Pavement Performance". A Paper Presented at Airfield Pavements, Challenges and New Technologies, ASCE, Las Vegas, Nevada.
- Pittman, D. W., and McCullough, B. F. (1997). "Development of a Roller-Compacted Concrete Pavement Crack and Joint Spacing Model". *Transportation Research Record* 1568, pp. 52-64.
- Poblete, M., Ceza, P., David, J., Espinosa, R., Garcia, R., and Gonzalez, J. (1991). "Model of Slab Cracking for Portland Cement Concrete Pavements". *Transportation Research Record* 1307, pp. 154-161.
- Ramsamooj, D. V. (1999). "Stresses in Jointed Rigid Pavements". *Journal of Transportation Engineering*, ASCE, Vol. 125, No. 2, pp. 101-107.
- Richardson, J. M., and Armaghani, J. M. (1887). "Stress Caused by Temperature Gradient in Portland Cement Concrete Pavements". *Transportation Research Record* 1121, pp. 7-13.
- Sargand, S. M., and Masada, T. (2001). "Laboratory Characterization of Ohio-SHRP Test Road Pavement Material". Final Report to Ohio Department of Transportation & Federal Highway Administration, ORITE, Department of Civil Engineering, Ohio University, Athens, Ohio, 189 p.
- Sargand, S. M., Edwards, W., and Khoury, I. (2003). "Evaluation of Forces in Dowel Bars under Controlled Conditions". Final Report to U.S. Department of Transportation & Federal Highway Administration, ORITE, Department of Civil Engineering, Ohio University, Athens, Ohio, 43 pp.
- Sargand, S., Green, R., and Khoury, I. (1997). "Instrumenting Ohio Test Pavement." *Transportation Research Record* 1596, pp. 23-30.
- Sargand, S.M. (1994). "Development of an Instrumentation Plan for the Ohio SPS Test Pavement (DEL-23-17.48)". Report FHWA/OH-94/019. Ohio Department of Transportation and FHWA, U.S. Department of Transportation.

Sargand, S.M. (1999). "Coordination of Load Response Instrumentation of SHRP Pavements". Report FHWA/OH-99/009. Ohio Department of Transportation and FHWA, U.S. Department of Transportation.

Sheehan, M. J., Snyder, M. B., Savage, B. M., Holt, E. E., and Janssen, D. J. (1996). "Early and Long-Term Effects of Curling and Warping on Jointed Concrete Pavement. Part II: Experimental and Gradient Modeling Plan". Interim Report, Washington State Transportation Center (TRAC), Seattle, Washington. 87 p.

Shoukry, S. N., and Fahmy, M. R. (2002). "Optimization of Concrete Slab Geometry for Enhanced Rigid Pavement Performance and Service Life". Final Report to West Virginia Department of Transportation and Federal Highway Administration, University of West Virginia, Morgantown, West Virginia.

Shoukry, S. N., Riad, M. Y., and William, G. W. (2003). "West Virginia Smart Road: Early Age Behavior of Doweled Concrete Pavements". A Paper Presented at the International Conference on Highway Pavement Data, Analysis and Mechanistic Design Applications, Columbus, Ohio.

Shoukry, S. N., William, G. W., and Riad, M. (2003). "Nonlinear Temperature Gradient Effects in Dowel Jointed Concrete Slabs". *International Journal of Pavement Engineering*, Vol. 4, Issue 3, pp. 131-142.

Suprenant, B. A. (2002). "Why Slabs Curl. Part II: Factors Affecting the Amount of Curling". *Concrete International*, Vol. 24, Issue 4, pp.59-64.

Swan, J. S., and Darter, M. I. (1978). "Structural Evaluation of PCC Shoulders". Transportation Research Record 666, pp. 51-60.

Tabatabaie, A. M., and Barenberg, E. J. (1978). "Finite Element Analysis of Jointed or Cracked Concrete Pavements". *Transportation Research Record* 671, pp. 11-19.

Tarr, S. M., Okamoto, P. A., Sheehan, M. J. (1998). "Concrete Pavement Warping, Curling, and Subbase Interaction". Report to Portland Cement Association, Construction Technology Laboratories, Inc., Skokie, IL, 52 p.

Tayabji, S. D., and Colley, B. E. (1986). "Analysis of Jointed Concrete Pavements". Report No. FHWA/RD-86/041, Construction Technology Laboratories, PCA, Skokie, IL, 68 p.

Timoshenko, S., and Woinowsky-Krieger, S. (1959). Theory of Plates and Shells. McGraw-Hill Book Company.

Uddin, W., Zhang, D., and Fernandez, F. (1994). "Finite Element Simulation of Pavement Discontinuities and Dynamic Load Response". *Transportation Research Record* 1448, pp. 100-106.

Weiss, W. J., Yang, W., and Shah, S. P. (1998). "Shrinkage Cracking of Restrained Concrete Slabs". *Journal of Engineering Mechanics*, ASCE, Vol. 124, No. 7, pp. 765-774.

Weiss, W. R., and Hall, J. W. (2002). "Performance of Concrete Airfield pavements at United States Air Force Bases". A Paper Presented at the Twenty-Seventh International Air Transport Conference, ASCE, Orlando, Florida.

Westergaard, H. M. (1927). "Analysis of Stresses in Concrete Roads Caused by Variations of Temperature". *Public Roads*, Vol. 8, No. 3, pp. 54-60.

William, G., and Shoukry, S. N. (2000). "3D Finite Element Analysis of Temperature –Induced Stresses in Dowel Jointed Concrete Pavements". A Paper Presented at the Second International Symposium on 3D Finite Element for Pavement Analysis, Design, and Search, Charleston, West Virginia.

Won, M. C., Kim, S-M., Merritt, D., and McCullough, B. F. (2002). "Horizontal Cracking and Pavement Distress in Portland Cement Concrete Pavement". A Paper Presented at the Twenty-Seventh International Air Transport Conference, ASCE, Orlando, Florida.

Ytterberg, R. F., "Shrinkage and Curling of Slabs on Grade, Part II – Warping and Curling" *Concrete International*, V. 9, No. 5, May 1987, pp.54-61.

Yu, H. T., Smith, K. D., and Darter, M. I. (1995). "Field and Analytical Evaluation of the Effects of Tied PCC Shoulder and Widened Slabs on Performance of JPCP". Final Report to Colorado Department of Transportation. ERES Consultants, Inc., 76 pp.

Zaghloul, S. M., White, T. D., and Kuczek, T. (1994). "Evaluation of Heavy Load Damage Effect on Concrete Pavements Using Three-Dimensional, Nonlinear Dynamic Analysis". *Transportation Research Record* 1449, pp. 123-133.

Zhang, J., Fwa, T. F., Tan, K. H., and Shi, X. P. (2003). "Model for Nonlinear Thermal Effect on Pavement Warping Stresses". *Journal of Transportation Engineering*, ASCE, Vol. 129, No. 6, pp. 695-702.

Zienkiewicz, O. C., and Cheung, Y. K. (1967). The Finite Element Method in Structural and Continuum Mechanics. McGraw-Hill Publishing Company Limited.

Zienkiewicz, O. C., and Taylor, R. L. (2000). The Finite Element Method, Volume 1: The Basis. Fifth Edition, Butterworth-Heinemann, Linacre House, Jordan Hill, Oxford OX2 8DP.



ORITE • 141 Stocker Center • Athens, Ohio 45701-2979 • 740-593-2476
Fax: 740-593-0625 • orite@bobcat.ent.ohiou.edu • <http://webce.ent.ohiou.edu/orite/>